

Mononuclear and Oligonuclear Transition Metal Complexes with Acyclic and Macrocyclic Ligands

Inauguraldissertation

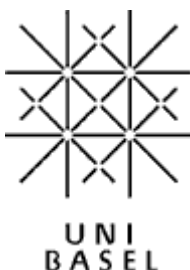
zur Erlangung der Würde eines Doktors der Philosophie
vorgelegt der Philosophisch-Naturwissenschaftlichen Fakultät der Universität Basel

von

Pirmin Rösel

aus Weil am Rhein, Deutschland

Basel, 2009



Genehmigt von der Philosophisch-Naturwissenschaftlichen Fakultät
auf Antrag von

Prof. Dr. Edwin Constable

Prof. Dr. Andreas Pfaltz

Prof. Dr. Jean-Pierre Sauvage

Basel, den 26.05.2009

Prof. Dr. Eberhard Parlow

Dekan

Originaldokument gespeichert auf dem Dokumentenserver der Universität Basel
edoc.unibas.ch



Dieses Werk ist unter dem Vertrag „Creative Commons Namensnennung-Keine kommerzielle Nutzung-Keine Bearbeitung 2.5 Schweiz“ lizenziert. Die vollständige Lizenz kann unter **creativecommons.org/licenses/by-nc-nd/2.5/ch** eingesehen werden.



Namensnennung-Keine kommerzielle Nutzung-Keine Bearbeitung 2.5 Schweiz

Sie dürfen:



das Werk vervielfältigen, verbreiten und öffentlich zugänglich machen

Zu den folgenden Bedingungen:



Namensnennung. Sie müssen den Namen des Autors/Rechteinhabers in der von ihm festgelegten Weise nennen (wodurch aber nicht der Eindruck entstehen darf, Sie oder die Nutzung des Werkes durch Sie würden entlohnt).



Keine kommerzielle Nutzung. Dieses Werk darf nicht für kommerzielle Zwecke verwendet werden.



Keine Bearbeitung. Dieses Werk darf nicht bearbeitet oder in anderer Weise verändert werden.

- Im Falle einer Verbreitung müssen Sie anderen die Lizenzbedingungen, unter welche dieses Werk fällt, mitteilen. Am Einfachsten ist es, einen Link auf diese Seite einzubinden.
- Jede der vorgenannten Bedingungen kann aufgehoben werden, sofern Sie die Einwilligung des Rechteinhabers dazu erhalten.
- Diese Lizenz lässt die Urheberpersönlichkeitsrechte unberührt.

Die gesetzlichen Schranken des Urheberrechts bleiben hiervon unberührt.

Die Commons Deed ist eine Zusammenfassung des Lizenzvertrags in allgemeinverständlicher Sprache: <http://creativecommons.org/licenses/by-nc-nd/2.5/ch/legalcode.de>

Haftungsausschluss:

Die Commons Deed ist kein Lizenzvertrag. Sie ist lediglich ein Referenztext, der den zugrundeliegenden Lizenzvertrag übersichtlich und in allgemeinverständlicher Sprache wiedergibt. Die Deed selbst entfaltet keine juristische Wirkung und erscheint im eigentlichen Lizenzvertrag nicht. Creative Commons ist keine Rechtsanwalts-gesellschaft und leistet keine Rechtsberatung. Die Weitergabe und Verlinkung des Commons Deeds führt zu keinem Mandatsverhältnis.

Die vorliegende Arbeit wurde unter Anleitung von Prof. Dr. Edwin Constable, Prof. Dr. Jean-Pierre Sauvage und Prof. Dr. Catherine Housecroft in der Zeit von Juli 2005 bis Mai 2009 im Departement Chemie der Universität Basel (Kapitel 2-5) und der Fakultät für Chemie der Universität Louis Pasteur (Kapitel 1) in Strassburg angefertigt.

Auszüge dieser Arbeit wurden bereits veröffentlicht:

F. Durola, D. Hanss, P. Rösel, J. P. Sauvage, O. S. Wenger, *Eur. J. Org. Chem.* **2007**, 125.

E. C. Constable, C. E. Housecroft, M. Neuburger, P. Rösel, S. Schaffner, *Dalton Trans.*, accepted.

Acknowledgements

My thanks go first to my supervisors, Prof. Dr. Edwin Constable, Prof. Dr. Jean-Pierre Sauvage, and Prof. Dr. Catherine Housecroft, who gave me the opportunity to do my PhD and to work in collaboration with University Louis Pasteur in Strasbourg. I am very grateful to work for supervisors who provided me with support, advice, encouragement and an excellent working environment.

I thank Prof. Dr. Andreas Pfaltz for being my co-referee and co-examiner and Prof. Dr. Thomas Ward for being my chairman.

Markus Neuburger, Dr. Silvia Schaffner and Dr. Jennifer Zampese are gratefully acknowledged for X-ray structure elucidation.

Dr. Daniel Häussinger's excellent expertise and advice were very helpful and I thank him for recording NMR spectra on the 600 MHz machine. Jon Beves, Kate Harris, Ana Hernandez and Valerie Jullien are thanked for recording 500 MHz NMR spectra.

The following people are also thanked: William Kylberg (electrochemical measurements), Dr. Conor Brennan and Tünde Vig (atomic absorption spectroscopy), and Emma Dunphy (measurements on various other instruments).

Stefan Graber and Dr. Bernhard Jung are gratefully acknowledged for computer help.

I am thankful for technical and administrative support from the University Basel and the University Louis Pasteur staff, especially from Beatrice Erismann and Markus Hauri.

For proof reading parts of this thesis I thank Kate Harris, Jennifer Zampese, Biljana Bozic-Weber, Ralf Schmitt and Peter Kopecky and especially Prof. Dr. Housecroft for very helpful proof reading of my entire thesis.

Thanks go to all members of the Constable-Housecroft group in Basel and the Sauvage group in Strasbourg for their help and friendship. Dr. David Hanss, Dr. Oliver Wenger and Fabien Durola particularly helped me during my first year in Strasbourg.

Financial support is gratefully acknowledged from Stiftung Stipendien Fonds des Verbandes der Chemischen Industrie e. V. and University of Basel.

A very big thank you goes to my parents and sisters for their care and support.

Szczególne podziękowania dla mojej wspaniałej dziewczyny Pauliny za miłość, pomoc i wsparcie.

Table of Contents

Acknowledgements.....	i
Table of Contents	ii
Abstract.....	v
Abbreviations.....	vi
1 A Biisoquinoline Chelate	1
1.1 Introduction	1
1.2 Aims and Overview.....	8
1.3 Results and Discussion.....	10
1.4 Summary	17
2 Macrocyclic Tris(bipyridine) – A Metal Templated Synthesis for Trivial Knots.....	19
2.1 Introduction	19
2.2 Aims and Overview.....	24
2.3 Synthesis.....	26
2.4 Characterisation.....	36
2.5 Summary and Outlook	45
3 Oligonuclear Ruthenium(II) Complexes with Macrocyclic Ligands	47
3.1 Introduction	47
3.2 Aims and Overview.....	51
3.3 Synthesis.....	52
3.4 Characterisation and Crystal Structures	56
3.5 Photophysical Properties and Redox Potentials	64
3.6 NMR Enantiodifferentiation of Chiral Ruthenium(II) Complexes	68
3.7 Determination of Coordinated Sodium in 64 via Atomic Absorption Spectroscopy.....	73
3.8 Summary and Outlook	76
4 Diversification of Ligand Families.....	77
4.1 Introduction	77
4.2 Aims and Overview.....	79
4.3 Results and Discussion.....	80
4.4 Summary	92
5 Complexes of [Ru(bpy)₃]²⁺-type bearing Pyrene Moieties.....	93
5.1 Introduction	93
5.2 Aims and Overview.....	97
5.3 Synthesis.....	98
5.4 Crystal Structures and Characterisation	102
5.5 Photophysical Properties	110
5.6 Summary and Outlook	115

6 Experimental Part	117
6.1 General Experimental.....	117
6.2 Experimental for Compounds in Chapter 1.....	121
6.3 Experimental for Compounds in Chapter 2.....	135
6.4 Experimental for Compounds in Chapter 3.....	156
6.5 Experimental for Compounds in Chapter 4.....	164
6.6 Experimental for Compounds in Chapter 5.....	177
7 Appendix	183
7.1 Crystal Structures from Chapter 2.....	183
7.2 Crystal Structures from Chapter 3.....	185
7.3 Crystal Structures from Chapter 4.....	187
7.4 Crystal Structures from Chapter 5.....	189
7.5 Overview Crystal Structures	191
8 References	193
Curriculum vitae	203

Abstract

Chapter 1 describes an efficient multi-step synthesis of an endotopic but sterically unhindered bisoquinoline decorated with long alkyl groups for better solubility. This chelate is ideally suited for macrocycle formation around transition metal ions and therefore a valuable new building block for topological chemistry.

Sokolov's concept to use an octahedral metal template for the syntheses of macrocycles and molecular knots is discussed in **Chapter 2**. The concept was successfully realised for the synthesis of a macrocyclic, hexadentate ligand that incorporates three bipyridine units. One-to-one complexes with this ligand and zinc(II), iron(II) and ruthenium(II) were prepared and a crystal structure of the latter was obtained.

Three novel oligonuclear, macrocyclic ruthenium(II) complexes are presented in **Chapter 3**. The complexes are mononuclear, dinuclear and trinuclear and were prepared from bidentate, tetradentate or hexadentate macrocyclic ligands, respectively. The compounds were extensively characterised and their physical properties have been investigated.

Chapter 4 describes the diversification of ligand families into neocuproin (suited for coordination to copper(I)), ferroin (suited for coordination to iron(II)) and heteroditopic structure type. Proof-of-principle conversion into palladium(II) and copper(I) complexes were prepared and their structures are discussed.

The synthesis of a symmetric bipyridine ligand which possesses pyrene domains is shown in **Chapter 5**. Homoleptic and heteroleptic iron(II) and ruthenium(II) complexes with this ligand are presented and their solid state structures and photophysical properties are examined.

Abbreviations

AAS	atomic absorption spectroscopy	ESI	electrospray ionisation
AES	atomic emission spectroscopy	Et ₂ O	diethyl ether
ADP	adenosine diphosphate	EtOH	ethanol
ATP	adenosine triphosphate	exc	excitation
COSY	correlated spectroscopy	Φ	quantum yield
CT	charge transfer	FAB	fast atom bombardement
CV	cyclic voltammetry	<i>fac</i>	facial
b.p.	boiling point	Fc	ferrocene
bpy	2,2'-bipyridine	FT	Fourier transformation
Bu	butyl	GS	ground state
BuLi	butyl lithium	h	Planck's constant
d	doublet	HMBC	heteronuclear multiple bond correlation
δ	chemical shift	HMQC	heteronuclear multiple quantum correlation
DCE	1,2-dichloroethane	H ₂ Na ₂ Edta	disodium ethylenediamine-tetraacetic acid
DCM	dichloromethane	HPLC	high performance liquid chromatography
DEPT	distortionless enhancement by polarisation transfer	Hz	hertz, s ⁻¹
dmbp	5,5'-bis(3-methoxyphenyl)-2,2'-bipyridine	IC	internal conversion
DME	dimethoxyethane	IR	infrared spectroscopy
DMF	<i>N,N'</i> -dimethylformamide	ISC	intersystem crossing
DMSO	dimethylsulfoxide	IUPAC	International Union of Pure and Applied Chemistry
dppf	1,1'-bis(diphenylphosphino)ferrocene	J	coupling constant
dppp	1,3-bis(diphenylphosphino)propane	λ	wavelength
ϵ	molar extinction coefficient	LC	ligand centred
EI	electron impact	m	multiplet or medium (IR)
		M	molarity

MALDI	matrix assisted laser desorption ionisation	TIPSCl	triisopropylsilyl chloride
MC	metal centred	tlc	thin layer chromatography
MeCN	acetonitrile	TOF	time of flight
MeLi	methyl lithium	tpy	2,2':6',2''-terpyridine
MeOH	methanol	TRISPHAT	tris(tetrachlorobenzene- diolato)phosphate(V)-ion
<i>mer</i>	meridional	UV-Vis	ultra-violet visible spectroscopy
MLCT	metal to ligand charge transfer	w	weak (IR)
m.p.	melting point		
MS	mass spectrometry		
μ W	microwave		
<i>m/z</i>	mass to charge ratio		
ν	frequency (cm^{-1} or Hz)		
NEt ₃	triethyl amine		
NHE	Normal Hydrogen Electrode		
NMR	nuclear magnetic resonance spectroscopy		
NOESY	nuclear overhauser effect spectroscopy		
phen	1,10-phenantroline		
ppm	parts per million		
py	pyridine		
q	quartet		
RCM	ring closing metathesis		
RT	room temperature		
s	singlet or strong (IR)		
t	triplet		
τ	lifetime of emission		
TBAF	tetra- <i>n</i> -butylammonium fluoride		
Tf	triflate		
THF	tetrahydrofuran		
TIPS	triisopropylsilyl		

1 A Biisoquinoline Chelate

Biological motors^[1] are proteins (for example, myosins, kinesins and dyneins) and are important in biological processes including muscle contraction, intracellular transport and signal transduction. The ATP synthase^[2, 3] is an enzyme that is another genuine example for a molecular motor able to synthesise adenosine triphosphate (ATP) from adenosine diphosphate (ADP) using energy usually in the form of protons moving down an electrochemical gradient. ATP is the common immediate energy source of cells.

Nature has had roughly 4.5 billion years time to develop molecular machines whereas mankind has only been working for several decades on synthetic molecular machines. Clearly, the natural molecular machines are superior in terms of complexity and functionality to their artificial analogues.

Synthetic molecular motors are often based on catenanes or rotaxanes in which motion can be triggered and controlled at will; hence act as molecular machines or at least like their prototypes.

1.1 Introduction

Interlocked molecules are built from two or more modules that are mechanically linked together. Figure 1.1-1 illustrates a [2]catenane^a and a [2]rotaxane – two of the simplest and most common compounds that are intertwined. The name catenane is derived from the Latin word *catena* which means “chain”. The interlocked rings cannot be separated without breaking a covalent bond. A [2]rotaxane is comprised of a linear, dumbbell-shaped fragment that is threaded through a cyclic component. Bulky groups (stoppers) trap the two components such that they are not free to separate unless a covalent bond is broken.

^a The number in brackets designates the number of components.

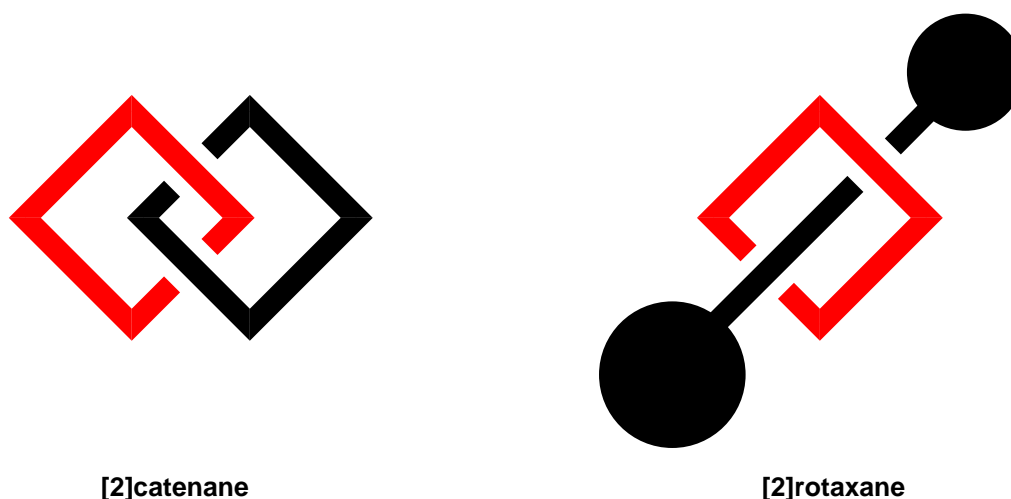
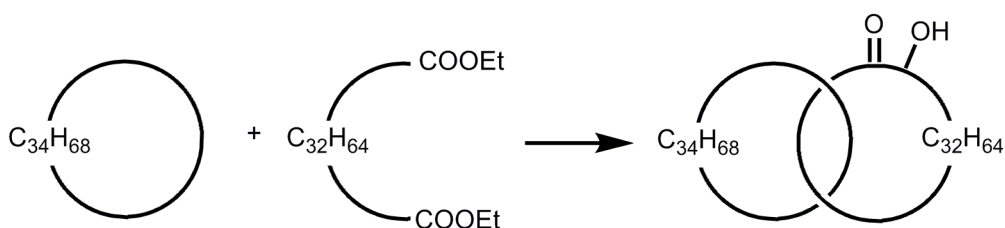


Figure 1.1-1. Schematic representation of a [2]catenane and a [2]rotaxane.

R. M. Willstätter discussed the possibility of interlocked rings in a talk in Zürich almost a century ago.^[4] He could not conjecture that his early “visionary” speculations would become true and that today’s chemists are not only able to synthesise catenanes in high yields but also geometrical structures of much higher topological complexity. In 1960, Wasserman published for the first time the synthesis of a catenane by a statistical threading approach.^[5] The intramolecular acyloin condensation of a diester to form a macrocycle in the presence of a large alkane ring should deliver a statistical amount of a catenated species supposing that during the reaction some molecules of the diester have been threaded in the ring. With this very intuitive, though not efficient, method, only one percent of the species with interlocked rings could be isolated after extensive chromatographic purification (see Scheme 1.1-1).



Scheme 1.1-1. Wasserman’s statistical synthesis^[5] via intramolecular acyloin condensation in the presence of a cyclic alkane yielded approximately one percent of the catenane.

The directed synthesis of catenanes has been performed by Schill et al. and published in 1971.^[6, 7]

With the appearance of various templated approaches in the 1980’s, the research area of topologically unusual but doubtlessly beautiful molecules and their applications literally

exploded. Since 1983, a copper-metal template strategy introduced by Sauvage et al.^[8, 9] that allowed catenanes, rotaxanes and knots to be obtained in reasonable to excellent yields. Figure 1.1-2 shows the first example of an extremely short and convenient synthetic route to a catenane, that is based on a generalized template effect around a metal ion.^[10] In the first step the complex **2**⁺ is formed quantitatively with ligand **1** and Cu(MeCN)₄⁺. This very stable, deep red complex was reacted further under high dilution conditions with a diiodo chain, derived from pentaethylene glycol, in the presence of Cs₂CO₃ affording **3**⁺ in 27% yield.

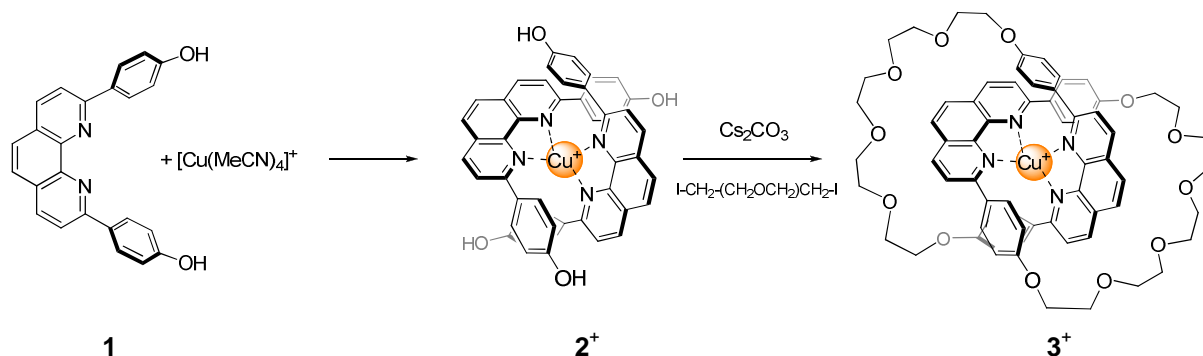


Figure 1.1-2. Synthesis of a catenand (metalated catenane) around a copper(I) ion in 27% yield. Adapted from reference.^[10]

In 2006, Beer et al.^[11] reported the synthesis of a [2]catenane that was templated by a chloride anion (see Figure 1.1-3). Equimolar solutions of **4a** (chloride salt) and **4b** (hexafluorophosphate salt) were mixed and subjected to a ring closing metathesis (RCM) affording the catenane in 78% yield. Interestingly, analogous RCM reactions with pure **4a** or **4b** gave significantly lower yields, 34% and 16% respectively. The lower yield of catenane is explained by a favoured formation of a macrocycle in case of the pure chloride and the lack of anion templation from chloride in case of the pure hexafluorophosphate salt. However, catenane formation in the latter shows that π - π stacking and pyridinium CH \cdots O hydrogen bonds participate in the formation process.

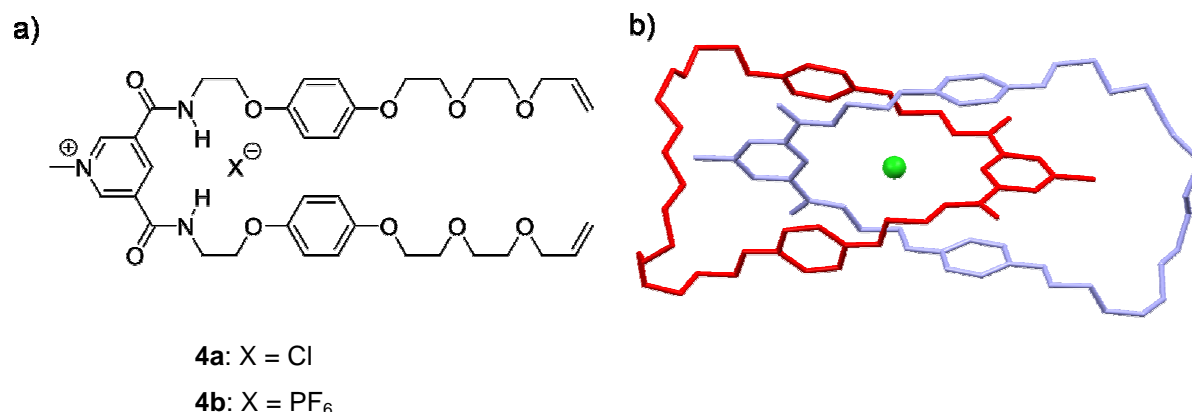


Figure 1.1-3. a) Structure of the catenane precursor; b) Crystal structure of the [2]catenane with a chloride ion in the binding cavity. Other counterions, hydrogen atoms and solvent molecules have been omitted for clarity. Adapted from reference.^[11]

In order to achieve good yields, the building blocks have to be pre-organised. Such pre-organisation has been very successfully demonstrated in many syntheses with the interactions including coordination to a metal ion,^[9, 10, 12] hydrophobic effects^[13], hydrogen bond formation,^[14, 15] charge-transfer interactions^[16, 17] and covalent bond formation.^[18] In particular, Stoddart and his group have worked on the synthesis of interlocked systems based on secondary dialkylammonium salts and crown ethers^[19, 20] and on systems based on π -electron-rich/ π -electron-deficient aromatic systems.^[16] Hunter^[21], Vögtle^[22, 23] and Leigh^[24] worked on catenane systems with hydrogen-bonds as templates, and cyclodextrin systems have been presented by Harada, Wenz and Ogino.^[13, 25, 26] Furthermore, one can also find rotaxanes based on crown ether frameworks reported by Gibson.^[27]

All these molecules display interesting physical properties such as photoinduced intramolecular electron transfer,^[28] electrochemically triggered molecular motion and photochemical dethreading processes. This leads us to multicomponent systems which can act as molecular machines, molecular devices or molecular computers.^[29-33]

One appealing example for a molecular machine is the hydrogen-bonded molecular shuttle^[31] developed by Leigh's group (see Scheme 1.1-2). A benzylic amide macrocycle is mechanically locked onto a thread bearing two potential H-bonding stations. In the ground state the ring is predominantly bound around the succinamide site (green). After irradiation and photoreduction of the naphthalamide site (red), the reduced naphthalamide (blue) is now the stronger H-bond acceptor, and the equilibrium shifts to the second station. After charge recombination, the macrocycle shuttles back to its original position. This process is reversible and has properties that are characteristic of an energy-driven piston.

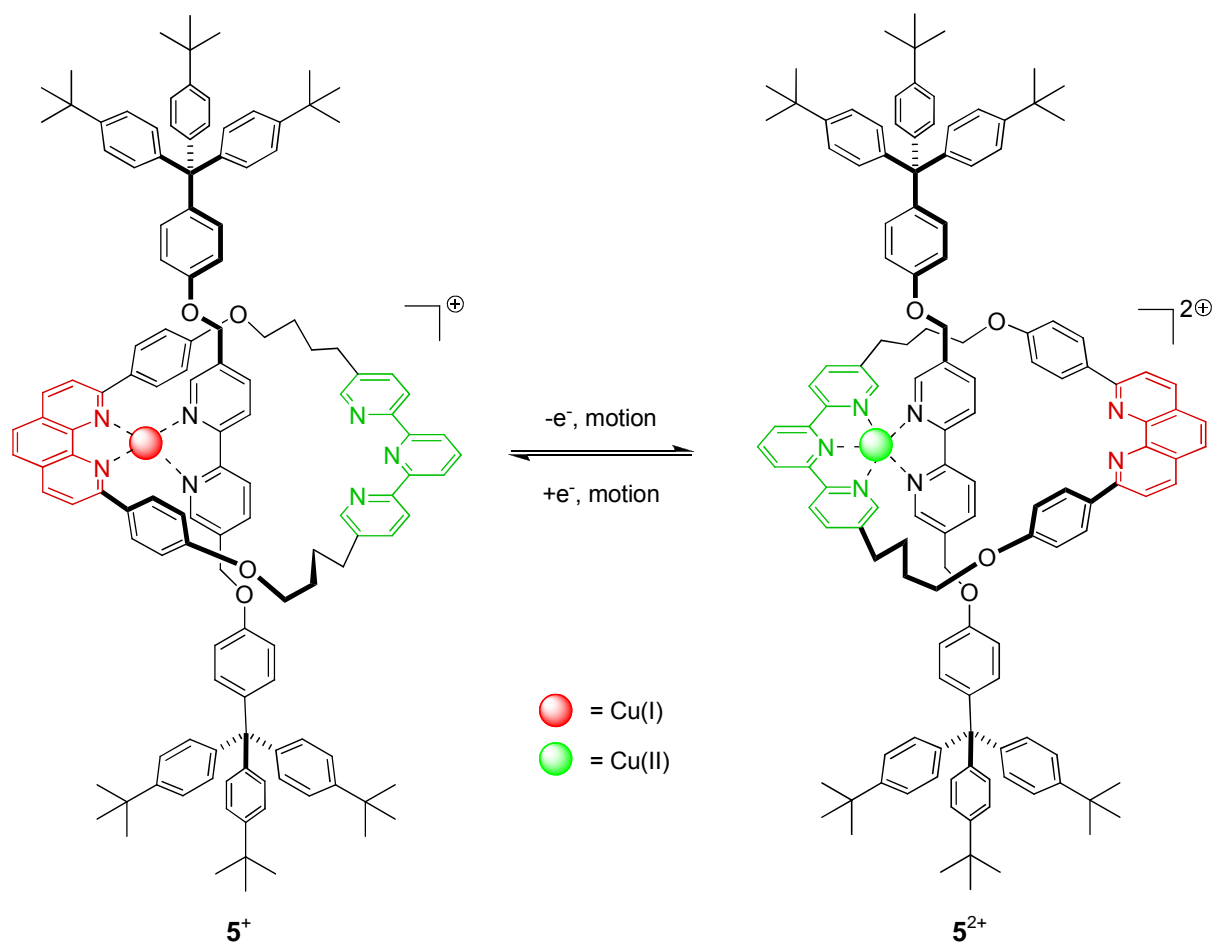
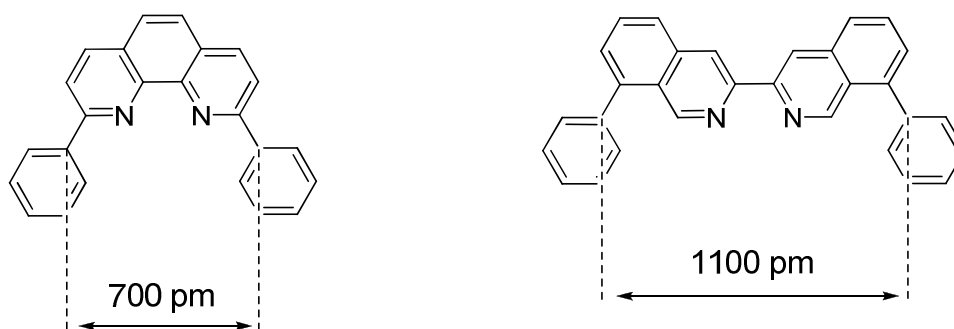


Figure 1.1-4. Electrochemically induced motion of the ring in rotaxane 5^{n+} . The bidentate chelate (red) and the tridentate fragment (green) are alternatively coordinated to the copper centre. Adapted from reference.^[35]

The 2,9-diphenylphenanthroline is a sterically more demanding ligand compared to the corresponding biisoquinoline system (see Scheme 1.1-3). The distances between the carbon atoms in the phenyl rings that are linked to the ligand moiety are 700 pm and 1100 pm^[41], respectively. The complexed metal centre will be remote from any organic group of the biisoquinoline ligand.



Scheme 1.1-3. Pronounced steric hindrance will occur once the dpp-fragment is coordinated to a metal (left). Substituted bisisoquinoline fragments allow endocyclic and sterically non-hindered coordination (right).

The homoleptic iron(II)-complex of ligand **6** illustrates the endocyclic but sterically non-hindering fashion of coordination (see Figure 1.1-5).^[38, 41]

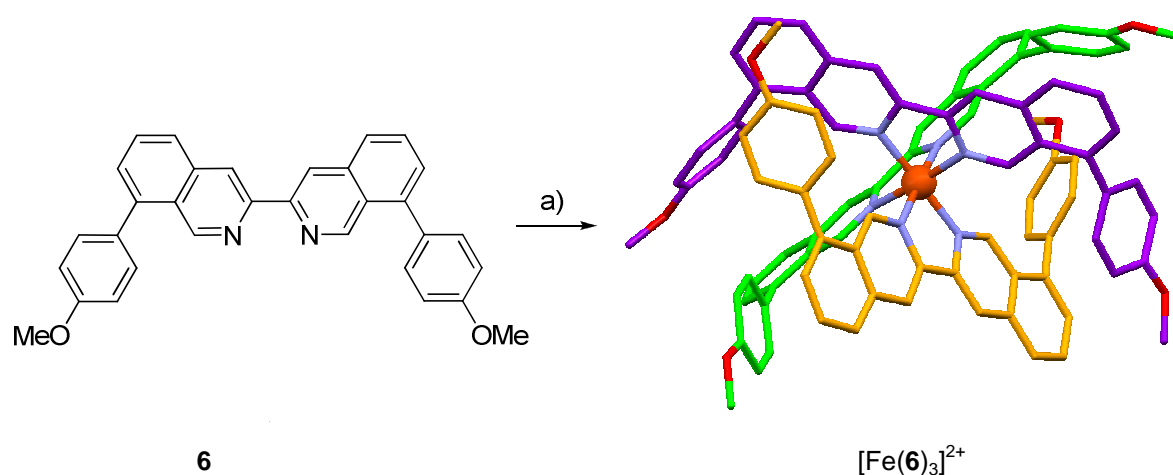


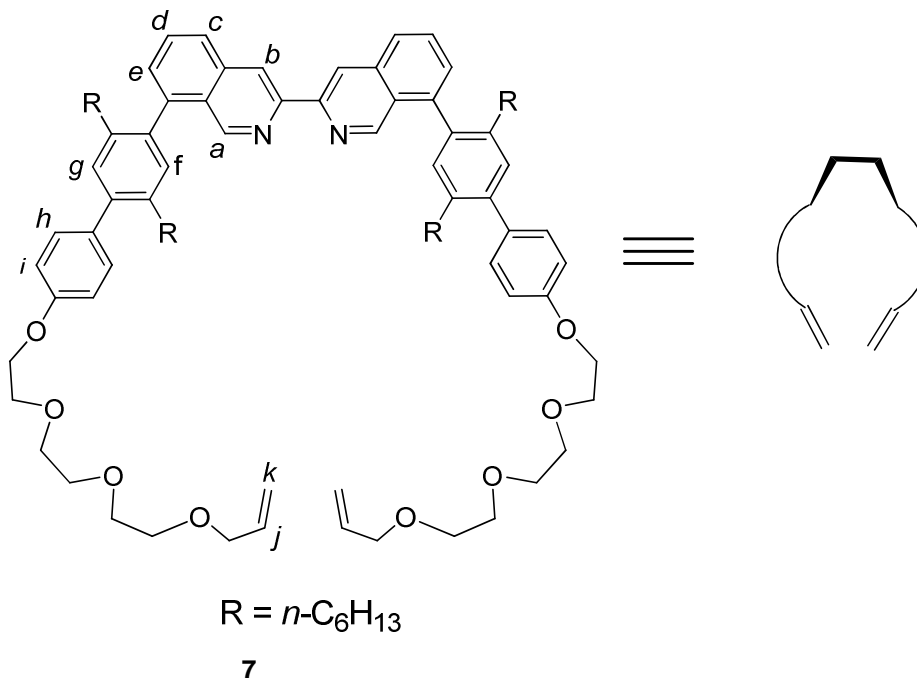
Figure 1.1-5. Reagents and conditions: a) $\text{Fe}(\text{BF}_4)_2$, CH_2Cl_2 . The crystallographic structure of the cation $[\text{Fe}(\mathbf{6})_3]^{2+}$ is shown on the right. Counterions, solvent molecules and hydrogen atoms have been omitted for clarity. Adapted from references.^[38, 41]

1.2 Aims and Overview

Ligands of the biisoquinoline family^[37-44] are ideally suited for macrocycle formation around transition metal ions and are promising novel building blocks for topologically unusual molecules. They feature two crucial properties that seem to be contradictory:

- (i) they coordinate in an unhindered or only very slightly hindered fashion since they have no substituents in α position.
- (ii) the binding site is inevitably arranged towards the endo part of the crescent shaped ligand that will lead unambiguously to an endocyclic coordination if the chelate is subsequently included in a ring.

This chapter describes the synthesis of the novel biisoquinoline ligand **7** (see Scheme 1.2-1). Alkyl chains render this ligand soluble. Ethylene glycol chains bearing terminal alkene functionalities ready to undergo olefin metathesis and macrocycle formation are attached at the termini of the aromatic system.



Scheme 1.2-1. Biisoquinoline ligand **7**. Note the terminal alkene function ready for RCM and long alkyl side chains that help to solubilise the ligand.

Grubbs' catalysed ring closing metathesis (RCM) has proven to be very efficient in such cyclisation reactions and, furthermore, features very mild reaction conditions.^[45, 46]

This sterically unhindered endotopic ligand **7** paves the way to molecules with unusual chemical topologies. The synthesis of a cyclic [3]catenane has never been reported to date. One possible route to this compound using ligands of the biisoquinoline family and an octahedral transition metal as templating agent is outlined in Figure 1.2-1.

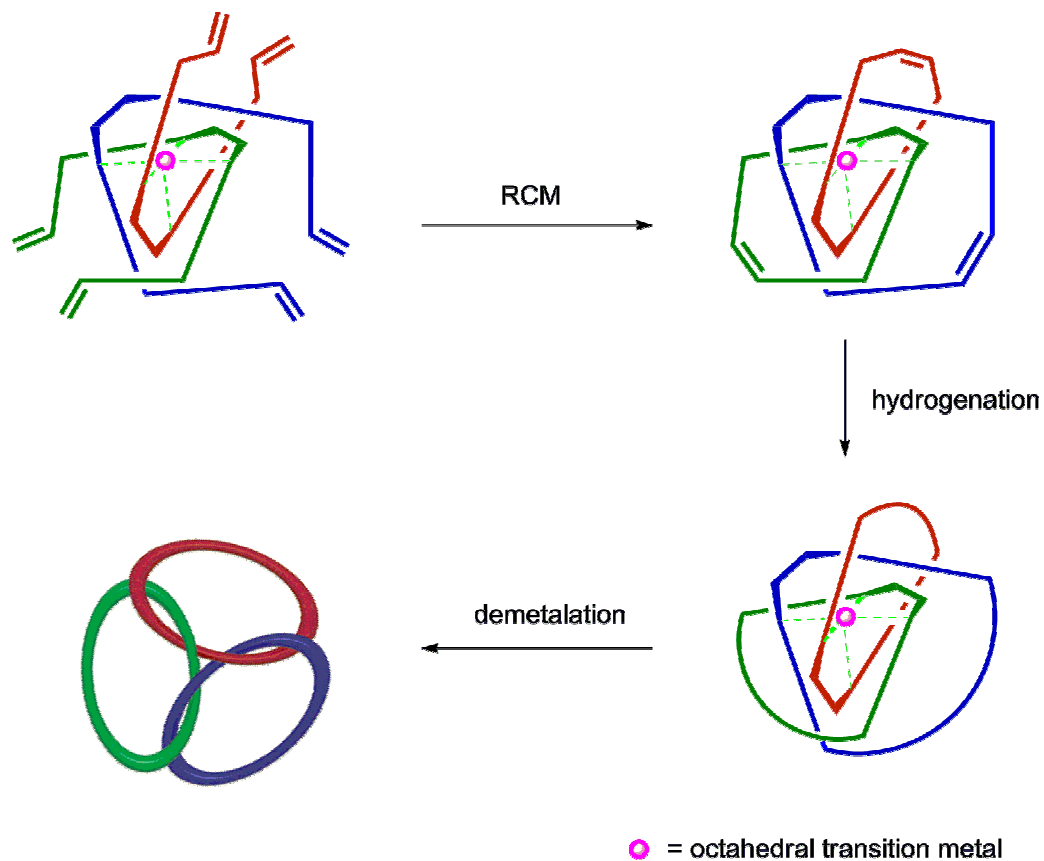
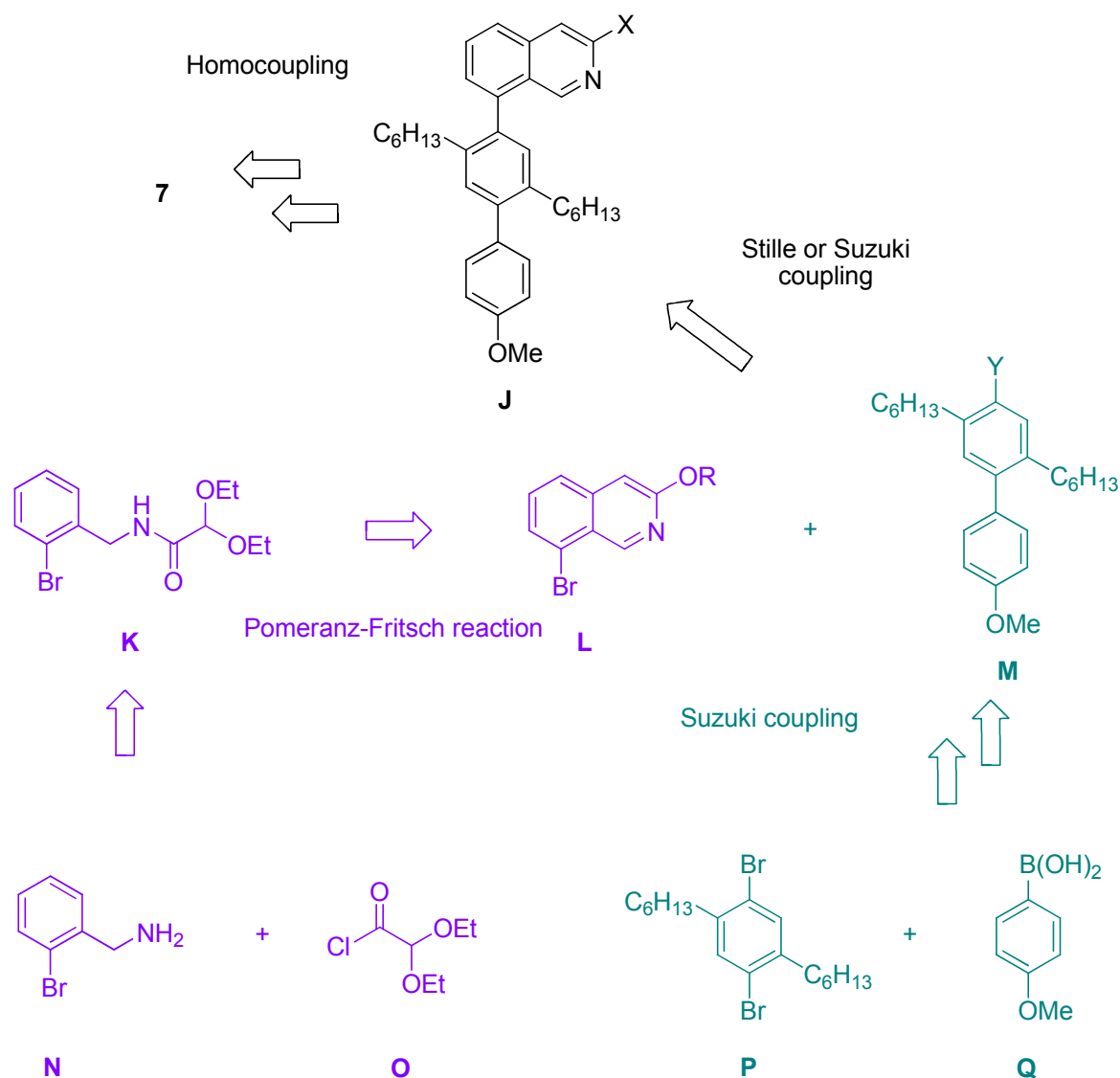


Figure 1.2-1. Synthetic strategy towards a cyclic [3]catenane.

The synthesis of a [3]catenane has been attempted using this strategy and the outcome and insights are discussed in this chapter.

1.3 Results and Discussion

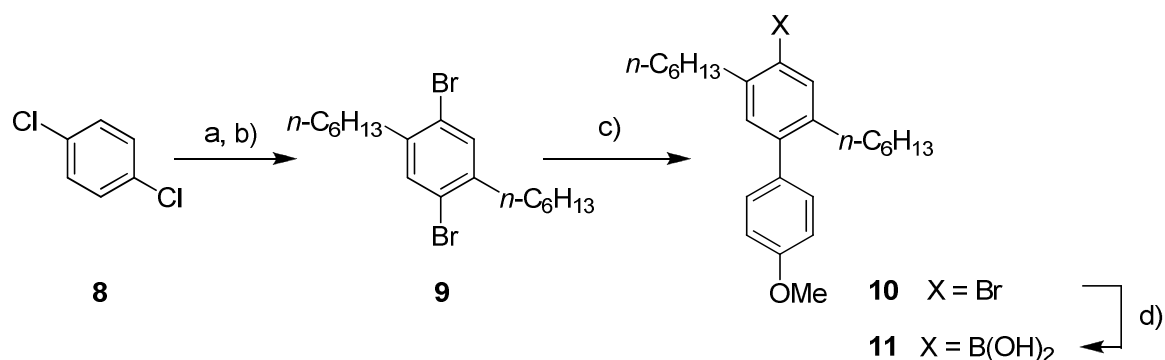
The retrosynthetic route towards biisoquinoline **7** is shown below. Ligand **7** is accessible via a homocoupling of the corresponding substituted (e. g. X = OTf) isoquinoline **J**. The phenolic functions can be deprotected in refluxing pyridinium chloride, and a double Williamson ether synthesis using a glycolic chain with a terminal olefinic function will yield our target molecule **7**. With the help of typical coupling reactions like the Stille (Y = SnR₃) or Suzuki (Y = BOR₃) reaction between the brominated part **L** and the biphenyl **M**, compound **J** can be prepared. The reaction yielding isoquinoline **L**, functionalized at the 3 and 8 positions, can be carried out following an existing literature procedure.^[47] 2,2-Diethoxyacetyl chloride (**O**) condensed with 2-bromobenzylamine (**N**) results in amide **K** which can be cyclised in a Pomeranz-Fritsch reaction to yield **L**. The biphenyl **M** can be made via a statistical Suzuki coupling of building blocks **P** and **Q**, which are prepared with relative ease or can be purchased commercially.



Scheme 1.3-1. Proposed synthetic route to ligand 7.

It has been shown that the solubility of rigid and other very poorly soluble species can be greatly enhanced by attaching flexible side chains.^[48]

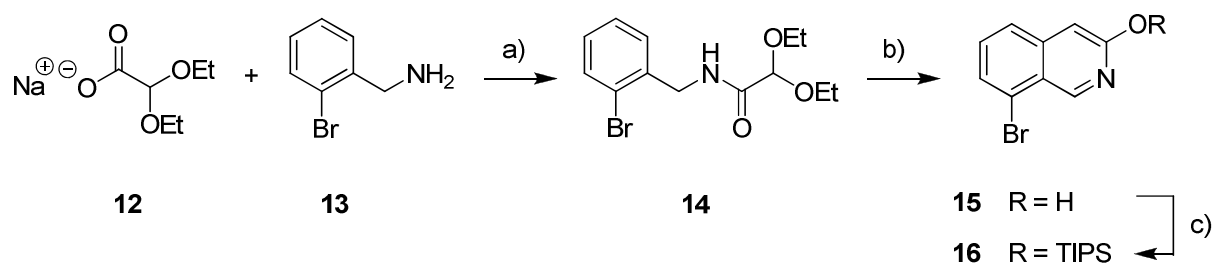
The 1,4-di-*n*-hexylbenzene was obtained by a method analogous to the literature procedure.^[49] Thus, *n*-hexylmagnesium bromide was coupled with 1,4-dichlorobenzene (**8**) using nickel-catalysis to give the respective product in almost quantitative yield (98%). In the next step, 1,4-di-*n*-hexylbenzene was brominated as a neat liquid under rigorous exclusion of light. The crude product could easily be isolated and was recrystallized from ethanol. Analytically pure **9**, made in excellent yield (82%), showed bromination exclusively at C-1 and C-4 (see Scheme 1.3-2).



Scheme 1.3-2. Preparation of the biphenyl part of the ligand. Reagents and conditions: a) $n\text{-C}_6\text{H}_{13}\text{MgBr}$, [(dppp) Cl_2Ni], Et_2O , reflux (98%); b) Br_2 (2.1 eq), I_2 (0.01 eq), RT (82%); c) 4-methoxyphenylboronic acid, $[\text{Pd}(\text{PPh}_3)_4]$ (2 mol%), Na_2CO_3 , toluene/ $\text{EtOH}/\text{H}_2\text{O}$ (80:15:5, v/v, 79%); d) $n\text{-BuLi}$, THF, $-78\text{ }^\circ\text{C}$ then $\text{B}(\text{OMe})_3$, THF, $-78\text{ }^\circ\text{C} \rightarrow \text{RT}$ then $\text{H}^+/\text{H}_2\text{O}$ (80%-quant). dppp = 1,3-bis(diphenylphosphino)propane.

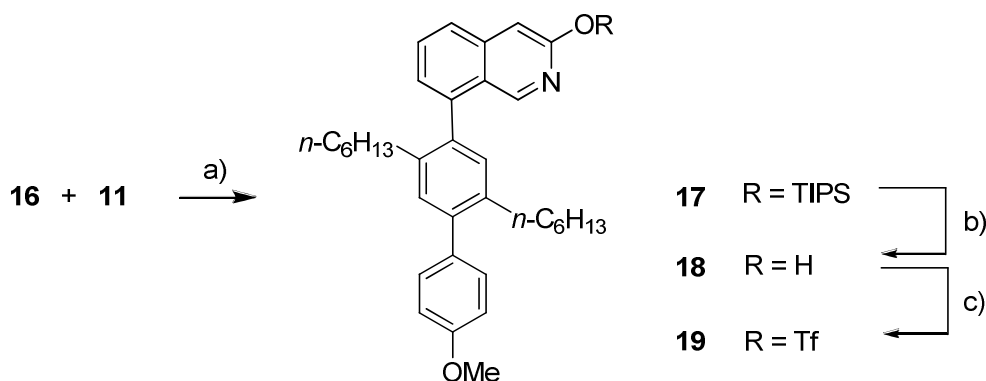
The statistical Suzuki coupling between the dibromo compound **9** and 4-methoxyphenylboronic acid turned out to be very successful. In the presence of a catalytic amount of $[\text{Pd}(\text{PPh}_3)_4]$, with sodium carbonate as a base in a solvent mixture of toluene, ethanol and water, product **10** was synthesised in 79% yield. The Suzuki coupling is considered as “green chemistry” because water or mixtures of water and organic solvents are used. Boronic acids are harmless unlike the carcinogenic stannane compounds used in Stille couplings.^[50] The boronic acid **11** was formed in 80% to quantitative yield depending on the quality of n -butyllithium solution used. The crude product was sufficiently pure to be used without further purification.

Sodium diethoxyacetate **12** was activated with thionyl chloride and subsequently condensed with 2-bromobenzylamine **13** in 72% yield. The amide **14** can be cyclised in concentrated sulfuric acid and forms 8-bromoisoquinoline-3-ol (**15**) in a so-called Pomeranz-Fritsch reaction.^[41] For the coupling reaction between the isoquinoline part and the biphenyl part, the phenolic function needs to be protected as shown by preliminary experiments. The TIPS-protecting group (triisopropylsilyl) was introduced using TIPSCl in the presence of imidazole in DMF (see Scheme 1.3-3).



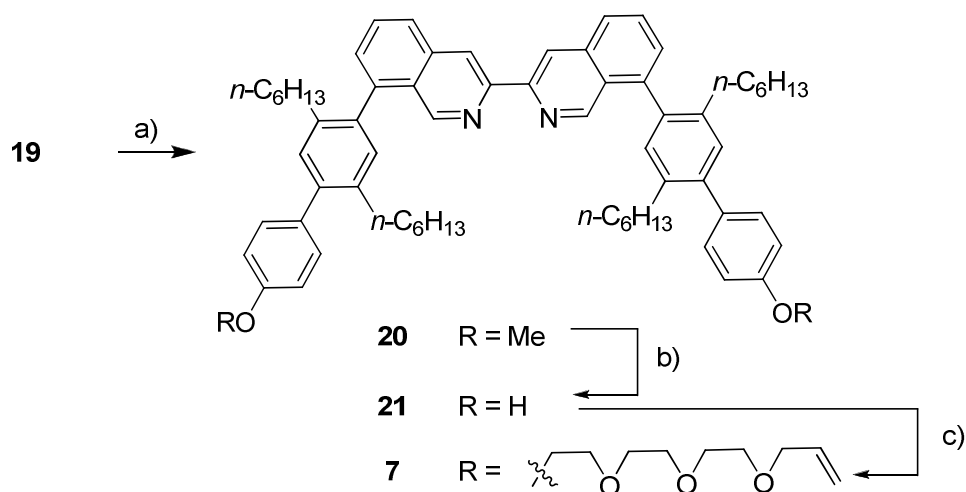
Scheme 1.3-3. Preparation of the isoquinoline part of the ligand. Reagents and conditions: a) SOCl_2 , Et_2O , reflux then pyridine/toluene, reflux (72%); c) H_2SO_4 , RT (30-40%); d) TIPS-Cl, imidazole, DMF, RT (82%). TIPS-Cl = triisopropylsilyl chloride.

Although the TIPS-protecting group can be removed under basic aqueous conditions, the Suzuki-coupling between the brominated isoquinoline **16** and the boronic acid **11** was performed in excellent yield (65% over three steps from **16** to **19**). During the reaction, the coupled product was partially deprotected. It was preferable not to isolate the TIPS-protected coupling product, so for simplicity the deprotection was completed with TBAF in THF. The crude phenol **18** was filtered to remove less polar side products and was directly converted to the triflate **19**, which could be readily purified by chromatography since the product is the least polar component and there is a large difference between the retention factors of the product and the impurities (see Scheme 1.3-4).



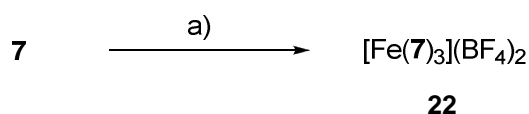
Scheme 1.3-4. Coupling between the isoquinoline part and the biphenyl part and subsequent reactions: Reagents and conditions: a) $[\text{Pd}(\text{PPh}_3)_4]$ (4 mol%), $\text{Ba}(\text{OH})_2$, DME/ H_2O (5:1, v/v); b) TBAF, THF, RT; c) Tf_2O , Et_3N , CH_2Cl_2 (65%; 3 steps). TBAF = tetra-*n*-butylammonium fluoride.

Ligand **20** was obtained in 74% yield by a palladium-catalyzed homocoupling reaction between two molecules of **19** with triflate functionalities using elemental zinc as the electron source. The use of high triflate concentrations ($> 1 \text{ mM}$) was of pivotal importance for favouring bimolecular homocoupling over undesired triflate/hydrogen exchange. Furthermore, the use of dry *N,N'*-dimethylformamide was imperative.^[51]



Scheme 1.3-5. Homocoupling and subsequent reactions: a) $[\text{PdCl}_2\text{dppf}]$, Zn, KI, DMF (74%); b) pyridinium chloride, reflux (92%); c) 3-(2-(2-(2-bromoethoxy)ethoxy)ethoxy)prop-1-ene (**28**), Cs_2CO_3 , DMF (74%). dppf = 1,1'-bis(diphenylphosphino)ferrocene.

The dimethoxy compound **20** was deprotected in refluxing pyridinium chloride to give **21** in 92% yield, which was converted via a double Williamson ether synthesis to ligand **7** in 74% yield (Scheme 1.3-5).

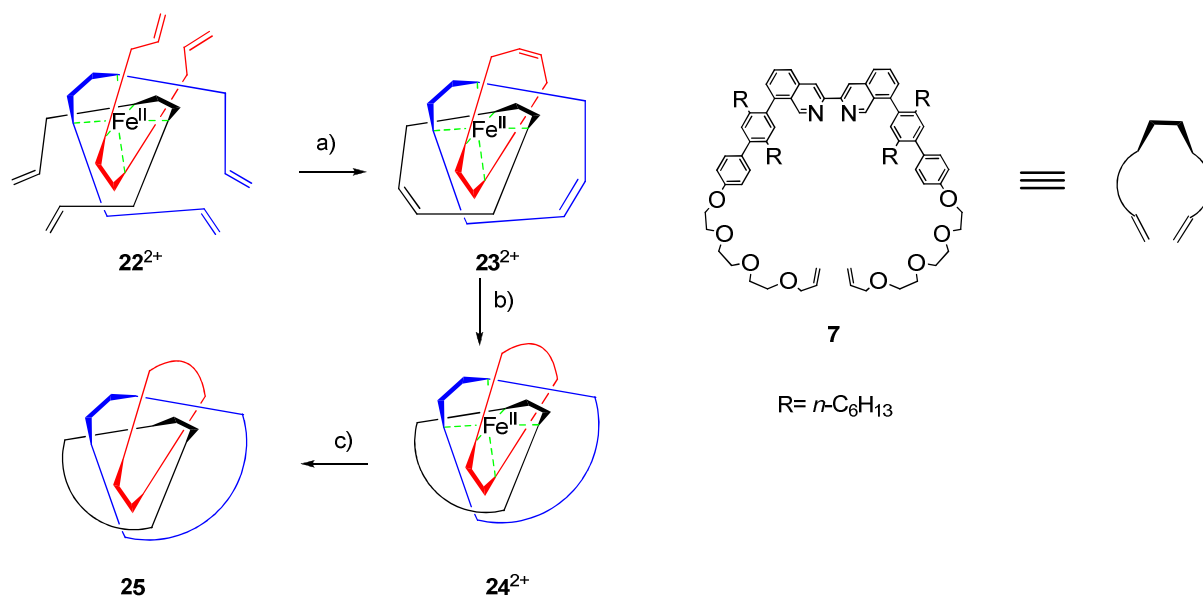


Scheme 1.3-6. Synthesis of the homoleptic iron(II) complex **22**. Reagents and conditions: a) $\text{Fe}(\text{BF}_4)_2 \cdot 6 \text{H}_2\text{O}$, reflux, CH_2Cl_2 , MeOH.

The iron(II) complex $[\text{Fe}(\mathbf{7})_3](\text{BF}_4)_2$ (**22**) was obtained in very good yield (93%) by mixing $\text{Fe}(\text{BF}_4)_2 \cdot 6\text{H}_2\text{O}$ (1.5 eq, in methanol) and ligand **7** (3 eq, in CH_2Cl_2). The reaction mixture was heated at reflux overnight and purified via column chromatography to remove traces of free ligand and excess iron tetrafluoroborate. The ESI-MS spectra exhibited one peak for the **22**²⁺ cation at $m/z = 1938.2$ (calc. 1938.2). The measured isotopic pattern matches the calculated pattern.

After complexation, complex **22** was subjected to intramolecular threefold RCM with Grubbs catalyst 1st generation. The ¹H-NMR showed the disappearance of the two typical multiplets for terminal alkenes at δ 5.9 ppm and δ 5.2 ppm and the appearance of one new singlet at δ 5.88 ppm that can be assigned to the protons of the closed double bonds in complex **23**. Reduction of the double bonds was carried out with molecular hydrogen in the presence of palladium on charcoal. The singlet at δ 5.88 ppm vanished in the ¹H-NMR spectrum. The

removal of the metal was assumed to be beneficial for the purification process. All attempts to remove the iron(II) ion in a reductive manner failed ($\text{H}_2\text{O}_2/\text{KOH}$). Refluxing complex $\mathbf{24}^{2+}$ in 1,2-dichloroethane in the presence of an excess of phen (1,10-phenanthroline) (10 eq) resulted in the formation of the more stable $[\text{Fe}(\text{phen})_3]^{2+}$ complex and yielded free ligand $\mathbf{25}$ (see Scheme 1.3-7).



Scheme 1.3-7. Synthesis of $\mathbf{25}$. Reagents and conditions: a) Grubbs 1st generation catalyst, CH_2Cl_2 (80-90%); b) H_2 , Pd/C, CH_2Cl_2 (90%); c) 1,10-phenanthroline (10 eq), DCE, chromatography. DCE = 1,2-dichloroethane.

A MALDI-TOF-MS spectrum of $\mathbf{25}$ was measured. The suspected [3]catenane $\mathbf{25}$ has a calculated mass of $m/z = 3742.4$. A peak at $m/z = 3741.1$ (isomer with one unreacted double bond plus one proton) and at $m/z = 3802.9$ ($\mathbf{25} + \text{Mg}^{2+} + \text{Cl}$) with matching isotopic pattern were observed.

Pleasingly, the ^1H NMR spectrum of $\mathbf{25}$ looked very similar to the spectrum of the ligand $\mathbf{7}$ before RCM. Signals a-e (see Figure 1.3-1) are much broader in the proposed [3]catenane, which may be due to dynamic processes such as hindered rotation of one ring around the others or partial protonation of nitrogen atoms. Already in the spectrum of ligand $\mathbf{7}$ signals a-e are much broader than signals h-i, which are sharp in both cases. The signals of the terminal alkene functionality are no longer present in $\mathbf{25}$.

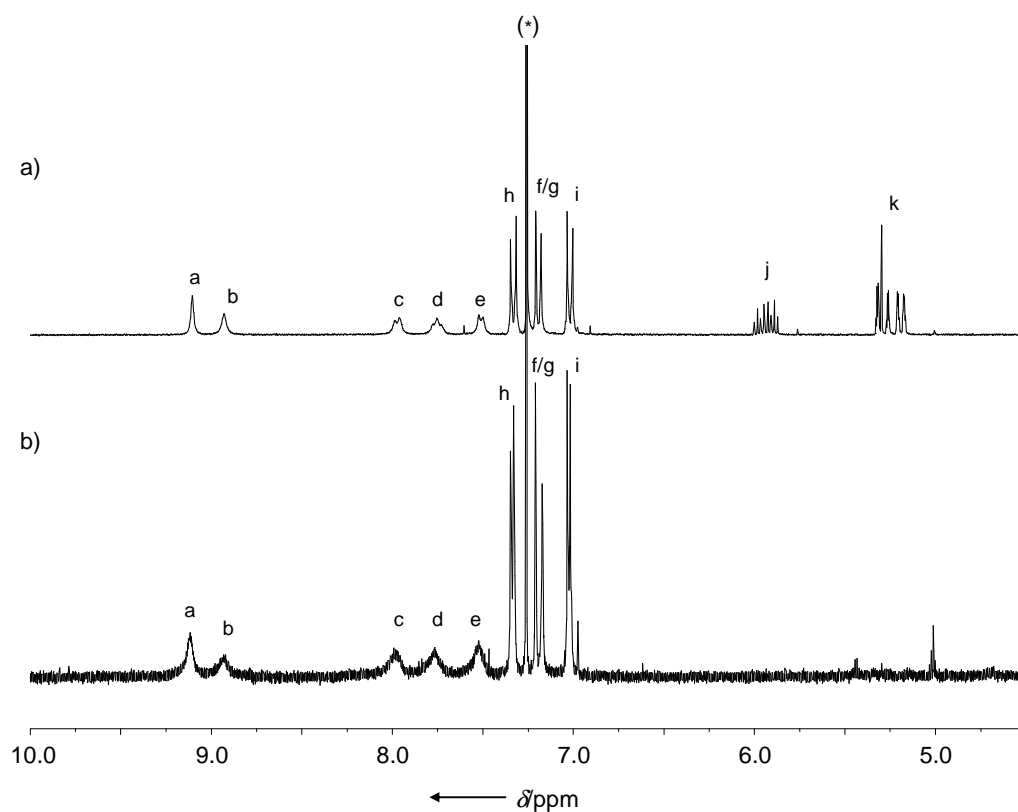


Figure 1.3-1. ¹H NMR spectra in CDCl₃ at 400 MHz of a) ligand **7** and b) proposed [3]catenane **25**. The solvent residual signal is marked with an asterisk (*). For labelling see Scheme 1.2-1.

No X-ray structure of **25** was obtained, and therefore its structure remains therefore unconfirmed.

1.4 Summary

In summary, an efficient multi-step synthesis of an endotopic biisoquinoline ligand has been developed. This chelate is ideally suited for macrocycle formation around transition metal ions and is thus a valuable new building block for topological chemistry. In contrast to the vast majority of previously reported endotopic diimine ligands, this 8,8'-diaryl-3,3'-biisoquinoline is sterically unhindered.

Long alkyl chains attached to extended aromatic systems have the advantage of rendering these molecules more soluble and to facilitate their manipulation. Otherwise, the synthetic effort is usually considerably higher and the chances to obtain crystals suitable for X-ray analysis that might be necessary for unambiguous structure determination are smaller due to an increased number of degrees of freedom.

2 Macrocyclic Tris(bipyridine) – A Metal Templated Synthesis for Trivial Knots

It is probably surprising that “simple” objects from daily life like knots can become subject to advanced scientific investigation. Mathematics developed knot theory more than a century ago^[52] and insight into these systems is today of great use for physicists, chemists and molecular biologists working on fields that deal with this kind of topology. Chemists synthesised molecular knots, at first for the synthetic challenge, emphasizing the viability and potential of their synthetic methods and tools, and secondly for possible future applications. The demand for novel devices on the molecular scale with various properties in nanotechnology and information technology is clearly a motivation in addition to purely fundamental viewpoints. Obviously, chirality is an essential property in many areas of chemistry, and the chirality arising from knots stems from their topology and not from the classical stereogenic units (points, axes, helices and planes). This makes them especially interesting for asymmetric induction, for instance in asymmetric catalysis.

2.1 Introduction

The discovery of natural knotted forms of DNA^[53-55] and proteins^[56-60] verifies the captivating beauty of nature that is able to produce such highly complex three dimensional structures. But the unusual geometry also has an impact on the biological properties. For example, the activity for the transport of iron(III) ions is remarkably higher in the knotted form of lactoferrin (see Figure 2.1-1a) than for its linear analogue.^[56] Enhanced chirality and rigidity due to the knotted topology seem to play a critical role in the antiviral activities of proteins circulin A and B, and make them promising anti-HIV drugs.^[61, 62] With the development of elaborate techniques like electron microscopy, it is today possible to give an unambiguous topological characterisation of catenated and knotted DNA. Figure 2.1-1b shows exquisite electron micrographs of knotted DNA.^[53]

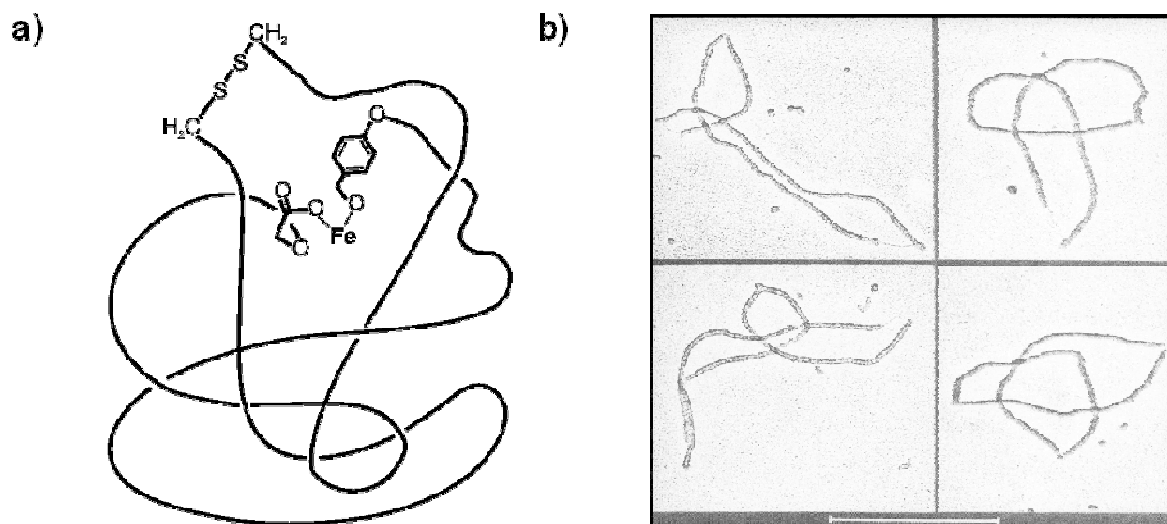


Figure 2.1-1. a) Schematic representation of lactoferrin,^[56] a naturally occurring knotted protein. b) Electron micrographs of trefoil DNA molecules.^[53]

These findings initiated a new field of research that has been named “Biological Topology”.^[55] Besides the fascinating naturally occurring knotted and catenated DNA, Seeman and co-workers accomplished and reported the synthesis of artificial single-stranded DNA knots and many intriguing topologies have been produced.^[63-69]

In knot theory^[52], the simplest knot of all is the unknotted circle, which is called the unknot or the trivial knot. The next simplest knot is a trefoil knot, its topological structure and its three topological isomers are depicted in Figure 2.1-2. One is the planar cycle (**III**) whose graph contains no crossings in contrast to the two trefoil knots. In chemical topology^[4, 70] the molecule or the molecular assembly is schematically represented on paper as a graph. The two non-planar knots (**I**, **II**) are enantiomers and topologically chiral. Their chirality can be evidenced by rationalising that their image and their mirror image are non-superposable.

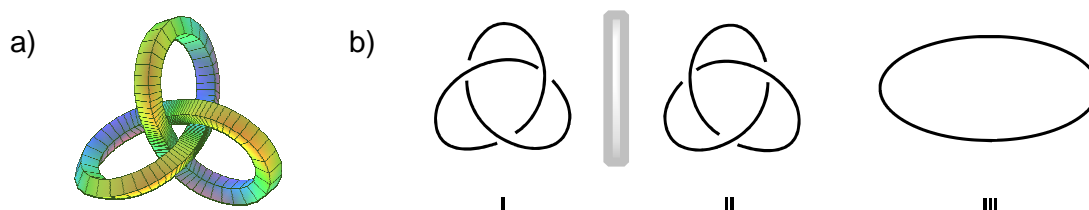


Figure 2.1-2. a) Computed structure of a trefoil knot (MAPLE 10); b) Schematic representations of the two enantiomers of the trefoil knot (**I**, **II**) and its planar isomer the cycle (**III**).

After the isolation of the first [2]catenane by Wasserman^[5] in 1960, a lively discussion about the synthesis of a molecular knot emerged in the chemical literature. Scientists suggested using a Möbius strip as a precursor^[4, 71], a covalent template^[72, 73] or metal coordination.^[74, 75] Sokolov^[74] proposed an octahedral tris(chelate) template. This chapter describes the realisation of his design with the help of recent achievements in modern chemistry – at least for the synthesis of a trivial knot. None of these early designs could be realised to date. Reviews by Walba^[76] and Sauvage and Dietrich-Buchecker^[77] describe the ideas and prospects of these early attempts in more detail. A more recent review from Vögtle and co-workers^[61] gives a very good background on molecular knots and their assemblies and provides an overview on molecular knots that have been prepared in the laboratory.

The first successful synthesis of a molecular knot was reported 20 years ago by Sauvage and co-workers.^[78] They conceived a seminal method taking advantage of the template effect of a transition metal and the particular geometry of helical dinuclear complexes (see Figure 2.1-3).

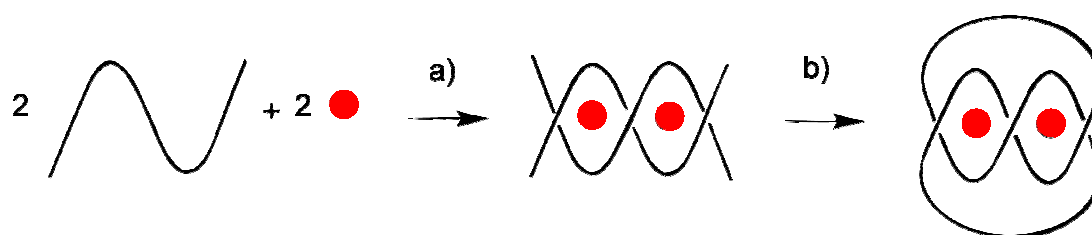
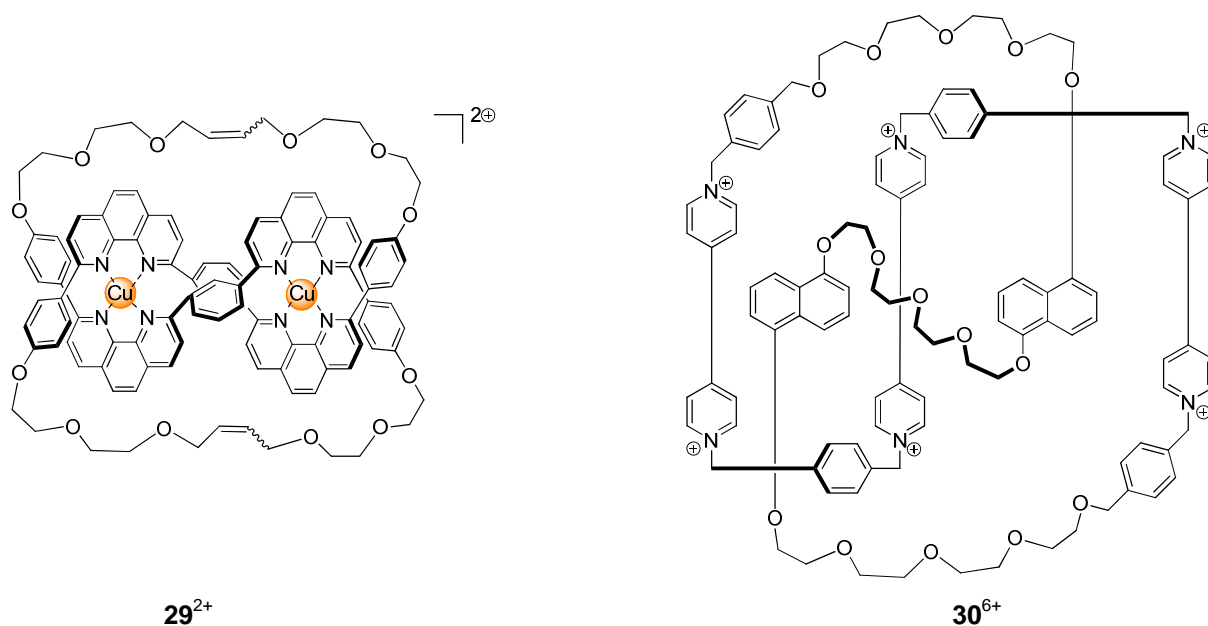


Figure 2.1-3. Strategy used to make a trefoil knot.^[78] a) Two bis(chelate) molecular strands are coordinated to a transition metal forming a helical complex; b) The ends of the double stranded helix are cyclised leading to the knotted structure.

Two bis-chelating molecular threads were coordinated to two copper(I) metal centres to form a helical dinuclear complex. The helical geometry is a prerequisite, and the stability of the copper complex is of utmost importance. The knot was formed after linking the ends with oligoethyleneglycol chains. Variation of length and rigidity in the bridge that links the chelating units and the chains used during cyclisation led to a variety of knots and improvement in yield.^[79, 80] The best yield of this topologically non-trivial molecule (35% over seven steps from commercially available starting materials) was achieved by employment of the highly efficient ring-closing metathesis (RCM) methodology^[79] (see Scheme 2.1-1, compound **29**). The knots obtained by the concept of helical copper(I)-phenanthroline complexes were characterised by X-ray structure analysis^[81] and the resolution into its enantiomers was also successful.^[82] Furthermore, two knotted moieties

were fused to a composite knot whose isomeric composition involves a *meso* form and a pair of enantiomers.^[83]



Scheme 2.1-1. Molecular trefoil knots that have been synthesised from a helical precursor. The dicopper complex 29^{2+} was prepared in very good yields.^[79] The cation 30^{6+} was synthesised in very poor yield but does not need an external template.^[84]

The synthesis of the trefoil knot **30** in extremely low yields was reported by Stoddart and co-workers in 1997.^[84] Their design logic relied on the formation of a double stranded supramolecular complex between π -electron rich and π -electron deficient strands by π -donor/ π -acceptor interactions. Irreversible covalent bond formation connecting the termini of the precursors afforded both a trefoil knot and a macrocycle. The compounds could be purified by high performance liquid chromatography (HPLC) and were characterised by means of liquid secondary-ion mass spectrometry (LSIMS).

After the successful employment of a transition metal and π -donor/ π -acceptor interactions, another templating mode was introduced by Vögtle and co-workers^[85] in 2000 for the synthesis of trefoil knots. An intramolecular hydrogen-bonding pattern of oligoamides and the folding of the loop provided conditions in which a one-pot procedure afforded the desired molecules in reasonable yields. Their concept is especially intriguing due to the simplicity of the synthesis, unique possibilities of further derivatization and that the assembly of the amide-knots has much in common with the formation of tertiary structural motifs found in natural proteins.^[86] A huge variety of derivatized knots has been prepared, including dendrimers, rotaxanes with knots acting as stopper groups, and other assemblies that link knots in linear,

triangular or cyclic fashions.^[61] Chiral resolution of the latter knot assemblies into their isomers could be performed in some cases by HPLC with a chiral stationary phase.

More recently, a trefoil knot was made from amino acids and steroids as building blocks.^[87] The unexpected knotted geometry was observed in cyclic oligoamides that were built from alternating sequences of aminodeoxycholic acid and a natural amino acid. The authors state that the knot was prepared only as one diastereoisomer due to asymmetric induction from chiral optically pure building blocks. The topology must have been preorganized prior to the final ring-closure because an amide bond is formed irreversibly. The chain of backbone atoms is depicted in Figure 2.1-4b displaying the knot topology.

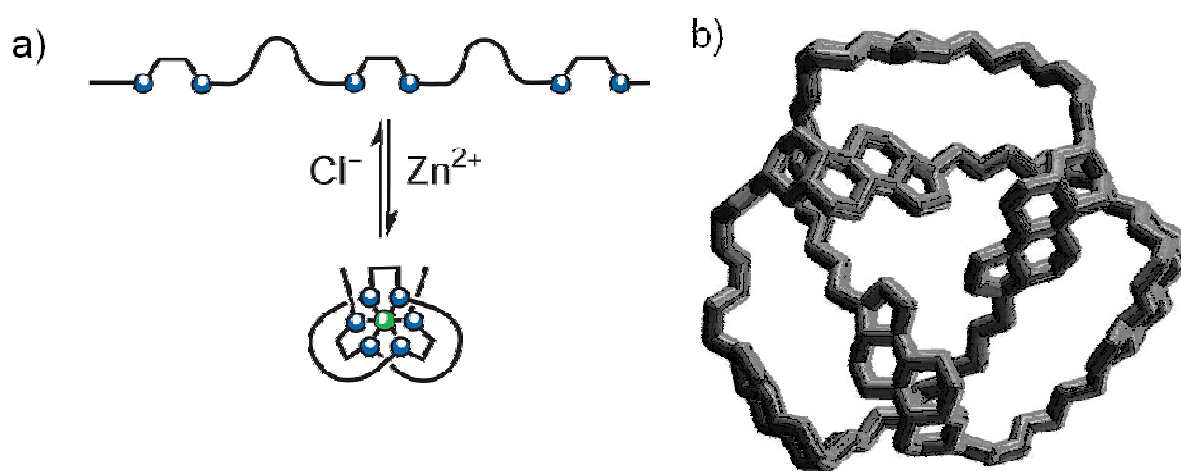


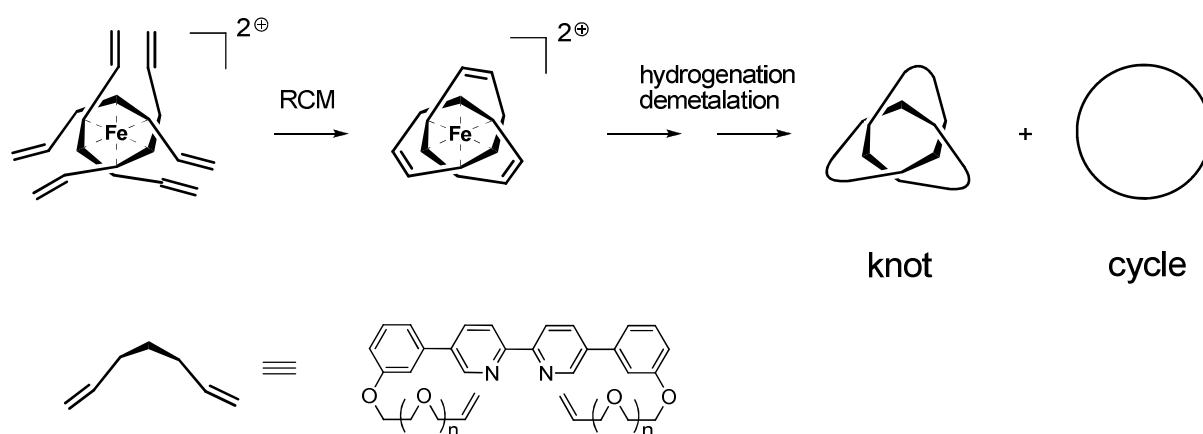
Figure 2.1-4. Two examples for molecular knots: a) Reversible folding of a tris(chelate) oligomer around zinc(II) into an open knot^[88]; b) Chain of backbone atoms illustrating the non-trivial topology of a knot that was prepared from amino acids and steroids.^[87]

A linear tris(bipyridine) oligomer that folded around an octahedral zinc(II) metal centre forming an open knot was reported by Hunter and co-workers.^[88] The folding process was found to be fully reversible. Addition of chloride quantitatively yields the free oligomer and addition of silver ions (which precipitate as AgCl) refolds it (see Figure 2.1-4a).

2.2 Aims and Overview

The Russian chemist Sokolov suggested a very interesting approach towards a molecular trefoil knot in his review from 1973.^[74] Three bidentate ligands coordinated in a suitable fashion around an octahedral transition metal used as a matrix might, after connection of their ends, lead to a molecular knot. The ends have to be connected two by two in an appropriate way. Clearly, there are many possibilities that lead to different compounds with a low probability for the desired knot.

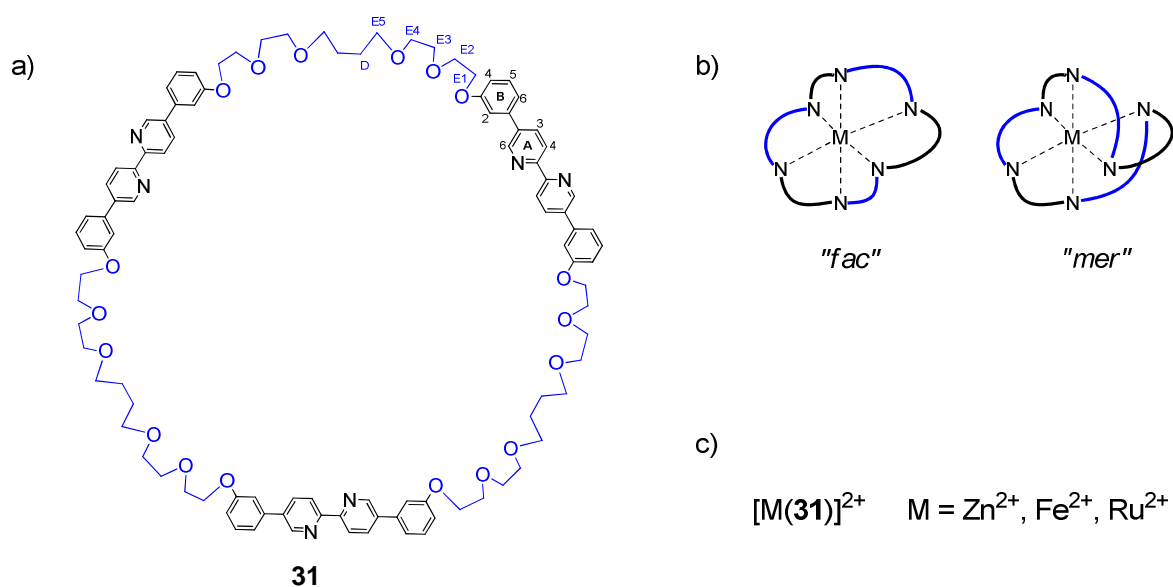
Scheme 2.2-1 illustrates a possible realisation of Sokolov's application of an octahedral tris(chelate) template for the synthesis of a trefoil knot using olefin metathesis. Extended bipyridine ligands bear chains that allow a certain degree of flexibility and have terminal alkene functionalities. Olefin metathesis can be performed under very mild conditions (ambient temperature, neutral pH, compatibility with various functional groups), is a reversible reaction and the products are usually formed in high yields. Assuming that intermolecular reactions can be excluded by using high dilution conditions and that the chains have a length too short to allow reaction of two double bonds stemming from the same ligand and just long enough to react with the right end, then there are only two possible outcomes from such a threefold ring closing metathesis after complete conversion: a knot and a cycle.



Scheme 2.2-1. Synthetic pathway that will lead to a knotted and/or a cyclic molecule after ring closing metathesis (RCM), hydrogenation and demetalation.

The reaction sequence was successfully performed yielding the macrocyclic molecule **31**. No knotted species was found.

Compound **31** is a large macrocycle with a ring size of 96 atoms. If the hexadentate cyclic ligand is coordinated to an octahedral transition metal, there is the possibility for two geometrical isomers (see Scheme 2.2-1b). One has only facial linkages whereas the other has two meridional linkages and four facial linkages. Searle investigated isomers of cobalt(II) complexes with the cyclic hexaazacyclen ligand and proposed to describe the isomers as *fac* and *mer*, respectively.^[89] No IUPAC-nomenclature for this type of isomerism is known and the proposed nomenclature from Searle was used for novel complexes in this chapter. Others have suggested a presumably more accurate but also more intricate nomenclature.^[90, 91]



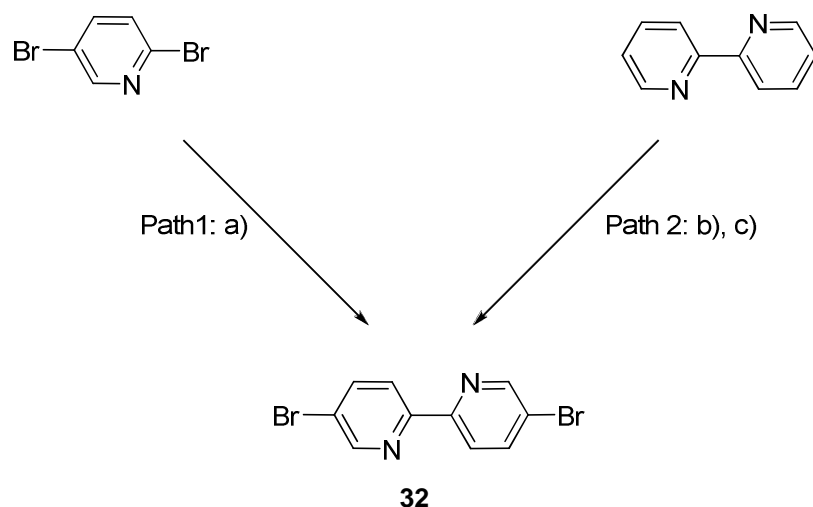
Scheme 2.2-1. a) Novel hexadentate and macrocyclic ligand **31** with ring and atom labelling for NMR spectroscopic assignments; b) Two possible geometrical isomers of complexes with ligand **31** and an octahedral transition metal; c) Novel zinc(II), iron(II) and ruthenium(II)-complexes with **31**.

One-to-one complexes of ligand **31** with zinc(II), iron(II) and ruthenium(II) have been prepared and will be presented in this chapter. A crystal structure of the “*mer*” isomer of the latter was obtained and the influence of the reduced symmetry on the spectroscopic properties is described.

2.3 Synthesis

The preparation of extended bipyridine ligands bearing chains with terminal alkene functionalities, their assembly around an octahedral transition metal and the metal templated synthesis of macrocyclic ligand **31** and complexes of the type $[M(\mathbf{31})]^{2+}$ ($M = \text{Zn}^{2+}, \text{Fe}^{2+}, \text{Ru}^{2+}$) are described below.

The synthesis of 5,5'-dibromo-2,2'-bipyridine (**32**) can be realised via two synthetic pathways: a palladium(0)-catalysed Stille reaction or the direct reaction of protonated 2,2'-bipyridine with molecular bromine under very harsh conditions (see Scheme 2.3-1). Ziessel and Romero^[92] reported for the latter synthesis a yield of 42%. However, in our hands, considerably smaller yields were obtained and other groups also share this experience.^[93, 94] The 2,2'-bipyridine was protonated with hydrobromic acid and the precipitate dried under vacuum. The salt and bromine were then heated to 180 °C in a sealed tube for 72 hours. The reaction is difficult to monitor and degradation and the formation of side-products is expected. Ligand **32** was isolated in 21% yield after column chromatography.

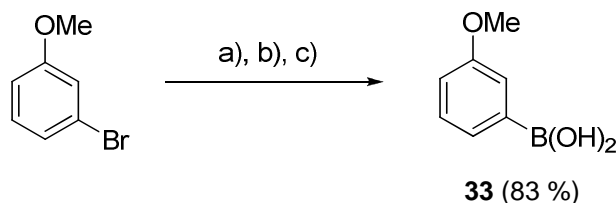


Scheme 2.3-1. Reagents and conditions for compound **32**. Path 1: a) $n\text{-Bu}_6\text{Sn}_2$ (0.5 eq), $[\text{Pd}(\text{PPh}_3)_4]$ (2 mol%), toluene, reflux, 3 d, 79%. Path 2: b) HBr, 99%; c) Br_2 (2 eq), 180 °C, 3 d, 21%.

A more efficient method was reported by Michel^[94] and co-workers in 2002 using 50 mol% of hexa-*n*-butylstannane and a catalytic amount of palladium(0). First, approximately half of the 2,5'-dibromopyridine are transformed to 2-tributylstannylpyridine *in situ* taking advantage of the different reactivity of the two bromine substituents. Secondly, the Stille cross coupling reaction is performed in the presence of $[\text{Pd}(\text{PPh}_3)_4]$ yielding ligand **32** in very good yield.

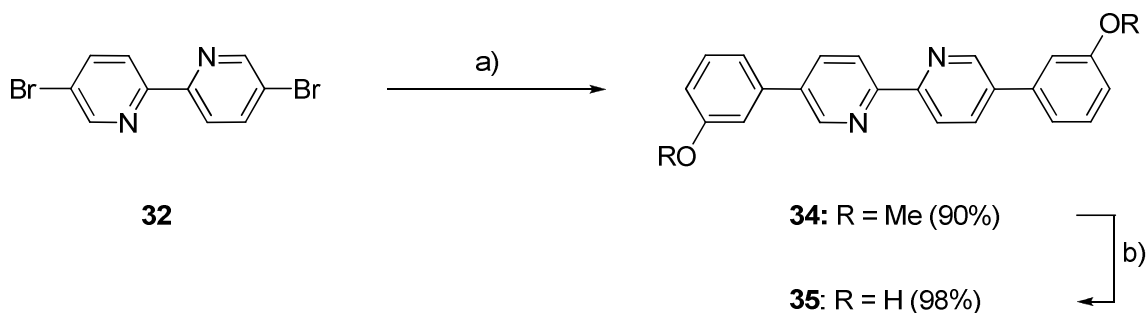
Boronic acid **33** is commercially available but can also be prepared easily on a large scale. Lithiation of 3-bromoanisole followed by treatment with trimethylborate led to a boronic

ester. The ester was hydrolysed in an aqueous hydrochloric acid solution yielding **33**. The product can be conveniently purified via extraction.



Scheme 2.3-2. Reagents and conditions: a) n-BuLi (1.1 eq), $-78\text{ }^{\circ}\text{C}$, THF, 2 h; b) $\text{B}(\text{OMe})_3$ (1.1 eq), $-78\text{ }^{\circ}\text{C} \rightarrow \text{r.t.}$; c) $\text{H}^+/\text{H}_2\text{O}$, 83% (over three steps).

The bis(methoxy) compound **34** was prepared according to a procedure published by Constable and co-workers.^[95] The ligand **34** was synthesised by Suzuki coupling of 5,5'-dibromo-2,2'-bipyridine (**32**) with 3-methoxyphenylboronic acid (**33**) in biphasic conditions in the presence of $[\text{Pd}(\text{PPh}_3)_4]$ and was isolated after column chromatography in 90% yield as a white crystalline solid (see Scheme 2.3-3).

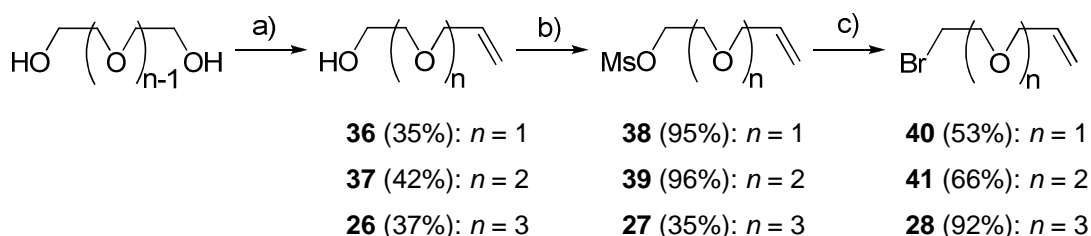


Scheme 2.3-3. Reagents and conditions: a) 3-methoxyphenylboronic acid (**33**, 2.5 eq), $[\text{Pd}(\text{PPh}_3)_4]$ (4.5 mol%), Na_2CO_3 (5 eq), toluene/ H_2O , reflux, 20 h, 90%; b) pyridinium chloride, reflux, 4 h, 98%.

Deprotection of **34** is conveniently achieved by heating the compound in refluxing pyridinium chloride at $210\text{ }^{\circ}\text{C}$ and the bis(phenol) derivative **35** was obtained in almost quantitative yield despite the harsh reaction conditions.

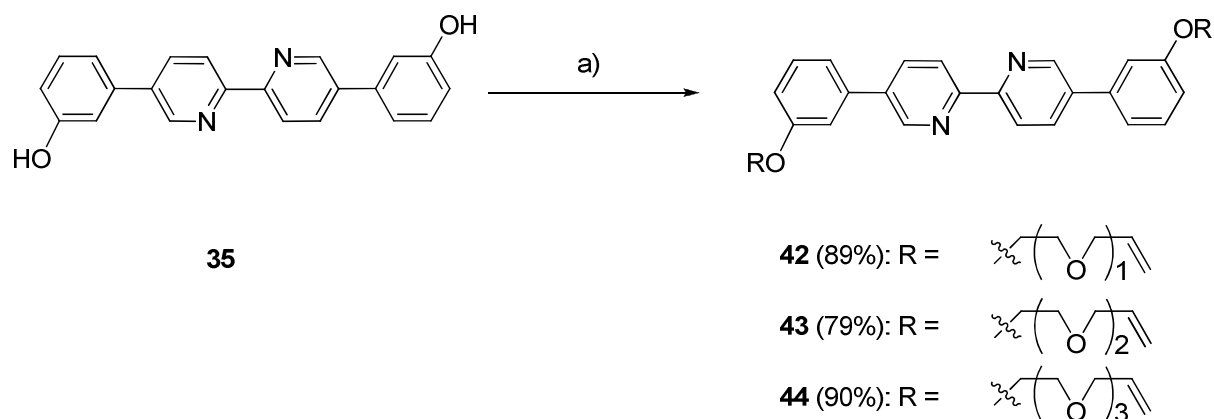
A modular approach appeared to be advantageous for designing ligands that can assemble around a single octahedral metal centre into a trefoil knot after a ring closing reaction on terminal alkene functionalities. The outcome of the ring closing reaction will most likely also depend on the length of the chains that are attached to the bis(phenol) ligand **35**. Thus, a series of chains with varying lengths bearing terminal alkene functionalities and a bromo group to function as leaving group have been prepared (see Scheme 2.3-4). Commercially

available diols were reacted with allyl bromide leading to mono-allyl compounds **36**, **37** or **26** in moderate yields. The latter were transformed to the corresponding mesylates **38**, **39** and **27** which can then be converted to the bromo-derivatives **40**, **41** and **28** in very good yields. Mesylate is expected to be a poorer leaving group than bromide. Little synthetic effort was required to prepare the bromo-derivatives since they can be prepared in large-scale and are easily purified. It was assumed that it would be beneficial to have a good leaving group for the subsequent Williamson ether synthesis and therefore to synthesise the bromo-compounds instead of using the mesylates.



Scheme 2.3-4. Reagents and conditions: a) KOH (1 eq), allyl bromide (0.5 eq), 80 °C, 2 h; b) Mesyl chloride (1.6 eq), NEt₃ (20 eq), CH₂Cl₂, -78 °C → r.t.; c) LiBr (5 eq), acetone, reflux, 12 h.

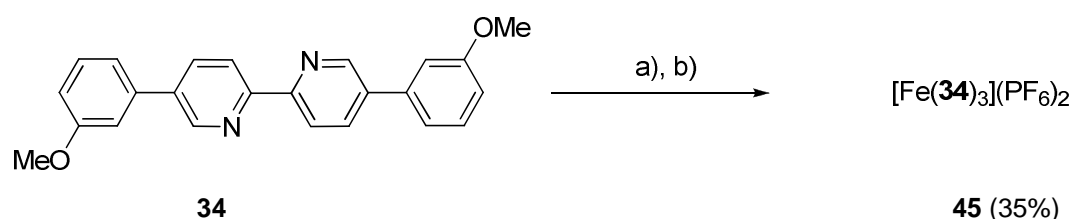
The Williamson ether synthesis was developed by Alexander Williamson in the 1850s.^[96] It is the most common synthetic method to prepare symmetric or asymmetric ethers. Ligands **42**, **43** and **44** were prepared in the presence of caesium carbonate and the corresponding bromo-compounds in very good yields (see Scheme 2.3-5). Instead of caesium carbonate the cheaper potassium carbonate was also employed successfully with a negligible drop in yields. A wide range of solvents was tested (acetone, acetonitrile, tetrahydrofuran) but only DMF and heating to 120 °C over several days showed satisfying conversions probably due to the poor solubility of bis(phenol) **35**.



Scheme 2.3-5. Reagents and conditions: a) Cs_2CO_3 (4 eq), **40** or **41** or **28** (2.2 eq), DMF, 120 °C, 4 d.

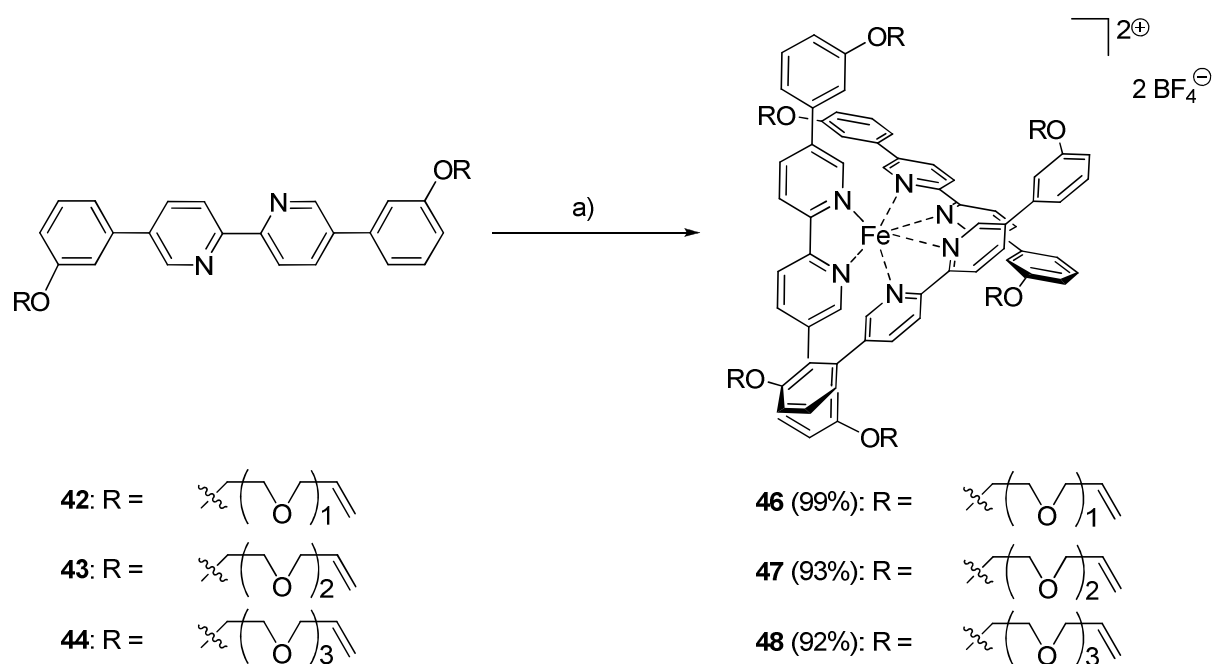
Iron(II) is a d^6 metal and has a preference for octahedral geometry (imposed by crystal field stabilisation energy) with chelating bipyridine ligands.

Scheme 2.3-6 shows the synthesis of the homoleptic iron(II) complex **45** with ligand **34**.



Scheme 2.3-6. Reagents and conditions: a) $[\text{FeCl}_2] \cdot 4 \text{ H}_2\text{O}$, $\text{CH}_3\text{CN}/\text{H}_2\text{O}$, reflux, 16 h; b) NH_4PF_6 .

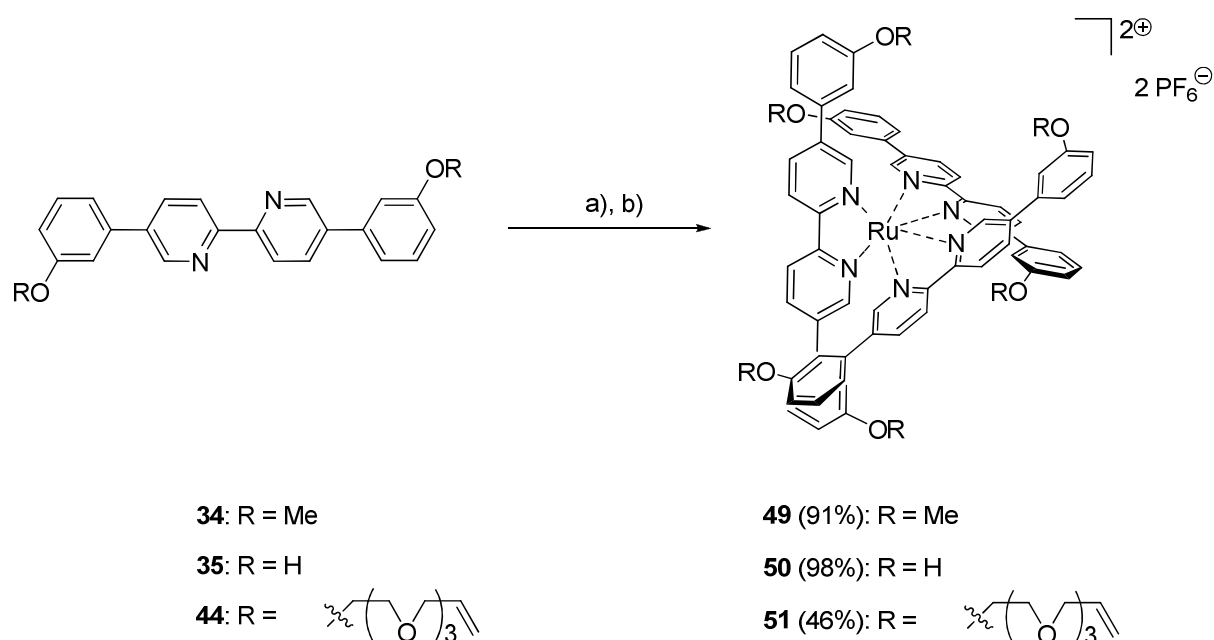
Iron(II) complexes of **42**, **43** and **44** were prepared in excellent yields by treatment of the ligand with the required iron salt $[\text{Fe}(\text{BF}_4)_2] \cdot 6 \text{ H}_2\text{O}$ in acetonitrile. The typically deep-red colour emerged instantaneously. Full conversion was surprisingly only achieved after heating the reaction mixture for several days at reflux. The formation of complexes of the $[\text{Fe}(\text{bpy})_3]^{2+}$ motif usually happens within minutes and no thermal excitation is needed. The iron salt was used in excess and the products were purified via extraction or filtration.



Scheme 2.3-7. Reagents and conditions: a) $[\text{Fe}(\text{BF}_4)_2] \cdot 6 \text{H}_2\text{O}$, CH_3CN , reflux, 3 d.

Ruthenium(II) also has the d^6 electronic configuration and the complexes formed with chelating polypyridyl-ligands display an octahedral geometry. The formation requires thermal excitation. In a microwave reactor, the reaction mixtures can be heated beyond the boiling point of the solvent and shorter reaction times compared to reactions under conventional conditions are mainly due to thermal effects but solubility issues may also play an important role.

Ruthenium(II) complexes **49** and **50** could be obtained in excellent yields and **51** was synthesised in good yield. Their synthesis is depicted in Scheme 2.3-8. The ruthenium(II) complexes with the ligands **34** and **44** were prepared by heating a mixture of the corresponding ligand and 0.33 equivalents of $[\text{Ru}(\text{DMSO})_4\text{Cl}_2]$ in a microwave reactor to 140°C in ethanol for 25 min or 1 h, respectively. The synthesis of complex **50** with the very poorly soluble ligand **35** was not successful under these reaction conditions. It was necessary to heat the reaction mixture in ethylene glycol to 230°C in a microwave reactor in order to achieve complete conversion. The counterion was exchanged for all the ruthenium(II) complexes by adding an aqueous solution of ammonium hexafluorophosphate to the reaction mixture and the precipitates were collected. Pure compounds **49** and **50** could be obtained after a simple filtration over aluminium oxide. Complex **51** needed to be purified via column chromatography.



Scheme 2.3-8. Reagents and conditions: a) for **49**: **34**, $[\text{Ru}(\text{DMSO})_4\text{Cl}_2]$, μW , EtOH, 140 °C, 1h; for **50**: **35**, $[\text{Ru}(\text{DMSO})_4\text{Cl}_2]$, μW , ethylene glycol, 230 °C, 30 min; for **51**: **44**, $[\text{Ru}(\text{DMSO})_2\text{Cl}_2]$, μW , EtOH, 140 °C, 25 min; b) all compounds: NH_4PF_6 .

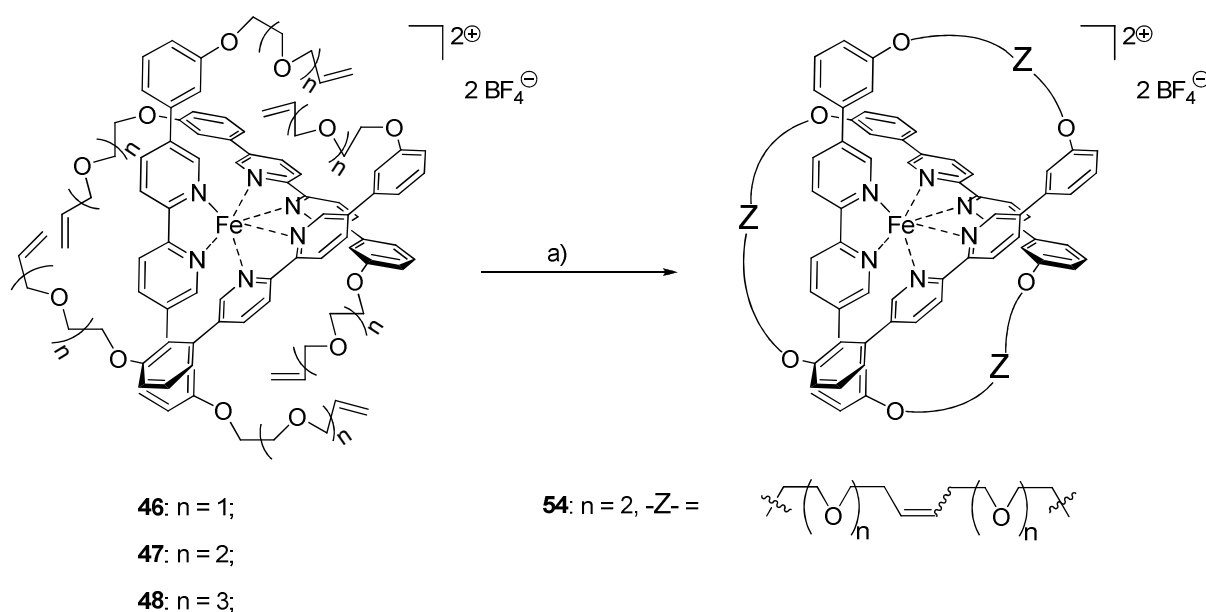
If a ring closing metathesis (RCM) is carried out on e.g. iron complex **46** (see Scheme 2.3-9) the formation of a trefoil knot is possible. This issue was already discussed in chapter 2.2. For a proof-of-principle, ruthenium(II) complex **51** was subjected to a RCM reaction. The formation of three new double bonds could be confirmed via NMR- and ESI-MS techniques but it was soon apparent that several isomers had been formed and an efficient purification method was needed. Chromatography is usually easier to perform on an organic molecule than on a complex, and so it was decided to use the labile iron complexes rather than the very stable ruthenium(II) complexes. Iron can be removed with various methods, but for ruthenium, no demetalation procedure is known for complexes presented in this chapter.

The RCM was tried on the three iron(II) complexes **46**, **47** and **48**. They all possess six oligo ethylene glycol chains with terminal alkene functionalities and differ in their chain lengths. In the presence of Hoyveda-Grubbs catalyst 2nd generation (**53**, see Scheme 2.3-11) the complexes (1 mM) were stirred for 30 days in dichloromethane. The complex with the medium length chain **47** was successfully converted to the intermediate complex **54**. The reaction could easily be monitored via ESI-MS (see Figure 2.4-7). The ¹H-NMR spectrum clearly showed the disappearance of the terminal olefin protons at δ 5.2 ppm and δ 5.8 ppm and the appearance of two new sets of signals at δ 5.9 ppm and δ 5.7 ppm for the newly

formed double bond (*cis*- and *trans*-isomers). Scheme 2.3-9 illustrates the reaction and only one of the isomers of **54** is shown. Each double bond can be oriented in a *cis*- or *trans*-configuration and there are other optical and geometrical isomers. The complex is drawn such that a macrocycle was formed. It was shown later that the cyclic molecule was the main product and no proof for the other isomer, the trefoil knot, was found.

Even though the threefold olefin metathesis was performed successfully on **48**, its chains seem to be too long because not only was the desired reaction between two double bonds of different ligands observed, but the unwanted metathesis between two double bonds stemming from the same ligand was also possible. Attempts to purify the organic products after hydrogenation and demetalation did not succeed.

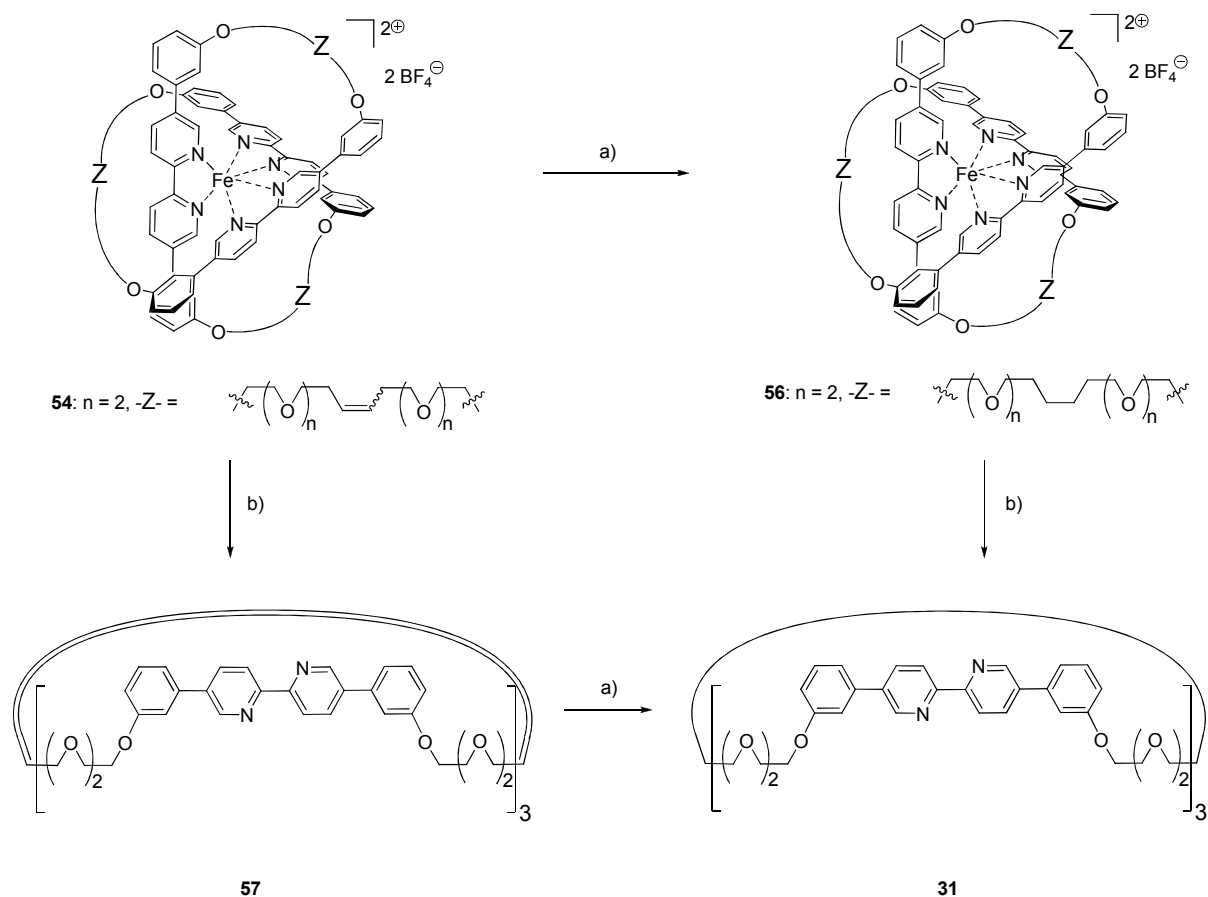
Molecular models confirmed that the compound with the short chains **46** should be able to assemble into a knot or a macrocycle. The RCM showed almost full conversion of precursor to product but only the smaller [2+2]-macrocycle **55** (see Scheme 2.3-11) could be identified after hydrogenation and demetalation.



Scheme 2.3-9. Reagents and conditions: a) Hoyveda-Grubbs catalyst 2nd generation (20 mol%), CH₂Cl₂, r.t., 30 d. Only one isomer is shown.

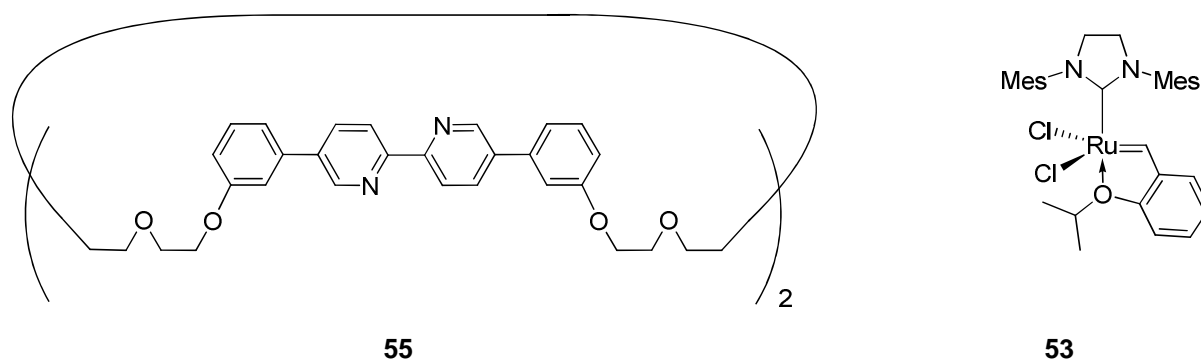
There are two complementary synthetic paths to the hexadentate, macrocyclic ligand **31** (see Scheme 2.3-10). First, the three double bonds in the iron complex **54** can be hydrogenated in the presence of palladium on charcoal in an ethanol-dichloromethane mixture. In the second step the iron can be removed with the disodium salt of ethylenediaminetetraacetic acid (H₂Na₂Edta) in the presence of sodium carbonate in a water-acetonitrile mixture. The order of

the steps can also be reversed. Ligand **31** was obtained in 26% yield over three steps (from **47** to **31**). The hydrogenation and the removal of the metal probably occur in an almost quantitative manner. If the threefold RCM is counted as three synthetic steps then the average yield for each of the five steps is 76%.



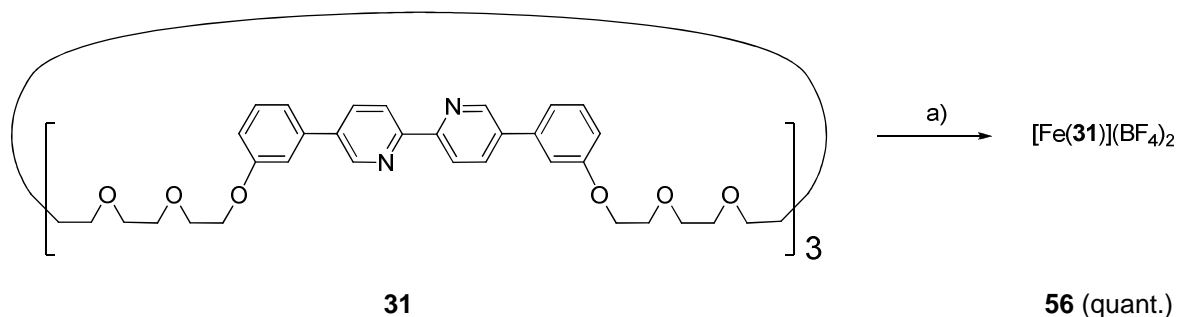
Scheme 2.3-10. Reagents and conditions: a) H_2 (1 atm), Pd/C (25 mol%), $\text{CH}_2\text{Cl}_2/\text{EtOH}$ (1:1), 12 h; b) $\text{H}_2\text{Na}_2\text{EDTA}$ (5 eq), Na_2CO_3 (10 eq), CH_3CN , 50°C , 3 h, 26% (over three steps).

Attempts to remove the iron with cyanide, or with mixtures of hydrogen peroxide and sodium hydroxide, caused decomposition of the ligand. The stability constant for $[\text{Fe}(\text{terpy})_2]^{2+}$ is several orders of magnitudes higher than that for $[\text{Fe}(\text{bpy})_3]^{2+}$. Iron could also be removed with an excess of a terpyridine ligand. The disadvantage is that the terpyridine ligand has to be removed chromatographically, too. The method using $\text{H}_2\text{Na}_2\text{Edta}/\text{Na}_2\text{CO}_3$ proved to be superior.



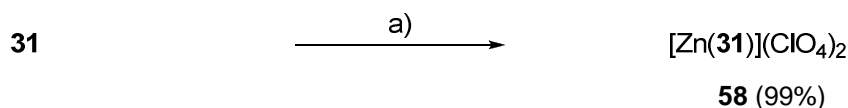
Scheme 2.3-11. Tetradentate macrocycle **55** and Hoyveda-Grubbs catalyst 2nd generation.

Iron complex **56** was obtained as an intermediate on the synthetic path towards macrocyclic hexadentate compound **31** (see Scheme 2.3-10). It can also be obtained by reacting pure **31** with one equivalent of an iron salt (see Scheme 2.3-12) and could be unambiguously identified by ESI-MS (see Figure 2.4-9b). The $^1\text{H-NMR}$ spectrum exhibited many signals and broad peaks assumed to be due to the possible formation of different geometrical isomers causing the loss of symmetry. Traces of paramagnetic iron(III) might also have contributed of the complex nature of the spectrum. A separation of the isomers was not attempted because the iron complex is kinetically labile and the complexes will most likely return to their initial equilibrium, once separated.



Scheme 2.3-12. Reagents and conditions: a) $[\text{Fe}(\text{BF}_4)_2] \cdot 6 \text{H}_2\text{O}$ (1 eq), CH_3CN , reflux, 4 d.

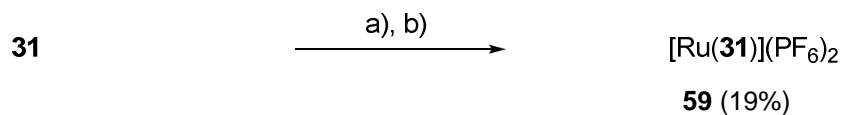
Clear ESI-MS evidence (see Figure 2.4-9a) was also found for the zinc [1+1]-complex **58**. The $^1\text{H-NMR}$ spectrum showed typically shifted signals with the expected relative integrals.



Scheme 2.3-13. Reagents and conditions: a) $[\text{Zn}(\text{ClO}_4)] \cdot 6 \text{H}_2\text{O}$ (1 eq), $\text{CH}_2\text{Cl}_2/\text{CH}_3\text{CN}$, r.t., 16 h.

In contrast to iron(II) and zinc(II), ruthenium(II) usually forms kinetically inert complexes with polypyridyl ligands. Ruthenium(II) complex **59** was obtained in moderate yield by heating **31** and $[\text{Ru}(\text{DMSO})_4\text{Cl}_2]$ in a microwave reactor in ethanol. Ion exchange and

chromatography yielded the pure [1+1]-complex **59**. The molecule was characterised via one and two-dimensional NMR techniques (see Figure 2.4-6), ESI-MS (see Figure 2.4-9c), X-ray crystallography (see Figure 2.4-1) and elemental analysis.



Scheme 2.3-14. Reagents and conditions: a) $[\text{Ru}(\text{DMSO})_4\text{Cl}_2]$ (1 eq), EtOH, μW , 1 h; b) NH_4PF_6 .

Other kinetic products including oligo and polymeric structures can also be envisaged if one ruthenium metal centre is bound to more than one ligand. That is presumably one reason for the moderate yield.

2.4 Characterisation

Ruthenium complex **59** was synthesised as described above and was analyzed via NMR-spectroscopy, ESI mass spectrometry, elemental analysis and single crystal X-ray crystallography. The latter could answer the crucial question as to whether the complexed ligand is in the form of a cycle or a knot.

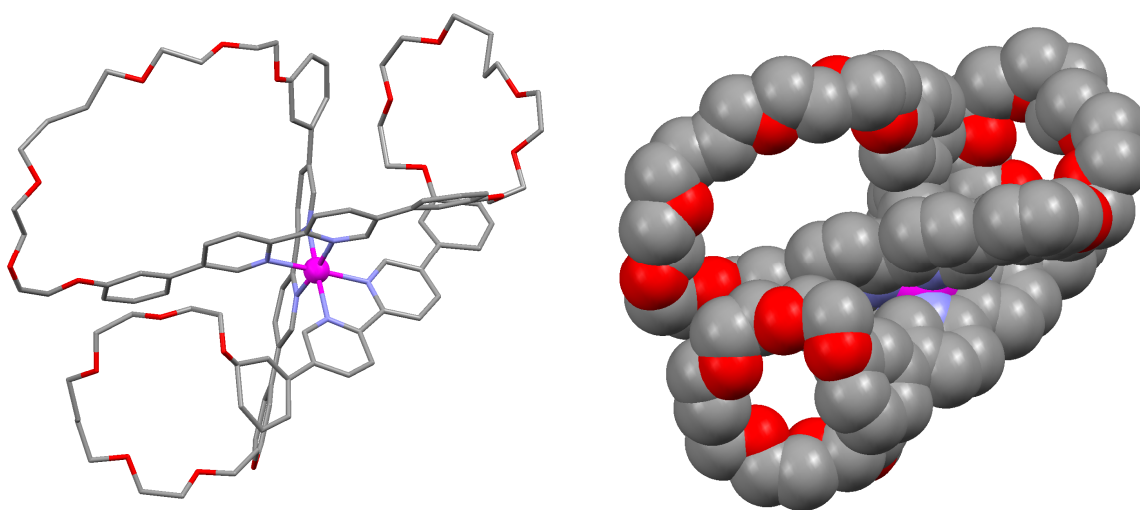


Figure 2.4-1. a) Molecular structure of the cation $[\text{Ru}(\mathbf{31})]^{2+}$ ($\mathbf{59}^{2+}$) depicted as capped stick representation; b) Space-filling representation of $\mathbf{59}^{2+}$. The ligand **31** is macrocyclic and hexadentate. Solvent molecules, counterions and hydrogen atoms have been omitted for clarity.

Despite the structure's poor quality, connectivity and the overall geometry were clearly established (see Figure 2.4-1).^[97] The organic molecule is macrocyclic and not knotted. The molecular skeleton is made up of a single 96-membered molecular chain that is assembled around the octahedral ruthenium core such that the bipyridine units can coordinate to the metal. The cation has effective C_1 symmetry and is therefore chiral. It contains only one trivial symmetry operation: the identity. Furthermore, careful analyses revealed that the molecules that crystallized have “*mer*”-configuration. It should be pointed out that from solution studies the “*mer/fac*”-ratio was deduced to be 2:1 (see later). The bond angles and lengths appeared to be in the expected range. Ruthenium – nitrogen bond distances vary from 206.4(9) pm to 215.6(9) pm.

Single crystals suitable for X-ray crystallography were obtained for the homoleptic complexes **45** and **49**. Their molecular composition differs only in the central metal that is iron(II) and ruthenium(II), respectively. Their molecular structures are shown in Figure 2.4-2.

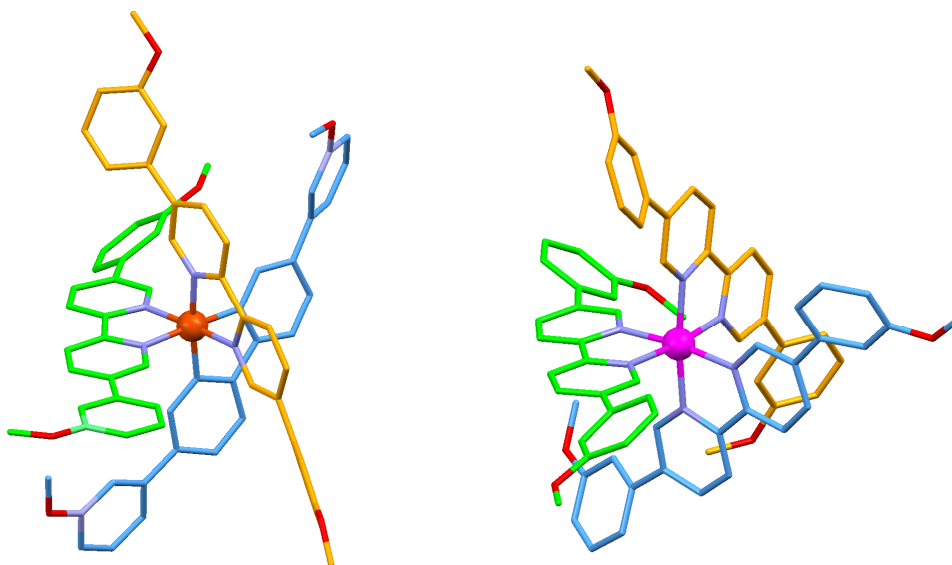


Figure 2.4-2. Molecular structures depicted as capped stick representations as they were found in single crystals of homoleptic iron and ruthenium complex cations: a) $[\text{Fe}(\mathbf{34})_3]^{2+}$ ($\mathbf{45}^{2+}$); b) $[\text{Ru}(\mathbf{34})_3]^{2+}$ ($\mathbf{49}^{2+}$). Solvent molecules, counterions and hydrogen atoms have been omitted for clarity.

The ionic radius of low spin iron(II) in octahedral complexes is with 61 pm^[98] smaller than the ionic radius of ruthenium(II). That is also mirrored in the nitrogen-metal bond length in the solid state of complexes **45** and **49**. The values are listed in Table 2.4-1 and the average N-Fe bond length was calculated as 196.3(7) pm and the average N-Ru bond length was found to be roughly 5% longer with 206.5(1) pm.

Table 2.4-1. Bond lengths between nitrogen atoms and central metal atoms that were found in crystal structures of $[\text{Fe}(\mathbf{34})_3]^{2+}$ and $[\text{Ru}(\mathbf{34})_3]^{2+}$.

	N1-X/pm	N2-X/pm	N3-X/pm	N4-X/pm	N5-X/pm	N6-X/pm	N-X/pm ^[a]
X = Fe(II)	196.2(2)	196.3(2)	196.7(3)	195.3(2)	197.4(2)	196.2(2)	196.3(7)
X = Ru(II)	206.4(3)	206.6(3)	206.4(3)	206.6(3)	206.4(4)	206.6(4)	206.5(1)

^[a]average bond length with standard deviation in brackets.

Single crystals of protonated ligand **34** suitable for X-ray analysis were found as a minor by-product while setting up crystallisation trials for the iron complex **45**. The unit cell contains the protonated ligand, one hexafluorophosphate anion and one water molecule that is hydrogen bonded to H1 (203 pm). The bond distance between H1 and N1 is 85.0 pm and H1

and N2 are separated by 226 pm through space. Carbon-carbon bond lengths were found in the range of 137.5(4) pm (C13-C14) and 148.3(4) pm (C9-C21) and all bond angles appeared to be in the expected range. The bipyridine unit containing N1 and N2 is essentially planar, with an angle between the least-square planes of the two pyridine rings of 3.7(1)°. The conformation of the protonated ligand with respect to the nitrogen atoms is *cis*. The angle between the least-square planes from the aromatic rings containing N2 and C22 is 38.6(1)° and for the two planes containing N1 and C15 an angle of 27.1(1)° was measured.

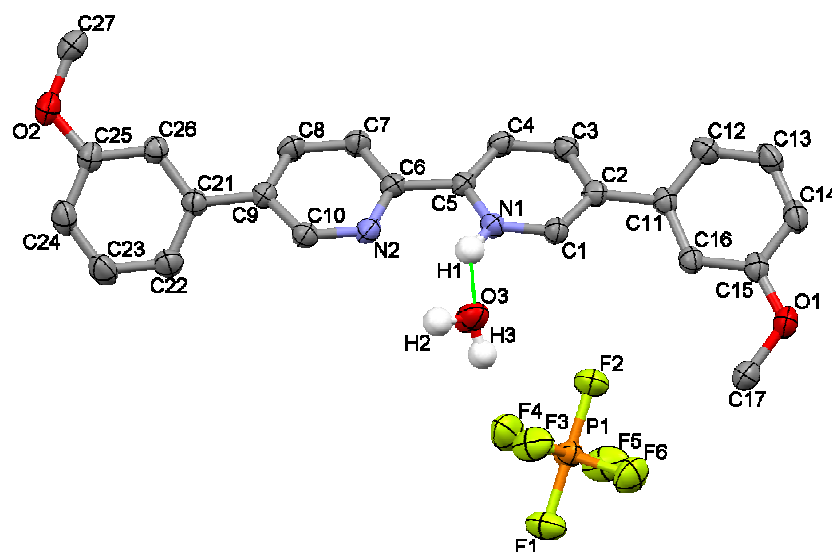


Figure 2.4-3. The molecular structure of $[34H]^+$ with atom labelling of selected atoms. Ellipsoids are drawn at the 50% probability level and protons are shown as small spheres of arbitrary radii. The hydrogen bond between H1 and O3 is shown as a green line. Hydrogen atoms have been omitted for clarity (except for H1-H3).

All ligands and complexes have been extensively studied via NMR spectroscopy. Most of the signals could be assigned. One example is presented in Figure 2.4-4: The ^1H -NMR and the ^{13}C -NMR spectrum of the macrocyclic ligand **31** that incorporates three bipyridine units. All ^1H and ^{13}C -NMR signals could be assigned with two dimensional NMR techniques (COSY, HMBC, HMQC, and NOESY). The symmetry of the molecule is reflected in the spectra and there are 13 distinguishable ^1H -NMR resonances and 17 peaks in the ^{13}C -NMR spectrum. The connectivity between the atoms was established by NMR spectroscopy, the molecular size was determined by ESI-MS and the molecular composition was determined by elemental analysis. The remaining question whether a knot or a macrocycle was formed could be answered with the help of crystal structure analysis (Figure 2.4-1). The chemical shifts are very similar and the relative peak positions are the same compared to the ligands bearing one bipyridine moiety (e.g. **34**, **42**).

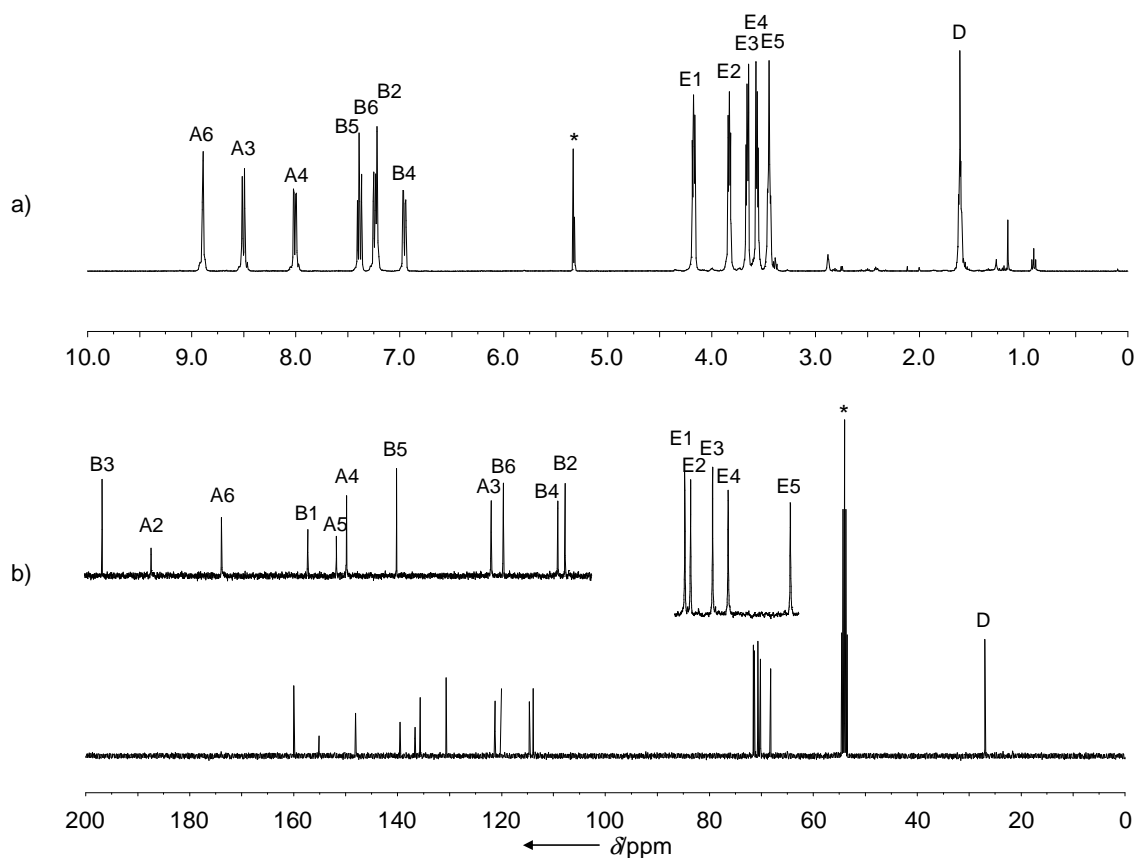


Figure 2.4-4. NMR-spectra of hexadentate, macrocyclic ligand **31** in CD_2Cl_2 : a) $^1\text{H-NMR}$ with assignments; b) $^{13}\text{C-NMR}$ with assignments. The insets show zooms in parts of the spectrum of interest. The solvent residual signal is marked with an asterisk (*). Labelling is given in Figure 2.2-1a.

Correlation spectroscopy in NMR is very useful in elucidating structural data that are not satisfactorily represented in a one dimensional spectrum. The most common is a COSY experiment whose spectrum displays diagonal peaks and cross peaks that result from a phenomenon called magnetisation transfer. If a cross peak appears in the spectrum between two resonances then the two atoms are spin-spin coupled over chemical bonds. The COSY spectrum for the aromatic and the aliphatic region of compound **31** is illustrated in Figure 2.4-5. For instance, a cross peak between the aromatic protons A3/A4 and A4/A6 was observed. That means that these atoms are magnetically coupled. Proton A3 couples over three bonds to A4 with $J = 8.3$ Hz and A4 and A6 (separated by four bonds) have a coupling constant of $J \approx 2$ Hz. The absolute value of the coupling constant can be compared to the intensity of the cross peak.

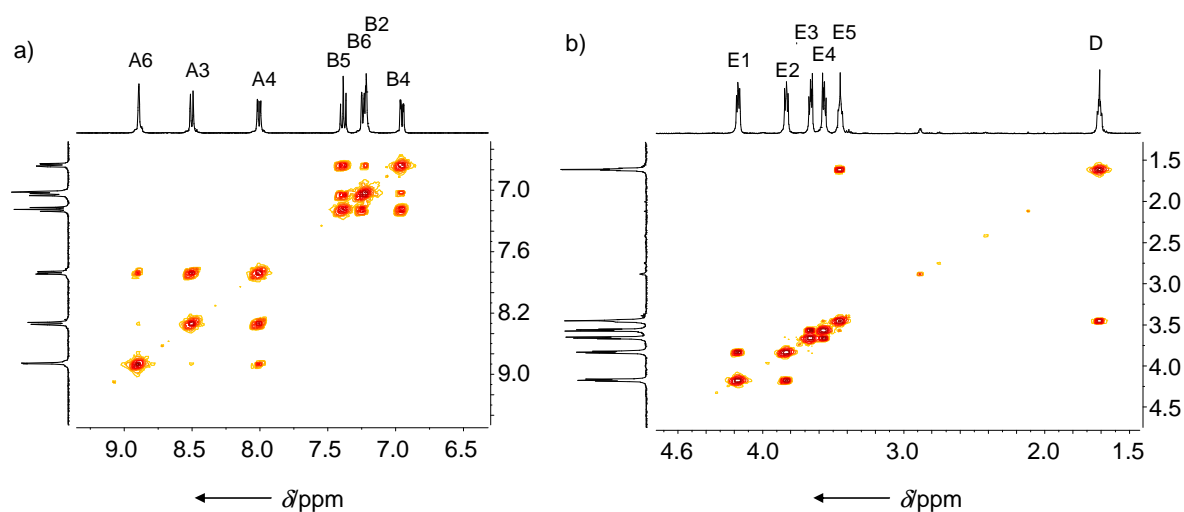


Figure 2.4-5. COSY spectra of **31** recorded in CD_2Cl_2 at 298 K and 500 MHz: a) Aromatic region displaying the typical coupling pattern; b) Aliphatic region showing coupling between protons.

In the aliphatic region (Figure 2.4-5b) a cross peak between protons E5 and D is detected indicating that they are adjacent to each other.

The ^1H -NMR spectra of the ruthenium complexes **59** and **49** are compared in Figure 2.4-6. The complex **49** with three bis(methoxyphenyl)-bipyridine (**34**) ligands has a high symmetry. This symmetry is lost if the ligands are connected to one cyclic hexadentate ligand like in **59**. Furthermore, two geometrical isomers are expected depending on how the connections were made. From the spectrum the ratio of the two isomers was found to be 2:1. Integration gives the expected values. The assignments for the aromatic protons in **59** were made by analysing COSY-NMR, peak position and shape compared to **49**, integrations and HMQC cross peaks of expected ^{13}C correlations.

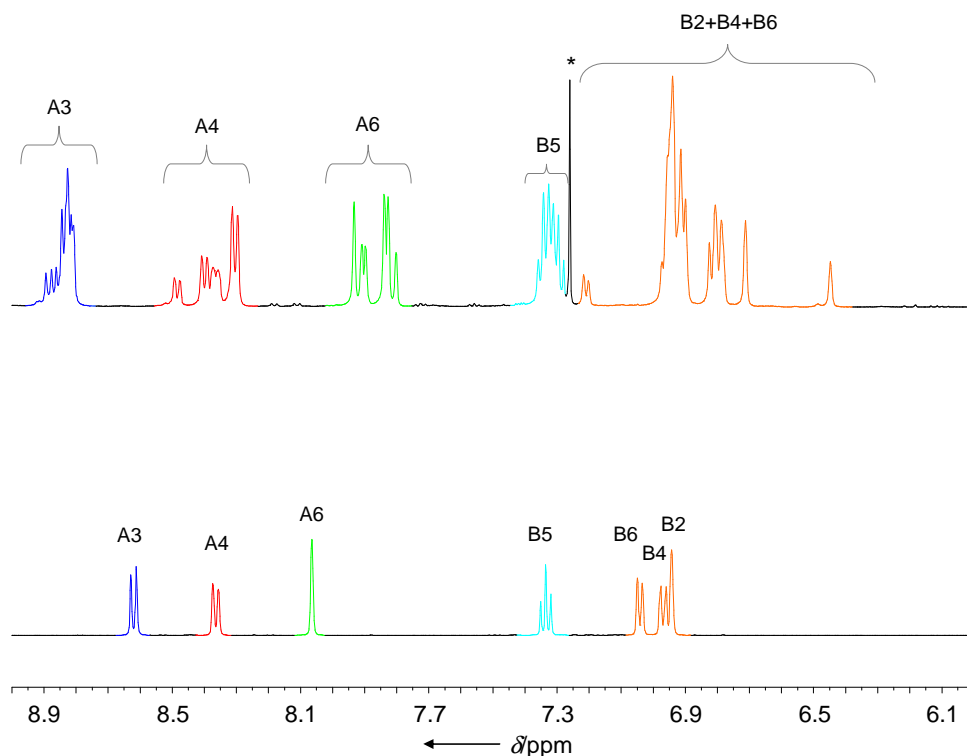


Figure 2.4-6. ¹H-NMR spectra at 298 K and 500 MHz of ruthenium complexes [Ru(**31**)](PF₆)₂ (**59**) (TOP) and [Ru(**34**)₃](PF₆)₂ (**49**) (BOTTOM). The asterisk (*) marks the solvent residual signal.

ESI-MS was a very versatile and valuable tool in following the ring closing metathesis (RCM) and characterizing metal complexes. The doubly charged cation of iron complex **47** with $m/z = 923.3$ was easily detected. Threefold RCM resulted in a loss of three ethene molecules and gave rise to a single peak of $m/z = 881.1$: the double charged cation **54**²⁺. Hydrogenation of three double bonds brought about a mass peak of three atomic mass units higher (**56**²⁺). The mass spectra are shown in Figure 2.4-7.

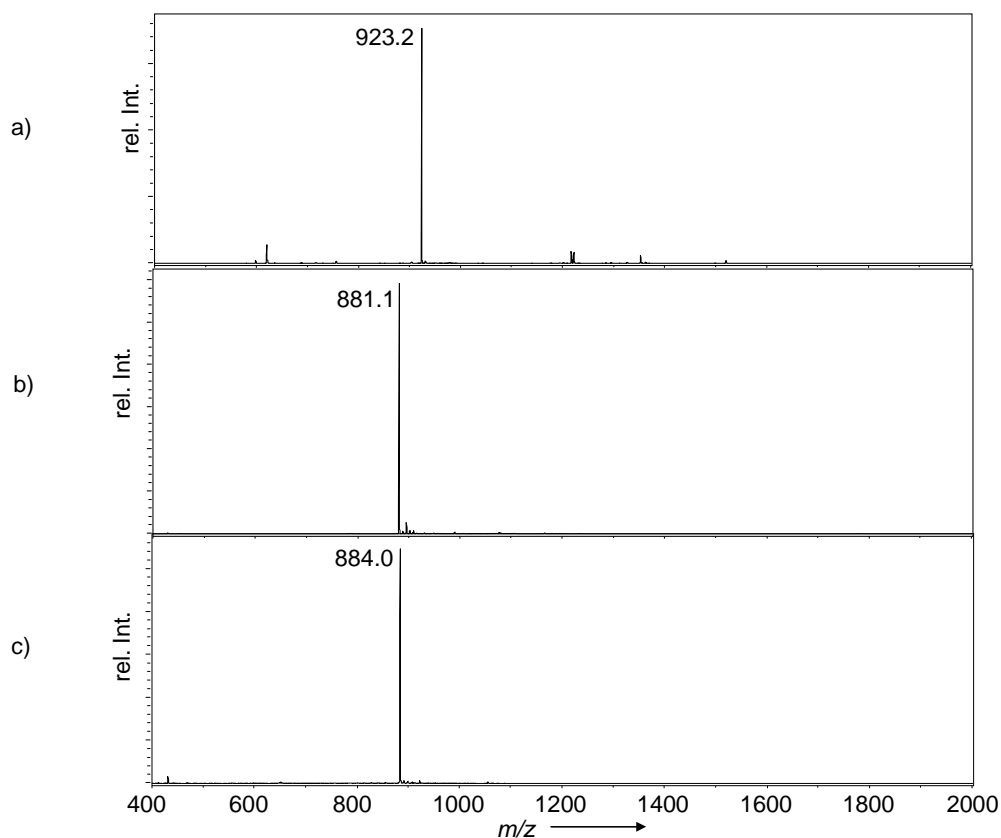


Figure 2.4-7. a) Iron(II) complex $[\text{Fe}(\mathbf{43})_3]^{2+}$ ($\mathbf{47}^{2+}$) before threefold olefin metathesis; b) Iron(II) complex $[\text{Fe}(\mathbf{57})]^{2+}$ ($\mathbf{54}^{2+}$) after olefin metathesis; c) Iron(II) complex $[\text{Fe}(\mathbf{31})]^{2+}$ ($\mathbf{56}^{2+}$) after hydrogenation.

Only charged species can be analysed via ESI-MS. Complexes usually lose one or more counterions if present and the cations are detected in the positive mode. For neutral molecules, the ions observed are created by the addition of a proton, another cation such as a sodium ion, or the removal of a proton (e.g. phenols, carboxylic acids).

The highest mass peak in the ESI mass spectrum of the neutral, hexadentate macrocyclic ligand **57** and **31** were observed as $[\text{M}+\text{Na}]^+$. The measured isotopic patterns matched the calculated patterns (see Figure 2.4-8).

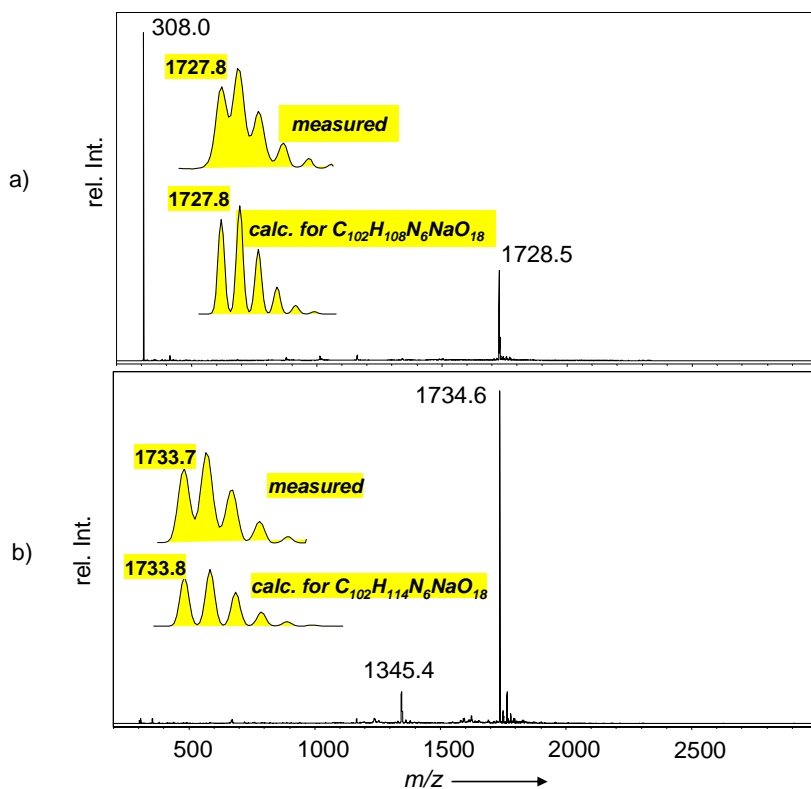


Figure 2.4-8. ESI-MS spectra of hexadentate, macrocyclic ligands: a) $[57+Na]^+$ with three double bonds; b) $[31+Na]^+$ after saturation of double bonds. The insets show the measured and calculated isotopic patterns.

Figure 2.4-9 displays the ESI-MS mass spectra of the zinc(II), iron(II), and ruthenium(II) complexes with macrocyclic ligand **31**. As already observed, the doubly charged cations were much more likely to be detected than singly charged species coming from the parent complexes.

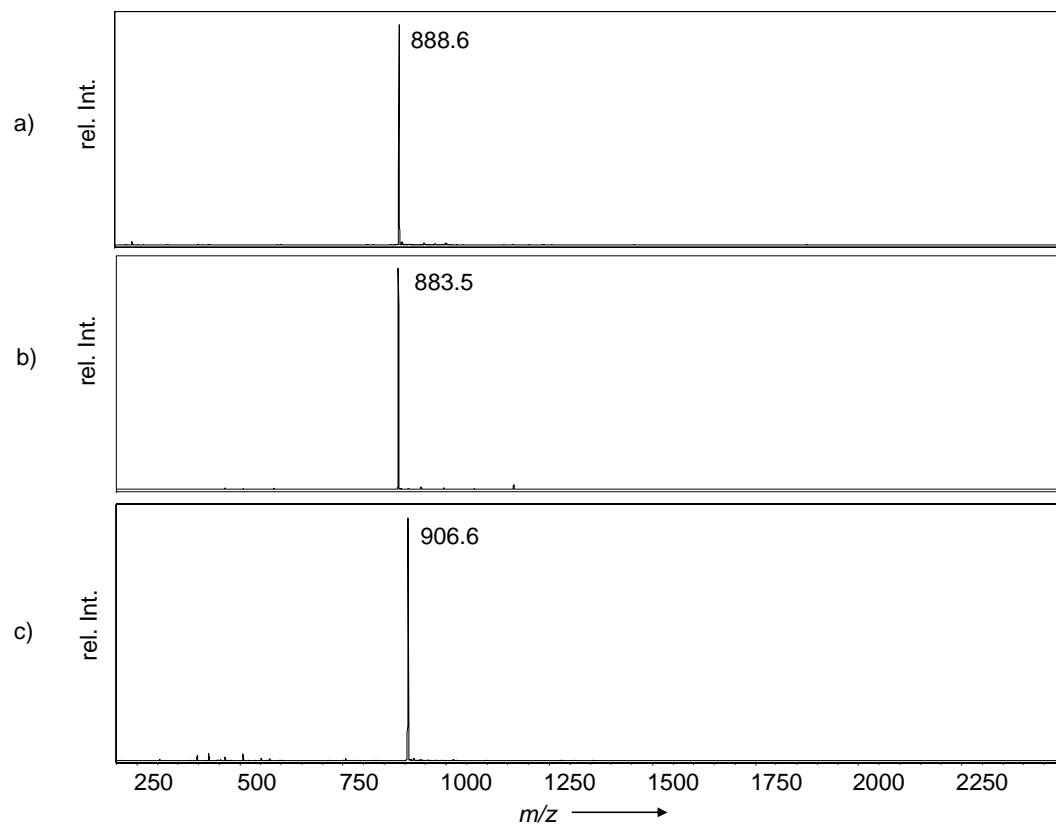


Figure 2.4-9. ESI-MS spectra of mononuclear complexes of macrocyclic **31**: a) $[\text{Zn}(\mathbf{31})]^{2+}$ ($\mathbf{58}^{2+}$); b) $[\text{Fe}(\mathbf{31})]^{2+}$ ($\mathbf{56}^{2+}$); c) $[\text{Ru}(\mathbf{31})]^{2+}$ ($\mathbf{59}^{2+}$).

2.5 Summary and Outlook

Sokolov's concept^[74] to use an octahedral metal core as template for the synthesis of a macrocycle (trivial knot) was for the first time successfully employed.

Three novel extended bipyridine ligands with chains having terminal alkene groups were prepared for this purpose. The chelating ligands were wrapped around iron(II) or ruthenium(II) and a threefold ring-closing metathesis (RCM) was performed that linked the termini two by two. In the case of iron complex **47** the RCM followed by hydrogenation and demetalation led to the isolation of a unique, macrocyclic, hexadentate ligand **31** that incorporates three bipyridine units. One-to-one complexes with this ligand and zinc(II), iron(II) and ruthenium(II) were synthesised and a crystal structure of the latter was obtained.

The use of a single octahedral metal centre to control the assembly of ligand threads into a macrocycle was accomplished, it is apparent that changes in the ligand architecture that will fulfil geometrical prerequisites might lead to the preparation of a trefoil knot.

3 Oligonuclear Ruthenium(II) Complexes with Macrocyclic Ligands

This chapter will deal with complexes that are formed between ruthenium (a rare transition metal of the platinum group from the periodic table) and several organic ligands. One of the ligands is a macrocycle: a ring architecture of more than nine atoms that usually enables molecules to achieve a certain degree of pre-organisation but no rigidity. Not only chemists but everybody encounters macrocycles each day in an unavoidable way since they occur in many natural products. The active site in haemoglobin –a protein in our blood that transports oxygen– contains a macrocyclic moiety (the porphyrin). Other examples are vancomycin (an antibiotic) or chlorophyll (a photosynthetic pigment in plants). On the other hand, ruthenium is widely used in alloys, as a versatile catalyst, in mixed-metal oxides for cathodic protection and in dye sensitized solar cells that are potentially cheaper to produce than conventional silicon based solar cells.^[99, 100] The combination of both, ruthenium, being the central atom in its oxidation state two, and ligands that have donor atoms that can bind or form coordinate bonds is a complex. The metal is considered as a Lewis acid (electron pair acceptor) and the ligands are Lewis bases (electron pair donors).

3.1 Introduction

The prototype for ruthenium(II) polypyridyl complexes is $[\text{Ru}(\text{bpy})_3]^{2+}$ which has become one of the most investigated compounds in the past 40 years due to its particularly interesting combination of chemical stability, redox properties, excited state reactivity, luminescence emission and excited state lifetimes. Ruthenium(II) possesses a d^6 system and the bipyridine ligands coordinated to it have σ -donor orbitals localized on the nitrogen atoms and π donor and π^* acceptor orbitals localized on aromatic rings. A simplified orbital diagram showing the possible transitions during irradiation is depicted in Figure 3.1-1a. Transition of an electron from a metal π_M orbital to the ligand π_L orbitals leads to a metal to ligand charge transfer (MLCT) excited state – the transition with the lowest energy. Promotion of an electron from π_M to σ_M^* orbitals and from π_L to π_L^* orbitals give rise to metal centred (MC) and ligand centred (LC) excited states, respectively. If a photon is absorbed from the singlet ground state (^1GS), the $^1\text{MCLT}$ or higher singlet states are populated followed by an intersystem crossing

to the $^3\text{MCLT}$ state (with $\Phi_{\text{ISC}} = 1$). The system can return to the ground state either by emission (with $\Phi_{\text{emission}} = 0.06$) or radiationless decay. Schematic potential energy curves are represented in Figure 3.1-1b.

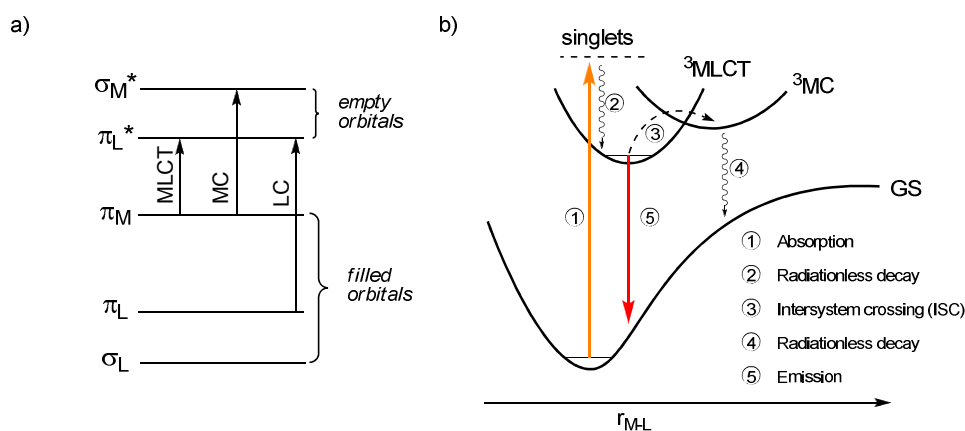
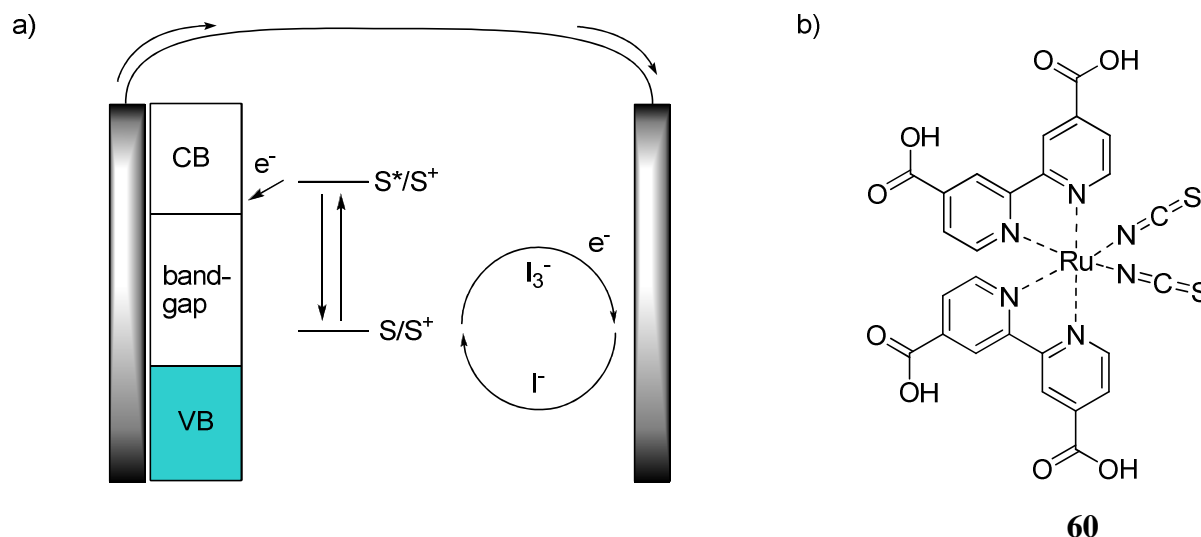


Figure 3.1-1. a) Simplified molecular orbital diagram for ruthenium(II) polypyridine complexes that show the three types of electronic transitions occurring at low energies. b) Schematic representation for the relative positions of ^3MC and $^3\text{MLCT}$ excited states that are found in $[\text{Ru}(\text{bpy})_3]^{2+}$ and transitions that take place. Adapted from references.^[101-103]

The area of research for this compound and its derivatives exploded in the 1970's with the awareness that it might be used to split water into molecular hydrogen and oxygen using sunlight.^[104, 105] The chemistry of ruthenium polypyridyl complexes has been reviewed extensively^[101, 106] covering initial findings, applications and possible future uses. Polynuclear complexes^[107] of this type and photochemical, photophysical and redox data^[102] have also been reviewed in detail.

Fossil energy carriers such as oil and gas are limited on Earth. It thus became a major challenge to convert solar energy to electric energy via solar cells. In the early 1990's, Grätzel and co-workers developed photovoltaic cells based on the principle of sensitization of wide-bandgap mesoporous semiconductors like nanocrystalline TiO_2 surfaces that are modified with monolayers of ruthenium complexes.^[108, 109] Dye-sensitized photoelectrochemical solar cells are a promising alternative to conventional junction based photovoltaic devices. Molecular sensitization is one of two general approaches that have been developed in order to use sunlight. The other approach doping is found in conventional photovoltaic devices. The operating principle of a dye-sensitized solar cell is depicted in Scheme 3.1-1b. A photoanode and a counter electrode are facing each other and the gap is filled with an electrolyte. The sensitizer (S) is converted to its excited state (S^*) by light and is able to inject an electron into the conduction band (CB) of the semiconductor. The sensitizer in its one-electron oxidized form (S^+) is rapidly reduced by I^- ions in solution. Photoinjected electrons flow in the circuit

and can perform electric work. They are also available at the counter electrode for the reduction of the electron mediator acceptor I_3^- . The system is then back at its initial point, ready for another catalytic cycle.



Scheme 3.1-1. a) Simplified operation principle of a dye sensitized solar cell. b) $[Ru(dcbpy)_2(NCS)_2]$ (dcbpy = 4,4'-carboxylbipyridine), also known as “red dye”.

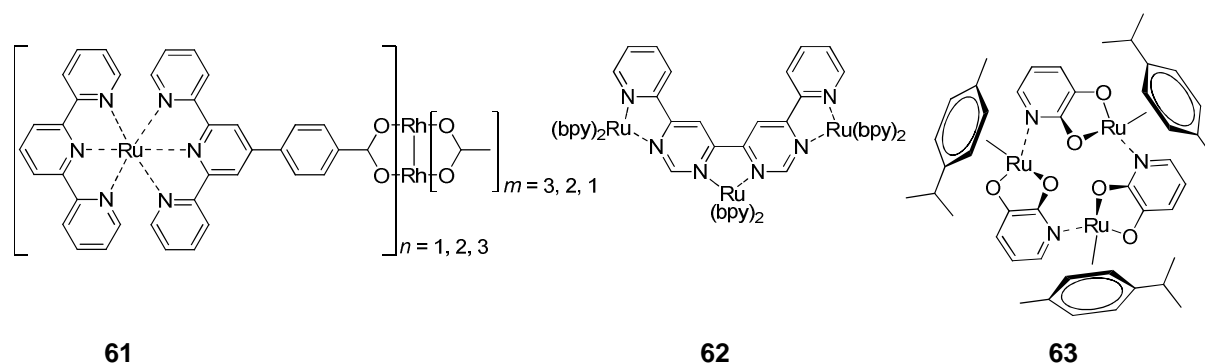
Sensitizers usually have functional groups such as $-COOH$, $-PO(OH)_2$ or $-B(OH)_2$ to ensure stable adsorption onto the semiconductor substrate. Ruthenium complexes such as **60** (“red dye”) are typically used but recently also copper complexes showed promising results.^[110] Several review articles describe past and recent progress in this area that often combines nanotechnology, material science, interfacial electron transfer and supramolecular photochemistry in a very multidisciplinary way.^[100, 111]

Ruthenium polypyridyl complexes were also utilised to mimic the photosystem II.^[112] Artificial light harvesting antenna systems^[113-115] can be constructed from mixed ruthenium-manganese complexes that are able to store photoinduced holes. The natural excited chlorophyll donor in the photosystem II can extract up to four electrons in a consecutive manner from the so-called manganese cluster. Oxygen can be produced from the four-times oxidized manganese cluster recycling the initial state that can undergo another photoinduced cycle.^[112]

Topological objects can be built using the specific geometry imposed by the ligand and the octahedral metal core of the ruthenium(II). The thermodynamic and kinetic stability of the resulting complexes is in general beneficial. Rack-type complexes are linearly arranged species and grid-type complexes are arranged species in a plane.^[116, 117] Ruthenium polypyridyl complexes have been examined photochemically and the emission in a rack could

be moved to the near-IR^[118] or was totally quenched in a tetranuclear mixed ruthenium-iron grid.^[119] These classes of compounds are usually constructed with terpyridine ligands but also pyrimidine-containing complexes have been reported.^[120]

Dendrimers are repeatedly branched molecules and those containing ruthenium(II) have been studied and the results have been reviewed.^[121-123] In one example the three chromophoric units, namely $[\text{Ru}(\text{bpy})_3]^{2+}$, naphthyl and 1,3-dimethoxybenzene were combined and properties of a light-harvesting antenna system and a possible frequency converter were investigated.^[124] The $[\text{Ru}(\text{tpy})_2]^{2+}$ motif was utilized to construct multinuclear arrangements and recently for a dye sensitized photoelectrochemical cell.^[125] The heteronuclear complex **61** illustrates an approach to build up polypyridylruthenium systems relying upon coordination to a tetracarboxylato metal dimer.^[126] Compound **62** is the first trinuclear ruthenium polypyridyl complex which was characterised by X-ray diffraction and was reported along with evidence of stereospecific complexation during its formation.^[127] There are a few examples of metallomacrocyclic multinuclear ruthenium complexes^[128-131] such as **63**^[132] whose extraction properties for alkali metal picrates have been investigated.

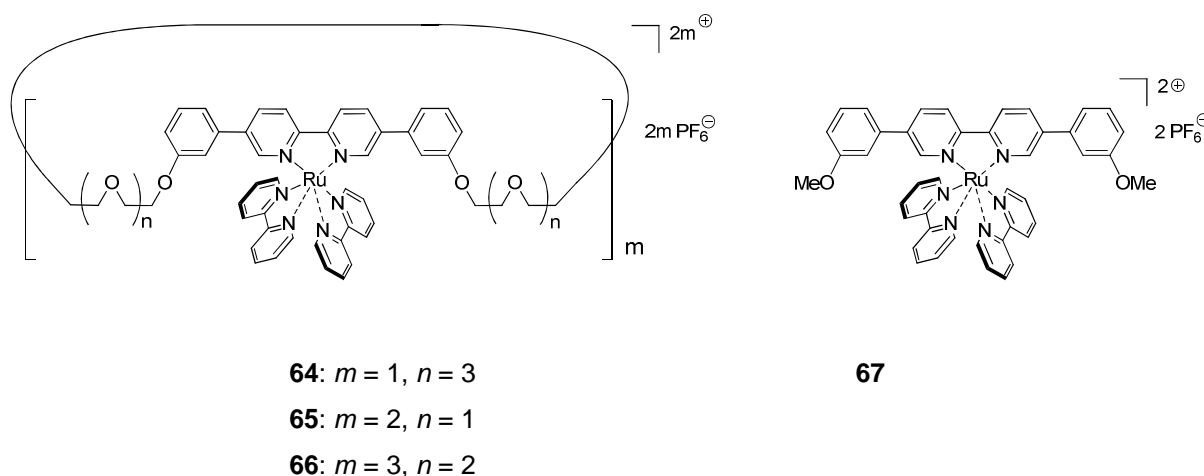


Scheme 3.1-2. Examples of multinuclear ruthenium(II) complexes. The mixed rhodium(II)-ruthenium(II) complex **61**, the trinuclear complex **62** and the metallomacrocyclic complex **63**. Charges are omitted for simplicity.

Metallomacrocycles can also be prepared with non-linear ditopic bis(terperidine) ligands.^[133, 134] Preorganisation and design of the ligand allow the control of dimensionality and nuclearity up to a certain degree. These complexes all have in common that the macrocycle is formed by coordinative bonds – they are metallomacrocycles. In these cases, kinetic or thermodynamic factors favour the formation of a cycle with precise size over linear, oligomeric or polymeric species. It has been shown that with labile metal ions metallopolymer or metallocycles are formed depending on the reaction conditions.^[135]

3.2 Aims and Overview

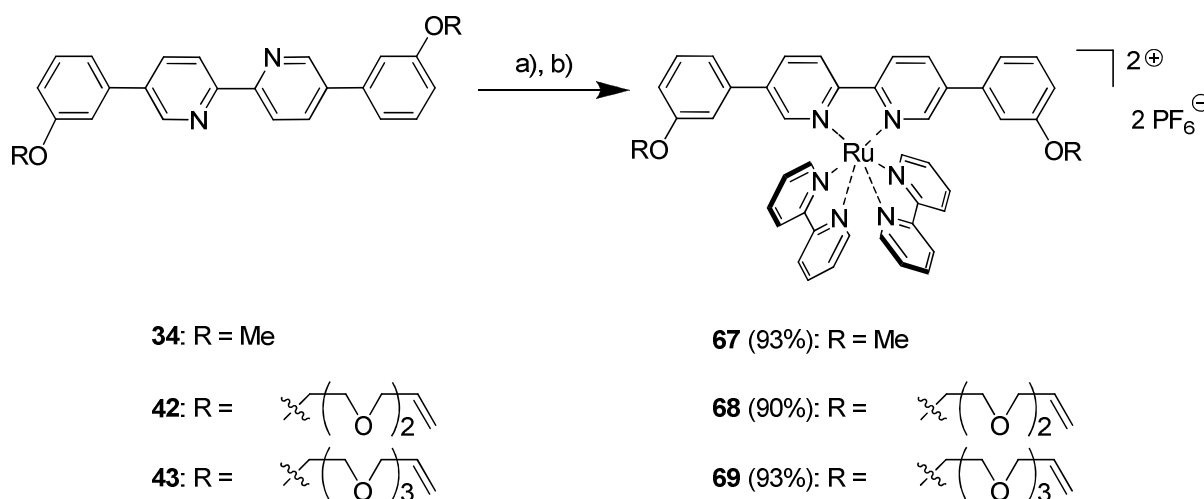
Is it possible to start with a macrocyclic ligand bearing multitopic binding sides and to coordinate several kinetically inert metals like ruthenium(II) to it? Multinuclear complexes displaying this particular kind of topology have not been reported yet, neither with ruthenium or other transition metals. This was one motivation to synthesise oligonuclear, macrocyclic complexes **64** (one metal centre), **65** (two metal centres) and **66** (three metal centres) along with their particularly appealing photophysical properties. Their molecular structures are represented in Scheme 3.2-1 together with [Ru(**34**)(bpy)₂](PF₆)₂ (**67**) which can be regarded as a reference compound displaying the properties of one complex subunit. The synthesis, characterisation, crystal structures of **67**, **64** and **65**, photophysical properties and the ability of **64** to act as a sodium receptor will be discussed in this chapter.



Scheme 3.2-1. Novel multinuclear complexes **64**, **65**, **66** and mononuclear reference complex **67**.

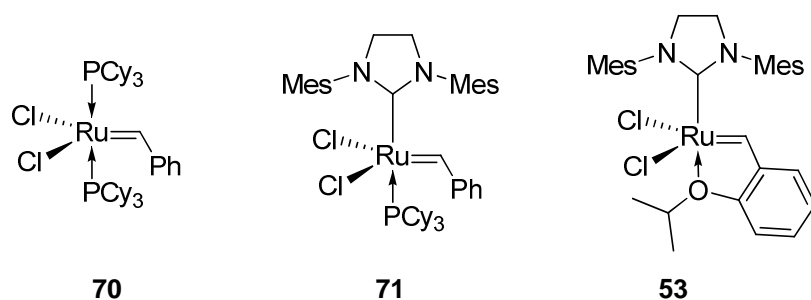
3.3 Synthesis

The synthesis of the open form ligands **34**, **42** and **43** is described in Chapter 2. Ruthenium(II)-complexes of the type $[\text{RuL}(\text{bpy})_2]^{2+}$ are available with relative ease in very good yields and short reaction times thanks to the employment of microwave technology. In a typical reaction, one equivalent of the ligand and a small excess of *cis*- $[\text{Ru}(\text{bpy})_2\text{Cl}_2]^{136}$ were heated in a microwave reactor in ethanol at 120 °C for 30 minutes. The reaction mixture was added to an aqueous solution containing an excess of ammonium hexafluorophosphate, the precipitate was collected and washed with water and diethyl ether (see Scheme 3.3-1). The crude products exhibited clean NMR spectra, but correct micro analysis necessitated a filtration over aluminium oxide.



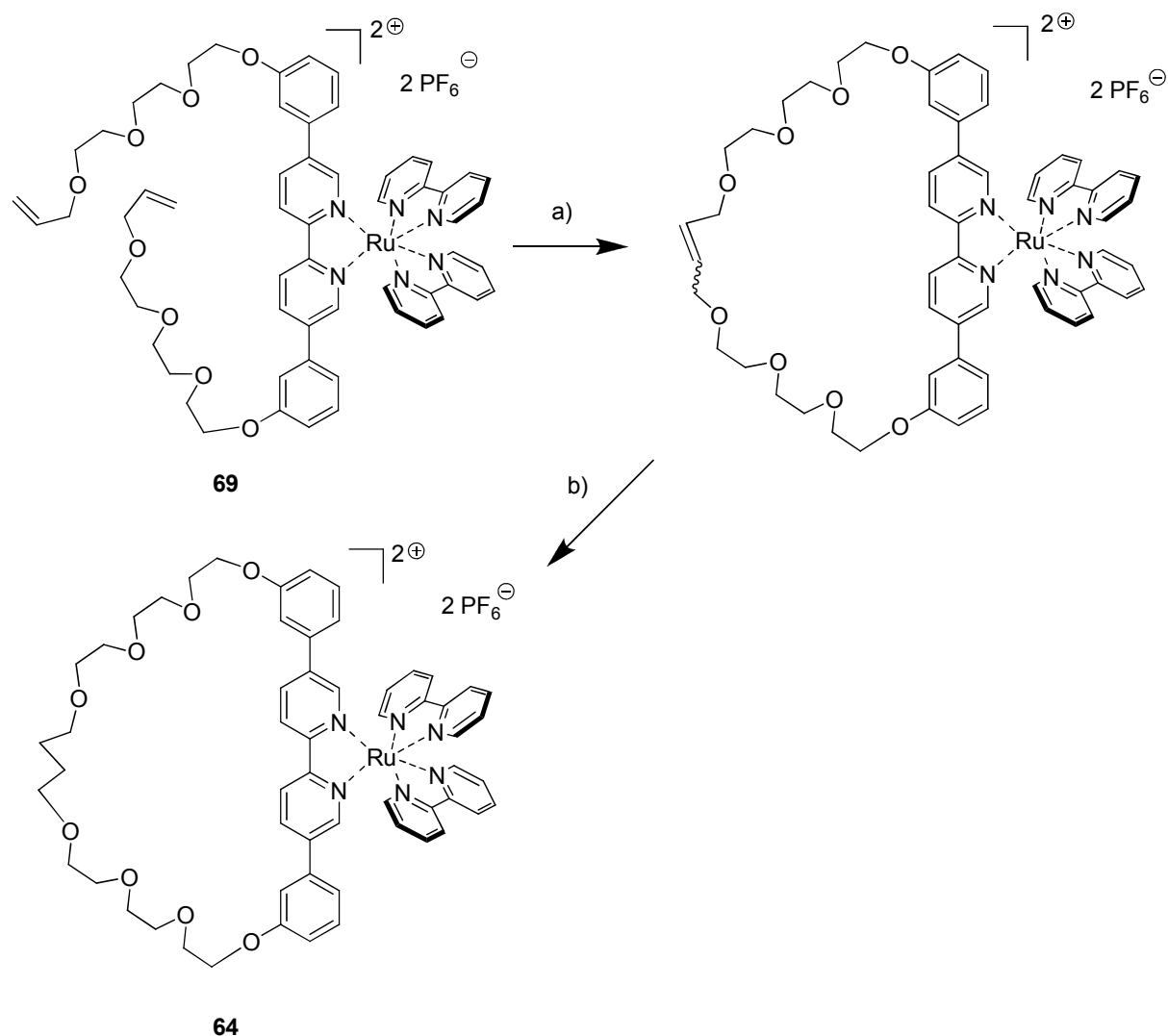
Scheme 3.3-1. Reagents and conditions: a) *cis*- $[\text{Ru}(\text{bpy})_2\text{Cl}_2]$ (1.01 eq), EtOH, 120 °C, microwave; b) NH_4PF_6 .

These mononuclear complexes can be made in high yields and are purified via filtration. In particular, no chromatography is needed. Once familiar with them, the synthetic protocol was used in similar reactions on multitopic macrocyclic ligands. Complex $[\text{Ru}(\mathbf{34})(\text{bpy})_2](\text{PF}_6)_2$ (**67**) will serve later as a reference compound, being used to help to interpret NMR spectra, photophysical properties, electrochemical properties and stereochemical considerations of the more intricate multinuclear ruthenium(II) complexes. The molecule **69** which has two terminal double bonds on the ethylene glycol chain is the starting material for the smallest macrocyclic ruthenium(II) complex presented in this chapter.



Scheme 3.3-2. Grubbs' catalyst 1st generation **70**, Grubbs' catalyst 2nd generation **71** and Hoyveda-Grubbs' catalyst 2nd generation **53**. Cy = cyclohexyl, Mes = 2,4,6-trimethylphenyl.

Ring closing metathesis (RCM) has been established as an efficient tool to synthesise macrocyclic molecules via intramolecular formation of a carbon-carbon double bond.^[137-140] As a first test, we tried the RCM in the presence of Grubbs' catalysts **70** of the first generation and **71** of the second generation. The reactions turned out to be very slow at room temperature and the purification of the product was demanding as a result of decomposition from the parent catalyst complexes. The diene **69** was then subjected to the air-stable and more reactive Hoyveda-Grubbs' catalyst of the second generation **53**^[141-143] (see Scheme 3.3-2). After hydrogenation with molecular hydrogen catalysed by palladium on charcoal, the desired macrocyclic complex **64** was obtained (see Scheme 3.3-3). The crystal structure revealed that one sodium cation coordinated to the ethylene glycol chain. This behaviour will be discussed in more detail in chapter 3.5.



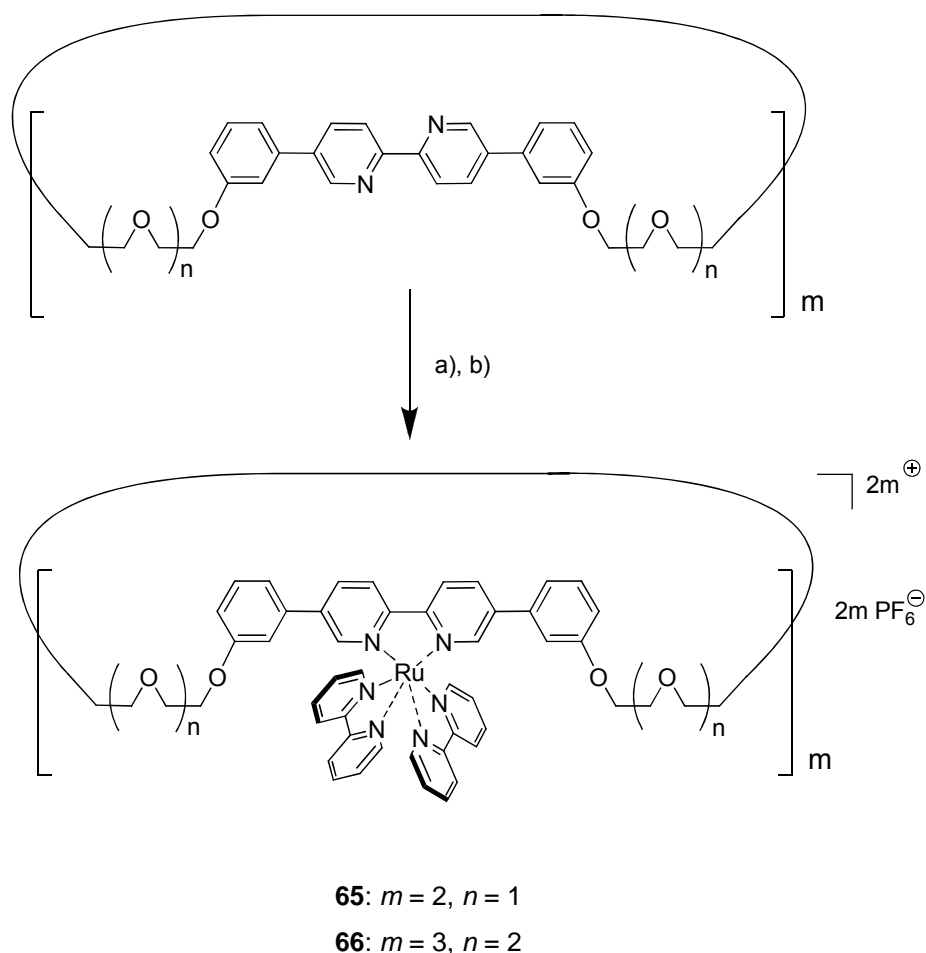
Scheme 3.3-3. Reagents and conditions: a) Hoyveda-Grubbs' catalyst 2nd generation (20 mol%), CH₂Cl₂, r.t.; b) H₂ (1 atm), Pd/C (11 mol%), EtOH/CH₂Cl₂ (1:1).

The RCM reaction cannot be performed on the free ligand. The ligand is not innocent and binds to the catalyst which is then blocked and “poisoned” for further conversion. The [Ru(bpy)₂]²⁺ moiety can, in this respect, be regarded as a protecting group even if its cleavage is not possible.

This example shows that it is possible to make a macrocyclic complex by carrying out the olefin metathesis on the complex. It is also feasible to synthesise first the macrocyclic ligand and then coordinate a transition metal to it.

Chapter 2 described how the macrocyclic ligands, **55** and **31**, with two and three bpy units are prepared. Our goal was to convert them into oligonuclear ruthenium(II) complexes. If the synthetic protocol for ligands bearing one bpy unit is adapted with a different stoichiometry,

the formation of **65** and **66** can be expected. The desired compounds were synthesised in good to very good yields (see Scheme 3.3-4).



Scheme 3.3-4. Reagents and conditions: a) *cis*-[Ru(bpy)₂Cl₂] (2.01 eq for **65**, 3.01 eq for **66**), EtOH, 120 °C, microwave; b) NH₄PF₆.

The dinuclear compound [Ru₂(**55**)(bpy)₄](PF₆)₄ (**65**) was obtained pure as the homochiral $\Delta\Delta/\Lambda\Lambda$ -form after chromatography on aluminium oxide. The other diastereoisomer namely the heterochiral $\Lambda\Delta$ -isomer could not be identified unambiguously and is not considered here. This explains the lower yield (46% compared to the usual 90%). Unfortunately, we were not able to separate the two diastereoisomers ($\Delta\Delta\Delta/\Lambda\Lambda\Lambda$ and $\Delta\Delta\Lambda/\Lambda\Lambda\Delta$) arising from the trinuclear complex **66**. Both complexes were comprehensively characterised by NMR and mass spectrometry. The purity of **66** and **65** was confirmed by microanalysis.

3.4 Characterisation and Crystal Structures

The molecular structures for **67**, **64**, **65** and a general labelling scheme are shown in Figure 3.4-1 and structural parameters are found in Table 3.4-1. As expected, the ligands coordinate in a propeller-like arrangement around the central metal atoms and the complexes are chiral. Only one of the two enantiomers present in the crystal is shown. All complexes exhibit distorted octahedral geometry with bond distances varying from 205.2(3) pm to 207.0(4) pm around the ruthenium(II) centres. Despite distortions, the Ru-N bond distances are similar to those in the molecular structure of $[\text{Ru}(\text{bpy})_3]^{2+}$ which was solved using X-ray crystallography in 1979 by Rillema.^[144] The Ru-N bond length (205.6 pm) in the D_3 symmetric $[\text{Ru}(\text{bpy})_3][\text{PF}_6]_2$ complex is to some extent shorter than in $\text{Ru}(\text{NH}_3)_6^{2+}$ (210.4 pm).^[145] This indicates a notable backbonding between the t_{2g} -orbitals of the metal core and the π^* -orbitals of the ligand.

The dihedral angles describing the twist between the two aromatic rings A and B in $[\text{Ru}(\mathbf{34})(\text{bpy})_2](\text{PF}_6)_2$ (**67**), **64** and **65** are different on the two sides of the bis(methoxy-phenyl)bipyridine moiety and vary between $11.2(2)^\circ$ (in **64**) and $42.3(2)^\circ$ (in **67**). Distortions from the ideal octahedral geometry can also be evaluated by the angles of coordinating atoms (not discussed here) and ascertained by angles of least square-planes calculated from the aromatic rings around the coordination environment. The values span from $1.0(3)^\circ$ to $9.8(2)^\circ$ (see Table 3.4-1).

For comparison, $[\text{Ru}(\text{bpy})_3]^{2+}$ displays a dihedral angle based on the twist about the pyridine rings in bipyridine of 9.97° .^[146]

Table 3.4-1. Angles between least-square planes of aromatic rings. Values are given in [°].

least-square planes of aromatic rings	$[\text{Ru}(\text{bpy})_3]^{2+}$	67	64	65
AA'	n.a.	7.8(2)	2.9(2), 5.0(2)	7.3(2), 10.1(2)
CC'	9.97 ^[a]	2.8(2), 9.8(2)	1.9(2), 5.5(2), 5.7(2), 7.9(2)	1.0(3), 2.8(3), 6.5(3), 6.8(3)
AB, A'B'	n.a.	34.1(2), 42.3(2)	11.2(2), 24.1(5), 31.0(3), 31.2(2)	21.5(3), 24.9(2), 32.0(2), 32.3(3)

^[a] from reference^[146]

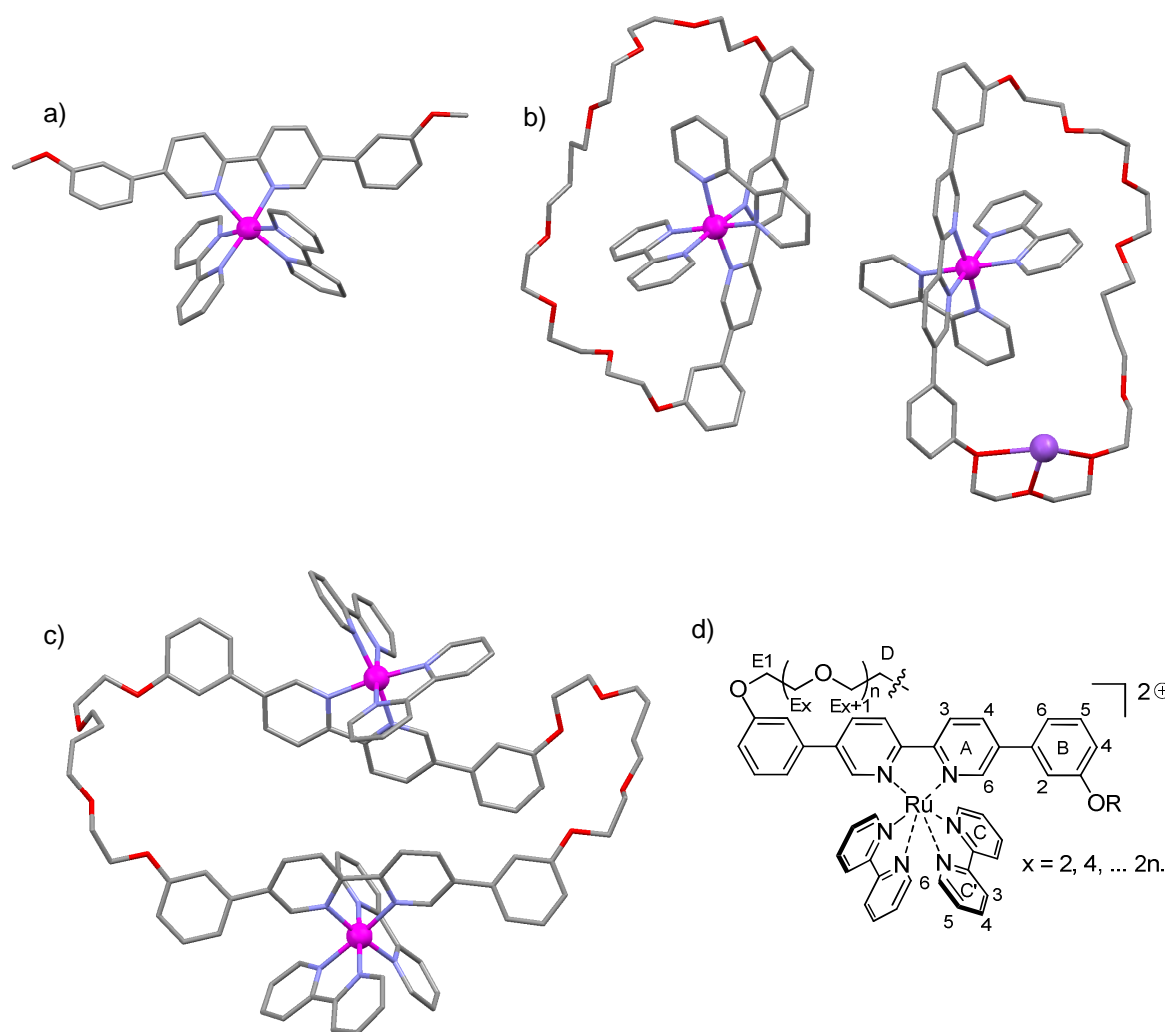


Figure 3.4-1. Molecular structures of a) 67^{2+} , b) 64^{2+} (two molecules per unit cell, one has a sodium cation coordinated to its ether chain) and c) 65^{4+} , depicted as stick representations as they were found in the single crystal. Hydrogen atoms, solvent molecules and counterions have been omitted for clarity. The colour coding is: ruthenium = violet, nitrogen = blue, carbon = black and oxygen = red. A general labelling mode is presented in d).

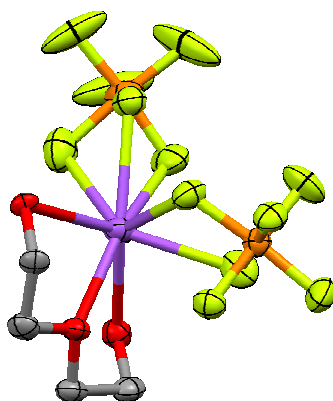


Figure 3.4-2. Molecular structures of the coordination environment of the sodium cation in **64** with ellipsoids plotted at 20% probability level. The colour coding is: carbon = black, oxygen = red, phosphorus = orange, fluorine = yellow, sodium = violet.

Table 3.4-2. Crystal structure data collection information.

	67 ·CH ₃ CN	64 (squeeze)	65 ·C ₂ H ₂ Cl ₂ ·2.5C ₄ H ₈ O ₂
Empirical formula	C ₄₅ H ₃₉ N ₇ O ₂ P ₂ F ₁₂ Ru	C ₅₈ H ₆₂ Na _{0.5} N ₆ O ₈ P _{2.5} F ₁₅ Ru	C ₁₁₂ H ₁₁₆ Cl ₂ N ₁₂ O ₁₃ P ₄ F ₂₄ Ru ₂
Formula weight [g mol ⁻¹]	1112.85	1446.13	2691.12
Temperature [K]	446	173	123
Wavelength [Å]	0.71073	0.71073	0.71073
Crystal system	Triclinic	Triclinic	Triclinic
Space group	<i>P</i> -1	<i>P</i> -1	<i>P</i> -1
Unit cell dimensions [Å, °]	a = 12.44(3)	a = 15.154(3)	a = 14.1156(13)
	b = 13.75(3)	b = 17.614(4)	b = 20.075(2)
	c = 14.219(3)	c = 126.892(5)	c = 23.409(2)
	α = 76.49(3)	α = 86.54(3)	α = 77.354(5)
	β = 74.54(3)	β = 82.28(3)	β = 73.193(5)
	γ = 83.29(3)	γ = 84.31(3)	γ = 85.179(11)
Volume [Å ³]	2278.23	7070,	6194.7(11)
Z	2	4	2
Absorption coefficient [mm ⁻¹]	0.512	0.372	0.437
F(000)	1118	2952	2748
Crystal size [mm]	0.30 x 0.27 x 0.07	0.45 x 0.28 x 0.16	0.05 x 0.13 x 0.29
Reflections collected	8048	89634	48405
Independent reflections	7300	21321	18510
Goodness-of-fit on <i>F</i> ² (all data)	1.096	1.054	1.0375
Final R indices	<i>R</i> 1 = 0.0572, ω <i>R</i> 2 = 0.1435	<i>R</i> 1 = 0.0658, ω <i>R</i> 2 = 0.1683	<i>R</i> 1 = 0.0679, ω <i>R</i> 2 = 0.0723
R indices (all data)	<i>R</i> 1 = 0.0629, ω <i>R</i> 2 = 0.1493	<i>R</i> 1 = 0.0763, ω <i>R</i> 2 = 0.1755	<i>R</i> 1 = 0.1455, ω <i>R</i> 2 = 0.1851

Interestingly, the complex **64** crystallizes in two forms per unit cell: the complex and the complex which has one sodium cation coordinated to its ether chain. In this macrocyclic complex, the chain goes around the side that is occupied by the bipyridine ligands. In the unit cell, the two metal cores are separated by 1.40 nm and the bond length between the oxygen atoms and the sodium cation are 230.4(5) pm, 268.6(4) pm and 261.8(5) pm.

There are five more short contacts to the sodium cation from the fluorine atoms of two hexafluorophosphate counterions (242.9(5) pm, 247.3(5) pm, 248.8(5) pm, 250.7(6) pm and 253.2(6) pm, see Figure 3.4-1c and Figure 3.4.2). That results in a coordination number of eight for the singly charged alkali metal. The closest distances between a carbon atom in the chain and a carbon atom in bipyridine ligand are found between E7 and C5 with 380 pm.

Chiral dinuclear macrocyclic complex **65** was synthesised as a racemate and turned out to be homochiral, therefore the stereochemical descriptors for the two enantiomers are $\Delta\Delta$ and $\Lambda\Lambda$, respectively. Both enantiomers are found in the unit cell. The two ruthenium metal atoms are separated by 1.00 nm. The closest distance between the two complex entities is found between carbon atoms A3 and C4 with ≈ 360 pm. In the solid state, the same couple on the other side of the complex is separated by ≈ 440 pm, therefore the two complex entities are not completely symmetric in the crystal structure.

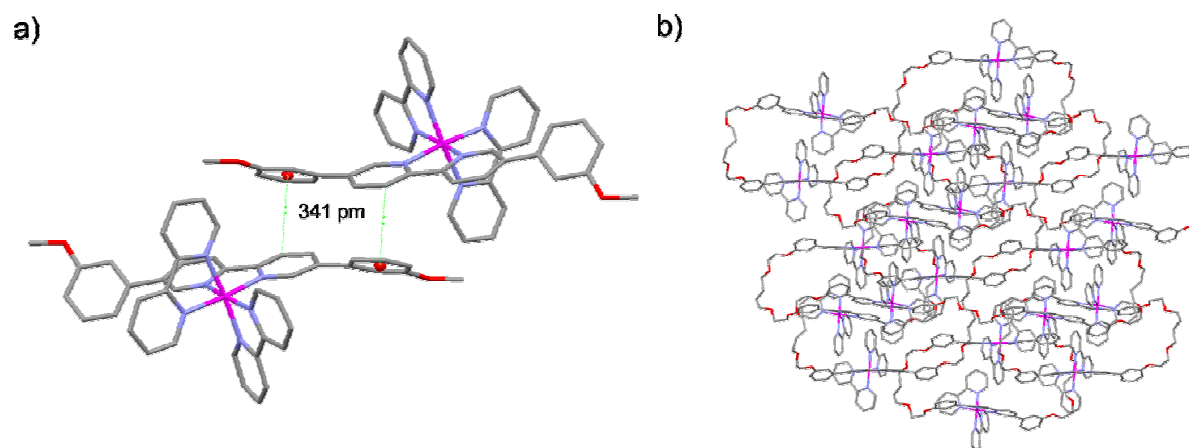


Figure 3.4-3. Packing in solid state structures of a) **67** and b) **65**. Hydrogen atoms, solvent molecules and counterions have been omitted for clarity.

The analysis of short contacts reveals a close proximity of a methoxyphenyl ring (B) to a pyridine ring (A) of an adjacent molecule in the solid state packing. The distance between the centroid of the aromatic B-ring and the carbon atom A3 was calculated as 341 pm (see Figure 3.4-3).

No particular packing effects were observed for the complexes **64** and **65**.

The ruthenium(II) complexes were studied extensively via NMR spectroscopy. All proton and carbon nuclei could be assigned with the help of two dimensional COSY, HMBC, HMQC, NOESY and DEPT experiments (for all data see Experimental part). For a labelling scheme see Figure 3.4-1d. The protons of the free ligand 5,5'-bis(3-methoxyphenyl)-2,2'-bipyridine (**34**) are shifted distinctively in the ruthenium(II) complexes. The A6-proton in α -position to

the nitrogen is the only signal that is shifted to a higher field from δ 8.9 ppm to δ 7.8 ppm in the complex. The protons A4, B2, and B6 exhibit resonances at lower field ($\Delta\delta \approx 0.3$ ppm) and the other signals are hardly affected. By analysing the molecular structure of $[\text{Ru}(\mathbf{34})(\text{bpy})_2](\text{PF}_6)_2$ (**67**), it is apparent that the symmetric bipyridine now has two different moieties in the complex. By considering, for example, the neighbouring proton to the N-atom (C6 and C'6), one can see that the C6-proton points towards the aromatic A-ring from ligand **34** and the C'6-proton points towards the aromatic C-ring from the other bipyridine. Therefore, the two bipyridine units are diastereotopic and chemically non-equivalent.

Figure 3.4-4 shows the proton spectra of the aromatic region of the mononuclear compound $[\text{Ru}(\mathbf{34})(\text{bpy})_2](\text{PF}_6)_2$ (**67**) (top) and the dinuclear compound **65** (bottom). The dinuclear compound **65** seems to be composed of two sets of signals that can in particular be observed for protons A3, C6 and A4. Furthermore, protons A3 and A4 are shifted to lower frequencies by about $\Delta\delta = 0.2$ ppm and $\Delta\delta = 0.1$ ppm, respectively. The reason may be a stronger shielding due to the close proximity of the second complex entity (for visualisation compare crystal structure Figure 3.4-1c).

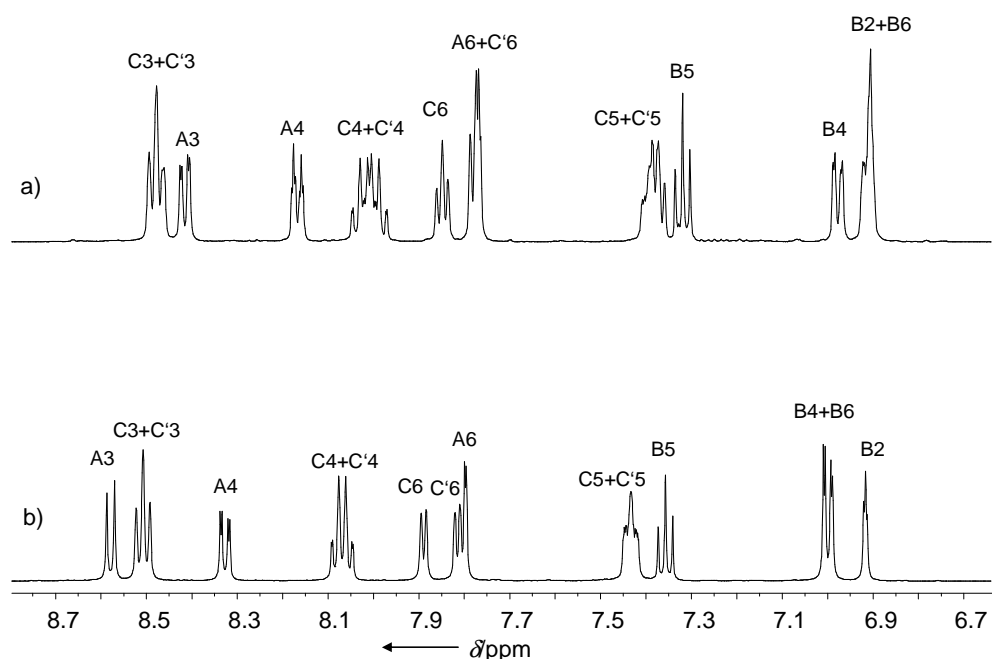


Figure 3.4-4. ^1H -NMR spectra in d_3 -acetonitrile of a) dinuclear complex **65** and b) mononuclear reference complex **67**.

The mononuclear, macrocyclic compound **64** exhibits downfield shifted nucleus B6 ($\Delta\delta = 0.27$ ppm) and upfield shifted nucleus B2 ($\Delta\delta \approx 0.2$ ppm) compared to **67**. A different dihedral angle between the aromatic rings A and B, and therefore different degrees of shielding or deshielding, rationalizes this outcome. The trinuclear macrocyclic complex **66**

and **67** have very similar chemical shifts. The molecular complex moieties are separated far enough from each other in space by the ethylene glycol chain to not influence each other (see Table 3.4-3).

Table 3.4-3. ^1H NMR spectroscopic shift data (500 MHz and 600 MHz, 298 K, CD_3CN) for the aromatic region.

proton		67	64	65	66
A	3	8.58	8.56	8.41	8.55
	4	8.33	8.35	8.19 – 8.14	8.29
	6	7.80	7.82	7.81 – 7.75	7.79
B	2	6.92	6.75 – 6.70	6.91	6.99 – 6.90
	4	7.00	6.96	6.98	6.99 – 6.90
	5	7.36	7.38	7.32	7.30
	6	7.00	7.27	6.91	6.99 – 6.90

The 3J coupling constant for aromatic protons is observed between 7.9 Hz and 8.6 Hz except for the protons in α -positions to the nitrogen atoms (A6, C6 and C'6) with $^3J \approx 5.5$ Hz.

In the aliphatic region, the signals for the methylene protons adjacent to an oxygen atom (E) are found between δ 4.1 ppm and δ 3.3 ppm and the signals for methylene protons that are neighboured by other methylene groups (D) are found at $\approx \delta$ 1.6 ppm. An unusual feature was observed for the E7 proton from mononuclear macrocyclic complex **64**. Its resonance is at very high field (δ 2.3 ppm). This might stem from an anisotropy effect. In the solid state (see crystal structure Figure 3.4-1b) the chain reaches around the side of the complex which is occupied by the bipyridine ligands. If we assume the structure to be similar in solution then the protons might lie in the zone where the magnetic field B_0 is reduced (shielding is increased above and below the ring) by the ring current of the electrons from the aromatic bipyridine. This is opposite to the effect that causes aromatic protons outside the ring (e.g. in benzene) to be shifted to low fields.^[147]

The ^{13}C spectrum ranges in the aromatic region from δ 161 ppm (B3) to δ 113 ppm (B2). The nuclei from the methylene groups adjacent to an oxygen atom (E) are usually found between δ 68 ppm and δ 72 ppm and the nuclei from the methylene group neighboured by other groups (D) appear around δ 27 ppm. Again, the nucleus E7 in **64** exhibits an unusual upfield shifted signal at δ 35 ppm.

Electrospray ionisation (ESI) was the technique applied to produce ions for mass spectrometry (MS). It is a very mild method that is very useful for complexes and macromolecules because the ionisation energy is low enough that usually no fragmentation is observed (except for the fragmentation of a salt into cations and anions as in the case of complexes presented in this chapter). In 2002, the development of ESI-MS was rewarded with the Nobel Prize in Chemistry to John Bennet Fenn.^[148]

All compounds presented in this chapter could be studied via ESI-MS and showed correct spectra with expected masses. One typical example is illustrated in Figure 3.4-5. The trinuclear ruthenium(II) complex **66** deconvolutes into its +6, +5, +4, +3, +2 and +1 (not shown) cations which are detected in the positive mode of the mass spectrometer. The isotopic pattern can be examined by recording a zoom scan on these cations.

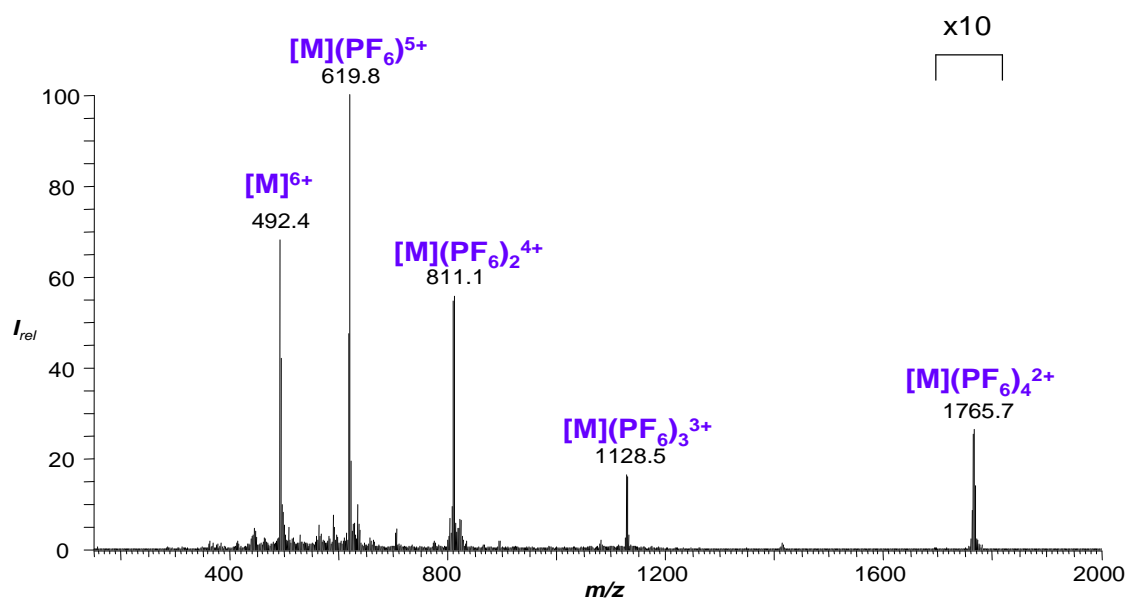


Figure 3.4-5. ESI-MS spectrum of trinuclear complex **66** showing its deconvolution in +2, +3, +4, +5 and +6 charged cations.

The measured isotopic pattern can be compared to a simulated pattern. The line spacing reflects the ratio mass over charge (m/z) of the fragment in question, that will for example lead to a difference of $1/5$ atomic mass units between two adjacent isotopes for a +5 charged cation (see Figure 3.4-6).

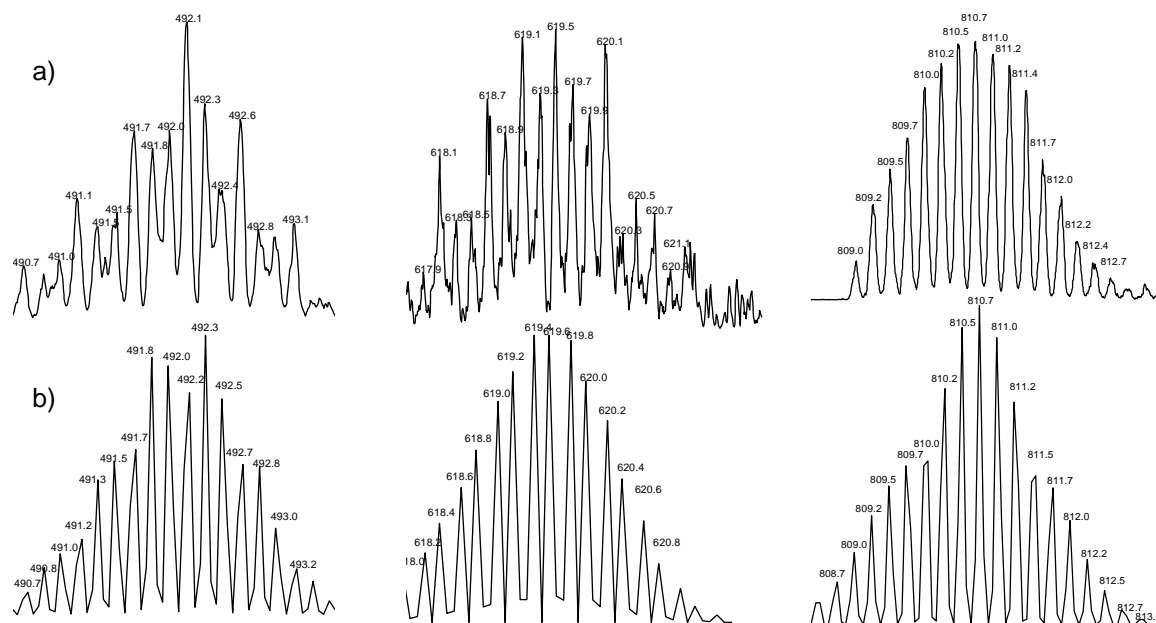


Figure 3.4-6. a) Measured isotopic pattern of +6, +5 and +4 charged cations from **66**. The m/z ratio is also reflected in the line spacing. b) Simulated isotopic pattern of the same cations.

Infrared spectra and melting points have been determined for all compounds and the data is documented the Experimental part of this thesis.

For compounds **67**, **68**, **69**, **65** and **66** correct micro analysis could be obtained.

3.5 Photophysical Properties and Redox Potentials

Absorption spectroscopy is an easy method to get some cursory information about the electronic structure and electronic transitions that take place in a molecular species.

The absorption spectra of macrocyclic complexes **64**, **65** and **66** are shown in Figure 3.5-1. The band around 290 nm is probably a spin-allowed LC $\pi \rightarrow \pi^*$ transition. The two bands at 240 nm and 460 nm can be assigned to spin-allowed MLCT $d \rightarrow \pi^*$ transitions. The shoulders at 320 nm and 355 nm might be MC transitions. Assignments have been made by referring to the properties of $[\text{Ru}(\text{bpy})_3]^{2+}$, the prototype of ruthenium(II) polypyridine complexes^[101], which has an MLCT band at $\lambda_{\text{max}} = 452 \text{ nm}$ ($\epsilon = 14600 \text{ M}^{-1} \text{ cm}^{-1}$).

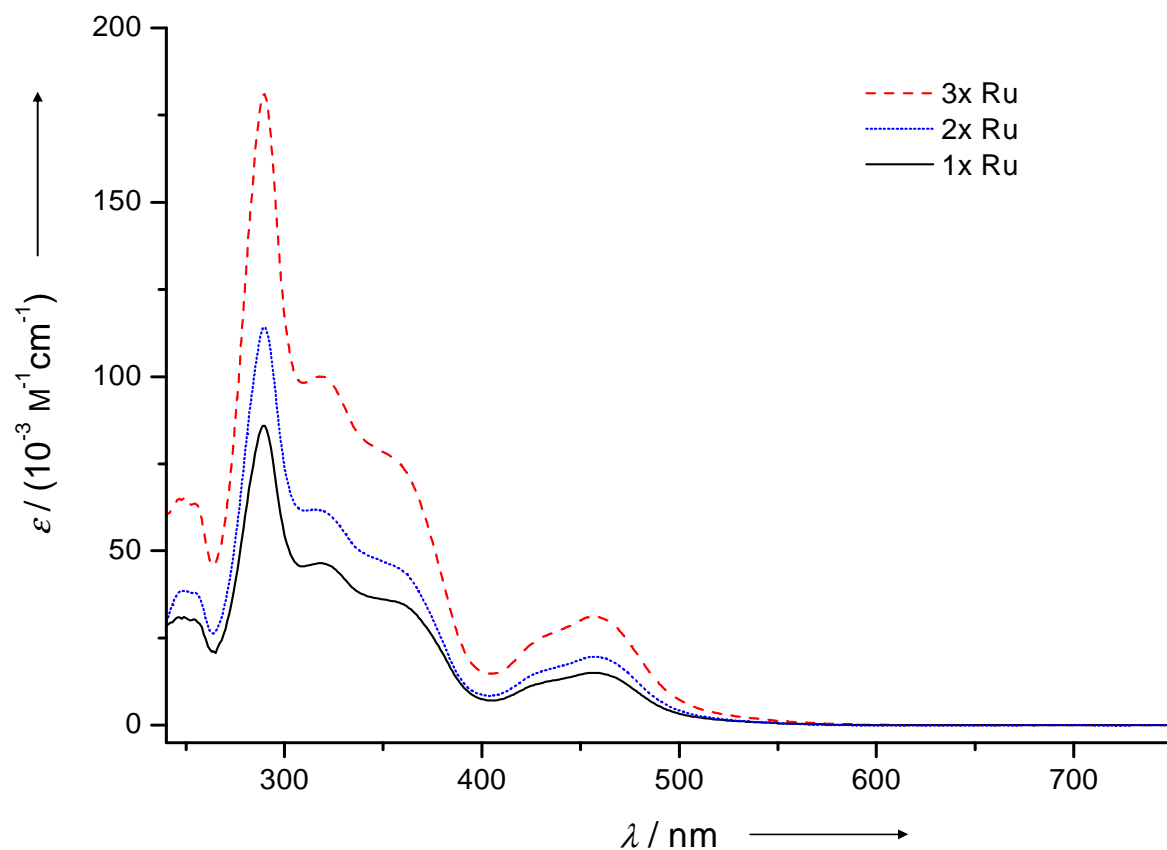


Figure 3.5-1. Absorption spectra of complexes **64** (black, solid line), **65** (blue, dotted line) and **66** (red, dashed line).

It is noteworthy to mention that the extinction coefficients are almost increased by a factor of two for the dinuclear compound **65** and by a factor of three for the trinuclear compound **66**

compared to the mononuclear compound **64**. These molecules contain one, two or three chromophoric groups, respectively.

In 1959 Paris and Brandt^[149] first reported the luminescence of $[\text{Ru}(\text{bpy})_3]^{2+}$ whose intensity, lifetime and energy position are more or less temperature dependent. At room temperature the maximum lies at 615 nm ($\tau \approx 1 \mu\text{s}$) in acetonitrile. The ruthenium(II) compounds introduced in this chapter exhibit an emission at ≈ 620 nm except for **64** which has its emission band at lower energy (641 nm).

Table 3.5-1. Absorption data (10^{-5} M in dichloromethane) and emission data (10^{-4} M in dichloromethane or acetonitrile) of ruthenium complexes.

	Absorption		Emission
	λ_{max} [nm]	ϵ [$\text{M}^{-1} \text{cm}^{-1}$]	$\lambda_{\text{exc}} = 355 \text{ nm}$ λ_{max} [nm]
67	457	15 000	616
	318 (shoulder)	46 500	
	289	85 900	
64	457	14 700	641
	354 (shoulder)	39 200	
	321 (shoulder)	45 700	
	290	86 800	
65	457	19 700	617
	316 (shoulder)	61 800	
	290	114 300	
66	457	31 200	621
	355 (shoulder)	77 000	
	318 (shoulder)	100 100	
	290	181 000	

The redox properties of the ruthenium(II) complexes have been investigated by means of cyclic voltammetry (CV). One typical example is shown in Figure 3.5-2 for the cyclic voltammogram of **64** in degassed acetonitrile.

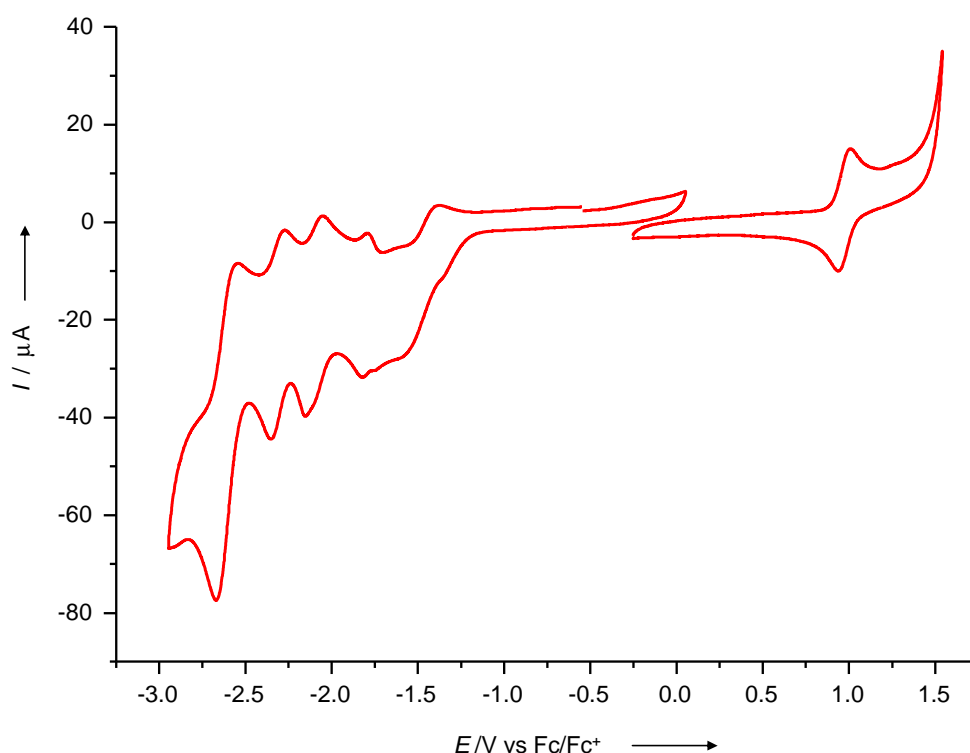


Figure 3.5-2. Cyclic voltammogram of **64** (1 mM) in degassed acetonitrile containing 0.1 M $[NnBu_4]PF_6$, $\nu = 100 \text{ mV s}^{-1}$.

Usually, the oxidation of ruthenium(II) in the complexes introduced in this chapter happens between 900 – 930 mV and there are four reduction processes which are reversible for the mononuclear complexes **67** and **64**, but not for the multinuclear complexes **65** and **66**. The potentials have been measured versus Ferrocene⁰/Ferrocenium⁺ (Fc/Fc⁺). The cyclic voltammogram of $[Ru(bpy)_3]^{2+}$ in degassed acetonitrile was measured for comparison and exhibits one oxidation process (890 mV) and four reduction processes (-1.73V, -1.93V, -2.17V), all are monoelectronic and reversible.^[150] Many references are found in the literature for $[Ru(bpy)_3]^{2+}$ and oxidation of ruthenium(II) to ruthenium(III) is usually reported at 1260 mV versus the NHE (Normal Hydrogen Electrode) in acetonitrile or water.^[151-154]

Table 3.5-2. Redox potentials measured for complexes **64-67** in argon-purged solutions of acetonitrile. $E_{1/2}$ values are given for reversible processes from the cyclovotammetry and are peak potentials for irreversible processes from square wave.

	Potential [V] versus Fc/Fc ⁺	
	oxidation	reduction
[Ru(bpy) ₃] ²⁺	0.890	-1.73, -1.93, -2.17
67	0.903	-1.60, -1.87, -2.10, -2.41
64	0.904	-1.60 ^[a] , -1.92, -2.12, -2.41
65	0.919	-1.48 ^[a] , -1.60 ^[a] , -1.85 ^[a] , -2.15 ^[a] , -2.44 ^[a]
66	0.927 ^[b]	-1.57 ^[a] , -1.97 ^[a] , -2.21 ^[a] , -2.42 ^[a]

[a] irreversible process, peak potential from square wave. [b] reversible process, peak potential from square wave.

3.6 NMR Enantiodifferentiation of Chiral Ruthenium(II) Complexes

Chirality in coordination compounds will occur when chelating ligands are bonded to an octahedral core. If the mirror image of a molecule and the original molecule are non-superposable then the molecule is optically active (chiral).^[98] Another more general definition says that any object that does not have any symmetry elements of the second kind (mirror plane, centre of inversion, rotation reflection axis) will be chiral.^[155] A demonstrative example is the cation $[\text{Ru}(\text{bpy})_3]^{2+}$ which is optically active and can appear in the form of the Δ - and Λ -enantiomer.

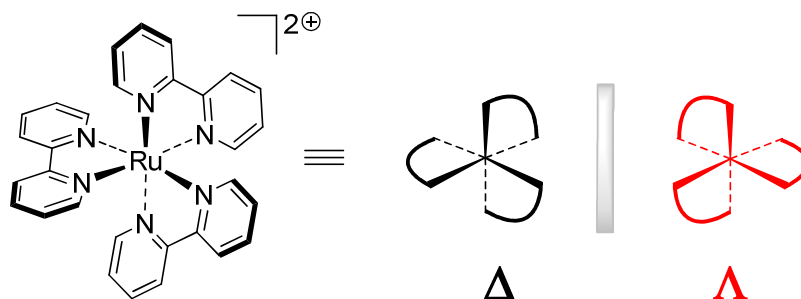


Figure 3.6-1. Optical isomers of the coordination complex $[\text{Ru}(\text{bpy})_3]^{2+}$. The Δ -isomer and the Λ -isomer are non-superposable and they are mirror images of each other.

In an achiral environment, $[\text{Ru}(\text{bpy})_3]^{2+}$ will be formed as a racemate (equal quantities of Δ - and Λ -enantiomers).

Pentavalent hexacoordinated phosphorus of octahedral geometry allows the formation of chiral phosphate anions if three identical bidentate ligands are coordinated. In 1997, Lacour and co-workers reported the synthesis and resolution of the configurationally stable TRISPHAT-anion (tris(tetrachlorobenzenediolato)phosphate(V)-ion)^[156] (see Figure 3.6-2). The non-substituted tris(benzenediolato)phosphate(V) anion is readily synthesised as an ammonium salt from catechol, PCl_5 and an amine but it is unfortunately configurationally labile and its enantioenriched form undergoes fast epimerisation in solution.^[157, 158] However, the use of catechols substituted with electron-withdrawing groups as in the case of TRISPHAT, prevents the epimerisation due to steric hindrance and electronic effects.

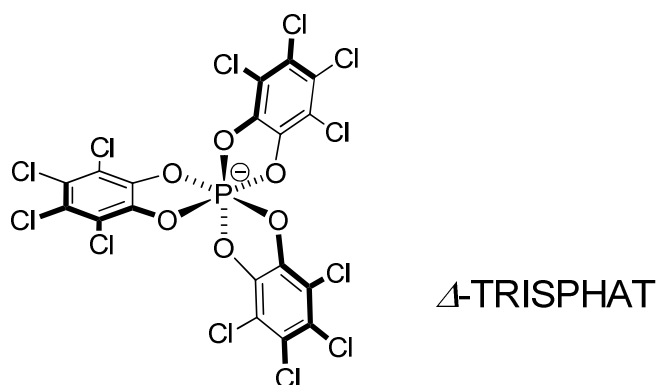


Figure 3.6-2. Hexacoordinated phosphate anion TRISPHAT (tris(tetrachlorobenzenediolato)-phosphate(V)). The Δ -enantiomer is shown.

Both enantiomers of the TRISPHAT anion can be obtained on a multigram scale through a reported resolution procedure^[159] and one isomer is also commercially available. It has found many applications as a NMR chiral shift reagent^[160-164], as a resolving auxiliary^[165-168], as an asymmetry-inducing agent^[169-172] and solubilising reagent^[173, 174] for organic, organometallic, metallo-organic and polymeric substances.

The advantage of an NMR spectroscopic investigation via chiral shift reagents over chiro-optical methods is that there is no need for parameters which characterise the pure enantiomers.^[175] In the case of a racemic ruthenium(II) complex, one has to replace the achiral counterions (e.g. PF_6^-) by enantiopure optically active counterions (e.g. Δ -TRISPHAT). The racemic mixture of enantiomers will be converted to a mixture of diastereoisomers.

Since we prepared cyclic complexes with one, two and three chiral centres, the study of their chirality appeared to be interesting.

For a first test, the racemic ruthenium(II) complex **67** as its hexafluorophosphate salt was dissolved in dichloromethane, two equivalents of Δ -TRISPHAT were added and the reaction mixture was extracted with water. Figure 3.6-3 shows the ^1H NMR spectrum of the complex with the achiral hexafluorophosphate counterion (top) and the spectrum of the complex with the enantiopure Δ -TRISPHAT counterion (bottom). The signals for protons A3, C3+C'3 and B5 clearly split into two sets of signals in roughly equal intensities. This can be explained by the formation of the two diastereoisomers [Δ -**67**][Δ -TRISPHAT] and [Λ -**67**][Δ -TRISPHAT] that have different chemical shifts.

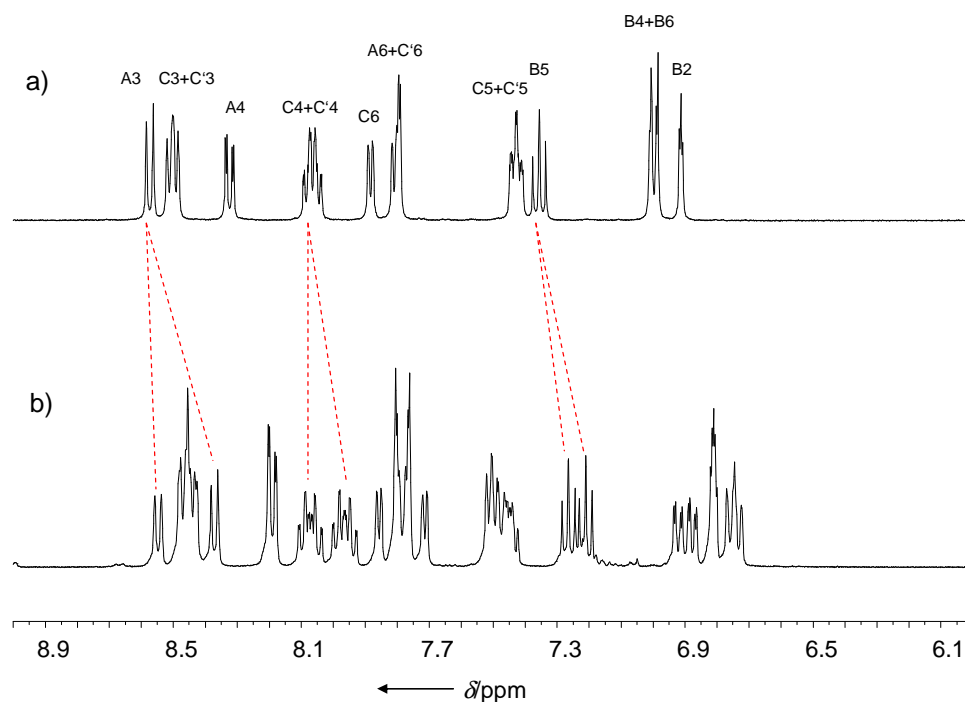
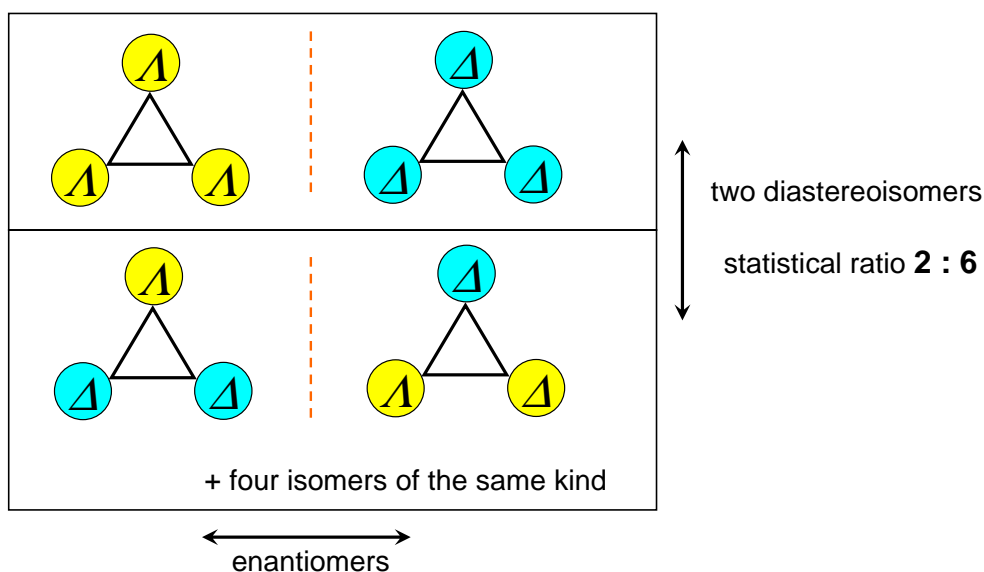


Figure 3.6-3. ^1H NMR spectra of a) *rac*-**67** as its hexafluorophosphate salt; b) *rac*-**67** with approximately two equivalents of $[\text{Et}_4\text{N}][\Delta\text{-TRISPHAT}]$. Both spectra are recorded at 500 MHz in CD_2Cl_2 at 25 $^\circ\text{C}$.

The trinuclear complex **66** has three stereogenic metal centres, and for each there is the possibility of Λ - or Δ -configuration. Two racemic diastereoisomers which are distinguishable in an achiral environment are possible: the homochiral $\Lambda\Lambda\Lambda/\Delta\Delta\Delta$ -stereoisomer-pair and the heterochiral $\Lambda\Lambda\Delta/\Delta\Delta\Lambda$ -stereoisomer-pair. The situation is depicted in Scheme 3.6-1. Any compound with n -stereocentres will give rise to 2^n isomers.^[176] Statistically, there are eight isomers ($2^3 = 8$) expected for the complex **66**. The heterochiral forms $\Lambda\Lambda\Delta/\Delta\Delta\Lambda$ are triple degenerated because a rotation of $\pm 120^\circ$ around the axis in the plane of paper will convert one isomer into one of the others (e.g. $\Lambda\Lambda\Delta = \Lambda\Delta\Lambda = \Delta\Lambda\Lambda$). In summary, there are two isomers from the homochiral form and two threefold degenerate isomers from the heterochiral form. Therefore, the ratio between these two diastereoisomeric pairs is expected to be 2:6.



Scheme 3.6-1. The four possible isomers of complex **66**.

Figure 3.6-4 shows the $^1\text{H-NMR}$ spectra of the trinuclear complex as the hexafluorophosphate salt (top) and with Δ -TRISPHAT as counterion (bottom).

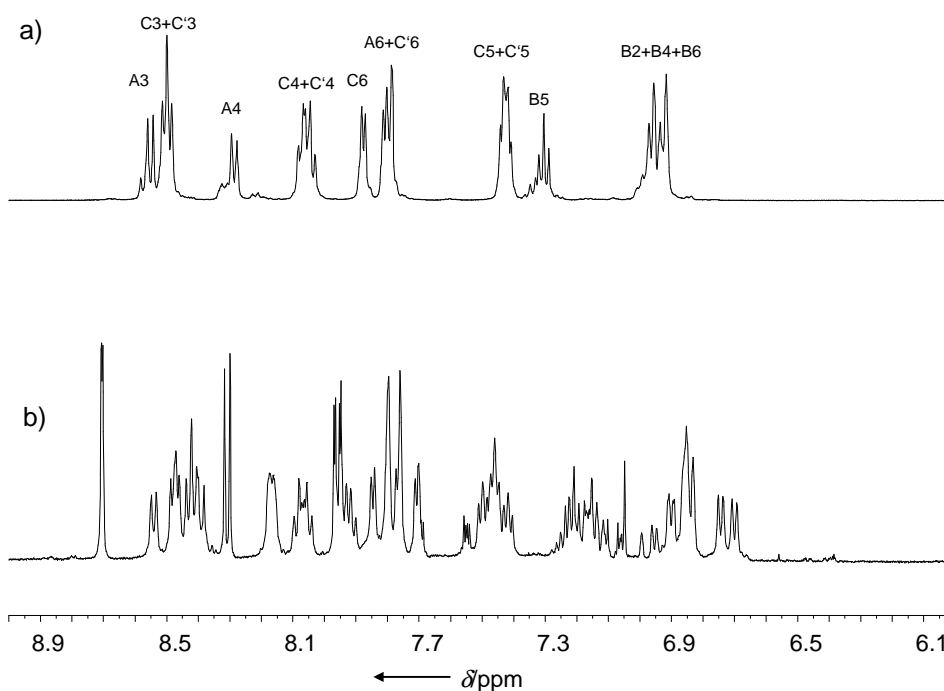
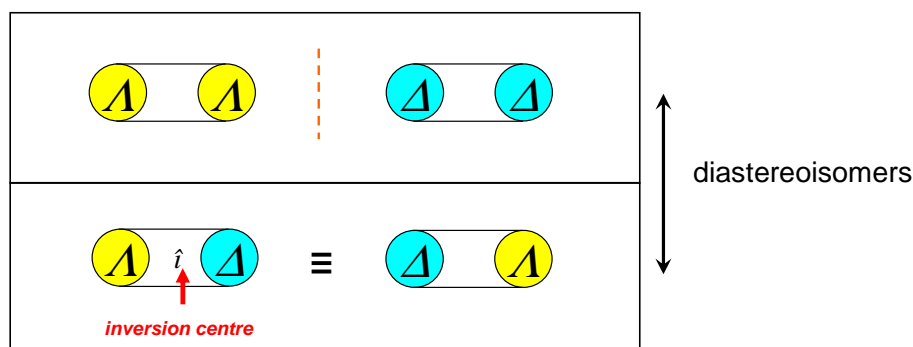


Figure 3.6-4. $^1\text{H NMR}$ spectra of a) *rac*-**66** as hexafluorophosphate salt; b) *rac*-**66** with approximately six equivalents of $[\text{Et}_4\text{N}][\Delta\text{-TRISPHAT}]$. Both spectra are recorded at 500 MHz in CD_2Cl_2 at 25 $^\circ\text{C}$.

The spectrum of the trinuclear complex **66** exhibits a similar pattern to that of the mononuclear complex **67**. Chemical shifts and coupling patterns are comparable. It seems to

be composed of a major component and a minor component in a 5:1 ratio. Once the counterion is replaced by enantiopure Δ -TRISPHAT, the proton spectrum appears to be more complex. Four different species are assumed to be distinguishable: ($[\Lambda\Lambda\Lambda\text{-66}][\Delta\text{-TRISPHAT}]$, $[\Delta\Delta\Delta\text{-66}][\Delta\text{-TRISPHAT}]$, $[\Lambda\Delta\Delta\text{-66}][\Delta\text{-TRISPHAT}]$ and $[\Delta\Delta\Lambda\text{-66}][\Delta\text{-TRISPHAT}]$). They will occur in different ratios. From the spectrum one cannot tell unambiguously how many compounds are present but there are more than two.

The dinuclear ruthenium(II) complex **65** has three isomers: The chiral $\Delta\Delta$ -form and $\Lambda\Lambda$ -form and the achiral $\Delta\Lambda$ -form. The latter is a *meso*-compound.^[177] The crucial property is that it contains an inversion centre that makes it achiral despite the fact that it possesses two asymmetric metal cores.^[98] Furthermore, the molecule and its mirror image are identical.^[178] The situation is depicted in Scheme 3.6-2. Only the homochiral form of the complex could be isolated, no treatment with TRISPHAT has been done to date.



Scheme 3.6-2. The three possible isomers of complex **65**.

3.7 Determination of Coordinated Sodium in 64 via Atomic Absorption Spectroscopy

Atomic absorption spectroscopy (AAS) and atomic emission spectroscopy (AES) are widely used in micro analyses^[179] and elements such as sodium, potassium, lithium and calcium, for example in biological liquids and tissues, are easily detected.

Most of the sodium atoms are in the ground state at room temperature.^[180] The valence electron occupies the 3s-orbital. Thermal excitation (heat of the flame) can cause a transition from the ground state to a higher energy level. As the transition back to a ground state occurs energy is emitted in form of a photon with the characteristic energy between the two energy levels. In the case of sodium, the transition from the 3p to the 3s-orbital can be detected at 589.0 nm and 589.6 nm. These wavelengths are also responsible for the typical yellow colour of sodium salts in a flame. The detection limit for sodium is lower in the case of flame atomic emission spectroscopy (0.1 ng/mL) than for atomic absorption spectroscopy (20 ng/mL).^[180, 181] That is the reason why the AES (atomic emission spectroscopy) is usually preferred for this element over AAS (atomic absorption spectroscopy).

Table 3.7-1. Standards with known concentration of sodium and calculated concentration of the sample.

solution	Concentration [μM]	absorption a. u.	Relative SD [%]
standard 1	2.0	0.0223	1.5
standard 2	3.0	0.034	1.3
standard 3	4.0	0.0481	0.54
standard 4	6.0	0.065	0.49
standard 5	10.0	0.1144	1.9
sample	4.46	0.0507	1.8

A calibration curve was obtained after measurement of three standard solutions containing exactly known concentrations (see Table 3.6-1 and Figure 3.6-1). For all measurements, the typical yellow colour of the flame was observed which indicated the presence of sodium.

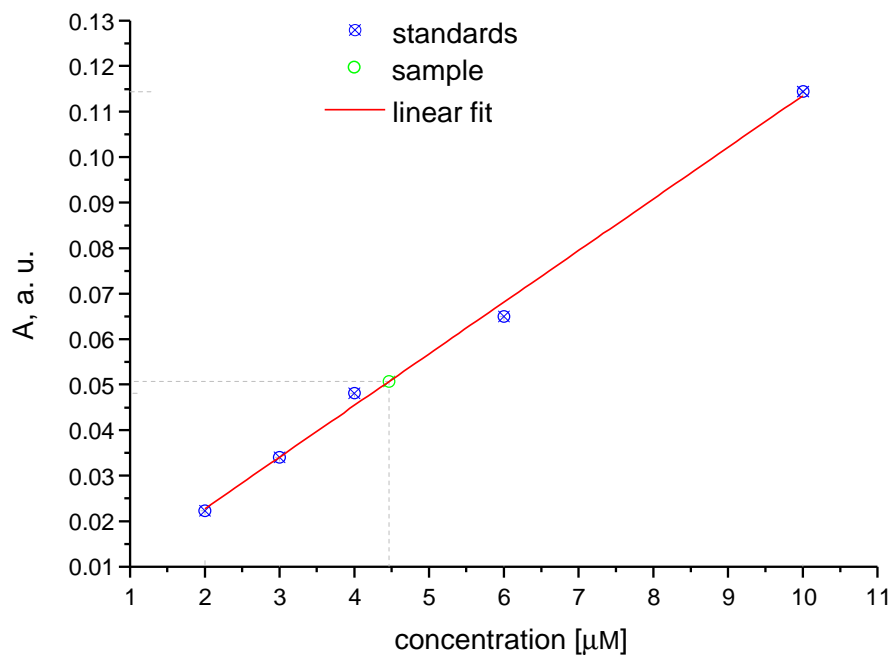


Figure 3.7-1. Linear calibration plot for standard solution and sample.

The sodium concentration was found to be $4.5 \mu\text{M}$ in the sample solution. Deduced from the weighed complex, the concentration compound **64** in the sample was $12.9 \mu\text{M}$. Therefore, roughly $(35\pm 10)\%$ of the molecules had a sodium cation coordinated to the ether chain in solution. This value is comparable to the results found in the crystal structure with 50% of the molecules containing sodium. The relative error was estimated from the standard error coming from the linear regression and the unknown nature of one third of the counterions (chloride was assumed).

A few more comments have to be made. The main question is how the sodium came to be in the complex if during its synthesis no sodium in the form of salts or any other form has been used. One explanation is that the aluminium oxide used for chromatography usually contains up to one gram sodium per kilogram. Another way to rationalize the appearance of the sodium is that the counterion hexafluorophosphate might decompose to fluoride and its conjugate acid, hydrofluoric acid, which is well known for its ability to dissolve glass. Common laboratory glassware such as borosilicate contains, for example, around 4% sodium oxide.

Trials to synthesise **64** without any extra coordinating sodium were unsuccessful. Either it was impossible to purify the compound solely over ultrapure silica gel or sodium, which is difficult to exclude completely, found its way to the molecule.

No matrix effects were considered, especially those coming from the ruthenium complex might interfere with the analyte. This can be avoided by utilizing the Standard Addition Method or the Internal Standard Method.^[180] Those methods have not been applied because of

the more demanding employment and only the nature of the coordinated species and the approximate amount of analyte were of interest.

3.8 Summary and Outlook

Three novel oligonuclear, macrocyclic ruthenium(II) complexes have been presented in this chapter. In contrast to well-known metallomacrocycles, the cycle is not formed by coordinative bonds but by covalent bonds. The complexes consist of bipyridine ligands and one ligand that is either a bidentate, tetradentate or hexadentate macrocycle leading to mononuclear (**64**), dinuclear (**65**) or trinuclear (**66**) complexes, respectively. The macrocyclic complex can be synthesised in two ways: reaction of a multitopic macrocyclic ligand with *cis*-[Ru(bpy)₂Cl₂] or direct ring-closing metathesis (RCM). The compounds could be comprehensively characterised and single crystals suitable for X-ray crystallography analysis were obtained for **67**, **64** and **65**. Cyclic voltammetry, absorption and emission spectroscopy revealed that the particular macrocyclic topology of these compounds hardly influence their physical properties. Molecules with more than one octahedral metal centre and bidentate ligands lead to a mixture of isomers. Diastereoisomers can often be separated chromatographically. It will be very interesting to synthesise these multinuclear complexes in an enantioselective synthesis providing only one of the possible diastereoisomers. Enantiopure Δ -[Ru(bpy)₂(py)₂]²⁺ can be prepared by a known procedure^[182] and could be used instead of racemic *cis*-[Ru(bpy)₂Cl₂] during the synthesis. The resulting complexes will be homochiral and optically pure.^[183]

4 Diversification of Ligand Families

The crystal field theory^[98] is a good model to describe colour, magnetism and other properties of transition metal complexes. The theory which was introduced by the physicists Bethe and van Vleck^[184] in the 1930s considers ligands to be negative point charges that surround a positively charged metal ion. In octahedral complexes, the negative charges are located on the six vertices and the electrons in the *d*-orbitals from the metal core experience repulsion. This leads to a splitting of the originally degenerate *d*-orbitals. Crystal field theory does not attempt to describe bonding. Crystal field theory and molecular orbital theory were then combined to ligand field theory which gives more insight into chemical bonding in metal complexes.

The stability of complexes is not only governed by electronic factors but also by steric interactions.

4.1 Introduction

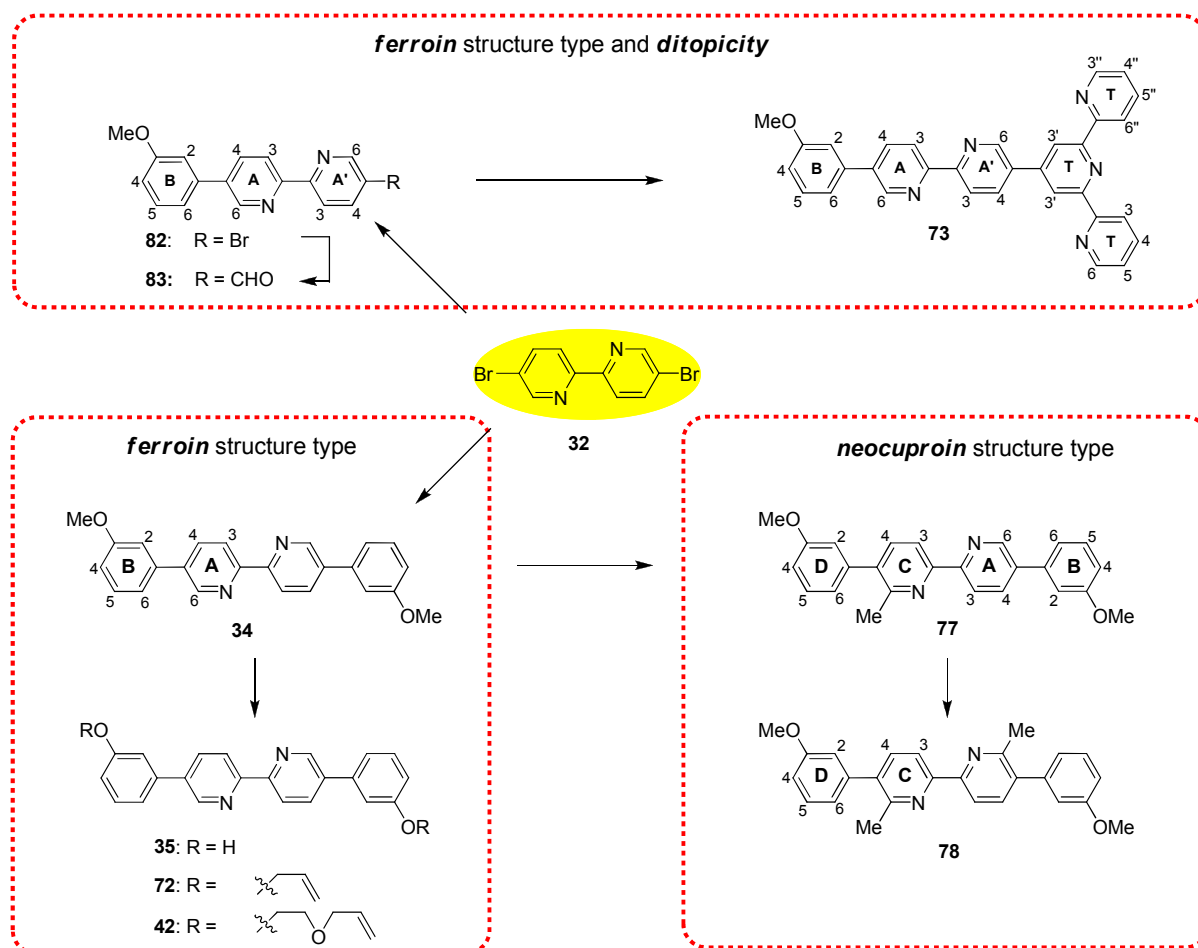
Diaryl-functionalized 2,2'-bipyridines (bpy), 1,10-phenanthrolines (phen) and 2,2':6',2''-terpyridines (tpy) are commonly utilized scaffolds in metallosupramolecular chemistry. The aryl groups bear substituents which can be further elaborated or which contain desired functionalities and the metal-binding domain provides the recognition features for interaction with specific metal centres. The development of the metal-ion templated synthesis of catenanes, knots and other topologically complex systems^[77] was predicted on the organization of 6,6'-disubstituted bpy (or 2,9-disubstituted phen) ligands about tetrahedral copper(I) or silver(I) centres. Although the substituents adjacent to the nitrogen (*neocuproin* structure type) are critical for the stability of copper(I) complexes,^[185] formation of stable complexes with octahedral metal centres requires that the aryl substituents are attached to other positions (*ferroin* structure type). The synthesis of families of ligands with neocuproin or ferroin metal-binding domains is time-consuming and strategies have been developed for the direct conversion of ferroin metal-binding domains to the neocuproin type.

Ligands **35** and **34** (Scheme 4.2-1) have been previously reported,^[95] and the complexation of **35** with silver(I).^[186] Ligand **35** was also used as a building block for the formation of a heterotopic ligand in which the central bpy domain is linked by polyethyleneoxy spacers to two 2,2':6',2'' terpyridine (tpy) units. The flexibility of this ligand permits the binding of iron(II) and formation of a [1+1] ferramacrocycle.^[187] Apart from these studies, the

complexation of **35** and **34** remains unexplored. Heteroditopic bpy-tpy ligands^[188-195] are versatile building blocks in supramolecular chemistry, as they can behave as switches or tuners if one coordination site is transformed into a chromophore and the other coordination side is free (e. g. for coordination to a metal), and they can act as bridging ligands for multinuclear assemblies with different metals in different coordination environments. A convergent synthesis of a heptaruthenium metallostar with a heteroditopic ligand was reported.^[190] Photophysical and electrochemical properties were investigated on multinuclear assemblies^[188-190, 195] bridged by heteroditopic ligands. Electronic communication (energy transfer) was observed in some examples.

4.2 Aims and Overview

In this chapter, the formation of two ligands, **72** and **42** (Scheme 4.2-1) is described. They possess terminal alkene functionalities that are ideally suited to Grubbs' coupling and the assembly of polymeric or macrocyclic species. The diversity in coordination space has been extended beyond commonly studied 1 : 2 tetrahedral and 1 : 3 octahedral species to 1 : 2 square planar metal centres, and the preparation and characterisation of palladium(II) complexes of ligands **34**, **72** and **42** is described. Proof-of-principle conversion of **34** to ligands containing substituents adjacent to the nitrogen donors and the air-stable copper(I) complexes of these new ligands is described. The interconversion to the heteroditopic ligand **73** that bears bipyridine and terpyridine binding sides is presented.



Scheme 4.2-1. Diversification of ligand families to ferrioxalene structure type ligands, neocuproin structure type ligands or ferrioxalene structure type ditopic ligands.

4.3 Results and Discussion

Ligands for palladium(II) complexes

Ligands **72** and **42** were prepared using caesium-directed Williamson's methodology by treating **35** with allyl bromide or 3-(2-bromoethoxy)prop-1-ene, respectively, in the presence of Cs₂CO₃ in DMF. For **72**, the reaction was carried out in a microwave reactor at 100 °C and was complete in less than an hour. For **42**, the reaction mixture was heated at 120 °C for 4 days. Both ligands were obtained in high yield. The EI mass spectrum of each compound exhibited a parent ion ($m/z = 421.2$ for **72** and 508.2 for **42**), and the appearance of the solution ¹H and ¹³C NMR spectra of **72** and **42** confirmed the formation of symmetrical ligands. The spectra have been assigned using COSY, DEPT, HMQC and HMBC techniques. With the exception of the appearance of signals for the additional methylene groups in **42**, the ¹H NMR spectra for **72** and **42** are almost identical, as are their ¹³C NMR spectra. However, whereas in **72**, the signals for protons H^{B2} and H^{B6} (Scheme 4.2-1) appear at δ 7.14 and 7.18 ppm, in **42**, they overlap at δ 7.29 ppm. Since the ¹³C NMR spectroscopic signatures for the aromatic domain of the two ligands are virtually superimposable, the assignments of signals for C^{B2} and C^{B6} in **42** have been made by comparison with those of **72**, assigned from the HMQC spectrum.

Palladium(II) complexes: synthesis and solution characterisation

The reaction of [Pd(CH₃CN)₄][BF₄]₂ with two equivalents of ligand **34** in CH₃CN produced analytically pure [Pd(**34**)₂][BF₄]₂ as a yellow solid. The highest mass peaks in the FAB mass spectrum came at $m/z = 861.1$ and 842.1, and were assigned to [Pd(**34**)₂+F]⁺ and [Pd(**34**)₂]⁺, respectively. Fragmentation by ligand loss was also observed. The complex was poorly soluble in most common solvents, and the NMR spectra were recorded in DMSO-*d*₆. Compared to signals for the free ligand in DMSO-*d*₆, the most diagnostic indication of complex formation is the large shift to higher frequency for the signal for bpy proton H^{A4}. This presumably reflects the fact that in the square planar Pd(II) environment, the presence of the methoxy substituents restricts rotation about the C_{py}-C_{Ph} bond, and the aryl ring twists out of the plane of the bpy unit (this is confirmed in the crystal structures of ligand and complex described below). The bpy protons most affected by this will be those facing the aryl π -cloud, i.e. H^{A4} and H^{A6} (Figure 4.3-1). As Figure 4.3-1 shows, the peaks for the bpy unit are rather

broad compared to those of the free ligand in the same solvent. Addition of free ligand to an NMR sample of $[\text{Pd}(\mathbf{34})_2][\text{BF}_4]_2$ resulted in further broadening of the signal assigned to $\text{H}^{\text{A3+A4}}$ as well as broadening of the resonance for H^{B4} and loss of resolution for the signals for $\text{H}^{\text{B2+B6/HB5}}$. In spectra recorded for $[\text{Pd}(\mathbf{34})_2][\text{BF}_4]_2$ plus one and a half equivalents of ligand, no signals arising from the free ligand were observed. This observation is consistent with that observed by Milani *et al.*, in the DMSO- d_6 solution ^1H -NMR spectrum of $[\text{Pd}(\text{bpy})_2][\text{PF}_6]_2$, indicating that exchange occurs between free and coordinated ligand on the NMR spectroscopic timescale.^[196]

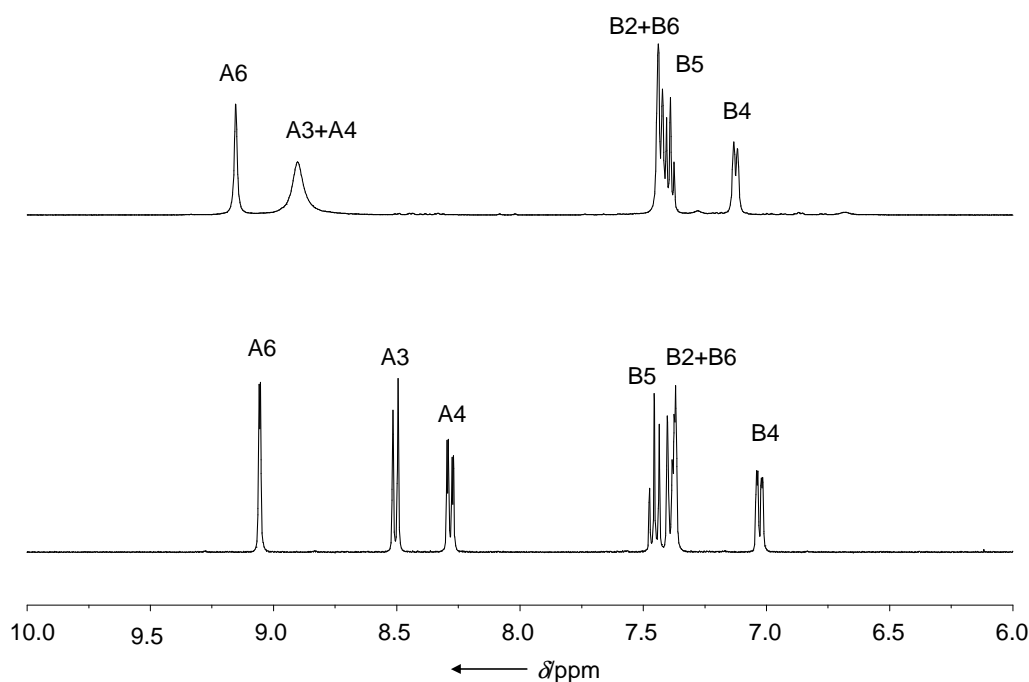


Figure 4.3-1. 500 MHz NMR spectra of DMSO- d_6 solutions of $[\text{Pd}(\mathbf{34})_2][\text{BF}_4]_2$ (TOP) and ligand **34** (BOTTOM).

*Structural characterisation of $[\text{Pd}(\mathbf{34})_2][\text{BF}_4]_2$ (**74**)*

A solution of analytically pure $[\text{Pd}(\mathbf{34})_2][\text{BF}_4]_2$ (**74**) in a mixture of DMF and Et_2O in a vial surrounded by Et_2O was left at 4 °C for several weeks after which time, X-ray quality yellow plates had grown. Interestingly, the complex co-crystallized with the free ligand (which must have originated from the complex) and the single crystal structure of $[\text{Pd}(\mathbf{34})_2][\text{BF}_4]_2 \cdot \mathbf{34}$ determined. Figures 4.3-2a and 4.3-2b show the centrosymmetric structures of the $[\text{Pd}(\mathbf{34})_2]^{2+}$ cation and ligand **34**, respectively. Bond distances and angles within the bpy and phenyl rings are unexceptional. As expected, the free ligand adopts a *transoid* conformation, but flips to a *cisoid* arrangement upon binding to palladium(II). The C–O bond distances and C–O–C bond angles in both ligand and complex (see figure caption) are consistent with delocalization of π -

character from phenyl ring to the oxygen atom. Two features of the structure deserve note: the ligand distortion in $[\text{Pd}(\mathbf{34})_2]^{2+}$, and the packing. In $[\text{M}(\text{bpy})_2]^{n+}$ complexes and in the absence of electronic factors (i.e. crystal field stabilisation energy), the metal ion is typically in a tetrahedral environment. However, a square planar environment is preferred for a d^8 metal centre such as palladium(II) or platinum(II). In such a bis(bpy) complex, steric interactions between the H^6 protons on adjacent ligands lead to one of the two types of distortion illustrated in Scheme 4.3-1.^[197] A search of the Cambridge Structural Database (v. 5.30)^[198] using Conquest11^[199] revealed 24 structures containing either a $[\text{Pd}(\text{bpy})_2]^{2+}$ or $[\text{Pt}(\text{bpy})_2]^{2+}$ motif, including substituted derivatives and $[\text{M}(\text{phen})_2]^{2+}$ (phen = 1,10-phenanthroline).^[200-217] Excluded from this set are compounds in which adjacent bpy domains are connected directly^[69, 218, 219] or indirectly through the 6-positions. Of the 24 structures, twelve distort at the metal centre (distortion A in Scheme 4.3-1) and twelve undergo ligand distortion (B in Scheme 4.3-1, the so called 'bow-incline' distortion). These distortions have been discussed in detail by Marzilli,^[214] but with a sample size of only six complexes. In $[\text{Pd}(\mathbf{34})_2]^{2+}$, $\text{H}^6 \dots \text{H}^6$ repulsions are relieved by ligand distortion B as shown in Figure 4.3-2b.

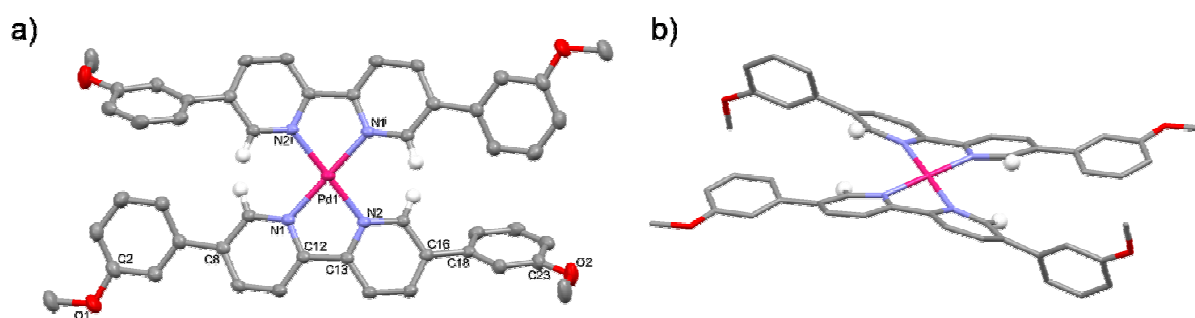
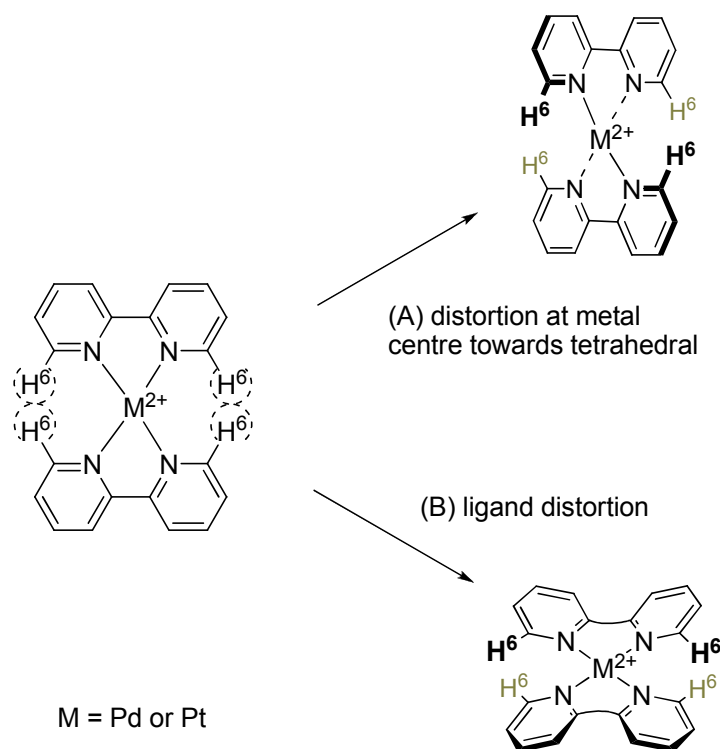


Figure 4.3-2. a) Molecular structure of the $[\text{Pd}(\mathbf{34})_2]^{2+}$ cation in $[\text{Pd}(\mathbf{34})_2][\text{BF}_4]_2 \cdot \mathbf{34}$ with ellipsoids plotted at 50% probability level; b) Distortions of the bpy units alleviates steric hindrance between H^6 protons. Counterions and hydrogen atoms except for H^6 have been omitted for clarity.



Scheme 4.3-1. Modes of distortion in $[\text{Pd}(\text{bpy})_2]^{2+}$, $[\text{Pt}(\text{bpy})_2]^{2+}$ and related cations.

In ligand **34** (Figure 4.3-3), the bpy unit is planar, and the phenyl substituent is twisted $23.44(9)^\circ$ with respect to this plane. This compares to $32.2(6)^\circ$ and $32.4(6)^\circ$ in the two independent molecules of **34** in the previously determined structure of the ligand alone. In $[\text{Pd}(\mathbf{34})_2][\text{BF}_4]_2 \cdot \mathbf{34}$ the MeO group is oriented on the side opposite the N atom of the adjacent pyridine ring (Figure 4.3-3), whereas in the previous structure of **34**, it lies on the same side of the molecule as the N atom. This difference probably originates from packing effects. In **34**, molecules interact through weak C–H_{methyl}...O hydrogen bonds to form interconnected, undulating chains; offset face-to-face π -stacking occurs between adjacent bpy domains and between adjacent phenyl rings. In $[\text{Pd}(\mathbf{34})_2][\text{BF}_4]_2 \cdot \mathbf{34}$, ligands and $[\text{Pd}(\mathbf{34})_2]^{2+}$ cations are interleaved to form stacks with the pyridine ring containing atom N1 in $[\text{Pd}(\mathbf{34})_2]^{2+}$ is π -stacked over the bpy unit of the free ligand at a distance of 333 pm. The stacks are connected by non-classical hydrogen bonds between atom O3 of the free ligand and C24H241 of a methyl group of the $[\text{Pd}(\mathbf{34})_2]^{2+}$ cation (C24H241...O3i = 250 pm, C24...O3i 325.8(2) pm, C24–H241...O3i = 135° , symmetry code $i = -1 + x, 1 + y, -1 + z$) (Figure 4.3-4).

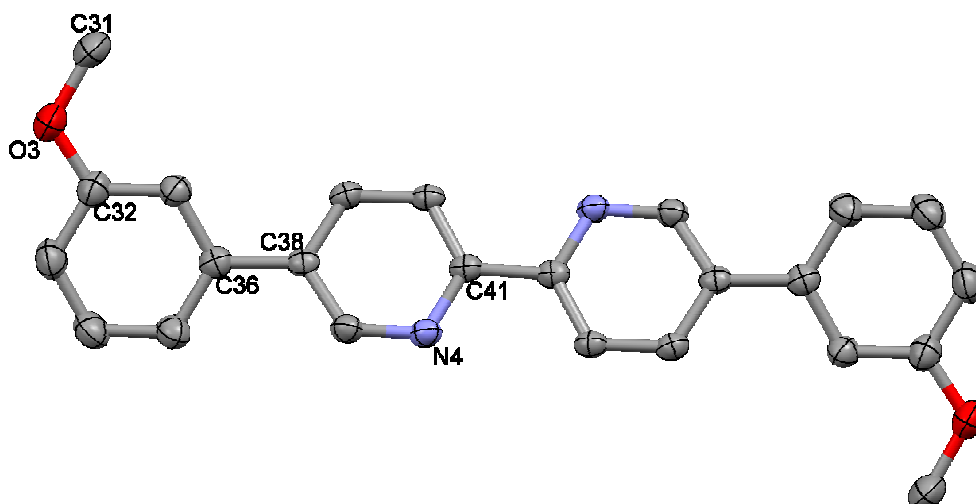
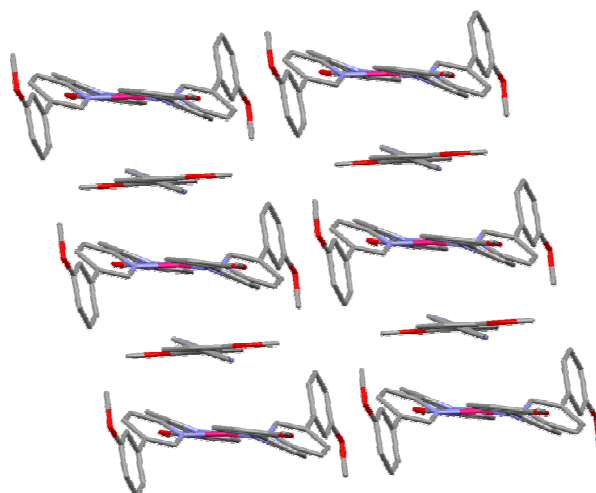


Figure 4.3-3. a) Molecular structure of the **34** in $[\text{Pd}(\mathbf{34})_2][\text{BF}_4]_2 \cdot \mathbf{34}$ with ellipsoids plotted at 50% probability level. Counterions and hydrogen atoms have been omitted for clarity.

a)



b)

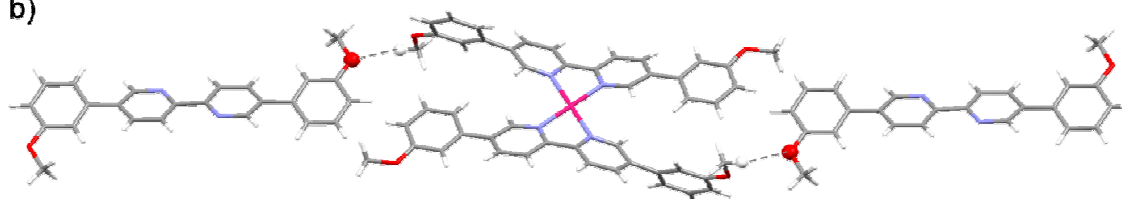


Figure 4.3-4. a) Stacking of $[\text{Pd}(\mathbf{34})_2]^{2+}$ cations and ligand **34** in $[\text{Pd}(\mathbf{34})_2][\text{BF}_4]_2 \cdot \mathbf{34}$. b) Hydrogen bonding between free ligands and cations (see text).

The reaction of $[\text{Pd}(\text{CH}_3\text{CN})_4][\text{BF}_4]_2$ with two equivalents of either **72** or **42** resulted in the formation of $[\text{Pd}(\mathbf{72})_2][\text{BF}_4]_2$ (**75**) or $[\text{Pd}(\mathbf{42})_2][\text{BF}_4]_2$ (**76**), respectively, each isolated as a yellow solid. The two complexes were characterised by NMR spectroscopic and mass spectrometric methods, and by elemental analysis. A comparison of the $^1\text{H-NMR}$ spectrum of

acetone- d_6 solutions of ligand **72** and of the palladium(II) complex showed that the most significant changes were in the chemical shifts of the signals (assigned by 2D techniques) arising from protons H^{A4} (δ 9.00 to 9.33 ppm) and H^{A6} (δ 8.21 to 8.86 ppm), consistent with the formation of a square planar palladium(II) complex (see earlier discussion). A comparison of the 1H -NMR spectra of **42** and $[Pd(\mathbf{42})_2][BF_4]_2$ was made using $CD_3CN/CDCl_3$ solutions of the compounds, and the change in the chemical shift of proton H^{A4} (δ 8.03 to 8.46 ppm) was indicative of coordination. Attempts to grow X-ray quality crystals of $[Pd(\mathbf{72})_2][BF_4]_2$ and $[Pd(\mathbf{42})_2][BF_4]_2$ were unsuccessful. Our interest in these complexes is the reactivity of the terminal alkene functionalities. Applications of Grubbs' catalysts to the formation of macrocyclic species have included the formation of macrocycles, catenanes and knots templated within a metal coordination sphere.^[46, 79, 220-222] Molecular modelling indicated that in both $[Pd(\mathbf{72})_2]^{2+}$ and $[Pd(\mathbf{42})_2]^{2+}$, the terminal alkene chains are long enough to permit ring-closing metathesis with concomitant formation of a palladium(II)-bound macrocyclic ligand. However, attempts at ring closure were unsuccessful with either first generation Grubbs' or Hoveyda-Grubbs' catalysts in CH_2Cl_2 or CH_3NO_2 at room temperature or reflux, and also under microwave heating conditions. In each case, the 1H -NMR spectrum of the crude mixture indicated no signs of the formation of a new double bond. The 1H -NMR spectrum of the crude mixture showed the presence of the unreacted palladium(II) complex. The problem lies probably in the lability of the palladium(II) complexes which release free ligands capable of poisoning the catalyst. Although ruthenium carbene catalysts exhibit an exceptional tolerance towards many functional groups, catalyst inhibition by complex-formation involving the reagents is known to be problematical.^[140, 223]

The ferrocene-cuproin interconversion

In order to broaden the scope of our investigation of 4-coordinate complexes with ligands related to **34**, the attention was turned to the preparation of copper(I) complexes. The crucial factor for the isolation of air-stable complexes containing an $[Cu(bpy)_2]^+$ core is the presence of substituents in the 6- and 6'-positions.^[185] The syntheses of ligands **77** and **78**, and their reactions with copper(I) are described below.

Ligand **77** was prepared by methylation of **34** using MeLi adapting the procedure reported for the methylation of 1,10-phenanthrolines and 2,2'-bipyridines.^[8, 224, 225] The optimum yield of **77** (82%) was obtained when MeLi (one equivalent) was added at -78 °C, and the reaction then carried out at room temperature followed by a period of heating. After quenching the reaction with water, oxidation with MnO_2 resulted in the formation of **77**. Ligand **78** was

subsequently synthesised by methylation of **77**. Attempts to prepare **78** directly by the reaction of **34** with two or more equivalents of MeLi were unsuccessful. The highest mass peak in the ESI MS of each ligand corresponded to the parent ion. The symmetrical appearance of the ^1H and ^{13}C -NMR spectra of **78** was consistent with methylation at both the 6- and 6'-positions, and this is confirmed by the disappearance of the signal assigned to H^{A6} on going from **34** to **78** (Figures 4.3-5a and 4.3-5b). Figures 4.3-5c and 4.3-5d also illustrate that the introduction of the methyl substituents causes the signals for the remaining bpy protons and the *ortho*-protons of the phenyl substituent (H^{D2} and H^{D6}) to shift to a lower frequency. This can be rationalized in terms of a change in the relative orientations of pyridine and aryl rings (see structural details below) which results in the ring protons lying over the π -cloud of the adjacent ring. The resonances for the aryl protons remote from the bpy unit and for the methoxy protons are only slightly affected by methylation. The ^1H -NMR spectrum of **80** (Figure 4.3-5c) is readily assigned by comparison with those of **34** and **78** (Figures 4.3-5), and the assignments have been confirmed by 2D techniques.

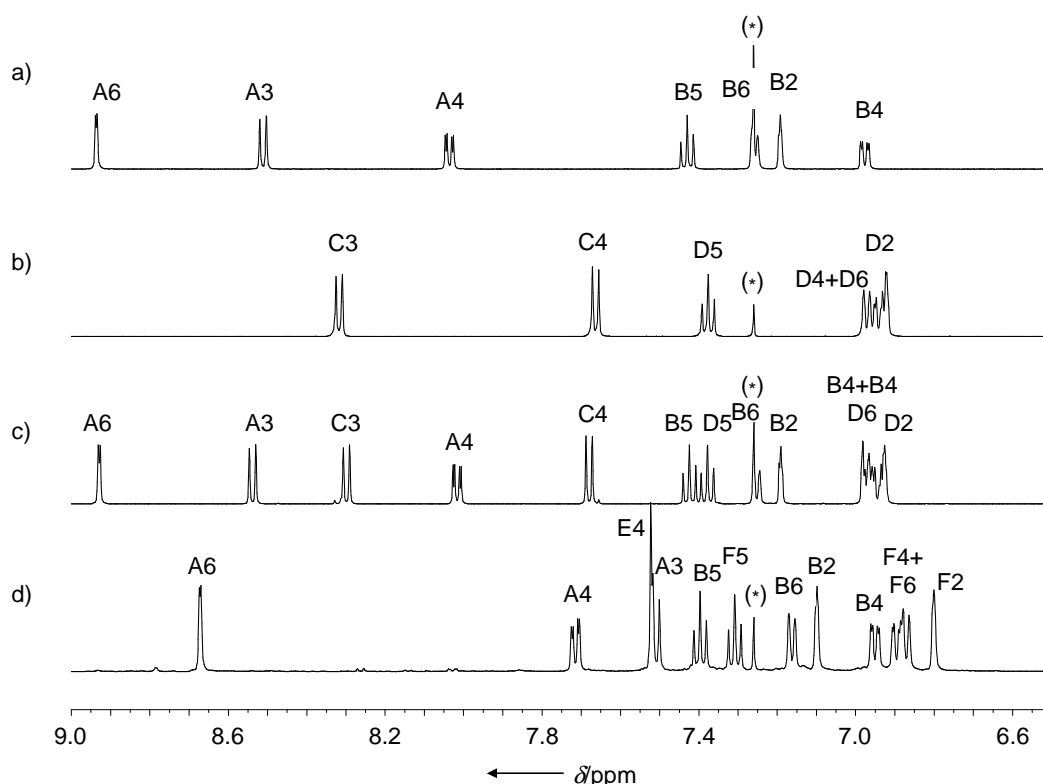


Figure 4.3-5. Room temperature 500 MHz NMR spectra of CDCl_3 solutions of a) **34**; b) **78**; c) **77**; d) **79**. Asterisks mark the residual CHCl_3 . Proton labelling is given in Scheme 4.2-1 and Scheme 4.3-3.

Single crystals of **78** were grown by slow evaporation of a CDCl_3 solution of the ligand. The centrosymmetric molecular structure of **78** is shown in Figure 4.3-6. The plane of the aryl substituent deviates $55.16(6)^\circ$ from the plane of the bpy unit, and so, as expected, 6,6'-dimethyl substitution results in a significantly greater twist of the 3-anisyl groups than is observed in **34** (Figure 4.3-3). This deviation affects the way in which the molecules are able to pack. In **34**, π -stacking is important, whereas in **78**, there is no analogous stacking, and the molecules pack so that each 6-methyl or 6'-methyl substituent points obliquely towards a pyridine ring on an adjacent molecule.

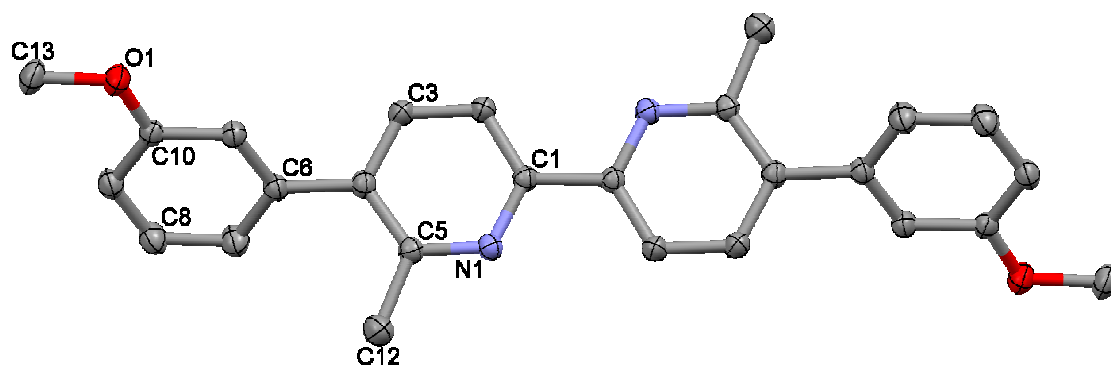
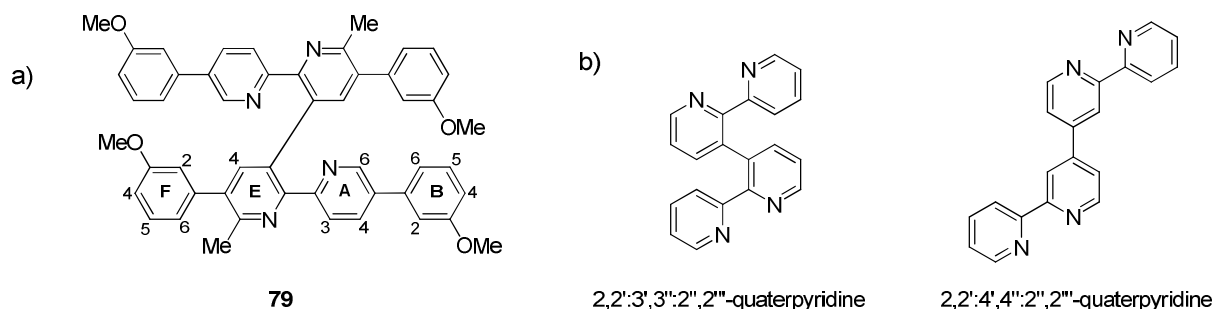


Figure 4.3-6. Molecular structure of **78** with ellipsoids plotted at 50% probability level. Hydrogen atoms have been omitted for clarity.

In our initial attempts to synthesise the monomethyl derivative **77**, one equivalent of MeLi was added to **34** at room temperature. After quenching the reaction in water, and oxidation of the intermediate using MnO_2 , spot thin layer chromatography showed the presence of two products. These colourless compounds were separated by column chromatography, and the first fraction was identified as **77**. The highest mass peak in the ESI MS of the second product, **79**, was observed at $m/z = 763.4$ (i.e. approximately twice the molecular mass of **77**). The CDCl_3 solution ^1H NMR spectrum of **79** showed the presence of two MeO signals (δ 3.81 and 3.72 ppm, relative integrals 1 : 1), both shifted to lower frequency with respect to those in **77** (δ 3.88 and 3.84 ppm). A singlet at δ 2.62 ppm (relative integral with respect to each OMe = 1 : 1) replicated that in **77**. Figure 4.3-5d shows the aromatic region of the ^1H NMR spectrum of **79** (see Scheme 4.3-2 for atom labelling).

Crucial observations that aid identification of **79** are a similarity between the phenyl regions of the spectra of **77** and **78**, the appearance of a singlet at δ 7.54 ppm, significant changes in the chemical shifts of signals for the bpy protons, and the loss of one bpy signal with respect to the number of resonances in **77**. A comparison of the ^{13}C and DEPT NMR spectra revealed the presence of ten quaternary ^{13}C nuclei in **79** compared to nine in **77**. The NMR and ESI

MS data are consistent with C–C bond formation between two bpy units of **77** to produce **79**. The equivalence of the bpy units deduced from the ^1H and ^{13}C NMR spectra gave two possibilities: the formation of a tetramethoxyphenyl derivative of 2,2':3',3":2",2"'- or 2,2':4',4":2",2"'-quaterpyridine (Scheme 4.3-2). The singlet in the ^1H -NMR spectrum can be assigned to either $\text{H}^{\text{E}3}$ or $\text{H}^{\text{E}4}$, and the appearance in the NOESY spectrum of a cross peak from this singlet to the signal for $\text{H}^{\text{F}2}$ confirms an assignment of $\text{H}^{\text{E}4}$. Single crystals of **79** were not forthcoming. To date, attempts at metal complexation using **79** have been unsuccessful.



Scheme 4.3-2. a) Compound **79**; b) structures of two isomers of quaterpyridine.

Treatment of $[\text{Cu}(\text{NCMe})_4][\text{PF}_6]$ with either ligand **77** or **78** led to the formation of red $[\text{Cu}(\text{77})_2][\text{PF}_6]$ (**80**) or $[\text{Cu}(\text{78})_2][\text{PF}_6]$ (**81**), respectively. The highest mass peaks in the ESI mass spectra of the products were assigned to $[\text{M}-\text{PF}_6]^+$ in each case, with isotope distributions matching those calculated. The diagnostic changes in the ^1H -NMR spectrum on going from **77** (in CDCl_3) to $[\text{Cu}(\text{77})_2]^+$ (in CD_3CN) involve the signals for protons $\text{H}^{\text{A}4}$ and $\text{H}^{\text{C}4}$. Both signals are shifted to higher frequency (δ 8.00 to 8.24 ppm for $\text{H}^{\text{A}4}$, and δ 7.66 to 7.83 ppm for $\text{H}^{\text{C}4}$), while the remaining signals are little affected. Similarly, on going from **78** to $[\text{Cu}(\text{78})_2]^+$, the signal assigned to $\text{H}^{\text{C}4}$ is the only resonance to undergo significant perturbation (δ 7.64 to 7.98 ppm). This mirrors the effects described earlier for coordination of ligands **34** and **72** to palladium(II).

Crystals of $[\text{Cu}(\text{77})_2][\text{PF}_6] \cdot 0.1\text{C}_2\text{H}_4\text{Cl}_2 \cdot 0.15\text{CH}_2\text{Cl}_2$ of X-ray quality were grown by slow vapour diffusion of Et_2O to a mixture of CH_2Cl_2 and $\text{C}_2\text{H}_4\text{Cl}_2$ containing $[\text{Cu}(\text{77})_2][\text{PF}_6]$. Figure 4.3-7 depicts the structure of the $[\text{Cu}(\text{77})_2]^+$ cation. The structure suffers from disorders in the cation, anion and solvent molecules. In the cation, the methyl group of one ligand is disordered over two sites modelled with 70% (atom C50 in Figure 4.3-7) and 30%

occupancies. In the other ligand, one methoxyphenyl unit (the one containing atom O11, Figure 4.3-7) is disordered and has been modelled over two sites with 70/30% occupancies. Despite the problems associated with the structure, it confirms that the coordination geometry of the copper(I) centre approaches tetrahedral (angle between the least squares planes of the two bpy domains = $70.0(1)^\circ$). In the ligand containing atoms N1 and N2, the phenyl ring containing atom C21 is approximately coplanar with the bpy rings (angles between the least squares planes of the rings = $6.5(2)$ and $11.9(5)^\circ$), while the second phenyl ring is twisted through $67.7(2)^\circ$ with respect to the bpy unit. The coplanar rings are π -stacked with those of adjacent cations (alternating distances between least squares planes = 349 pm and 366 pm). Extensive C–H_{phenyl}...O, C–H_{methyl}...O and C–H_{bpy}...F hydrogen bonding contribute to the solid state packing.

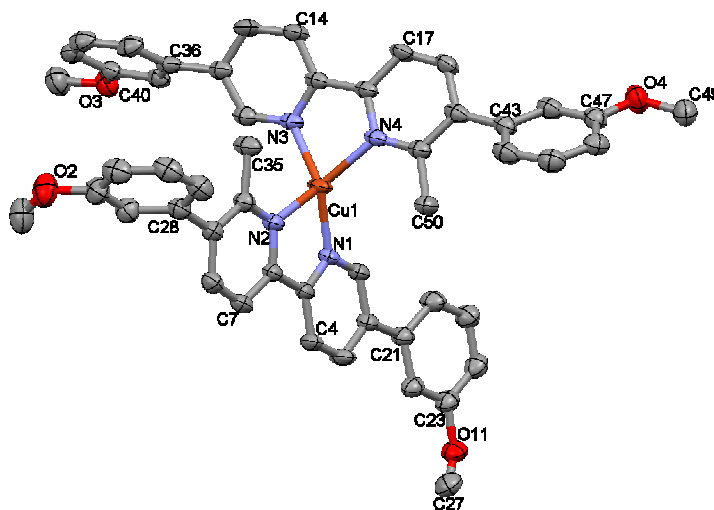
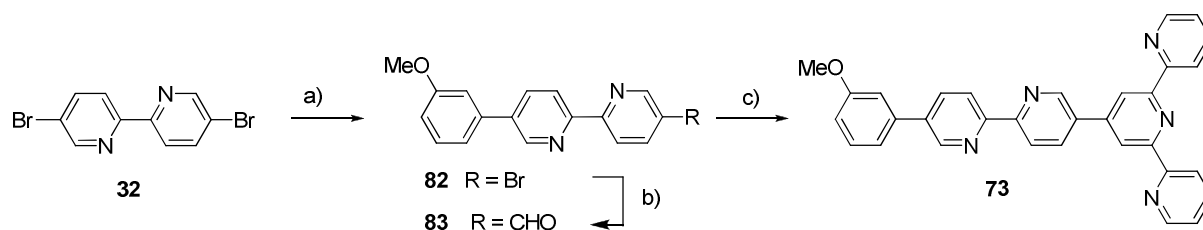


Figure 4.3-7. a) Molecular structure of the $[\text{Cu}(\mathbf{77})_2]^+$ ($\mathbf{80}^+$) cation in $[\text{Cu}(\mathbf{77})_2][\text{PF}_6] \cdot 0.1\text{C}_2\text{H}_4\text{Cl}_2 \cdot 0.15\text{CH}_2\text{Cl}_2$ with ellipsoids plotted at 30% probability level. Counterions and hydrogen atoms have been omitted for clarity. For disordered sites (see text), only the major occupancy atoms are shown.

The interconversion towards the heteroditopic bpy-tpy ligand 73

5-Bromo-5'-(3-methoxyphenyl)-2,2'-bipyridine (**82**) was prepared in a statistical Suzuki coupling reaction by reacting the dibromo compound **32** with roughly one equivalent of 3-methoxyphenylboronic acid in the presence of a palladium catalyst under biphasic conditions. Unreacted starting material (**32**) and the disubstituted compound **34** were removed as side products via column chromatography on silica gel. Treatment of **82** with *n*-butyllithium initiated halogen-metal exchange and addition of excess DMF and aqueous work-up produced

aldehyde **83** in moderate yield. The bpy-tpy ligand **73** was synthesised following a known procedure^[189] by reacting aldehyde **83** with 2-acetyl pyridine in the presence of potassium hydroxide and ammonia in ethanol at 50 °C for 30 min. The ligand was obtained in 26% yield. The EI mass spectrum for each compound exhibited a parent ion ($m/z = 340.0$ for **82**, 290.1 for **83**, 493.2 for **73**) and ¹H and ¹³C-NMR spectra confirmed the formation of the compounds. The spectra have been assigned using COSY, DEPT, HMQC and HMBC techniques.



Scheme 4.3-3. Reagents and conditions: a) 3-methoxyphenylboronic acid (0.93 eq), [Pd(PPh₃)₄] (2.7 mol%), Na₂CO₃ (5 eq), toluene/H₂O, reflux, 20h, 40%; b) *n*-butyllithium (1.05 eq), DMF (20 eq), toluene, -78 °C, then H₂O, r.t., 29%; c) 2-acetyl pyridine (2.2 eq), KOH (2.2 eq), NH₃, EtOH, 50 °C, 26%.

Figure 4.3-8 shows the ¹H-NMR spectrum of the heteroditopic ligand **73** along with assignments.

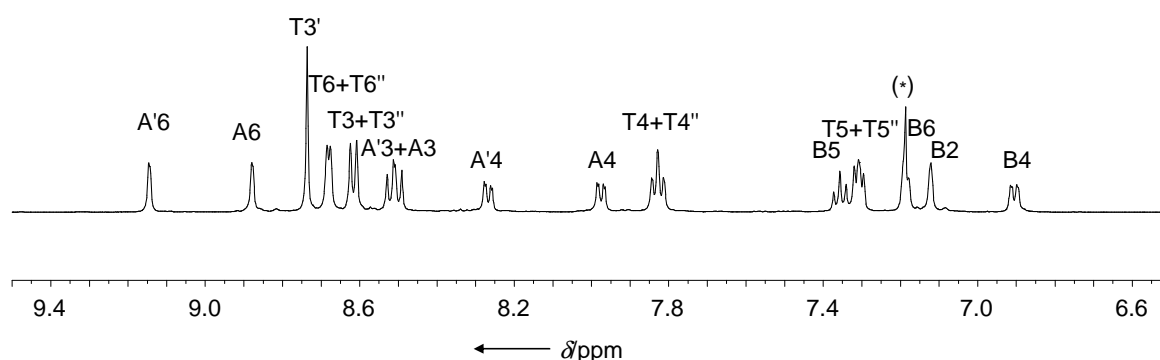


Figure 4.3-8. Room temperature 500 MHz NMR spectrum of CDCl₃ solution of **73**. The asterisk marks the residual CHCl₃. Proton labelling is given in Scheme 4.2-1.

Single crystals of **73** were grown by slow evaporation of a CDCl₃ solution of the ligand. The molecular structure with *transoid* conformation around the bipyridine and the terpyridine units is shown in Figure 4.3-9.

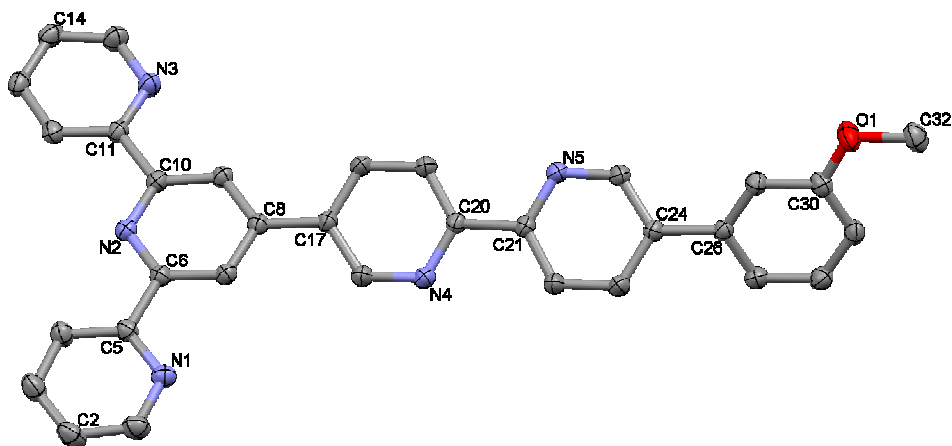


Figure 4.3-9. Molecular structure of **73**. Hydrogen atoms have been omitted for clarity.

The arrangement of molecules of **73** in the solid state is depicted in Figure 4.3-10. The molecules exhibit parallel displaced π -stacking over tpy domains. Adjacent molecules with the same spatial arrangement form stacks at a distance of 329 pm and adjacent molecules with opposite spatial arrangement stack at a distance of 335 pm (see Figure 4.3-10b). The distances were determined from the parallel least square planes of the tpy units.

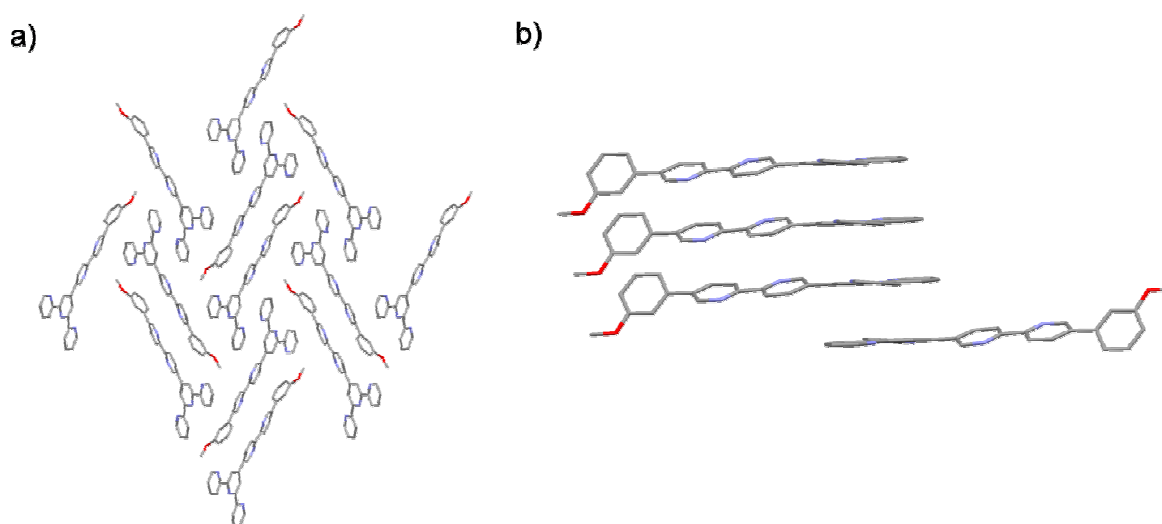


Figure 4.3-10. a) View in packing along the crystallographic a-axis; b) π -stacking between adjacent tpy domains.

4.4 Summary

The preparation of two ligands, **72** and **42**, which possess bpy domains terminated in alkene functionalities and the syntheses and characterisation of $[\text{Pd}(\mathbf{72})_2][\text{BF}_4]_2$ and $[\text{Pd}(\mathbf{42})_2][\text{BF}_4]_2$ have been described. For the related complex $[\text{Pd}(\mathbf{34})_2][\text{BF}_4]_2$ in which **34** is 5,5'-bis(3-methoxyphenyl)-2,2'-bipyridine, the labile nature of the complex leads to co-crystallization with free ligand to give $[\text{Pd}(\mathbf{34})_2][\text{BF}_4]_2 \cdot \mathbf{34}$. Rather than undergoing distortion the coordination sphere towards a tetrahedral geometry, the $\text{H}^6 \dots \text{H}^6$ repulsions between the two bpy domains in $[\text{Pd}(\mathbf{34})_2]^{2+}$ are alleviated by a “bow-incline” distortion, within each ligand. Compound **34** has been converted to 5,5'-bis(3-methoxyphenyl)-6-methyl-2,2'-bipyridine (**77**) and 5,5'-bis(3-methoxyphenyl)-6,6'-dimethyl-2,2'-bipyridine (**78**) to produce ligands capable of forming air-stable copper(I) complexes. The syntheses of $[\text{Cu}(\mathbf{77})_2][\text{PF}_6]$ and $[\text{Cu}(\mathbf{78})_2][\text{PF}_6]$ and crystal structures of **78** and $[\text{Cu}(\mathbf{77})_2][\text{PF}_6] \cdot 0.1\text{C}_2\text{H}_4\text{Cl}_2 \cdot 0.15\text{CH}_2\text{Cl}_2$ have been described. By altering the conditions under which **34** is methylated, competitive formation of 5,5',5'',5'''-tetrakis(3-methoxyphenyl)-2,2':3',3'':2'',2'''-quaterpyridine (**79**) occurs. The preparation of heteroditopic ligand **73** and its crystal structure have been described.

5 Complexes of $[\text{Ru}(\text{bpy})_3]^{2+}$ -type bearing Pyrene Moieties

Photosynthesis^[226] is one the most crucial biological processes on Earth, since it provides oxygen which is essential for most living creatures. It is a process used by plants, algae, and many species of bacteria to reduce carbon dioxide and fix it into biomass. The energy needed for this process comes from sunlight that is absorbed by proteins called photosynthetic reaction centres containing chlorophyll. Leaves appear green because they contain chlorophyll, a green pigment common to all photosynthetic cells. Chlorophyll molecules absorb visible light of all wavelengths except green, and this is responsible for the green colour perception to our eyes. Photosynthesis can be regarded as the opposite of cellular respiration, where glucose is converted and carbon dioxide and water and energy is released.

5.1 Introduction

Excimers

An excimer^[227] (originally short for *excited dimer*) is a dimer formed from two molecular species, at least one of which is in an electronic excited state. The lifetime of an excimer is usually very short. The aromatic excimer of pyrene (Figure 5.1-1) was first observed by Förster and Kasper^[228] in a concentrated solution of pyrene by fluorescence spectroscopy. In a 10^{-5} M solution of pyrene in hexane, the excited monomer is the predominant species with a violet fluorescence at $\lambda_{\text{max}} = 377$ nm and the spectrum has vibronic structure. However, at higher concentrations, the blue fluorescence ($\lambda_{\text{max}} = 480$ nm) of the excimer becomes the major emission feature in the spectrum. Figure 5.1-1c shows the proposed mechanism for the photophysics of pyrene.^[229] The lowest lying singlet excited state S_1 is populated during irradiation. The energy can dissipate via internal conversion or fluorescence occurs (with $h\nu_1$) and brings the molecule back to its ground state S_0 . Other relaxation processes including intersystem crossing and quenching also remove the excited state S_1 . The aromatic molecule in the S_1 state undergoes a reaction of the excited singlet with a ground state molecule of the same type at high concentrations, producing an electronically excited dimer (excimer). As described for the monomeric species, fluorescence from the excimer (with $h\nu_2$) and relaxation processes occur and yield the ground state S_0 .

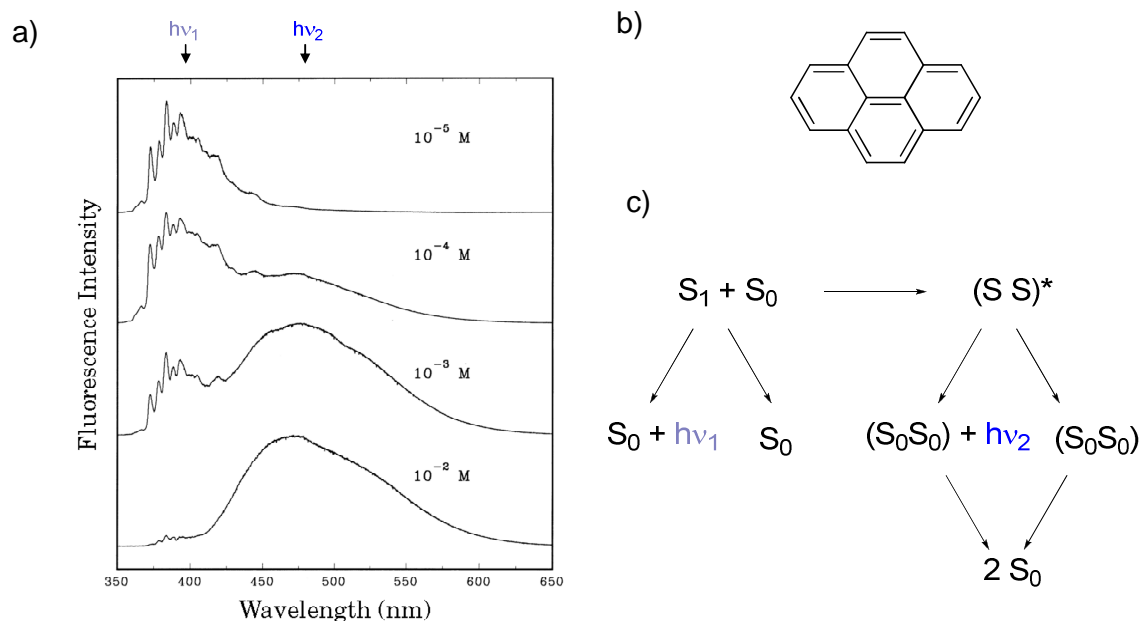


Figure 5.1-1. a) Pyrene emission spectra as a function of concentration: 10^{-2} M to 10^{-5} M in hexane. b) Molecular structure of pyrene. c) Proposed reaction scheme of pyrene photophysics and excimer formation in solution. Adapted from reference.^[227]

Excimers were investigated in seeded supersonic molecular beams^[230] where their electronic states and excited state dynamics can be characterised in detail. They play an important role in several areas of photophysics, including photodimerisation^[231, 232] and molecular probing.^[233, 234]

Dual emission in transition metal complexes

Kasha's rule^[235] says that photon emission (fluorescence or phosphorescence) occurs from the lowest-energy excited state in a species and the emission spectrum is therefore independent of the excitation energy. More precisely,^[236] fluorescence (spin-allowed emission) typically takes place from the lowest vibrational state of the lowest excited singlet level, phosphorescence (spin forbidden emission) usually occurs from the lowest vibrational state of the lowest excited triplet state, and intersystem crossing (ISC) happens usually from the lowest singlet electronic state, because vibrational relaxation is exceedingly fast. These descriptions are true for most luminescent organic systems with only a few exceptions.

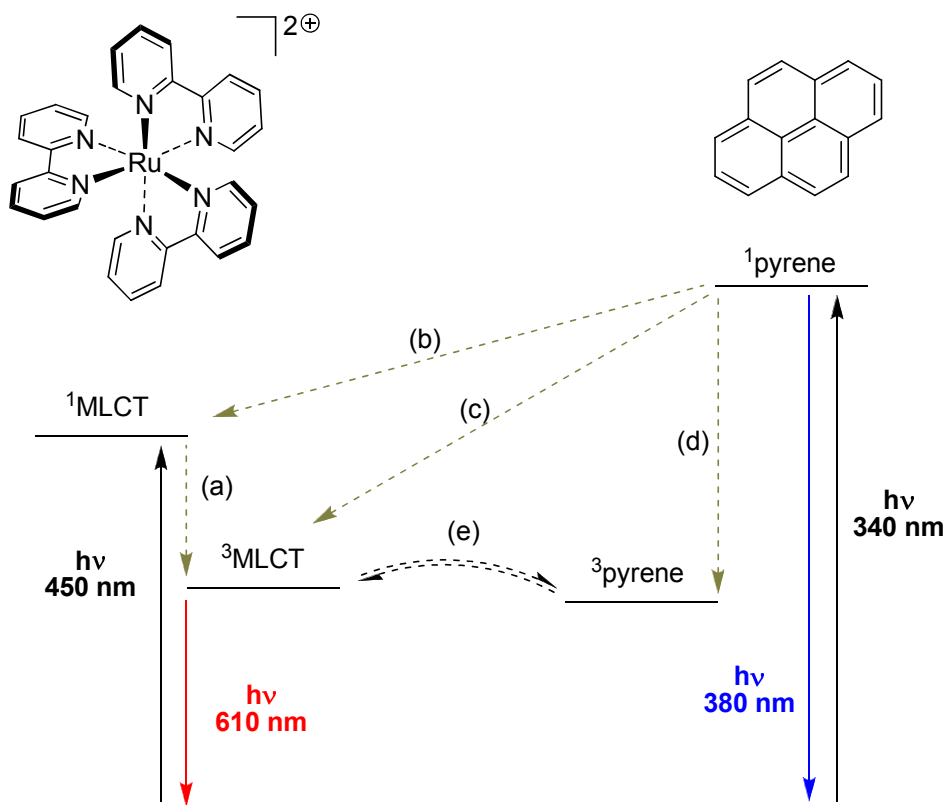
Phosphorescence is the predominant form of emission in d^3 (Cr(III)), and d^6 (Ru(II), Rh(III) and Ir(III)) transition metal complexes.^[236]

Dual emission defies Kasha's rule and was reported for small molecules^[237-240] at low temperature and in rigid media where thermal energy is not sufficient to overcome even low-energy barriers.

DeArmond^[241] classified multiple emissions of tris-chelated complexes with bidentate diimine ligands into the "spatially isolated" and "distinct orbital" type. Examples for the first type are $[\text{Rh}(\text{bpy})_n(\text{phen})_{3-n}]^{3+}$ ($n = 1, 2$) complexes^[242] where π - π^* -emissions are determined from the bpy and the phen moiety. These ligands are separated in space. $[\text{Ir}(\text{phen})_2\text{Cl}_2]^+$ ^[243] exhibits an emission coming from a π - π^* -transition and an emission from a d- π^* -transition. They have different orbital origins and the phenomenon is therefore called "distinct orbital". Nearly all heteroleptic ruthenium(II) complexes exhibit a single emissive state except for a few isolated systems that possess two emissive states.^[238-241, 244] Tor et al.^[245, 246] published mononuclear and dinuclear ruthenium(II) complexes with two simultaneous emissive states that were controlled by structural features.

Enhanced lifetimes and "energy reservoir" effects

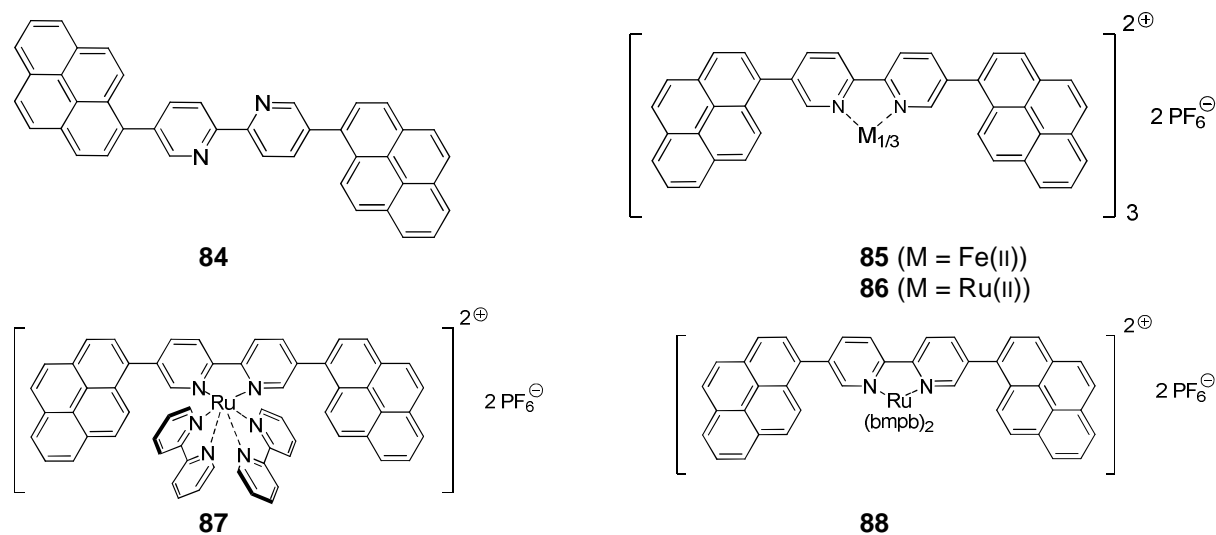
Transition metal complexes incorporating the motif $[\text{Ru}(\text{bpy})_3]^{2+}$ are particularly interesting due to their exceptional combination of luminescence and redox properties.^[102] Bi-chromophoric systems containing a $[\text{Ru}(\text{bpy})_3]^{2+}$ group and covalently linked arenes have been studied^[247, 248] and pyrene was identified as having its lowest lying triplet state at similar energy to the luminescent metal-based triplet level. Ford and Rodgers noted first that the luminescence lifetime of ruthenium(II) polypyridyl complexes can be prolonged by the presence of a coupled aromatic chromophore.^[249] Ruthenium(II) and pyrene units were tethered via saturated^[249-252] or unsaturated^[253] bonds. The excited state lifetime of the $[\text{Ru}(\text{bpy})_3]^{2+}$ unit can depend on the number of attached pyrene chromophores^[253] and a linear relationship between the number of pyrene chromophores and lifetime was found in a particular system.^[250] The basis of this behaviour is depicted in Scheme 5.1-1. Light can be absorbed by either the ruthenium or the pyrene unit and the observed ³MLCT luminescence can receive contributions from the ¹pyrene level over different pathways. Thermal redistribution between close lying ruthenium and pyrene centred triplet levels (path e) has a lifetime increasing effect. The pyrene unit acts in this respect as an "energy reservoir".



Scheme 5.1-1. Schematic representation of energy levels of relevant excited states. a) intersystem crossing (ISC) with $\Phi_{\text{ISC}}=1$; b) singlet-singlet energy transfer, $^1\text{pyrene} \rightarrow ^1\text{MLCT}$; c) direct ISC, $^1\text{pyrene} \rightarrow ^3\text{MLCT}$; d) ISC localized at pyrene followed by e) thermal redistribution between triplet levels.

5.2 Aims and Overview

In this chapter, the syntheses and characterisation of 5,5'-di(pyren-1-yl)-2,2'-bipyridine (**84**), homoleptic iron(II) and ruthenium(II) complexes, $[\text{Fe}(\mathbf{84})_3](\text{BF}_4)_2$ (**85**) and $[\text{Ru}(\mathbf{84})_3](\text{PF}_6)_2$ (**86**), and two heteroleptic ruthenium(II) complexes, $[\text{Ru}(\mathbf{84})(\text{bpy})_2](\text{PF}_6)_2$ (**87**, bpy = 2,2'-bipyridine) and $[\text{Ru}(\mathbf{84})(\text{bmpb})_2](\text{PF}_6)_2$ (**88**, bmpb = 5,5'-bis(3-methoxyphenyl)-2,2'-bipyridine), are described (see Scheme 5.2-1). Crystal structures for compounds **84**, **86**, **87** and **88** were obtained and intramolecular and intermolecular interactions were investigated in the solid state. The $[\text{Ru}(\text{bpy})_3]^{2+}$ and the pyrene domain are prominent chromophores, and intramolecular interactions were studied via absorption and emission spectroscopy and lifetimes of the excited states were determined.

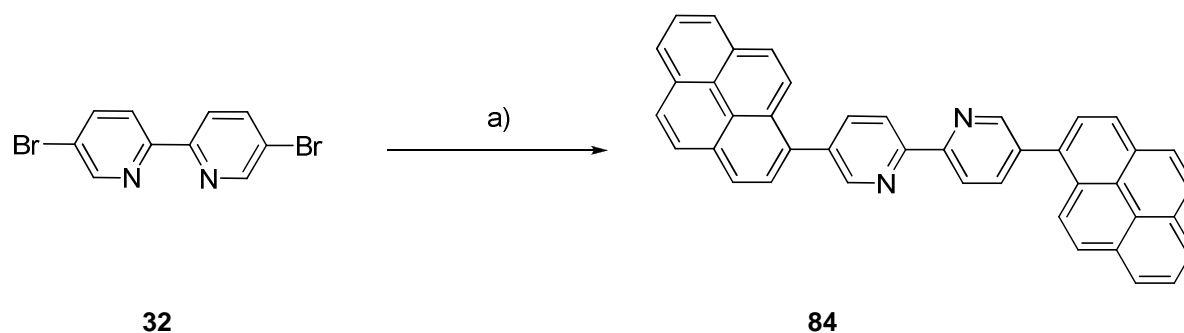


Scheme 5.2-1. Novel bipyridine ligand **84** bearing pyrene groups, homoleptic iron(II) (**85**) and ruthenium(II) (**86**) complexes and heteroleptic ruthenium(II) complexes, **87** and **88**, with that ligand. bmpb = 5,5'-bis(3-methoxyphenyl)-2,2'-bipyridine.

5.3 Synthesis

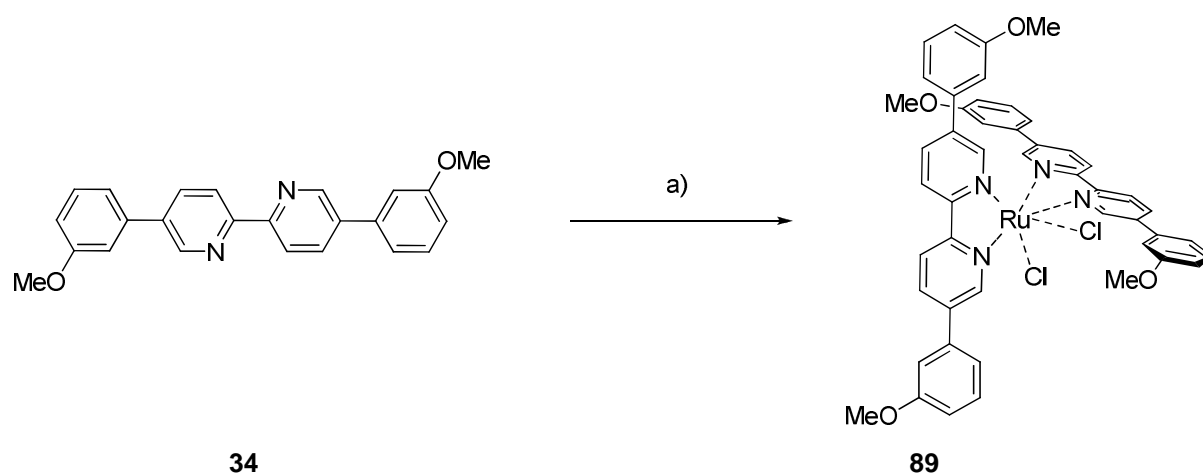
The preparation of 5,5'-di(pyren-1-yl)-2,2'-bipyridine (**84**), its homoleptic ruthenium(II) complex **86** and iron(II) complex **85** and the heteroleptic ruthenium(II) complexes **87** and **88** with that ligand are described below.

The bis(pyrene) compound **84** was synthesised with relative ease by Suzuki coupling of 5,5'-dibromo-2,2'-bipyridine (**32**) with commercially available pyren-2-ylboronic acid in biphasic conditions in the presence of $[\text{Pd}(\text{PPh}_3)_4]$ under rigorous exclusion of light. The reaction mixture was heated to reflux for three days and the precipitate was collected and washed with water and ether to yield spectroscopically pure **84** in excellent yield (see Scheme 5.3-1). The ligand is very poorly soluble in CH_2Cl_2 , not soluble in most other common solvents (including DMSO) and very soluble in its protonated form, for instance, in mixtures of trifluoroacetic acid and CH_2Cl_2 .



Scheme 5.3-1. Reagents and conditions: a) pyren-2-ylboronic acid (2.15 eq), $[\text{Pd}(\text{PPh}_3)_4]$ (10 mol%), Na_2CO_3 (4 eq), toluene/ H_2O , reflux, 3 d, 99%.

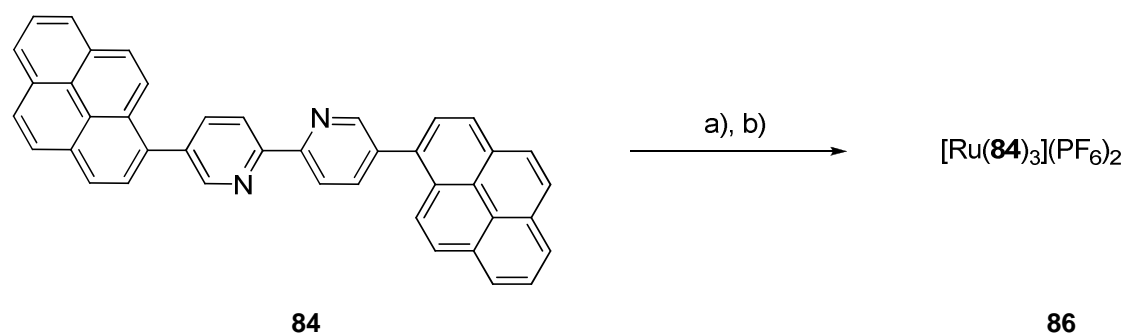
Complex **89** was prepared according to the literature procedure^[105] for its smaller analogue *cis*-dichlorobis(bipyridine)ruthenium(II). Commercial ruthenium trichloride trihydrate and the ligand **34** were heated to reflux in DMF. Purification was performed by several steps of filtration and crystallization producing the desired complex in good yield. The compound is poorly soluble in the most common solvents. $^1\text{H-NMR}$ spectroscopy showed the expected number of signals with the expected relative integrals for the molecule with the *cis*-configuration. The highest mass peaks in the FAB mass spectrum came at $m/z = 908.1$, 873.3 and 838.2, and were assigned to $[\mathbf{89}]^+$, $[\mathbf{89-Cl}]^+$ and $[\mathbf{89-2Cl}]^+$, respectively.



Scheme 5.3-2. Reagents and conditions: a) $\text{RuCl}_3 \cdot 3 \text{H}_2\text{O}$ (0.63 eq), DMF, reflux, 4 h, 44%.

The homoleptic ruthenium(II) complex **86** and the homoleptic ruthenium(II) complexes **87** and **88** were prepared by heating ligand **84** and the corresponding ruthenium(II) precursors in a microwave reactor yielding the desired complexes in good to very good yields.

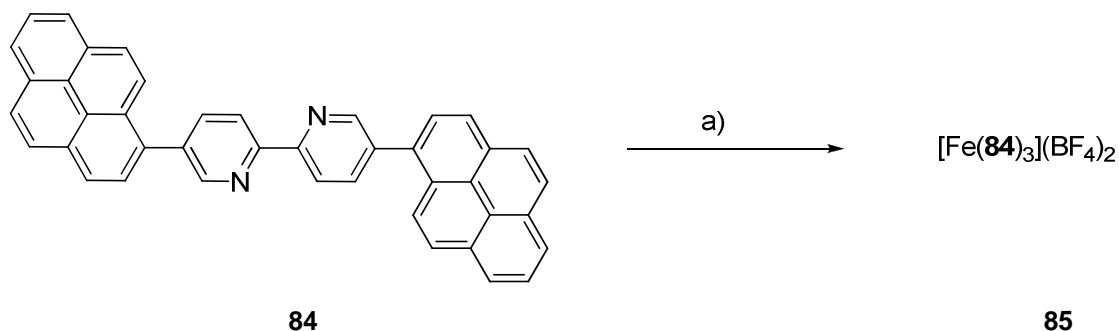
The synthesis of complex **86** required high thermal excitation and a mixture of ligand **84** and 0.34 equivalents of $[\text{Ru}(\text{DMSO})_4\text{Cl}_2]$ were therefore heated to 250 °C in ethylene glycol. The counterion was exchanged by adding an aqueous solution of ammonium hexafluorophosphate to the reaction mixture and the precipitate was collected. Filtration over Al_2O_3 produced analytically pure **86** (see Scheme 5.3-3).



Scheme 5.3-3. Reagents and conditions: a) $[\text{Ru}(\text{DMSO})_4\text{Cl}_2]$ (0.34 eq), μW , ethylene glycol, 250 °C, 2h; b) NH_4PF_6 , 83%.

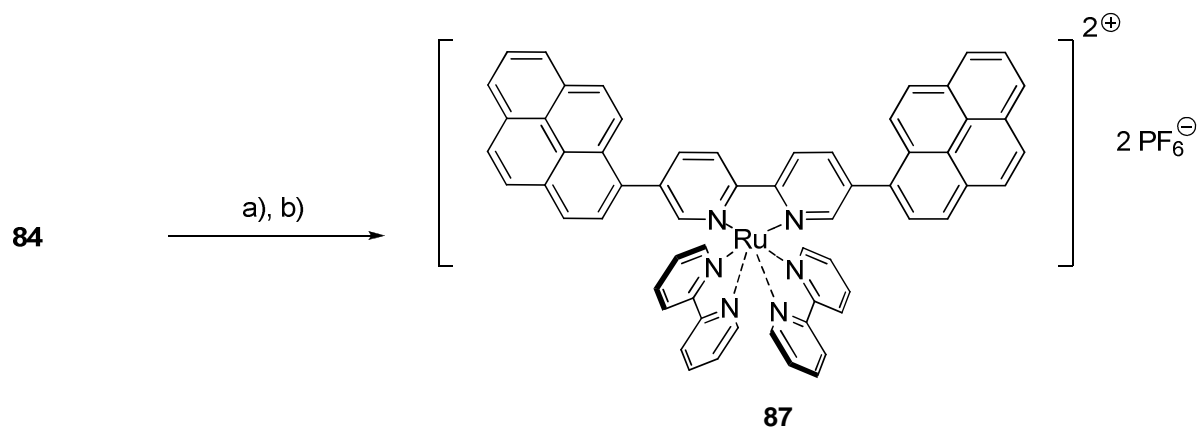
The iron(II) complex **85** was made by heating ligand **84** with an excess of the required iron salt in a microwave reactor. The resulting precipitate was washed with water and ether. ESI-MS showed the highest mass peak at $m/z = 863.1$ that was assigned to $[\mathbf{85}-2\text{BF}_4]^{2+}$. Due to its poor solubility, only a $^1\text{H-NMR}$ spectrum could be measured in $\text{DMSO}-d_6$. Furthermore, decolouration of the initially red solution was observed after several hours along with the disappearance of the resonances attributable to the compound in the $^1\text{H-NMR}$ spectrum (the

free ligand is not soluble in DMSO). The replacement of ligands by non-innocent solvent molecules in the labile complex explains these observations.

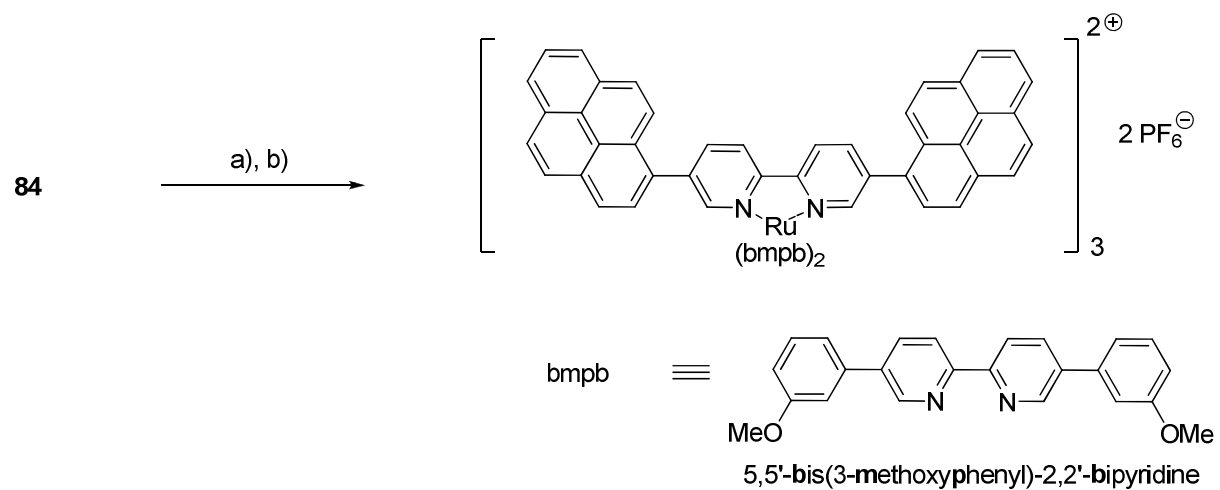


Scheme 5.3-4. Reagents and conditions: a) $[\text{Fe}(\text{BF}_4)_2] \cdot 6\text{H}_2\text{O}$ (1.0 eq), μW , CH_3CN , $110\text{ }^\circ\text{C}$, 30 min, 21%.

The ruthenium(II) complexes **87** and **88** were made in an analogous manner as described for **86** (see Scheme 5.3-5 and Scheme 5.3-6). Equimolar mixtures of ligand **84** and *cis*- $[\text{Ru}(\text{bpy})_2\text{Cl}_2]$ or **89** were heated in a microwave reactor to $140\text{ }^\circ\text{C}$, respectively. The work-up procedure was as described for **86**. Purification of compound **88** necessitated column chromatography.



Scheme 5.3-5. Reagents and conditions: a) *cis*- $[\text{Ru}(\text{bpy})_2\text{Cl}_2]$ (1.0 eq), μW , EtOH , $140\text{ }^\circ\text{C}$, 1 h; b) NH_4PF_6 , 94%.



Scheme 5.3-6. Reagents and conditions: a) **89** (1.03 eq), μW , EtOH, 140 °C, 1 h; b) NH_4PF_6 , 62%.

5.4 Crystal Structures and Characterisation

Single crystals of **84** suitable for X-ray analysis were obtained by layering ethyl acetate upon a dichloromethane and trifluoroacetic acid solution of **84**. After several weeks, X-ray quality pale yellow plates of the unprotonated ligand had grown (the trifluoroacetic acid had evaporated). The structure of the centrosymmetric ligand is shown in Figure 5.4-1.

Bond distances and angles within the bpy and pyrene rings are unexceptional. As expected, the ligand adopts a *transoid* conformation but flips to a *cisoid* arrangement upon binding to a metal ion. There is a surprisingly highly ordered geometry in the solid state. The two least squares planes of the two pyridine moieties perfectly overlap and are therefore in line. The same planarity is noticed for the two pyrene moieties having perfectly parallel least square planes. Moreover, the least square planes between one pyridine unit and one pyrene unit are twisted $45.1(1)^\circ$ with respect to each other. Figure 5.4-1 illustrates the described geometrical features.

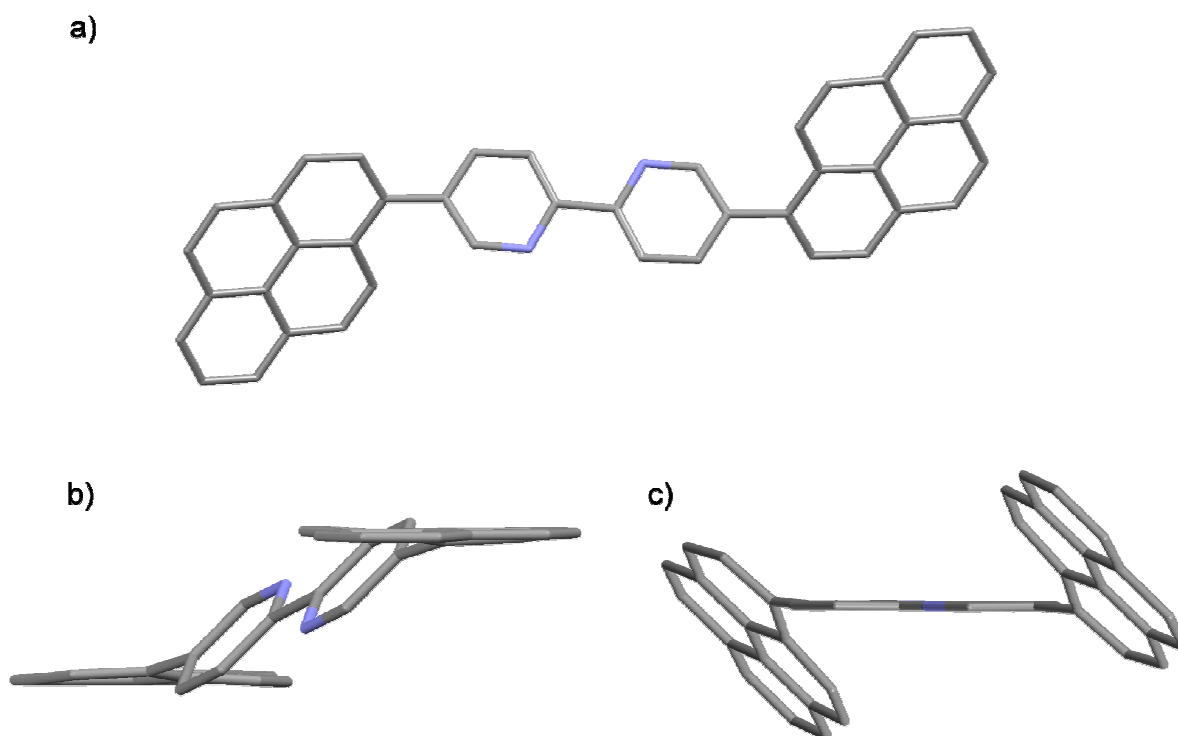


Figure 5.4-1. Molecular structure of **84** depicted in capped stick representation. Hydrogen atoms have been omitted for clarity. a) Front view that displays the *transoid* arrangement of the nitrogen atoms; b) View along the two parallel least square planes of the pyrene moieties; c) View along the two in line least square planes of the pyridine moieties. The angle between one pyrene least square plane and one pyridine least square plane is $45.1(1)^\circ$.

The packing of **84** is shown in Figure 5.4-2 and Figure 5.4-3. Contrary to expectations, no π -stacking was observed. A stacked formation in the crystal structure of pyrene was discovered by Robertson and White in 1947.^[254] Simple aromatic residues often prefer to associate via enthalpically favourable edge to face C-H \cdots π interactions rather than to interact through parallel π - π stacking interactions.^[255-258] Analysis of the close contacts in the packing of **84** indicates that the stabilisation occurs over C-H \cdots π interactions within a distance of 260 pm between the hydrogen atom and the centre of mass of an aromatic ring from another molecule in proximity (see Figure 5.4-2). The least square planes in which the hydrogen atom and the centroid of the ring that form the non classical hydrogen bond are inscribed, span an angle of 45° . The edge to face arrangements can also be seen as the origin of the known herringbone structure of crystalline benzene.^[259-261] Figure 5.4-3a displays the view along the crystallographic a-axis, emphasising the herringbone structure of the packing pattern for ligand **84** similar to those found in the crystal structure of benzene.

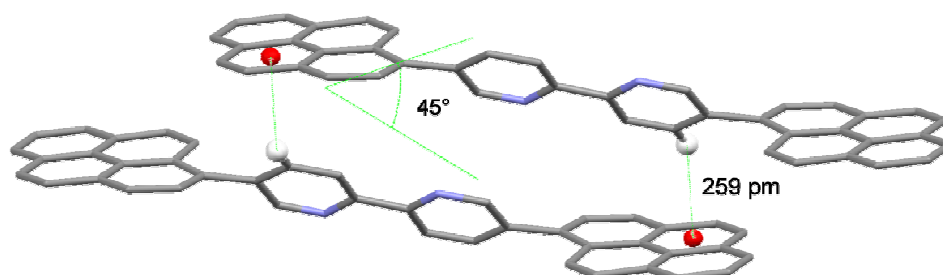


Figure 5.4-2. Molecular structure of **84** displaying the C-H \cdots π interactions between the individual molecules in the packing. The distance between the hydrogen atoms (white dots) and the centroid (red dots) of the aromatic ring is 260 pm. The planes of the aromatic ring in the pyrene unit and the plane in which the hydrogen lies are tilted 45° .

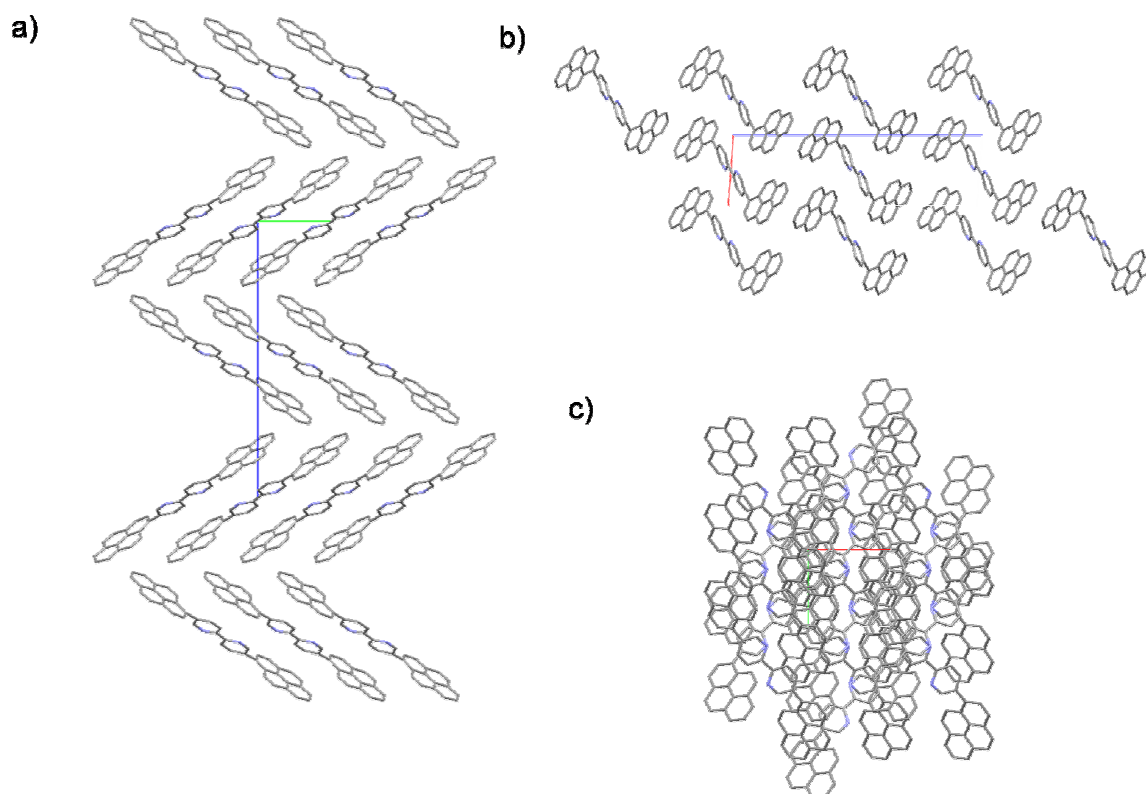


Figure 5.4-3. Stacking of **84** in the solid state. a) View along the crystallographic a-axis with the herringbone pattern; b) View along the crystallographic b-axis; c) View along the crystallographic c-axis. Hydrogen atoms have been omitted for clarity.

Single crystals of **87** and **88** suitable for X-ray analysis were grown by slow liquid diffusion at room temperature of diethyl ether to a solution of the complex in dimethylformamide or acetonitrile, respectively. The molecular structures of the heteroleptic ruthenium(II) complexes are shown in Figure 5.4-4. Bond lengths and bond angles appeared in the expected range. Both complexes exhibit distorted octahedral geometry around the metal centre with ruthenium-nitrogen bond lengths between 205.6(2) pm and 206.2(2) pm for **87** and between 204.4(2) pm and 205.9(2) pm for **88**.

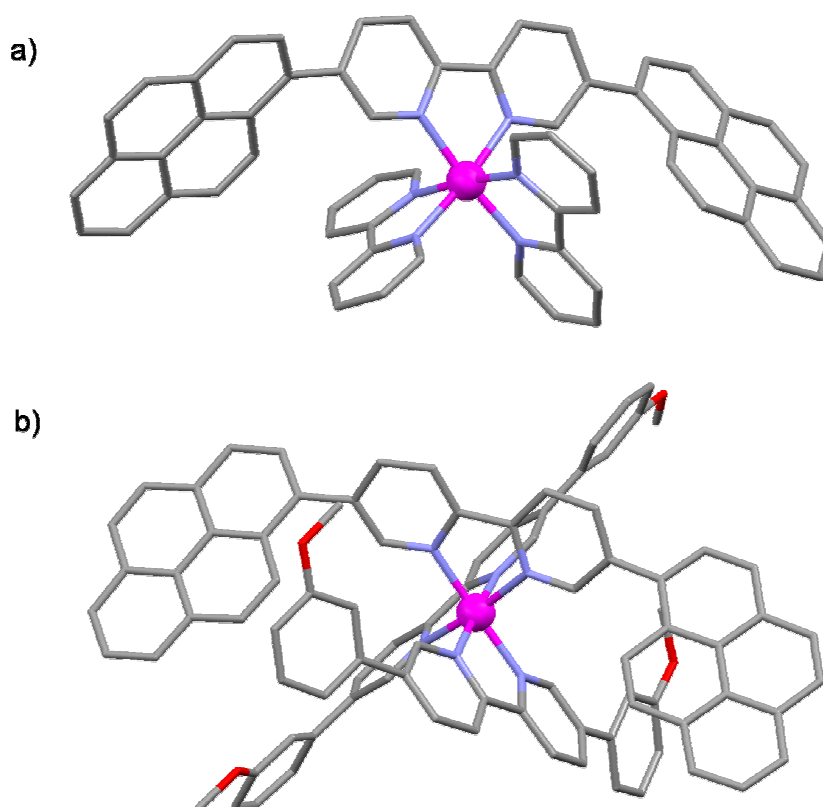


Figure 5.4-4. Molecular structures depicted as capped stick representations as they were found in the single crystals of heteroleptic ruthenium(II) complex cations: a) $\mathbf{87}^{2+}$; b) $\mathbf{88}^{2+}$. Solvent molecules, counterions and hydrogen atoms have been omitted for clarity.

Single crystals of **86** suitable for X-ray analysis were obtained by slow liquid diffusion of ethyl acetate into a solution containing the ruthenium(II) complex in dimethylformamide. The molecular structure is depicted in Figure 5.4-5a. Bond lengths and bond angles are unexceptional and ruthenium-nitrogen bond lengths were found between 205.1(3) pm and 205.5(3) pm. The ligands wrap around the slightly distorted octahedral metal centre such that the pyrene moieties adopt an *endo*-conformation by pointing towards the metal centre. Views along the crystallographic axis of the spacefilling model are shown in Figure 5.4-5. Two intramolecular C-H \cdots π interactions between two ligands that have roughly perpendicular pyrene moieties were determined within a distance of 251.1(5) pm. The cation is chiral but the complex crystallized in the non-chiral space group $C_{2/C}$ and so both enantiomers are present in the unit cell.

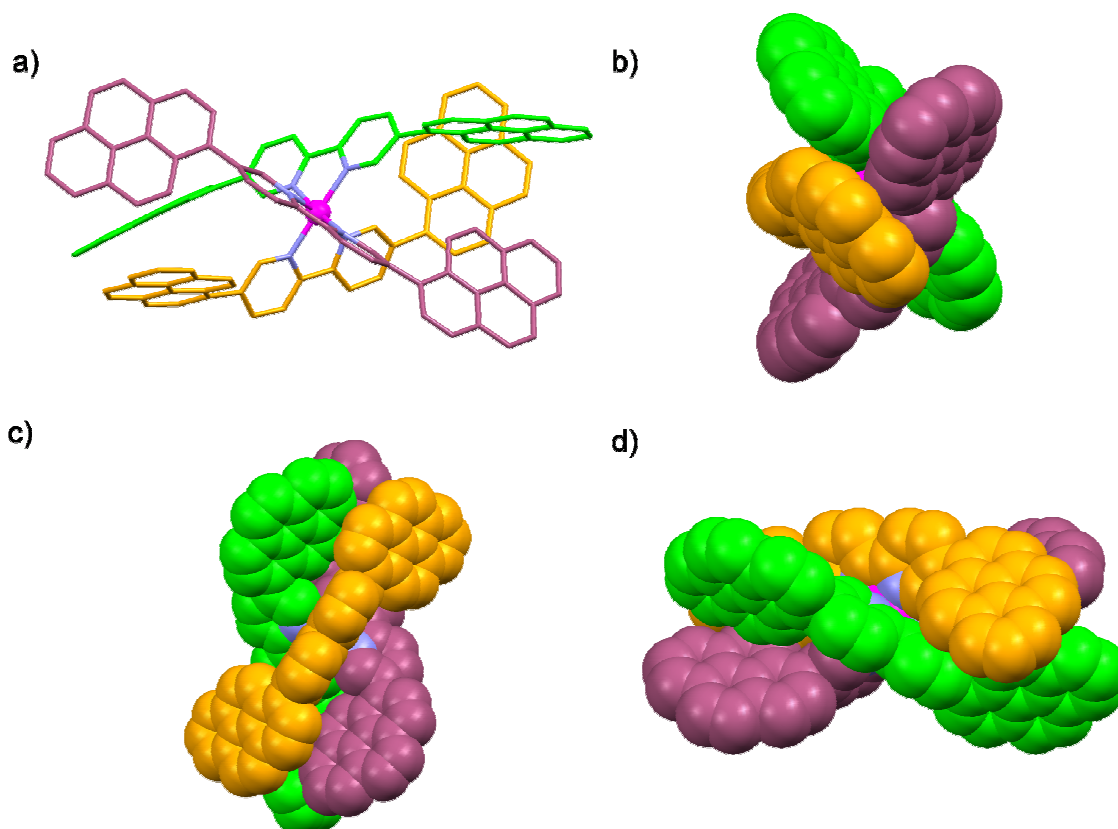


Figure 5.4-5. a) Molecular structure of **86** depicted as capped stick representations as it was found in the single crystal. The fashion in which the ligands wrap around the metal centre is depicted by space-filling representations and views along b) the crystallographic a-axis; c) the crystallographic b-axis; d) the crystallographic c-axis. Solvent molecules, counterions and hydrogen atoms have been omitted for clarity.

The bpy unit is planar in the free ligand **84** and has a *transoid* conformation. Upon coordination to ruthenium(II), it flips to an *cisoid* conformation with distortion to planarity up to $11.7(1)^\circ$ allowing a chelating binding mode. The least square planes of the two pyrene moieties are parallel in **84** whereas in the ruthenium(II) complexes angles from $18.92(9)^\circ$ to $85.5(3)^\circ$ were calculated. The results are summarized in Table 5.4-1.

Table 5.4-1. Angles between selected least squares planes as they were found in the crystal structure. Values are given in [°].

plane	84	87	88	86
py-py in bpy-moiety	0.00	0.8(1), 2.7(1), 7.22(8) ^[a]	3.1(1), 10.8(1), 11.7(1) ^[a]	1.6(2), 5.8(2) (2x)
pyrene-pyrene moiety	0.00	76.22(7)	18.92(9)	27.8(1) (2x), 85.1(3)

^[a] angle in the coordinated ligand **84**.

In contrast to the packing pattern of ligand **84**, π -stacking plays an important role in the packing of the ruthenium complexes **87**, **88** and **86**. In **87**, one pyrene moiety participates in π -stacking to the adjacent pyrene group of another complex molecule at a distance of 353 pm (distance of parallel least squares planes of the two pyrene units). These pyrene units form a stack of offset parallel planes with alternating distances of 353 pm and 711 pm (see Figure 5.4-6a). The short contact analysis of **88** reveals that both pyrene groups interact via π -stacking at a rough distance of 365 pm in a nearly parallel displaced manner to neighbouring pyrene moieties, and also the bis(methoxyphenyl)bipyridine ligand exhibits stacking interactions at a distance of ca. 380 pm (see Figure 5.4-6b). There are π -stacking interactions from all six pyrene groups of homoleptic complex **86** in a nearly parallel, but displaced, manner at a distance of 344 pm (see Figure 5.4-6c).

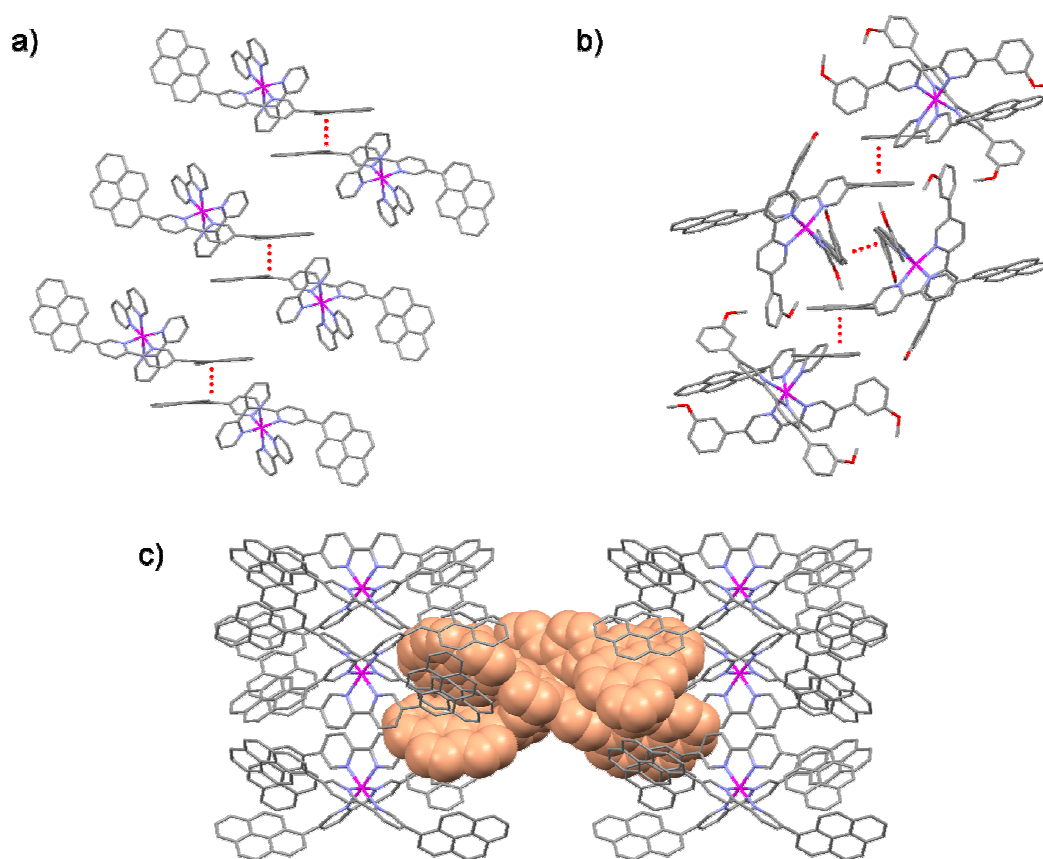


Figure 5.4-6. Intermolecular packing interactions as they were found in the crystal structures of a) **87**; b) **88**; c) **86**. Solvent molecules, counterions and hydrogen atoms have been omitted for clarity.

At room temperature the $^1\text{H-NMR}$ spectrum of **86** exhibits the expected resonances with appropriate integrals, but several peaks experience a considerable shift to lower frequency (up

to $\delta 6.88$ ppm) and are broadened. In the protonated free ligand $[\mathbf{84}+\text{H}]^+$ and in the heteroleptic ruthenium(II) complexes **87** and **88**, all resonances have sharp peak shapes and the protons from the pyrene moiety usually appear in the range of $\delta 8.5$ ppm to $\delta 7.7$ ppm.

$^1\text{H-NMR}$ spectra of **86** were recorded at variable temperatures and assignments have been made with COSY and NOESY techniques (see Figure 5.4-7). At 295 K signals P9 and P8 are very broad (200 Hz and 80 Hz line width at half height) and signal P7 and P6 are broad (20 Hz line width at half height). Upon heating, the signals sharpen and at 355 K the fine structure of all peaks is resolved.

The strong shift to lower frequencies and the broadness of some resonances deserve further note.

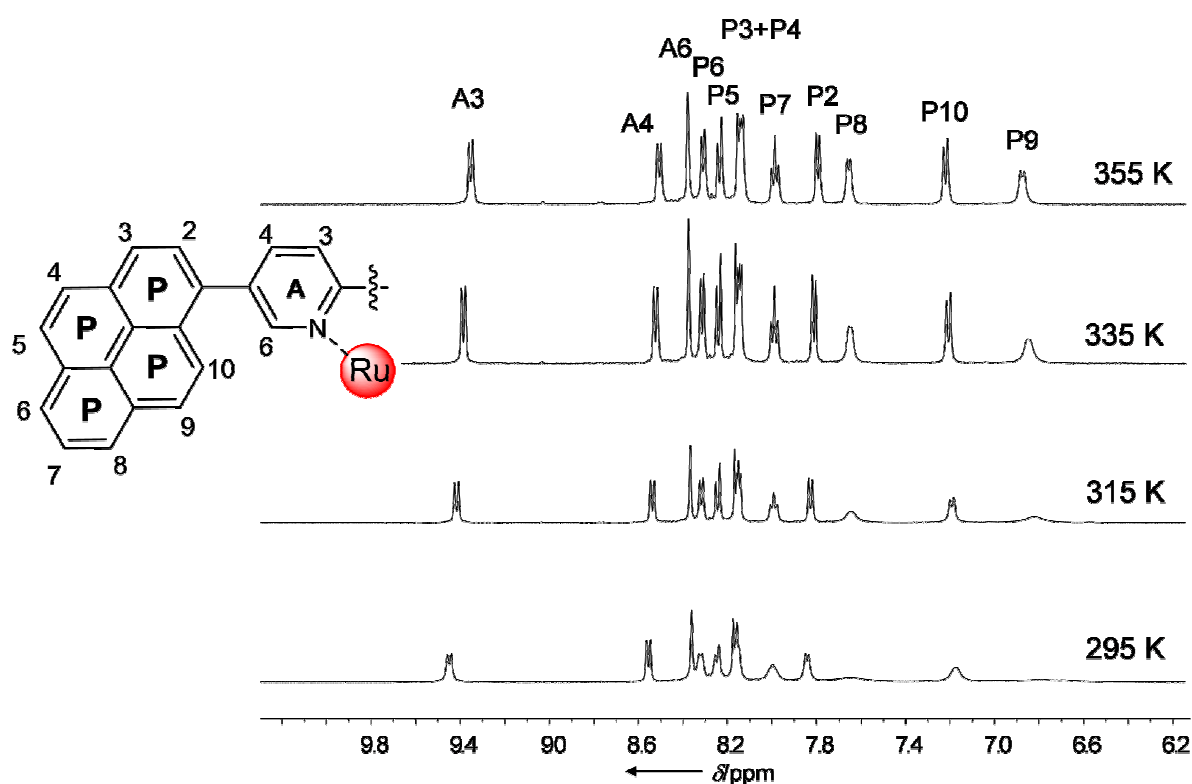


Figure 5.4-7. Variable temperature 500 MHz NMR spectra in $\text{DMSO-}d_6$ solutions of homoleptic ruthenium(II) complex **86**. Proton labelling is given on the left and temperatures at which the spectra were recorded are given on the right.

The crystal structure of **86** reveals the very close proximity of protons P7, P8 and P9 to a nearly perpendicular pyrene moiety. Facing the aryl π -cloud, these protons experience a strong shielding effect and are therefore shifted upfield. Moreover, the pyrene groups are not equivalent by symmetry in the solid state and only fast rotation around the carbon-carbon bond that bridges the pyrene to the bpy unit will render them chemically equivalent. A slow rotation on the NMR time scale leading to coalescence of signals from conformationally

different units explains the broadness of the peaks. Upon heating, the signals sharpen and differences in the conformations are no longer distinguishable due to a fast rotation on the NMR timescale.

The ^1H -NMR spectrum of the homoleptic iron(II) complex $[\text{Fe}(\mathbf{84})_3](\text{BF}_4)_2$ (**85**) displays a similar pattern most likely caused by the same effects as described for **86**.

More characterisation details (NMR, MS, IR, UV-Vis, emission, elemental analysis) for all compounds presented in this chapter are described in the experimental part of this thesis and are unexceptional.

5.5 Photophysical Properties

The UV absorption and emission spectra of ligand **84** and its protonated form (**84H⁺**) in CH_2Cl_2 are shown in Figure 5.5-1. Comparison of the absorption and emission profiles with the spectra of pyrene allows the following proposed assignments. For **84**, the strong absorption band at $\lambda = 357$ nm originates from a $S_0 \rightarrow S_2$ transition and the weak shoulder at $\lambda \approx 420$ nm might have its origin in a $S_0 \rightarrow S_1$ transition. These transitions are red shifted by 22 nm and 30 nm with respect to transitions in pyrene due to the extended conjugation. The emission at $\lambda_{\text{max}} = 444$ nm is broad and was determined in a 10^{-5} M solution in CH_2Cl_2 . Due to the poor solubility of **84**, it is not possible to prepare solutions of higher concentration and study potential excimer formation. The solubility of **84** can be considerably enhanced by protonation and the intense band at $\lambda = 357$ nm is red shifted into the visible region of the spectrum with its maximum lying at $\lambda = 454$ nm. The solution changes colour upon protonation from pale yellow to intense red. The emission of the protonated form is orange with $\lambda_{\text{max}} = 609$ nm.

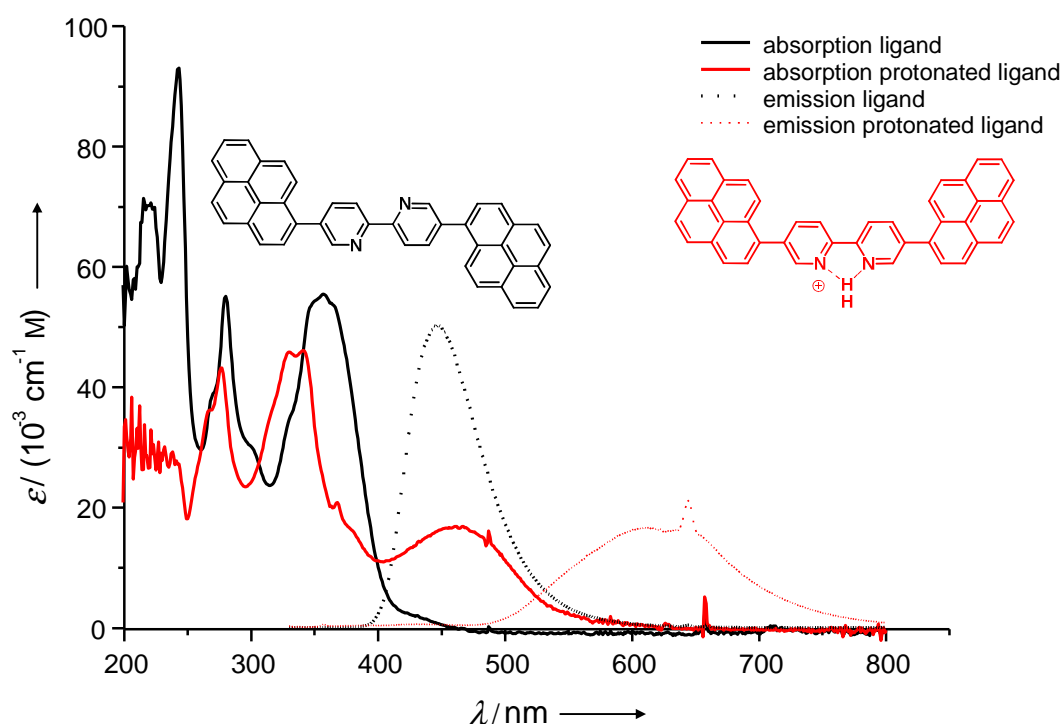


Figure 5.5-1. Absorption and emission spectra of ligand **84** (Absorption black solid line, emission dotted black line) and the protonated ligand **84H⁺** (Absorption red solid line, emission dashed red line).

The ruthenium(II) complexes **86**, **87**, **88** are bichromophoric species composed of pyrene and ruthenium(II) tris(diimine) domains. Table 5.5-1 summarized their steady-state spectroscopic

properties. The absorption and the emission spectra of **87** are depicted in Figure 5.5-2. The shoulder at $\lambda \approx 480$ nm might be assigned as MLCT in nature, the band at $\lambda = 405$ nm can be a π - π^* -transition from the pyrene domain or a MLCT transition. The emission profile of **87** exhibits two emission peaks, with $\lambda_{\text{em}} = 495$ nm and $\lambda_{\text{em}} = 645$ nm, respectively. Identification of species displaying authentic dual emission can be difficult, as possible contributions from luminescent impurities have to be excluded. Ruthenium(II) complex **87** exhibits clean NMR and mass spectra and correct elemental analysis. There is no indication of any impurities. The most likely impurities, ligand **84** and $[\text{Ru}(\text{bpy})_3]^{2+}$, have their emission maxima at different wavelengths (see Table 5.5-1).

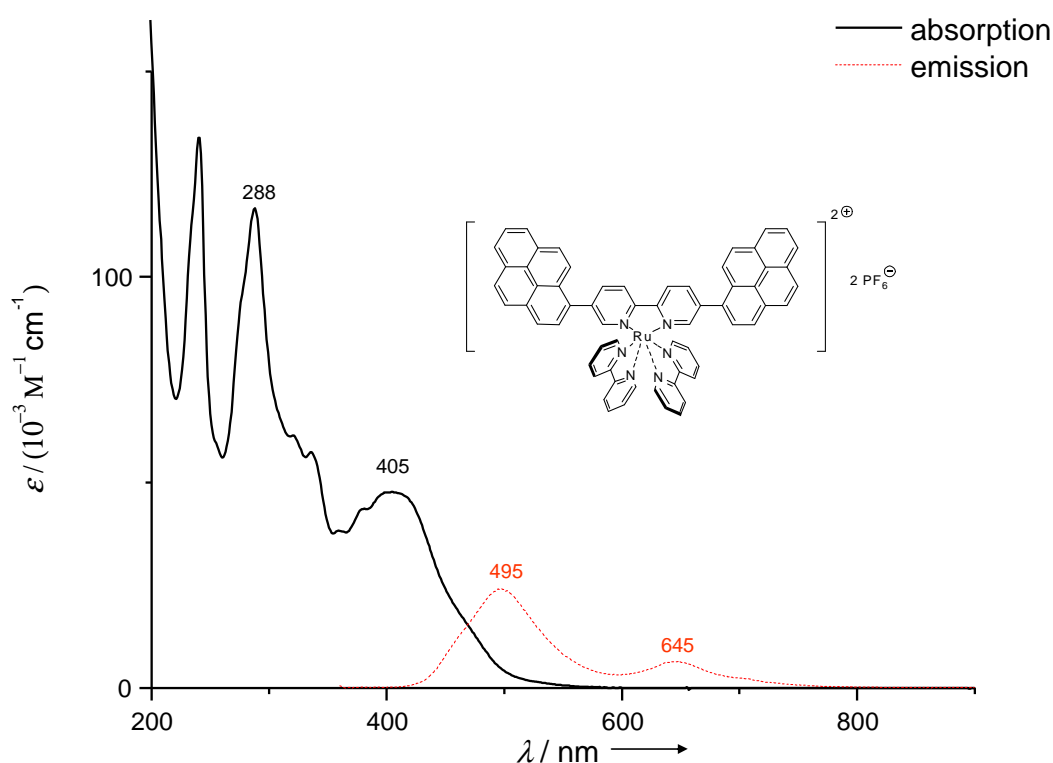


Figure 5.5-2. Absorption (black solid line) and emission (red dotted line) spectra of **87** in 10^{-5} M acetonitrile solutions. $\lambda_{\text{exc}} = 355$ nm.

An excitation spectrum records the intensity of the emission at a fixed wavelength while the excitation monochromator is varied. In a “well-behaved” system, the absorption spectrum and the excitation spectrum (corrected for instrumentation factors) are expected to match. Excitation spectra of **87** in acetonitrile were measured for the two emissions, $\lambda_{\text{em}} = 495$ nm and $\lambda_{\text{em}} = 645$ nm, and are displayed in Figure 5.5-3. The emission at higher energy exhibits a maximum at $\lambda = 356$ nm in the excitation spectrum and is ascribed to the fluorescence properties of the pyrene domain. The orange emission shows a maximum at $\lambda = 484$ nm in the excitation spectrum and has its origin probably from an emission of the $^3\text{MLCT}$ state.

Furthermore, it can be noticed that irradiation at $\lambda_{\text{exc}} = 356 \text{ nm}$ contributes mainly to emission at $\lambda_{\text{em}} = 495 \text{ nm}$ and to a smaller extent to an emission at $\lambda_{\text{em}} = 645 \text{ nm}$. Excitation at $\lambda_{\text{exc}} = 484 \text{ nm}$ populates only the emissive $^3\text{MLCT}$ level. These conclusions were verified by emission spectra with $\lambda_{\text{exc}} = 356 \text{ nm}$ and $\lambda_{\text{exc}} = 484 \text{ nm}$, respectively.

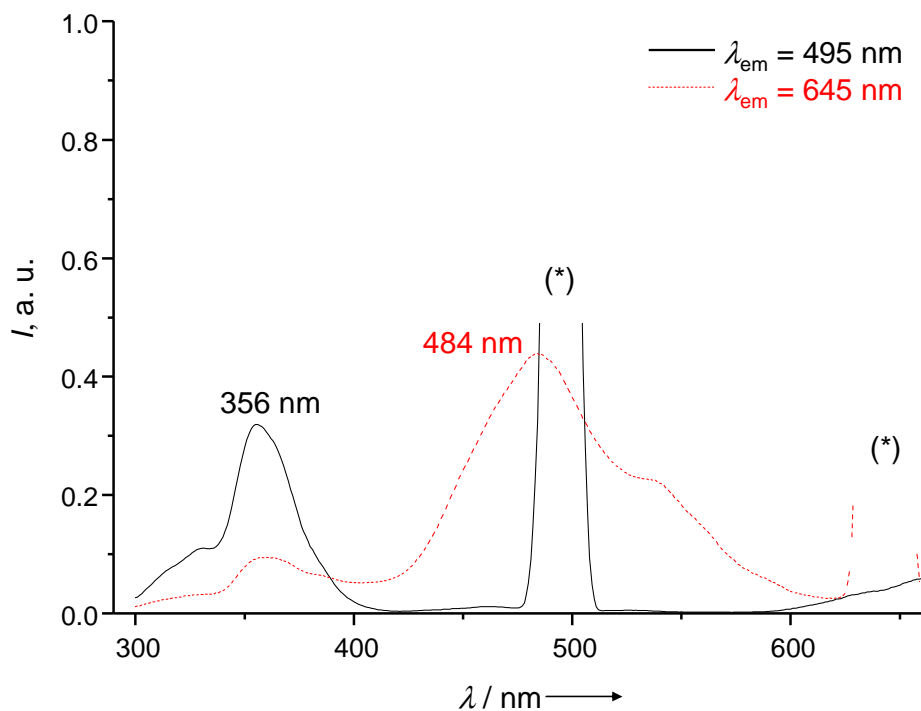


Figure 5.5-3. Uncorrected excitation spectra of **87** in acetonitrile solution with $\lambda_{\text{em}} = 495 \text{ nm}$ (black solid line) and $\lambda_{\text{em}} = 645 \text{ nm}$ (red dotted line). Asterisks mark stray light

The photophysical properties of heteroleptic ruthenium(II) complex **88** are described in Table 5.5-1.

The complexes **86** and **85** are isostructural and differ in the metal which is iron(II) or ruthenium(II). Another difference lies in their stability, as the iron(II) complex **85** decomposed in a DMSO solution and no such lability is expected, nor was found, for the corresponding ruthenium(II) complex **86**. For **85**, the optical properties are listed in Table 5.5-1 but should be considered with caution due to its instability in DMSO solutions and possible decomposition that will cause absorption and emission from the ligand. The absorption spectrum of 10^{-5} M solutions of **85** in acetonitrile showed a band at $\lambda = 544 \text{ nm}$ ($\epsilon = 8100 \text{ M}^{-1} \text{ cm}^{-1}$) which is responsible for the red colour of the compound and is diagnostic of the formation of a tris(bpy) iron(II) complex. The emission has its maximum at $\lambda = 479 \text{ nm}$ which is about 35 nm red shifted compared to the free ligand, the emission of which was not detected in the solution.

Emission and absorption spectra of an acetonitrile solution of **86** are shown in Figure 5.5-4. The absorption pattern is comparable to those for **87** and **88** with a broad maximum at $\lambda = 401$ nm. In contrast to **87**, no emission from the $^3\text{MLCT}$ occurs upon irradiation. The emission at $\lambda = 476$ nm most likely has its origin in fluorescence from an excited 1 pyrene state.

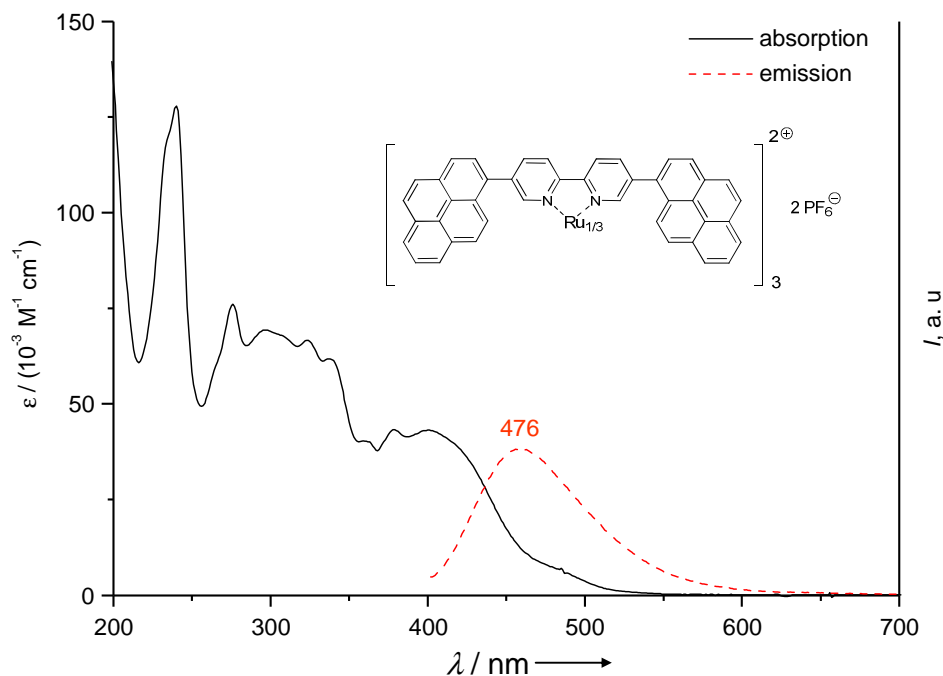


Figure 5.5-4. Absorption (black solid line) and emission (red dotted line) spectra of **86** in 10^{-5} M acetonitrile solutions. $\lambda_{\text{exc}} = 355$ nm.

The luminescence decay times were detected after irradiation at $\lambda_{\text{irr}} = 467$ nm of air-equilibrated and degassed samples in acetonitrile. The decay traces were mathematically analyzed according to an exponential decay law, $I(t) = a_1 \exp(-t/\tau_1) + a_2 \exp(-t/\tau_2) + \dots$ providing $\tau = 5.0, 2.6, 4.1$ μs for **87**, **88** and **86**. The decay traces did not fit to a mono-exponential curve, and so bi- or tri-exponential expressions have been used instead. Lifetimes in Table 5.5-1 and Table 5.5-2 are listed for the slowest decay rate. The luminescence lifetime is roughly one order of magnitude longer in **87**, **88** and **86** than in $[\text{Ru}(\text{bpy})_3]^{2+}$.

As in other examples in the literature^[247, 249-253, 262-264], a lifetime increasing effect or “energy reservoir effect” attributable to the pyrene domains was observed.

Table 5.5-1. Parameters for photophysical properties in degassed acetonitrile solutions.

	absorption		emission		
	λ_{\max}/nm	$\epsilon/(\text{M}^{-1} \text{cm}^{-1})$	λ_{\max}/nm	Φ	τ
[Ru(bpy) ₃] ²⁺ [101]	450	18000	608	0.086	900 ns
pyrene ^[227]	355	47000	377	n.d.	328 ns
84 ^[a]	357	55500	444	0.24	n.d.
84H ^{+[a]}	432	14500	609	0.035	n.d.
[Fe(84) ₃] ²⁺ (85 ²⁺)	544	8140	479	n.d.	n.d.
[Ru(84) ₃] ²⁺ (86 ²⁺)	401	43200	476	$1.0 \cdot 10^{-3}$	4.1(2) μs
[Ru(84)(bpy) ₂] ²⁺ (87 ²⁺)	405	47700	495 645	$3.1 \cdot 10^{-4}$ $3.0 \cdot 10^{-3}$	5.0(2) μs
[Ru(84)(dmbp) ₂] ²⁺ (88 ²⁺)	403	40200	646	$4.5 \cdot 10^{-3}$	2.6(1) μs

^[a]in degassed CH₂Cl₂.

In degassed acetonitrile solutions of ruthenium(II) complexes **87** and **88**, the luminescence quantum yields obtained by using $\lambda_{\text{exc}} = 450 \text{ nm}$ gave $\Phi = 3.0 \cdot 10^{-3}$ and $4.5 \cdot 10^{-3}$ for emissions around $\lambda = 645 \text{ nm}$, respectively. Table 5.5-1 summarises all quantum yields.

Table 5.5-2. Lifetime of the luminescence of selected ruthenium(II) complexes in degassed and air-equilibrated acetonitrile solutions.

	[Ru(bpy) ₃] ²⁺ [251]	86	87	88
air-equilibrated	220 ns	160(10) ns	180(10) ns	200(10) ns
O ₂ -free	900 ns	4.1(2) μs	5.0(2) μs	2.6(1) μs

5.6 Summary and Outlook

The preparation of symmetric ligand **84** which possesses a bpy domain and pyrene units linked over one carbon bond in the 5 and 5'-positions is described. The compound changes colour upon protonation from pale yellow to red and the maximum of the luminescence is considerably shifted. The bpy domain can therefore be used for protonation and obviously also for coordination to a metal ion. Particular output signals can be addressed by external stimuli and this makes this compound a promising building block for molecular logic elements.^[265]

The coordination behaviour of ligand **84** was initially demonstrated by two homoleptic complexes, $[\text{Fe}(\mathbf{84})_3](\text{BF}_4)_2$ (**85**) and $[\text{Ru}(\mathbf{84})_3](\text{PF}_6)_2$ (**86**), which are very similar in structure but different in their stability and inertness. The iron(II) complex **85** was thermodynamically unstable in solutions with non-innocent solvent molecules contrary to the expected behaviour of compounds of the $[\text{Fe}(\text{bpy})_3]^{2+}$ type. The crystal structure of the isostructural ruthenium(II) complex **86** illustrated a sterically demanding environment with the three pyrene domains on either side of the complex with exceptionally short intramolecular C-H \cdots π interactions. In order to broaden the scope of the investigated compounds, two heteroleptic ruthenium complexes, $[\text{Ru}(\mathbf{84})(\text{bpy})_2](\text{PF}_6)_2$ (**87**, bpy = 2,2'-bipyridine) and $[\text{Ru}(\mathbf{84})(\text{bmpb})_2](\text{PF}_6)_2$ (**88**, bmpb = 5,5'-bis(3-methoxyphenyl)-2,2'-bipyridine), were prepared and their crystal structures were studied. The photophysical properties of all the compounds were examined. Heteroleptic ruthenium(II) complex **87** was found to be dual emitting with emissions from excited pyrene and $^3\text{MLCT}$ states upon irradiation at $\lambda_{\text{exc}} = 355$ nm, whereas excitation at $\lambda_{\text{exc}} = 484$ leads to exclusive emission from the $^3\text{MLCT}$ state. For **86**, only emission from a pyrene state was observed. It is therefore desirable to synthesise the ruthenium(II) complex with two **84** and one bpy ligand, $[\text{Ru}(\mathbf{84})_2(\text{bpy})](\text{PF}_6)_2$, which is assumed to display properties lying somewhere in between the two other complexes. Furthermore, advanced optical measurements such as transient spectroscopy and low temperature luminescence should reveal more features of these compounds.

Analysis of the time resolved emissions indicated a significant increase in lifetimes for ruthenium(II) complexes decorated with pyrene units (**86**, **87**, **88**) compared to $[\text{Ru}(\text{bpy})_3]^{2+}$.

6 Experimental Part

6.1 General Experimental

Chemicals

The following chemicals were obtained commercially and were used without further purification: ammonium chloride (Aldrich), ammonium hexafluorophosphate (Alfa Aesar), 3-bis(triphenylphosphino)propane nickel(II) chloride (Strem), barium hydroxide octahydrate (Aldrich), 1,1'-bis(diphenylphosphanyl)ferrocenedichloropalladium(II) (Aldrich), bromine (Aldrich), 2-bromobenzylamine (Alfa Aesar), 1-bromohexane (Aldrich), *n*-butyllithium in hexanes (1.6 M solution) (Aldrich), caesium carbonate (Lancaster), 2,5-dibromopyridine (Lancaster), 1,4-dichlorobenzene (Alfa Aesar), dichlorobis(triphenylphosphane)palladium(II) (Aldrich), 1,2-dimethoxyethane (Aldrich), ethyl diethoxyacetate (Aldrich), hexabutyl-distannane (Aldrich), first generation and second generation Grubbs' and second generation Hoyveda-Grubbs' catalysts (Aldrich), imidazole (Acros), iron(II) tetrafluoroborate hexahydrate (Aldrich), lithium chloride (Merck), magnesium as ribbons (Riedel-de Haën), methanesulfonyl chloride (Acros), 4-methoxyphenylboronic acid (Aldrich), methyl lithium in hexane (1.6 M solution) (Acros), potassium carbonate (Prolabo), potassium hydroxide (Riedel-de Haën), potassium iodide (Prolabo), pyren-2-ylboronic acid (Aldrich), tetrabutylammonium fluoride trihydrate (Acros), tetrakis(triphenylphosphane)palladium(0) (Aldrich), tetrakis(acetonitrile)palladium(II) tetrafluoroborate (Aldrich), thionyl chloride (Prolabo), triethylamine (Riedel de Haën), trifluoromethanesulfonic anhydride (Alfa Aesar) triisopropylsilyl chloride (Acros), trimethyl borate (Aldrich), tris(dibenzylideneacetone)dipalladium(0) (Strem), potassium iodide (Prolabo), sulfuric acid (Riedel-de Haën), *p*-toluenesulfonic acid monohydrate (Aldrich), Δ -TRISPHAT tetrabutylammonium salt (Aldrich), zinc powder (Fluka).

Solvents

All solvents were commercially available. For chromatography, technical grade solvents were distilled prior to use. Reactions were performed in solvents of *reagents grade* quality or better and in dry and oxygen free solvents if necessary. Solvents were dried either by distilling over sodium (THF and diethyl ether) or sodium hydride (dichloromethane), or on a

solvent purification system “Pure Solv MD-5” (using several columns) by Innovative Technology inc.

For photophysical measurements, only HPLC quality solvents were used.

Column chromatography, preparative layer chromatography and spot thin layer chromatography

All silica column chromatography was performed using Merck silica gel 60 (0.063–0.200 mm). Fluka aluminium oxide 17994 and Merck aluminium oxide 90 standardized were used in alumina columns and for filtrations. Preparative layer chromatography was performed on silica gel (PLC plates 20 x 20 cm, silica gel 60 F₂₅₄, 2 mm, Merck) and aluminium oxide (PLC plates 20 x 20 cm, aluminium oxide 60 F₂₅₄, 1.5 mm, Merck). Spot thin layer chromatography was performed on silica gel plates (POLYGRAM[®] SILG/UV₂₅₄ and TLC silica gel 60 F₂₅₄, Merck) and aluminium oxide plates (TLC aluminium oxide 60 F₂₅₄, neutral, Merck).

Microwave reactor

Microwave reactions were carried out in a Biotage Initiator 8 reactor with sealed tubes allowing pressures of up to 20 bars.

NMR spectroscopy

NMR spectra were recorded on Bruker AM250 (250 MHz), Bruker AVANCE 300 (300 MHz), Bruker DPX400 (400 MHz), Bruker DRX500 (500 MHz) and on Bruker DRX600 (600 MHz). For full assignments COSY, DEPT, HMBC, HMQC and NOESY experiments were recorded on the Bruker DRX500 by either V. Jullien or J. Beves or K. Harris or A. Hernandez-Redondo. The measurements on the Bruker DRX600 were conducted by D. Häussinger. J. Beves performed measurements at variable temperatures.

¹H and ¹³C spectra were recorded at 25 °C and chemical shifts are relative to residual solvent peaks (¹H: CDCl₃ 7.26 ppm, CD₂Cl₂ 5.32 ppm, DMSO-*d*₆ 2.50 ppm, acetone-*d*₆ 2.05 ppm, acetonitrile-*d*₃ 1.94 ppm, methanol-*d*₄ 3.31 ppm; ¹³C: CDCl₃ 77.00 ppm, CD₂Cl₂ 54.00 ppm, DMSO-*d*₆ 39.51 ppm, acetone-*d*₆ 29.92 ppm, acetonitrile-*d*₃ 1.39 ppm, methanol-*d*₄ 49.15 ppm). An external reference was used for ¹⁹F (CF³⁵Cl₃ in CDCl₃) and ³¹P (H₃PO₄) spectra.

Mass spectrometry

FAB (NBA matrix) and electron impact (EI) mass spectra were recorded by P. Nadig using Finnigan MAT 312 and VG 70-250 instruments, respectively. Electrospray ionisation (ESI) mass spectra were measured using Finnigan MAT LCQ or Bruker esquire 3000^{plus} instruments.

Infrared spectroscopy

IR spectra were recorded on a Shimadzu FTIR-8400S spectrophotometer with neat samples using a golden gate attachment.

Melting points

Melting points were determined on a Stuart Scientific melting point apparatus SMP3.

UV-Vis spectroscopy

Electronic absorption spectra were recorded on Varian-Cary 5000 or on Agilent 8453 spectrophotometers.

Emission spectroscopy

Emission spectroscopy was performed on a Shimadzu RF-5301 PC spectrofluorophotometer. The excitation and emission slits were kept as close as possible and prior to the measurements, blank samples of the solvent were measured to assure that the solvent does not emit as well.

Lifetime measurements

The lifetime of the fluorescence was measured with an Edinburgh Instruments mini- τ apparatus equipped with an Edinburgh Instruments EPL-475 picosecond pulsed diode laser ($\lambda_{\text{exc}} = 467.0$ nm, pulse width = 75.5 ps) with the appropriate wavelength filter. The same solutions as for the fluorescence measurements were used.

Microanalysis

The microanalyses were performed with a Leco CHN-900 microanalyser by W. Kirsch.

Electrochemistry

Electrochemical measurements were done on an Eco Chemie Autolab PGSTAT 20 using a glassy carbon working electrode, a platinum mesh for the counter electrode, and a silver wire

as the reference electrode. The redox potentials ($E_{1/2}^{\text{ox}}$, $E_{1/2}^{\text{red}}$ [V]) were determined by cyclic voltammetry (CV) and by square wave and differential pulse voltammetry. The compounds were dissolved and measured in dry and degassed acetonitrile in the presence of 0.1 M [*n*-Bu₄N][PF₆] unless otherwise stated. The scanning rate for the CV was 100 mV·s⁻¹ in all cases and ferrocene (Fc) was added as an internal standard at the end of every experiment.

Atomic absorption spectroscopy and atomic emission spectroscopy

Measurements were performed on a Shimadzu AA-6300 atomic absorption spectrophotometer using a flame (acetylene/air) to atomise the samples. A sodium hollow cathode lamp (lamp current 12 mA, wavelength 489 nm, slit width 0.2 nm) was used as radiation source. The fuel gas flow rate was kept at 1.8 L/min and the support gas rate was kept at 15.0 L/min.

X-ray diffraction

The determination of the cell parameters and the collection of the reflection intensities of the single crystals were performed on an Enraf-Nonius Kappa CCD diffractometer (graphite monochromated MoK α radiation) by M. Neuburger or on a Stoe IPDS instrument by J. Zampese. For the data reduction, solution and refinement, the programs COLLECT,^[266] DENZO/SCALEPACK,^[267] SIR92,^[268] Stoe IPDS software,^[269] SHELXL97^[270] and CRYSTALS (version 12)^[271] were used by either M. Neuburger or S. Schaffner or J. Zampese. Structures have been analysed using Mercury v. 1.4.2.^[199]

Quantum yields

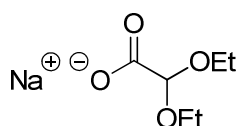
Luminescence quantum yields Φ were obtained by using equation 1, [Ru(bpy)₃]²⁺ as standard (R, $\Phi_R = 0.028$ in air-equilibrated water)^[272] for emissions around 620 nm and coumarin 307 (R, $\Phi_R = 0.95$ in methanol)^[273] as standard for emissions around 470 nm.

$$\Phi = \Phi_R \times \text{Int}/\text{Int}_R \times A_R/A \times n^2/n_R^2 \quad (1)$$

The area of the luminescence (Int) was calculated from spectra on an energy scale, *n* is the refractive index for the solvent ($n_{\text{water}} = 1.333$, $n_{\text{MeCN}} = 1.3442$, $n_{\text{MeOH}} = 1.329$, $n_{\text{DCM}} = 1.4242$) and A_R and *A* are absorbance values for the reference or the compound, respectively.

6.2 Experimental for Compounds in Chapter 1

Sodium 2,2-diethoxyacetate (**12**)

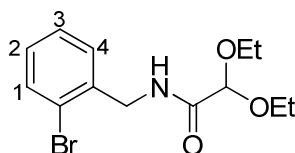


12

Ethyl 2,2-diethoxyacetate (115 g, 650 mmol) and NaOH (26.0 g, 650 mmol) were dissolved in 150 mL H₂O and 250 mL EtOH. The suspension was heated to reflux for 5 hours. Evaporation of solvents yielded pure **12** (110 g, 646 mmol, 99%) as a colourless solid.

¹H-NMR (300 MHz, CDCl₃): δ ppm = 6.48 (s, 1H, CH), 3.61-3.51 (m, 4H, CH₂), 1.18 (t, ³J = 7.0 Hz, 6H, CH₃).

N-(2-Bromobenzyl)-2,2-diethoxyacetamide (**14**)

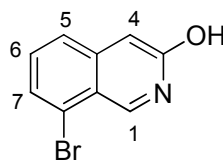


14

Sodium 2,2-diethoxyacetate (**12**) (22.8 g, 134 mmol) was dissolved in 100 mL dry diethyl ether. To the ice-cooled suspension was added drop wise SOCl₂ (15.9 g, 134 mol) over 10 min. The reaction mixture was heated to reflux for 30 min. In the meantime a solution of 50 mL pyridine, 80 mL toluene and (2-bromophenyl)methanamine (25 g, 134 mmol) was prepared. The latter solution was then transferred over 30 min to the *in situ*-formed acid chloride and stirred for 1 h at 0 °C. Ice-cooled water (250 mL) was added and the organic layer was separated. The aqueous phase was extracted with toluene (2 × 100 mL) and the combined organic phases were washed with 2% HCl (150 mL) and water (150 mL). The solvents were removed *in vacuo* yielding **14** (30.7 g, 97.1 mmol, 72 %) as a colourless oil.

$^1\text{H-NMR}$ (300 MHz, CDCl_3): δ ppm = 7.55 (dd, $J = 1.3, 7.9$ Hz, 1H, H^1), 7.38 (dd, $J = 1.8, 7.7$ Hz, 1H, H^4), 7.29 (td, $J = 1.3, 8.0$ Hz, 1H, H^2), 7.15 (td, $J = 1.8, 7.7$ Hz, 1H, H^3), 7.08 (sb, 1H, NH), 4.83 (s, 1H, CH), 4.55 (d, $J = 6.2$ Hz, 2H, CH_2NH), 3.75-3.56 (m, 4H, OCH_2), 1.24 (t, $J = 6.9$ Hz, 6H, CH_3).

8-Bromo-isoquinoline-3-ol (**15**)

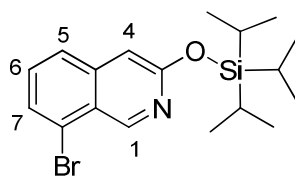


15

N-(2-Bromobenzyl)-2,2-diethoxyacetamide (**14**) (7.20 g, 22.7 mmol) was dissolved in 30 mL concentrated H_2SO_4 (95%) at 5 °C. The reaction mixture was stirred at room temperature for 16 h. Water (350 mL) was added under ice-cooling, a brown polymeric residue removed and the solution was neutralized to pH 7 with NH_3 (aq, 33%). The yellow precipitate was recrystallized in 150 mL EtOH (dissolved EtOH, filtered hot to remove a colourless impurity). The desired product **15** formed fine, yellow crystals (1.61 g, 7.19 mmol, 32%).

$^1\text{H-NMR}$ (300 MHz, CDCl_3): δ ppm = 9.08 (s, 1H, H^1), 7.63-7.54 (m, 2H, H^{5+7}), 7.37(t, 1H, H^6), 6.99 (s, 1H, H^4).

8-Bromoisoquinoline-3-(trisisopropyl)silyl ether (**16**)



16

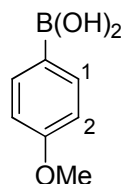
Imidazole (340 mg, 5.00 mmol) was added to a solution of 8-bromo-isoquinoline-3-ol (**15**) (448 mg, 2.00 mmol) and trisisopropylchlorosilane (463 mg, 2.40 mmol) in dry DMF (50 mL). The mixture was stirred for 3 h, diluted with 5% aqueous NaHCO_3 (200 mL) and extracted twice with CH_2Cl_2 (30 mL). The combined organic extracts were washed with water and the solvents removed *in vacuo*. Filtration over SiO_2 (pentane : diethyl ether (10:1)) yielded 623 mg (1.64 mmol, 82%) of a colourless solid.

$^1\text{H-NMR}$ (300 MHz, CDCl_3): $\delta_{\text{ppm}} = 9.20$ (s, 1H, H^1), 7.65-7.55 (m, 2H), 7.37-7.32 (m, 1H), 6.96 (s, 1H, H^4), 1.50-1.40 (m, 3H, CH), 1.13 (d, $J = 7.3$ Hz, 18 H, CH_3).

$^{13}\text{C-NMR}$ (75.5 MHz, CDCl_3): $\delta_{\text{ppm}} = 178.0, 160.0, 150.3, 141.0, 130.2, 127.9, 125.4, 122.5, 103.9, 18.0$ (CH_3), 12.6 (CH).

MS (ESI): $m/z = 380.1$ [$\mathbf{16} + \text{H}^+$] (calc. 380.1).

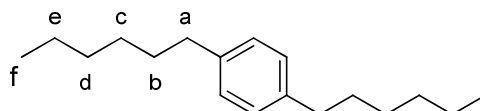
4-Methoxyphenylboronic acid



To a slight excess of Mg (3.60 g, 149 mmol) activated with a grain of I_2 in 50 mL dry THF was added drop wise 4-bromoanisole (16.9 mL, 135 mmol) in 50 mL dry THF to maintain slight reflux. The reflux was continued under argon for additional 45 min. The cooled solution was transferred to a degassed solution of trimethyl borate (30 mL, 264 mmol) in 250 mL of dry THF at -78 °C. The reaction mixture was stirred for 2 h and then allowed to warm at room temperature before hydrolysis with 300 mL of 4M hydrochloric acid. The solvents were removed and the milky precipitate was taken in 300 mL water and 300 mL diethyl ether. The organic phase was extracted twice with 200 mL 1M NaOH. The combined aqueous extracts were acidified to pH 1 with 37% HCl before extraction with two portions of diethyl ether (200 mL). The solvents were evaporated *in vacuo* to yield a white solid (12.6 g 82.9 mmol, 62%).

$^1\text{H-NMR}$ (300 MHz, acetone/ D_2O (~3:1)): $\delta_{\text{ppm}} = 7.73$ (d, $J = 8.5$ Hz, 2H, H^1), 6.84 (d, $J = 8.6$ Hz, 2H, H^2), 3.74 (s, 3H, CH_3).

1,4-Dihexylbenzene

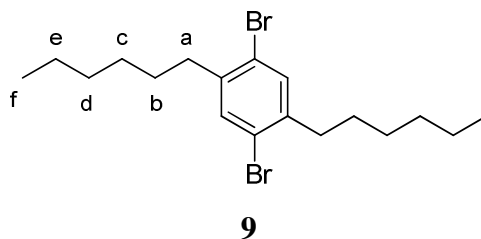


N-Hexyl-1-bromide (70 mL, 500 mmol) in 50 mL dry diethyl ether was added drop wise, over 30 min, to a suspension of Mg (13.4 g, 550 mmol) in 100 mL dry diethyl ether to maintain slight reflux. After complete addition, the solution was refluxed for additional 30 min. The *n*-

hexylmagnesium bromide, cooled to room temperature was transferred, over 30 min, to an ice-cooled and stirred mixture of 1,4-dichlorobenzene (29.4 g, 200 mmol) and [(dppp)Cl₂Ni] (108 mg, 200 μmol) in dry diethyl ether (200 mL). The cooling bath was removed and the solvent began to boil after an induction period of about 1 h. The mixture was then refluxed over night, cooled to 0 °C and quenched carefully with water (10 mL), followed by 2M HCl (100 mL). After separation of the layers, the aqueous phase was extracted with diethyl ether (2 × 50 mL), and the combined organic phases were washed with water (50 mL) and dried (MgSO₄). The solvent was removed to yield the crude but analytically pure title compound **151** (48.2 g, 196 mmol, 98%) as a slightly yellow oil.

¹H-NMR (300 MHz, CDCl₃): δ_{ppm} = 7.09 (s, 4H, H^{arom}), 2.57 (t, ³J = 7.7 Hz, 4H, H^a), 1.65-1.52 (m, 4H, H^b), 1.37-1.26 (m, 12H, H^{c+d+e}), 0.89 (t, ³J = 7.1 Hz, 6H, H^f).

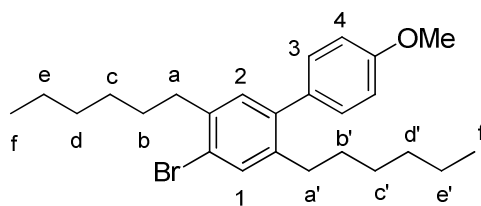
1,4-Dibromo-2,5-dihexylbenzene (**9**)



Bromine (67.1 g, 420 mmol) was added drop wise, over 30 min, to a stirred and ice-cooled solution of 1,4-dihexylbenzene (**151**) (49.3 g, 200 mmol) and iodine (~500 mg, 0.01 eq) under rigorous exclusion of light. After 1 d at room temperature, 20% aqueous KOH solution (100 mL) was added and the mixture was shaken under slight warming until the colour disappeared. The mixture was then cooled to room temperature, the aqueous solution was decanted and the remaining residue was recrystallized from EtOH to yield title compound **9** (65.9 g, 163 mmol, 82%) as colourless crystals.

¹H-NMR (300 MHz, CDCl₃): δ_{ppm} = 7.35 (s, 2H, H^{arom}), 2.64 (t, J = 7.7 Hz, 4H, H^a), 1.60-1.49 (m, 4H, H^b), 1.41-1.24 (m, 12H, H^{c+d+e}), 0.90 (t, ³J = 7.1 Hz, 6H, H^f).

4-Bromo-2,5-dihexyl-4'-methoxybiphenyl (**10**)

**10**

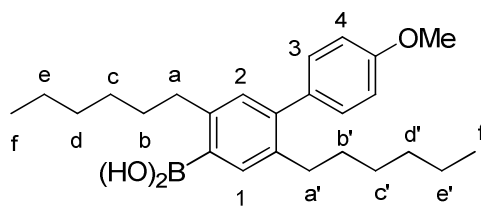
1,4-Dibromo-2,5-dihexylbenzene (**9**) (23.9 g, 59.2 mmol), 4-methoxyphenylboronic acid (4.50 g, 29.6 mmol) and Na_2CO_3 (5.02 g, 47.4 mmol) were dissolved in 800 mL toluene, 150 mL EtOH and 50 mL H_2O . The solution was degassed with argon (30 min) before addition of $[\text{Pd}(\text{PPh}_3)_4]$ (867 mg, 750 μmol). The reaction mixture was heated to reflux for 16 h, extracted twice with water (200 mL) and purified by column chromatography (SiO_2 , 0.4% ethyl acetate in pentane) to yield title compound **10** (10.1 g, 23.4 mmol, 79%) as a colourless oil.

$^1\text{H-NMR}$ (300 MHz, CDCl_3): $\delta_{\text{ppm}} = 7.41$ (s, 1H, H^1), 7.19 (d, $J = 8.8$ Hz, 2H, H^3), 7.01 (s, 1H, H^2), 6.93 (d, $J = 8.8$ Hz, 2H, H^4), 3.85 (s, 3H, OCH_3), 2.68 (t, $J = 7.7$ Hz, 2H, H^a), 2.49 (t, $^3J = 7.7$ Hz, 2H, $\text{H}^{a'}$), 1.65-1.52 (m, 2H, CH_2), 1.46-1.11 (m, 14H, CH_2), 0.88-0.75 (m, 6H, CH_3).

$^{13}\text{C-NMR}$ (75.5 MHz, CDCl_3): $\delta_{\text{ppm}} = 158.6, 140.7, 140.0, 139.1, 133.5, 133.0, 131.8, 130.2, 123.0, 113.5, 55.3$ (OCH_3), 35.8, 32.4, 31.7, 31.5, 31.1, 30.0, 20.2, 20.1, 22.6, 22.5, 14.1 (2 CH_3).

MS (EI): $m/z = 430.2$ [**10**] (calc. 430.2).

Boronic acid **11**

**11**

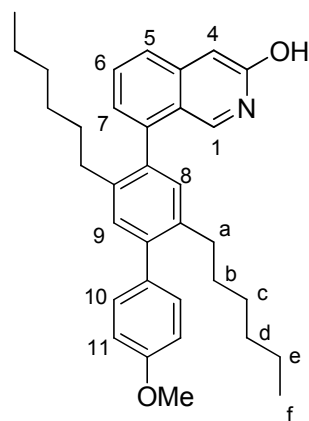
Bromo compound **10** (4.28 g, 9.92 mmol) was dissolved in 500 mL anhydrous THF and cooled to -78 $^\circ\text{C}$. *N*-Buthyllithium (12.4 mL, 1.6M solution in hexane, 19.8 mmol) was added drop wise to this solution. The reaction mixture was stirred over a period of 2 h at this temperature whereby a slight yellow colouring was observed. Trimethyl borate (2.2 mL, 19.8 mmol) was added, and the reaction mixture (now colourless) was stirred at room temperature over night. Hydrochloric acid (200 mL, 4M) was added and the solvents were

removed *in vacuo*. The white precipitate was dissolved in 150 mL diethyl ether and 150 mL water. The organic phase was separated and the solvent removed to yield a white solid (4.06 g, 10.3 mmol, quant.) which was used without further purification for the next step.

$^1\text{H-NMR}$ (300 MHz, acetone/ D_2O (~6:1)): $\delta_{\text{ppm}} = 7.47$ (s, 1H, H^1), 7.17 (d, $^3J = 8.8$ Hz, 2H, H^3), 6.94 (d, $^3J = 8.8$ Hz, 2H, H^4), 6.87 (s, 1H, H^2), 3.79 (s, 3H, OCH_3), 2.79 (t, $J = 7.7$ Hz, 2H, H^a), 2.49 (t, $J = 7.7$ Hz, 2H, H^a), 1.58-1.46 (m, 2H, CH_2), 1.42-1.03 (m, 14H, CH_2), 0.83-0.72 (m, 6H, CH_3).

MS (ESI): $m/z = 509.3$ [$\mathbf{11} + \text{CF}_3\text{CO}_2^-$] (calc. 509.4).

Compound 18



18

8-Bromo-isoquinoline-3-ol (**15**) (167 mg, 746 μmol), boronic acid **11** (340 mg, 859 μmol), potassium *tert*-butoxide (209 mg, 1.87 mmol) dissolved in 150 mL anhydrous dimethoxyethane. The solution was set under argon (30 min) before addition of $[\text{Pd}(\text{PPh}_3)_4]$ (86.0 mg, 74.6 μmol) and heated to reflux over night. The residue was washed with CH_2Cl_2 on SiO_2 in order to remove less polar impurities. The crude product was used without further purifications for triflation.

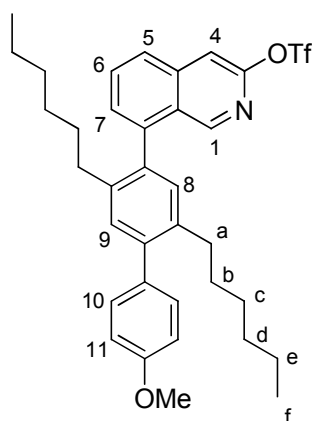
$^1\text{H-NMR}$ (300 MHz, CDCl_3): $\delta_{\text{ppm}} = 8.20$ (s, 1H, H^1), 7.50-7.48 (m, 2H), 7.35 (d, $^3J = 8.8$ Hz, 2H, H^{10}), 7.15 (s, 1H), 7.05-6.99 (m, 4H), 6.89 (s, 1H), 3.86 (s, 3H, OMe), 2.57-2.49 (m, 2H, H^a), 2.40-2.19 (m, 2H, H^a), 1.40-0.91 (m, 16H, H^{b-e}), 0.79 (t, $J = 6.8$ Hz, 3H, H^f), 0.72 (t, $J = 7.1$ Hz, 3H, H^f).

$^{13}\text{C-NMR}$ (75.5 MHz, CDCl_3): $\delta_{\text{ppm}} = 162.0, 158.5, 142.7, 142.3, 141.4, 141.0, 138.3, 137.8, 135.8, 134.2, 131.5, 131.0, 130.9, 130.3, 124.5, 124.2, 120.6, 113.5, 106.5, 55.3$

(OCH₃), 32.8, 32.6, 31.5, 31.3, 31.2, 29.2, 29.0, 25.6, 22.5, 22.4, 14.0 (CH₂CH₃), 13.0 (CH₂CH₃).

MS(ESI): $m/z = 496.3$ [**18** + H⁺] (calc. 496.3).

Trifluoro-methanesulfonic acid 8-(2,5-dihexyl-4'-methoxy-biphenyl-4-yl)-isoquinolin-3-yl ester (**19**)



19

Three steps

Triisopropylsilyl ether **16** (6.77 g, 17.8 mmol) and boronic acid **11** (8.72 g, 22.0 mmol) were dissolved in 90 mL dimethoxyethane and 15 mL H₂O. The solution was degassed with argon (30 min) before addition of [Pd(PPh₃)₄] (825 mg, 712 μmol) and Ba(OH)₂·8 H₂O (7.30 g, 23.2 mmol) and refluxed over night. The TIPS-protecting group was partially removed during the reaction. In order to complete the deprotection, the reaction mixture was evaporated to dryness, dissolved in 100 mL THF, TBAF·3H₂O (6.18 g, 19.6 mmol) was added and the reaction mixture was stirred during a period of 30 min. The solution was concentrated to dryness and the residue was filtered on SiO₂ (CH₂Cl₂ → CH₂Cl₂ : MeOH (9:1)) in order to remove less polar impurities. The crude phenol was dissolved in 250 mL anhydrous CH₂Cl₂ and 40 mL anhydrous NEt₃. The solution was cooled to -10 °C and trifluoromethanesulfonic anhydride (4.5 mL, 26.7 mmol) were added slowly. The reaction mixture was stirred for 16 h at room temperature, washed with saturated NH₄Cl and purified by column chromatography (SiO₂, pentane:Et₂O (20:1)) to provide triflate **19** (7.22 g, 65% with respect to **16**) as a slightly yellow oil.

The crude **18** was dissolved in 50 mL dry CH₂Cl₂ and 1.1 mL abs. NEt₃. The solution was cooled to -78 °C and trifluoromethanesulfonic anhydride (270 μL, ~2 eq) were added slowly. The reaction mixture was stirred for 16 h at room temperature washed with saturated NH₄Cl

and purified by column chromatography (SiO₂, pentane:Et₂O (10:1)) to provide triflate **19** (176 mg, 280 μmol, 38% with respect to **15**) as a yellow oil.

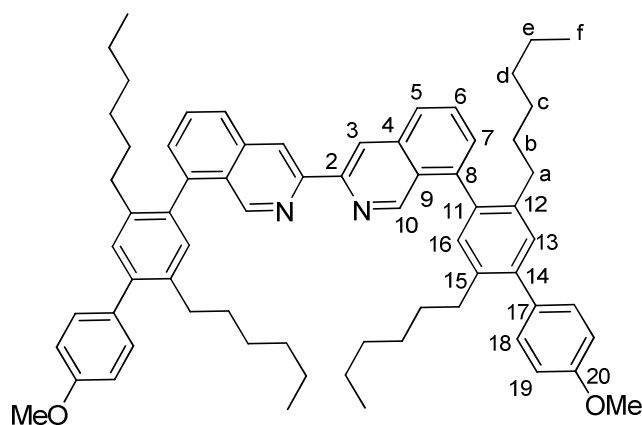
¹H-NMR (300 MHz, CDCl₃): δppm = 8.81 (t, ⁴J = 0.8 Hz, 1H, H¹), 7.93-7.81 (m, 2 H), 7.62-7.56 (m, 2 H), 7.32 (d, J = 8.8 Hz, 2H, H¹⁰), 7.19 (s, 1 H), 7.10 (s, 1 H), 7.00 (d, ³J = 9.0 Hz, 2H, H¹¹), 3.89 (s, 3H, OMe), 2.58-2.55 (m, 2H, H^a), 2.42-2.28 (m, 2H^{a'}), 1.40-0.91 (m, 16H, H^{b-c}), 0.80 (t, J = 6.8 Hz, 3H, H^f), 0.73 (t, J = 7.1 Hz, 3H, H^f).

¹³C-NMR (75.5 MHz, CDCl₃): δppm = 158.6, 152.4, 151.7, 141.7, 141.2, 138.6, 138.4, 137.9, 135.4, 134.0, 131.4, 131.2, 131.0, 130.3, 129.3, 127.8, 126.0, 113.5, 110.6, 76.6 (CF₃), 55.3 (OCH₃), 32.8, 32.6, 31.5, 31.3, 31.1, 29.7, 29.2, 28.9, 22.5, 22.3, 14.0 (CH₂CH₃), 13.9 (CH₂CH₃).

¹⁹F-NMR (282.4 MHz, CDCl₃): δppm = -73.4 (s).

MS (ESI): *m/z* = 628.3 [**19** + H⁺] (calc. 628.3).

Biisoquinoline **20**



20

Triflate **19** (1.68 g, 2.68 mmol), 1.75 g zinc (10 eq, activated by treatment of 20 g in 100 mL acetic acid for 1 h. After filtration the powder was washed three times with distilled water. It was dried under vacuum for 6 h at 120 °C), dry KI (1.78 g, 10.7 mmol) and [PdCl₂dppf] (218 mg, 268 μmol) were dissolved in 1.8 mL dry DMF and stirred for 16 h at 90 °C. The mixture was hydrolysed with 10% aqueous HCl (40 mL) and extracted with diethyl ether. The red solution was filtered three times over Al₂O₃ before purification by column chromatography (SiO₂, pentane: Et₂O (20:1)) to yield **20** (950 mg, 992 μmol, 74%) as a colourless solid.

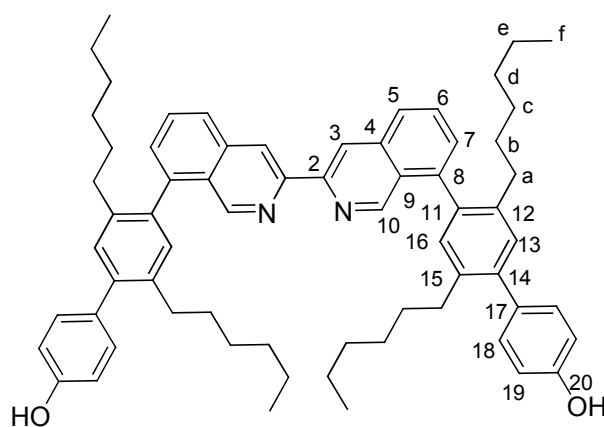
¹H-NMR (300 MHz, CDCl₃): δppm = 9.12 (s, 2H, H¹⁰), 8.94 (s, 2H, H³), 7.98 (d, ³J = 8.1 Hz, 2H, H⁵), 7.76 (t, ³J = 7.5 Hz, 2H, H⁶), 7.52 (d, J = 7.6 Hz, 2H, H⁷), 7.36 (d, J = 7.7 Hz, 4H,

H¹⁸), 7.23 (s, 2H, H^{13/16}), 7.20 (s, 2H, H^{13/16}), 7.02 (d, $J = 7.7$ Hz, 4H, H¹⁹), 3.91 (s, 6H, OCH₃), 2.65-2.55 (m, 4H, H^a), 2.49-2.37 (m, 2H, H^{a'}), 2.36-2.22 (m, 2H, H^{a''}), 1.52-0.93 (m, 32H, H^{b-e}), 0.82 (t, $J = 7.2$ Hz, 6H, H^f), 0.71 (t, $J = 7.2$ Hz, 6H, H^f).

¹³C-NMR (75.5 MHz, CDCl₃): δ ppm = 158.6 (C²⁰), 151.4 (C¹⁰), 149.8, 141.2, 140.6, 138.6, 137.7, 136.9, 136.4, 134.4, 131.4, 130.9, 130.4 (C¹⁸), 130.0, 128.4 (C⁷), 127.6, 126.9 (C⁵), 117.5 (C³), 113.5 (C¹⁹), 55.3, 32.9, 32.7, 31.5, 31.4, 31.3, 31.1, 29.2, 28.9, 22.5, 22.3, 14.0 (CH₃), 13.9 (CH₃).

MS (ESI): $m/z = 957.6$ [**20** + H⁺] (calc. 957.6).

Deprotected bisoquinoline **21**



21

Bisoquinoline **20** (130 mg, 136 μ mol) was refluxed in 5 g pyridinium chloride for 24 h. The mixture was cooled to 90 °C, water (20 mL) was added and the solution was neutralized with 0.5M KOH to pH 7. The solution was extracted with CH₂Cl₂ (3 \times 20 mL) and filtered over silica gel to yield a colourless solid (111 mg, 119 μ mol, 96%).

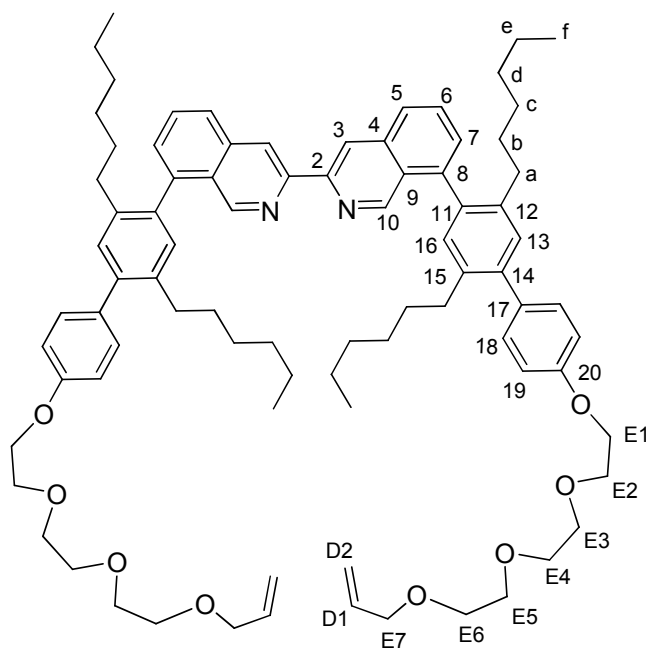
Pyridinium chloride was synthesised by drop wise addition of 108 mL HCl (37%) to 100 mL of pyridine at 0 °C. The product was dried under vacuum for 3 days.

¹H-NMR (300 MHz, CDCl₃): δ ppm = 9.17 (s, 2H, H¹⁰), 8.96 (s, 2H, H³), 8.00 (d, $^3J = 8.1$ Hz, 2H, H⁵), 7.78 (t, $J = 7.5$ Hz, 2H, H⁶), 7.54 (d, $J = 7.6$ Hz, 2H, H⁷), 7.30-7.20 (m, 8H, H¹³⁺¹⁶⁺¹⁸), 6.96 (d, $J = 7.7$ Hz, 4H, H¹⁹), 6.30 (sb, 2H, OH), 2.65-2.55 (m, 4H, H^a), 2.49-2.37 (m, 2H, H^{a'}), 2.36-2.22 (m, 2H, H^{a''}), 1.52-0.93 (m, 32H, H^{b-e}), 0.81 (t, $J = 7.2$ Hz, 6H, H^f), 0.71 (t, $J = 7.2$ Hz, 6H, H^f).

¹³C-NMR (75.5 MHz, CDCl₃): δ ppm = 155.0, 151.4, 149.5, 141.4, 140.7, 138.6, 137.7, 137.0, 136.2, 134.2, 131.4, 131.0, 130.5, 130.3, 128.7, 127.6, 127.0, 118.3, 115.2, 33.0, 32.7, 31.5, 31.4, 31.2, 29.7, 29.3, 29.0, 22.5, 22.4, 14.1, 14.0.

MS (ESI): $m/z = 929.6$ [**21** + H^+] (calc. 929.6).

Ligand **7**



7

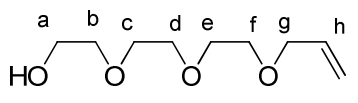
Dihydroxy biisoquinoline **21** (782 mg, 842 μmol), 3-(2-(2-(2-bromoethoxy)ethoxy)ethoxy)prop-1-ene (**28**) (859 mg, 3.45 mmol) and Cs_2CO_3 (1.12 g, 3.45 mmol) were dissolved in 50 mL freshly distilled DMF. The reaction mixture was stirred for 16 h at 90 °C. Water (15 mL) was added, leading to a milky solution, which was extracted with CH_2Cl_2 (5×10 mL) and Et_2O (3×40 mL). The combined organic layers were dried over Na_2SO_4 and the crude product was purified by column chromatography (SiO_2 , pentane: Et_2O (20:1) \rightarrow Et_2O) to **7** (794 mg, 620 μmol , 74%) as a slightly yellow oil.

$^1\text{H-NMR}$ (300 MHz, CDCl_3): δ ppm = 9.11 (s, 2H, H^{10}), 8.93 (s, 2H, H^3), 7.97 (d, $J = 8.1$ Hz, 2H, H^5), 7.75 (t, $J = 7.5$ Hz, 2H, H^6), 7.51 (d, $J = 7.6$ Hz, 2H, H^7), 7.33 (d, $J = 8.8$ Hz, 4H, H^{18}), 7.21 (s, 2H, $H^{13/16}$), 7.18 (s, 2H, $H^{13/16}$), 7.02 (d, $J = 8.8$ Hz, 4H, H^{19}), 6.02-5.84 (m, 2H, H^{D1}), 5.33-5.16 (m, 4H, H^{D2}), 4.22 (t, $J = 5.1$ Hz, 4H, H^{E1}), 4.06-4.03 (m, 4H, H^{E7}), 3.93 (t, $^3J = 5.1$ Hz, 4H, H^{E2}), 3.79-3.58 (m, 16H, H^{E3-E6}), 2.64-2.54 (m, 4H, H^a), 2.49-2.37 (m, 2H, H^a), 2.36-2.22 (m, 2H, H^a), 1.52-0.75 (m, 38H, $H^{b-c, f}$), 0.70 (t, $J = 7.3$ Hz, 6H, H^f).

$^{13}\text{C-NMR}$ (75.5 MHz, CDCl_3): δ ppm = 157.8, 151.5, 151.4, 149.4, 141.2, 140.6, 138.6, 137.7, 134.8, 134.5, 131.4, 130.9, 130.3, 130.0 (2 C), 128.5, 128.4, 127.6, 127.0, 117.1, 114.2, 72.3, 70.9, 70.8 (2 C), 69.9, 69.5, 67.5, 33.0, 32.7, 31.5, 31.3, 31.1, 29.7, 29.2, 29.0, 22.5, 22.3, 14.1, 14.0.

MS (ESI) $m/z = 1273.81 [7 + H^+]$ (calc. 1273.8).

2-(2-(2-(Allyloxy)ethoxy)ethoxy)ethanol (**26**)

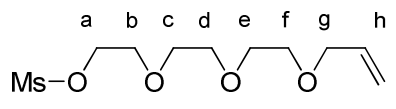


26

Finely crushed potassium hydroxide (56.1 g, 1.00 mol) and triethylene glycol (67.0 mL, 500 mmol) were put in a 500 mL flask. Allyl bromide (10.5 mL, 100 mmol) was added drop wise to the suspension at 90 °C. The heating was continued after complete addition for 3 h at 90 °C. To the cooled solution was added 250 mL water. The aqueous phase was extracted with toluene (3 × 30 mL) to remove the bis-allyl product. The aqueous phase was then extracted with CH₂Cl₂ (3 × 100 mL) to isolate the analytically pure mono-allyl alcohol **26** (7.34 g, 38.6 mmol, 39%) as a light yellow oil after solvent removal.

¹H-NMR (300 MHz, CDCl₃): δ ppm = 5.93-5.78 (m, 1H, H^h), 5.24-5.15 (m, 2H, Hⁱ), 3.95 (dt, $J = 5.7, 13.1$ Hz, 2H, H^g), 3.70-3.55 (m, 12H, H^{a,b,c,d,e,f}), 2.55 (s_b, OH).

2-(2-(2-(Allyloxy)ethoxy)ethoxy)ethyl methanesulfonate (**27**)

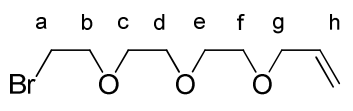


27

A degassed solution of **26** (7.34 g, 49.5 mmol) in anhydrous CH₂Cl₂ (200 mL) in presence of freshly distilled NEt₃ (41.4 mL, 297 mmol) was placed at -10 °C in a two-necked flask equipped with an argon gas inlet and a dropping funnel. Mesyl chloride (5.75 mL, 74.3 mmol) in anhydrous CH₂Cl₂ (30 mL) was slowly added to the mixture. The reaction was followed by TLC until complete disappearance of the starting materials (4 h). The solution was washed with water (4 × 100 mL) and the combined organic phases were extracted with CH₂Cl₂ (50 mL). The organic phases were combined, dried over MgSO₄ and the solvent was evaporated. The crude product was purified by column chromatography (Al₂O₃, CH₂Cl₂) to give title compound **27** (8.59 g, 38.0 mmol, 77%) as a slightly yellow oil.

$^1\text{H-NMR}$ (300 MHz, CDCl_3): δ ppm = 6.02-5.94 (m, 1H, H^{h}), 5.36-5.09 (m, 2H, H^{i}), 4.33-4.30 (m, 2H, H^{a}), 3.94 (td, $^3J = 6.7, 1.5$ Hz, 2H, H^{e}), 3.70 (m_c, 2H, H^{b}), 3.61-3.49 (m, 8H, $\text{H}^{\text{c,d,e,f}}$), 3.06 (s, 3 H, CH_3).

3-(2-(2-(2-Bromoethoxy)ethoxy)ethoxy)prop-1-ene (**28**)

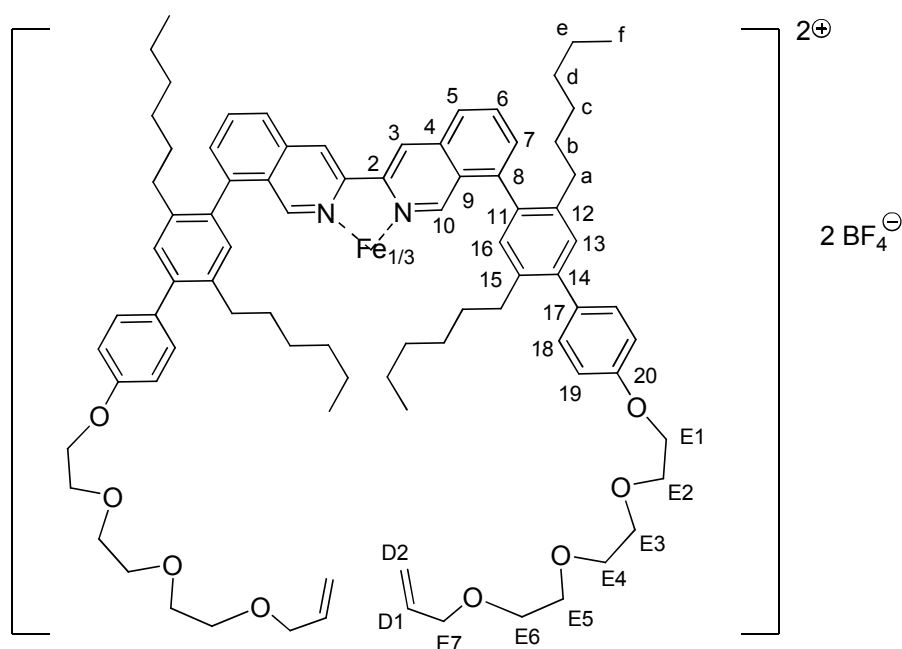


28

In a 500 mL two-necked flask equipped with a magnetic stirrer and a condenser was prepared a solution of the mesylate compound **27** (8.59 g, 40.0 mmol), lithium bromide (20.8 g, 240 mmol) in acetone (200 mL, analytical grade). The reaction mixture was heated to reflux over night. The acetone was evaporated and the crude mixture was dissolved in CH_2Cl_2 and washed with water (3×50 mL). The organic phase was dried over MgSO_4 and filtered. Evaporation of the solvent yielded the analytically pure bromide **28** (7.73 g, 36.6 mmol, 92%) as a yellow oil.

$^1\text{H-NMR}$ (300 MHz, CDCl_3): δ ppm = 5.92-5.79 (m, 1H, H^{h}), 5.25-5.10 (m, 2H, H^{i}), 3.96 (td, $J = 1.5, 5.5$ Hz, 2H, H^{e}), 3.75 (t, $J = 6.4$ Hz, 2H, H^{b}), 3.65-3.53 (m, 8H, $\text{H}^{\text{c,d,e,f}}$), 3.41 (t, $J = 6.3$ Hz, 2H, H^{a}).

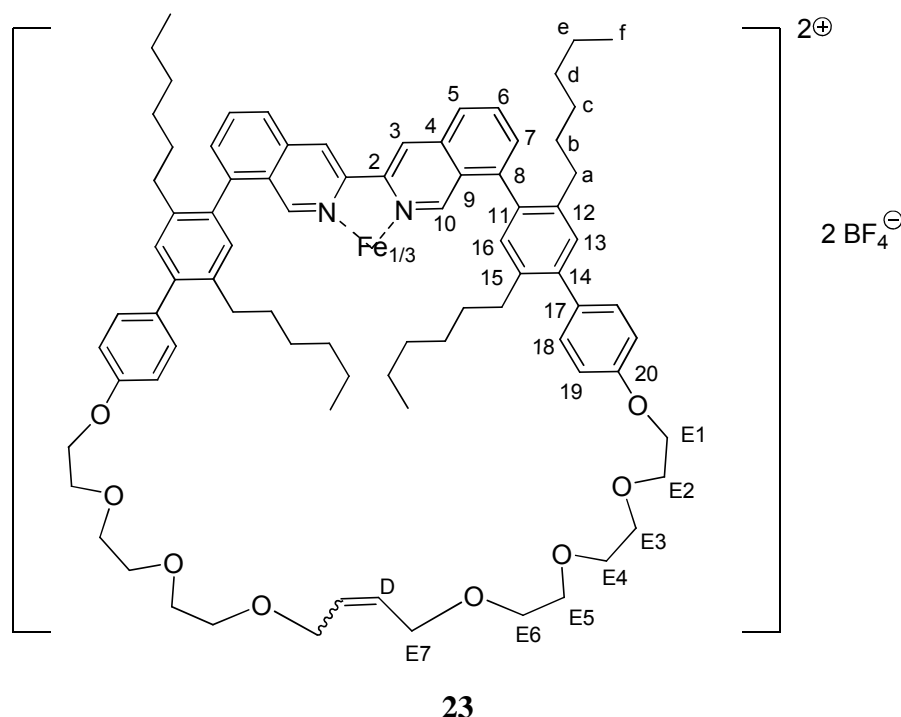
$[\text{Fe}(\mathbf{7})_3][\text{BF}_4]_2$ (**22**)



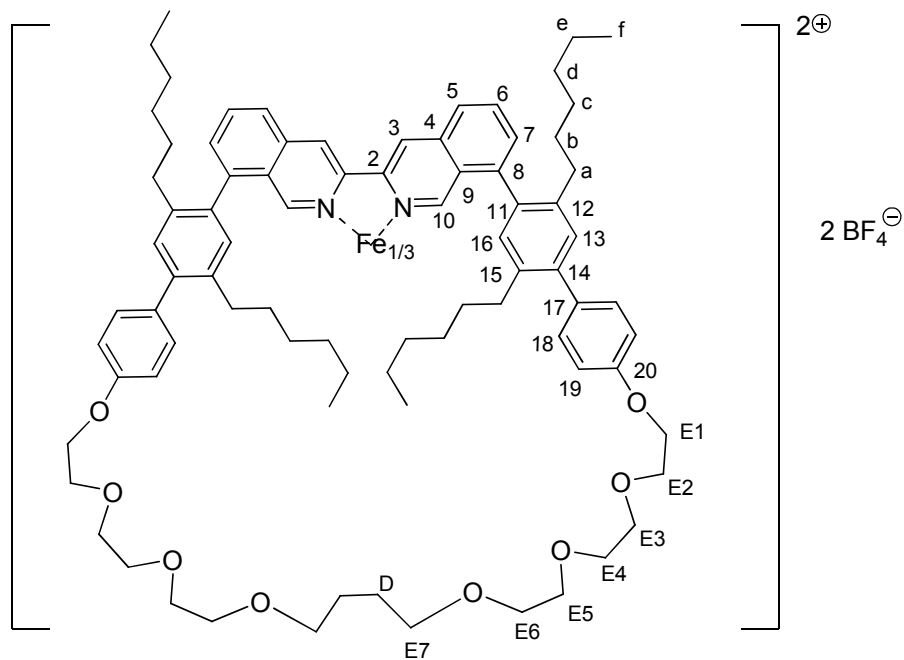
Ligand **7** (55.3 mg, 43.4 μmol) was dissolved in CH_2Cl_2 and $[\text{Fe}(\text{BF}_4)_2 \cdot 6 \text{H}_2\text{O}]$ (14.6 mg, 43.7 μmol) in MeOH was added and the solution turned immediately red. The solution was refluxed over night and purified by column chromatography (SiO_2 , $\text{Et}_2\text{O} \rightarrow \text{Et}_2\text{O} : \text{MeOH}$ (20:1)) to yield a red solid (54.7 mg, 13.5 μmol , 93%). The $^1\text{H-NMR}$ displayed a very complex spectrum due to an expected hindered rotation around the bond between the biphenyl part and the isoquinoline that renders the two sides different and gives rise to several isomers and desymmetrization. ESI-MS showed one peak of the double charged product and on TLC only one spot was seen.

MS (ESI): $m/z = 1938.2$ $[\text{Fe}(\mathbf{7})_3]^{2+}$ (calc. 1938.2).

Grubbs' reaction (**23**)



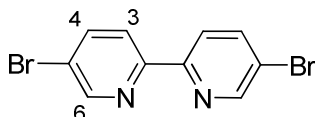
The iron complex **22** (150.0 mg, 37.0 μmol) was dissolved in 185 mL freshly distilled CH_2Cl_2 ($2 \cdot 10^{-4} \text{M}$ solution) and Grubbs catalyst (1st generation) (45.7 mg, 55.5 μmol) were added. The reaction mixture was stirred at room temperature over a period of 7 days under argon atmosphere. Every second day 30 mg of catalyst was added. The reaction was quenched with ethoxyethene (2 mL) and purified twice with column chromatography (SiO_2 , $\text{Et}_2\text{O} \rightarrow \text{Et}_2\text{O} : \text{MeOH}$ (20:1)) leading to 153 mg of the crude product. The $^1\text{H-NMR}$ spectrum showed the disappearance of the terminal allyl signals and one new broad singlet at δ 5.88 ppm that corresponds to the newly formed double bond.

Hydrogenation (**24**)**24**

The iron complex **23** (150 mg, 37.0 μmol) was dissolved in 20 mL CH_2Cl_2 and 30 mg of Pd/C (10% Pd) was added. Hydrogen gas was bubbled through the solution during a period of 8 h. The solution was filtered over Celite yielding after evaporation of the solvent 152 mg of a red solid. The $^1\text{H-NMR}$ showed no longer the peak at δ 5.88 ppm.

6.3 Experimental for Compounds in Chapter 2

5,5'-Dibromo-2,2'-bipyridine (**32**)



32

To a flask evacuated and put under Nitrogen, 2,5-dibromopyridine (16.2 g, 69.0 mmol) was dissolved in abs. toluene (500 mL) and *n*-Bu₆Sn₂ (20.0 g, 34.5 mmol) was added. Nitrogen was bubbled through the stirred solution for 1 h before [Pd(Ph₃)₄] (1.60 g, 1.38 mmol) was added. The reaction mixture was refluxed during 3 d until all starting material was consumed (TLC control). To the reaction mixture a NaOH-solution (0.1M, 400 mL) was added and the organic phase was separated. The water phase was extracted with CH₂Cl₂ (3 × 100 mL). The combined organic phases were dried over Na₂SO₄. After chromatography (SiO₂, CH₂Cl₂) compound **32** could be isolated as a colourless solid (8.5 g, 27.2 mmol, 79%).

An alternative synthesis starts with 2,2'-bipyridine (3.43 g, 22.0 mmol) which was dissolved in HBr (48%). The reaction mixture was reduced to dryness. The precipitate formed was collected and dried in vacuum (99%). The latter and bromine (7.0 g, 43.8 mmol) were placed in a sealed tube and heated to 180 °C during 72 h. The mixture was then allowed to cool and the hard solid was powdered and treated with Na₂SO₃ to remove unreacted bromine, then basified with sodium hydroxide solution (500 mL, 3M). Chromatography (SiO₂, CH₂Cl₂) yielded 4.11 g (13.1 mmol, 21%) **32**.

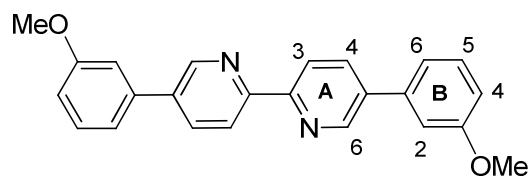
¹H-NMR (400 MHz, CDCl₃): δ/ppm = 8.70 (d, ⁴J = 2.8 Hz, 2H, H⁶), 8.27 (d, ³J = 8.8 Hz, 2H, H³), 7.93 (dd, ³J = 8.8 Hz, ⁴J = 2.8 Hz, 2H, H⁴).

¹³C-NMR (100.6 MHz, CDCl₃): δ/ppm = 153.7, 150.3, 139.6, 122.2, 121.4.

MS (EI): *m/z* = 313.9 [**32** + H⁺] (calc. 313.9).

IR (ATR): $\tilde{\nu}/\text{cm}^{-1}$ = 3049w, 2920w, 2850w, 1537m, 1454m, 1356s, 1084s, 858s.

Anal. calc. for C₁₀H₆N₂Br₂ C 38.25, H 1.93, N 8.92; found C 38.20, H 1.91, N 8.82.

5,5'-Bis(3-methoxyphenyl)-2,2'-bipyridine (**34**)**34**

3-Methoxyphenylboronic acid (**33**) (3.63 g, 23.9 mmol) was added to 5,5'-dibromo-2,2'-bipyridine (**32**) (3.00 g, 9.55 mmol) followed by toluene (200 mL), Na₂CO₃ (5.06 g, 47.8 mmol) and water (70 mL). The biphasic mixture was then degassed for 20 min by bubbling nitrogen through the solution. [Pd(PPh₃)₄] (500 mg, 432 μmol) was added and the mixture was heated to reflux for 20 h. After cooling to room temperature, the phases were separated and the aqueous layer extracted with CH₂Cl₂ (3 × 50 mL). The organic extracts were combined and dried with MgSO₄. After purification via chromatography (SiO₂, CH₂Cl₂ : MeOH (100:1)) a colourless solid (3.28 g, 8.90 mmol, 90%) could be isolated.

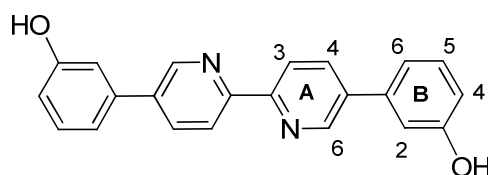
¹H-NMR (400 MHz, CDCl₃): δ/ppm = 8.94 (d, ⁴J = 2.8 Hz, 2H, H^{A6}), 8.51 (d, ³J = 8.2 Hz, 2H, H^{A3}), 8.04 (dd, ³J = 8.2 Hz, ⁴J = 2.4 Hz, 2H H^{A4}), 7.40 (t, ³J = 7.8 Hz, 2H, H^{B5}), 7.26 (dd, ³J = 7.8 Hz, ⁴J = 2.4 Hz, 2H, H^{B6}), 7.19 (d, ⁴J = 2.3 Hz, 2H, H^{B2}), 6.98 (dd, ³J = 7.9 Hz, ⁴J = 2.1 Hz, 2H, H^{B4}), 3.90 (s, 6 H, OMe).

¹³C-NMR (100.6 MHz, CDCl₃): δ/ppm = 160.2, 154.3, 147.5, 138.9, 136.5, 135.5, 130.2, 121.1, 119.5, 113.6, 112.8, 55.4.

MS (EI): *m/z* = 368.2 [M⁺] (calc 368.2).

IR (ATR): $\tilde{\nu}/\text{cm}^{-1}$ = 3007w, 2939w, 2839w, 1595s, 1501m, 1460m, 1429m, 1367m, 1305m, 1236m, 1224s, 1045m, 1028m, 864m, 694s.

Anal. calc. for C₂₄H₂₀N₂O₂ C 78.24 H, 5.47, N 7.60, O 8.69;. Found C 78.03, H 5.48, N 7.56.

3,3'-(2,2'-Bipyridine-5,5'-diyl)diphenol (**35**)**35**

Pyridinium chloride (30 g) and 5,5'-bis(3-methoxyphenyl)-2,2'-bipyridine (**34**) (2.15 g, 5.84 mmol) were refluxed during 4 h. The reaction mixture was allowed to cool to 120 °C, when water (300 mL) was added. The solution was neutralized to pH 7 with NaHCO₃. The product **35** was filtered off, washed with water and ether and dried to yield a pale yellow powder (2.16 g, 6.35 mmol, 98%).

¹H-NMR (400 MHz, DMSO-*d*₆): δ ppm = 9.87 (s_b, 2 OH), 8.97 (d, ⁴*J* = 2.8 Hz, 2H, H^{A6}), 8.50 (d, ³*J* = 8.2 Hz, 2H, H^{A3}), 8.21 (dd, ³*J* = 8.1 Hz, ⁴*J* = 2.2 Hz, 2H, H^{A4}); 7.33 (t, ³*J* = 8.0 Hz, 2H, H^{B5}); 7.23 (d, ³*J* = 7.8 Hz, 2H, H^{B6}); 7.16 (d, ⁴*J* = 2.3 Hz, 2 H^{B2}); 6.86 (dd, ³*J* = 7.8 Hz, ⁴*J* = 2.2 Hz, 2 H^{B4}).

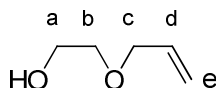
¹³C-NMR (100.6 MHz, DMSO-*d*₆): δ ppm = 158.0, 153.1, 146.9, 137.7, 135.9, 135.4, 130.2, 120.7, 117.5, 115.4, 113.5.

MS (EI): *m/z* = 340.1 [M⁺] (calc. 340.1).

IR (ATR): $\tilde{\nu}/\text{cm}^{-1}$ = ~3100br, 1585s, 1470s, 1443m, 1371m, 1325m, 1312m, 1298m, 1196s, 1151w, 1072w, 1020m, 997m, 889m, 823m, 777m, 736m, 679s.

Anal. calc. for C₂₂H₁₆N₂O₂·1.5 H₂O C 71.92 H 5.21 N 7.62; found C 72.13 H 4.81 N 7.55.

2-(Allyloxy)ethanol (**36**)



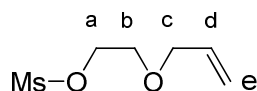
Finely crushed potassium hydroxide (84.2 g, 1.50 mol) and ethylene glycol (83.0 mL, 1.50 mol) were put in a 500 mL flask. Allyl bromide (64.9 mL, 750 mmol) was added drop wise to the suspension at 80 °C. The heating was continued after complete addition for 2 h at 80 °C. To the cooled solution was added 1 L water. The aqueous phase was extracted with toluene (3 × 30 mL) to remove the bis-allyl product (22.6 g, 21%). The aqueous phase was then extracted with CH₂Cl₂ (3 × 100 mL) to isolate the analytically pure mono-allyl alcohol **36** (26.9 g, 263 mmol, 35%) as a light yellow oil after solvent removal.

¹H NMR (400 MHz, CDCl₃) δ ppm = 5.99 – 5.80 (m, 1H, H^d), 5.28 (dq, *J* = 1.6, 17.2 Hz, 1H, H^{e, trans}), 5.19 (ddd, *J* = 1.2, 2.9 Hz, 10.4 Hz, 1H, H^{e, cis}), 4.05 – 4.01 (m, 2H, H^c), 3.76 – 3.71 (m, 2H), 3.57 – 3.52 (m, 2H).

¹³C NMR (101 MHz, CDCl₃) δ ppm = 134.48 (C^d), 117.24 (C^e), 72.10, 71.26, 61.80.

IR (ATR): $\tilde{\nu}/\text{cm}^{-1} = 3279\text{m}_{\text{broad}}, 3086\text{m}_{\text{broad}}, 2924\text{m}, 2862\text{m}, 1643\text{m}, 1543\text{w}, 1420\text{m}, 1350\text{w}, 1258\text{w}, 1211\text{w}, 1111\text{s}, 1065\text{s}, 995\text{m}, 926\text{m}, 887\text{w}, 833\text{w}.$

2-(Allyloxy)ethyl methanesulfonate (**38**)

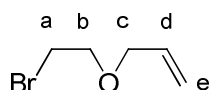


A degassed solution of **36** (16.5 g, 162 mmol) in anhydrous CH_2Cl_2 (200 mL) in presence of freshly distilled NEt_3 (100 mL) was placed at $-78\text{ }^\circ\text{C}$ in a two-necked flask equipped with an argon gas inlet and a dropping funnel. Mesyl chloride (20.0 mL, 258 mmol) in anhydrous CH_2Cl_2 (30 mL) was slowly added to the mixture. The reaction was followed by TLC until complete disappearance of the starting materials (4 h). The solution was washed with water ($4 \times 100\text{ mL}$) and the combined organic phases were extracted with CH_2Cl_2 ($2 \times 100\text{ mL}$). The organic phases were combined, dried over MgSO_4 and the solvent was evaporated yielding analytically pure **38** (27.8 g, 154 mmol, 95%) as a pale yellow oil.

^1H NMR (400 MHz, CDCl_3) $\delta_{\text{ppm}} = 5.94 - 5.82$ (m, 1H), 5.28 (dq, $J = 1.6, 17.2\text{ Hz}$, 1H), 5.20 (ddd, $J = 1.3, 2.8, 10.4\text{ Hz}$, 1H), 4.38 – 4.34 (m, 2H), 4.05 – 4.01 (m, 2H), 3.72 – 3.67 (m, 2H), 3.04 (s, 3H).

^{13}C NMR (101 MHz, CDCl_3) $\delta_{\text{ppm}} = 133.94, 117.61, 72.13, 69.12, 67.70, 37.62.$

3-(2-Bromoethoxy)prop-1-ene (**40**)



A solution of the mesylate compound **38** (27.8 g, 154 mmol), lithium bromide (67.0 g, 771 mmol) in acetone (500 mL, analytical grade) was prepared in a 1 L two-necked flask equipped with a magnetic stirrer and a condenser. The reaction mixture was heated to reflux over night. The acetone was evaporated and the crude mixture was dissolved in CH_2Cl_2 (250 mL) and washed with water ($3 \times 100\text{ mL}$). The organic phase was dried over MgSO_4 and filtered. Evaporation of the solvent yielded the analytically pure bromide **40** (13.5 g, 81.8 mmol, 53%) as a yellow oil.

^1H NMR (400 MHz, CDCl_3) $\delta_{\text{ppm}} = 5.91 - 5.77$ (m, 1H, H^{d}), 5.24 (dd, $J = 1.6, 17.2\text{ Hz}$, 1H, $\text{H}^{\text{e, trans}}$), 5.14 (ddt, $J = 1.2, 1.7, 10.4\text{ Hz}$, 1H, $\text{H}^{\text{e, cis}}$), 3.99 (ddd, $J = 0.8, 2.0, 5.6\text{ Hz}$, 2H, H^{c}), 3.69 (t, $J = 6.2\text{ Hz}$, 2H), 3.41 (t, $J = 6.2\text{ Hz}$, 2H).

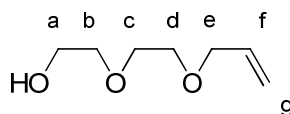
^{13}C NMR (101 MHz, CDCl_3) $\delta_{\text{ppm}} = 134.08 (\text{C}^{\text{d}})$, $117.16 (\text{C}^{\text{e}})$, 71.72 , 69.67 , $30.23 (\text{C}^{\text{a}})$.

IR (ATR): $\tilde{\nu}/\text{cm}^{-1} = 3078\text{w}$, 2970m , 2854m , 1728m , 1574w , 1458m , 1420m , 1350m , 1281m , 1219m , 1095s , 987m , 926s .

b.p.: $55\text{-}60\text{ }^\circ\text{C}$ (1 mbar).

Anal. calc. for $\text{C}_5\text{H}_9\text{BrO}$ C 36.39 H 5.50; found C 36.43 H 5.43.

2-(2-(Allyloxy)ethoxy)ethanol (**37**)



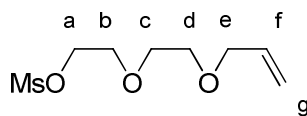
37

Finely crushed potassium hydroxide (52.1 g, 929 mmol) and diethylene glycol (68.0 mL, 743 mmol) were put in a 500 mL flask. Allyl bromide (32.4 mL, 372 mmol) was added drop wise to the suspension at $90\text{ }^\circ\text{C}$. The heating was continued after complete addition for 3 h at $90\text{ }^\circ\text{C}$. To the cooled solution was added 1 L water. The aqueous phase was extracted with toluene ($3 \times 30\text{ mL}$) to remove the bis-allyl product (13.9 g, 20%). The aqueous phase was then extracted with CH_2Cl_2 ($3 \times 100\text{ mL}$) to isolate the analytically pure mono-allyl alcohol **37** (22.7 g, 155 mmol, 42%) as a light yellow oil after solvent removal.

^1H -NMR (400 MHz, CDCl_3): $\delta_{\text{ppm}} = 5.97\text{-}5.84$ (m, 1 H_f), $5.31\text{-}5.17$ (m, 2 H_g), 4.03 (dt, $^3J = 6.0\text{ Hz}$, $^4J = 1.6\text{ Hz}$, 2 H_e), 3.74 (m, 2 H), $3.69\text{-}3.66$ (m, 2 H), $3.63\text{-}3.59$ (m, 4 H).

^{13}C -NMR (100.6 MHz, CDCl_3): $\delta_{\text{ppm}} = 134.5$, 117.4 , 72.5 , 72.3 , 70.4 , 69.4 , 61.8 .

2-(2-(Allyloxy)ethoxy)ethyl methanesulfonate (**39**)



39

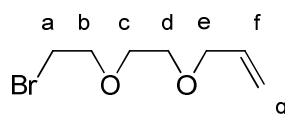
A degassed solution of **37** (22.2 g, 152 mmol) in anhydrous CH_2Cl_2 (250 mL) in presence of freshly distilled NEt_3 (150 mL) was placed at $-78\text{ }^\circ\text{C}$ in a two-necked flask equipped with an argon gas inlet and a dropping funnel. Mesyl chloride (20.0 mL, 258 mmol) in anhydrous CH_2Cl_2 (30 mL) was slowly added to the mixture. The reaction was followed by TLC until complete disappearance of the starting materials (4 h). The solution was washed with water ($4 \times 100\text{ mL}$) and the combined organic phases were extracted with CH_2Cl_2 ($2 \times 100\text{ mL}$).

The organic phases were combined, dried over MgSO_4 and the solvent was evaporated yielding analytically pure **39** (33.0 g, 147 mmol, 96%) as a pale yellow oil.

^1H NMR (400 MHz, CDCl_3) $\delta_{\text{ppm}} = 5.95 - 5.84$ (m, 1H), 5.30 - 5.24 (m, 1H), 5.19 (ddd, $J = 1.2, 2.9, 10.4$ Hz, 1H), 4.40 - 4.36 (m, 2H), 4.01 (ddd, $J = 1.4, 3.1, 5.7$ Hz, 2H), 3.80 - 3.76 (m, 2H), 3.69 - 3.65 (m, 2H), 3.62 - 3.58 (m, 2H), 3.07 (s, 3H).

^{13}C NMR (101 MHz, CDCl_3) $\delta_{\text{ppm}} = 134.48, 117.27, 72.21, 70.69, 69.31, 69.24, 69.04$.

3-(2-(2-Bromoethoxy)ethoxy)prop-1-ene (**41**)



41

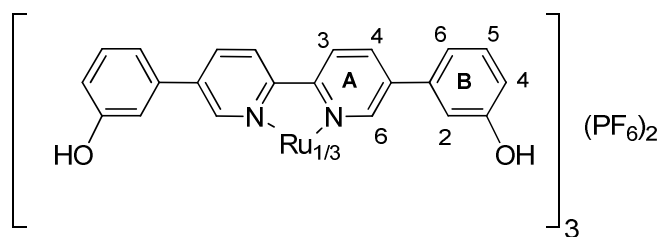
A solution of the mesylate compound **39** (30.0 g, 134 mmol), lithium bromide (59.1 g, 669 mmol) in acetone (500 mL, analytical grade) was prepared in a 1 L two-necked flask equipped with a magnetic stirrer and a condenser. The reaction mixture was heated to reflux over night. The acetone was evaporated and the crude mixture was dissolved in CH_2Cl_2 (250 mL) and washed with water (3×100 mL). The organic phase was dried over MgSO_4 and filtered. Evaporation of the solvent yielded the analytically pure bromide **41** (18.5 g, 88.5 mmol, 66%) as a yellow oil.

^1H NMR (400 MHz, CDCl_3) $\delta_{\text{ppm}} = 5.96 - 5.84$ (m, 1H), 5.27 (dq, $J = 1.6, 17.2$ Hz, 1H), 5.18 (ddd, $J = 1.2, 3.0, 10.4$ Hz, 1H), 4.05 - 4.00 (m, 2H), 3.81 (t, $J = 6.4$ Hz, 2H), 3.70 - 3.66 (m, 2H), 3.63 - 3.58 (m, 2H), 3.47 (t, $J = 6.4$ Hz, 2H).

^{13}C NMR (101 MHz, CDCl_3) $\delta_{\text{ppm}} = 134.58, 117.17, 72.25, 71.20, 70.54, 69.34, 30.21$.

Anal. calc. for $\text{C}_7\text{H}_{13}\text{BrO}$ C 40.21 H 6.27; found C 40.89 H 6.52.

$[\text{Ru}(\mathbf{35})_3](\text{PF}_6)_2$ (**50**)



3,3'-(2,2'-Bipyridine-5,5'-diyl)diphenol (**35**) (200 mg, 587 μmol) and $[\text{Ru}(\text{DMSO})_4\text{Cl}_2]$ (94.8 mg, 196 μmol) were suspended in ethylene glycol (7 mL). The reaction mixture was stirred in the microwave for 30 min at 230 $^\circ\text{C}$. The resulting orange solution was added to 100 mL of a NH_4PF_6 -solution (4.00 mmol). An orange precipitate formed which was filtered and washed with water (300 mL) and ether (100 mL) yielding the ruthenium complex **50** (271 mg, 98%).

^1H NMR (400 MHz, CD_3CN) δ ppm = 8.60 (d, $J = 8.5$ Hz, 6H), 8.30 (dd, $J = 1.9, 8.5$ Hz, 6H), 8.00 (d, $J = 1.8$ Hz, 6H), 7.23 (t, $J = 8.1$ Hz, 12H), 6.93 – 6.83 (m, 18H).

^{19}F NMR (376 MHz, CD_3CN) δ ppm = -73.98 (d, $J = 706.5$).

^{13}C NMR (101 MHz, CD_3CN) δ ppm = 158.61, 156.53, 150.90, 140.48, 137.38, 136.81, 131.59, 125.35, 119.67, 117.49, 114.93.

MS (ESI): $m/z = 561.4$ $[\text{M}-2\text{PF}_6]^{2+}$, 1121.6 $[\text{M}-\text{PF}_6-\text{H}]^+$, 1267.4 $[\text{M}-\text{PF}_6]^+$.

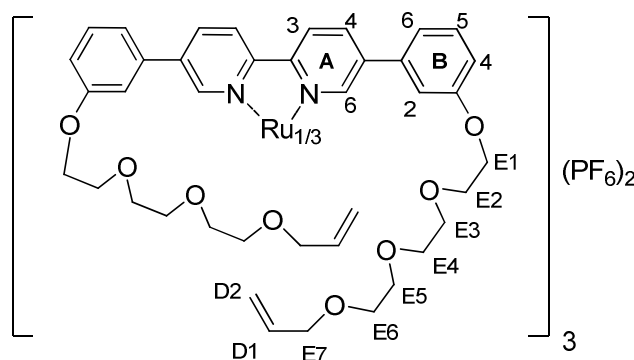
UV-Vis (MeCN, $\lambda_{\text{max}}(\text{nm})$ [ϵ ($\text{cm}^{-1} \text{M}^{-1}$)] = 467.0 [13900], 321.0 [102000].

Emission (MeCN, $\lambda_{\text{max}}(\text{nm})$) = 625.

IR (ATR): $\tilde{\nu}/\text{cm}^{-1} = 3522\text{w}, 3105\text{w}, 1740\text{m}, 1599\text{m}, 1583\text{m}, 1462\text{m}, 1448\text{m}, 1375\text{m}, 1304\text{m}, 1204\text{m}, 1165\text{m}, 997\text{w}, 893\text{m}, 824\text{s}, 779\text{m}, 731\text{w}, 698\text{w}$.

Anal. calc. for $\text{C}_{66}\text{H}_{48}\text{F}_{12}\text{N}_6\text{O}_6\text{P}_2\text{Ru} \cdot 2\text{H}_2\text{O}$ C 54.74, H 3.62, N 5.80; found C 54.77, H 3.68, N 5.64.

$[\text{Ru}(\mathbf{44})_3](\text{PF}_6)_2$ (**51**)



Ligand **44** (248 mg, 363 μmol), $[\text{Ru}(\text{DMSO})_4\text{Cl}_2]$ (58.7 mg, 121 μmol) and Ethanol (10 mL) were put in a microwave vessel. The reaction mixture was heated to 140 $^\circ\text{C}$ for 25 min, cooled to room temperature, reduced to 2 mL and poured to a saturated NH_4PF_6 -solution. An orange precipitate was formed. The solution was extracted with CH_2Cl_2 (3×20 mL).

Chromatography (SiO₂, CH₂Cl₂ → CH₂Cl₂ : MeOH (50:1)) yielded an orange solid (137 mg, 56.0 μmol, 46%).

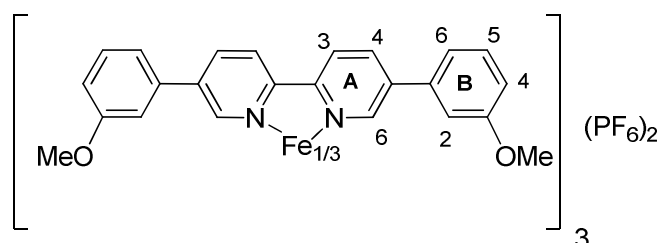
¹H-NMR (500 MHz, CDCl₃): δ/ppm = 8.80 (d, ³J = 8.8 Hz, 6 H, H^{A3}), 8.36 (dd, ³J = 8.5 Hz, ⁴J = 1.5 Hz, 6 H, H^{A4}), 7.87 (d, ⁴J = 1.5 Hz, 6H, H^{A6}), 7.29 (t, ³J = 8.0 Hz, 6 H, H^{B5}), 6.92 (d, ³J = 8.5 Hz, 6 H, H^{B6}), 6.83-6.82 (m, 12H, H^{B2+B4}), 5.86-5.81 (m, 6 H, H^{D1}), 5.23-5.08 (m, 12 H, H^{D2}), 4.05-4.00 (sb, 12 H, H^{E1}), 3.97 (d, ³J = 5.5 Hz, 12 H, H^{E7}), 3.80 (tb, 12 H, H^{E2}), 3.72-3.62 (m, 36 H, H^{E3+E4+E5}), 3.57 (m_c, 12 H, H^{E6}).

¹³C-NMR (125.8 MHz, CDCl₃): δ/ppm = 159.7 (C^{B3}), 155.1 (C^{A2}), 147.8 (C^{A6}), 140.7 (C^{B1}), 136.8 (C^{A4}), 135.1 (C^{A5}), 134.6 (C^{D1}), 131.0 (C^{B5}), 125.2 (C^{A3}), 119.2 (C^{B4}), 117.0 (C^{D2}), 116.4 (C^{B6}), 112.8 (C^{B3}), 72.1 (C^{E7}), 70.7, 70.5, 70.5 (C^{E2}), 69.4 (C^{E6}), 69.3 (C^{E1}), 67.5.

MS (ESI): *m/z* = 1077.9 [M-2PF₆]²⁺ (calc. 1077.5), 2299.4 [M-PF₆]⁺ (calc. 2299.9).

Anal. calc. for C₁₂₀H₁₄₄F₁₂N₆O₂₄P₂Ru · H₂O C 58.51, H 5.97, N 3.41; found C 58.54, H 6.12, N 2.97.

[Fe(**34**)₃](PF₆)₂ (**45**)



Ligand **34** (249 mg, 676 μmol) was dissolved in 2 mL of CH₂Cl₂ and 10 mL of CH₃CN. An excess of [FeCl₂ · 4 H₂O] (45.0 mg, 355 μmol) in H₂O was added and the solution turned immediately red. The reaction mixture was refluxed for 2 days and the organic solvents have been removed in vacuum and an excess of NH₄PF₆ was added. The water phase was extracted with CH₂Cl₂ (3 50 mL) and the combined organic layers were dried over MgSO₄. Removal of the solvents and recrystallisation from CH₂Cl₂/Et₂O yielded pure **45** (90 mmol, 35%).

¹H NMR (400 MHz, CDCl₃) δ/ppm = 8.52 (d, *J* = 8.3, 6H), 8.24 (d, *J* = 8.4, 6H), 7.52 (s, 6H), 7.18 (t, *J* = 8.0, 6H), 6.85 – 6.71 (m, 12H), 6.68 (s, 6H), 3.57 (s, 18H).

¹³C NMR (101 MHz, CDCl₃) δ/ppm = 159.77, 156.80, 151.27, 139.30, 136.57, 134.99, 130.21, 123.63, 118.58, 114.83, 111.81, 54.76.

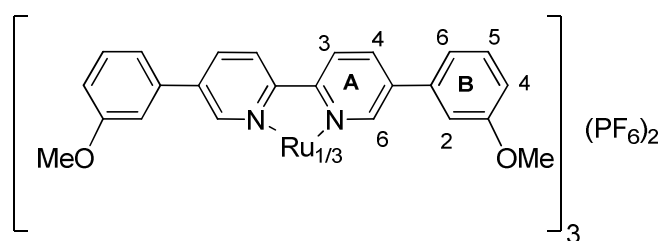
MS (ESI): *m/z* = 580.5 [M-2PF₆]²⁺ (calc. 580.2).

mp.: 179-182 °C.

IR (ATR): $\tilde{\nu}/\text{cm}^{-1}$ = 2935w, 2833w, 1717w, 1601m, 1582m, 1504m, 1470s, 1448m, 1433m, 1371m, 1304w, 1288m, 1246w, 1219m, 1173w, 1153m, 1051m, 1024m, 995m, 822s, 777m, 729m, 687w, 667m, 619m, 606m, 555m.

Anal. calc. for $\text{C}_{72}\text{H}_{60}\text{F}_{12}\text{FeN}_6\text{O}_6\text{P}_2$ C 59.60 H 4.17 N 5.79; found C 59.30 H 4.36 N 5.55.

[Ru(**34**)₃](PF₆)₂ (**49**)



5,5'-bis(3-methoxyphenyl)-2,2'-bipyridine (**34**) (115 mg, 313 μmol) and [Ru(DMSO)₄Cl₂] (50.5 mg, 104 μmol) in EtOH (7 mL) were stirred in a microwave at 140 °C for 1h. The reaction mixture was reduced to 5 mL and 50 mL of an aqueous NH₄PF₆ solution (2.00 mmol) was added. The precipitate was separated by filtration and washed with H₂O and ether yielding analytically pure complex **49** (142 mg, 94.9 μmol , 91%).

¹H NMR (500 MHz, CD₃CN) δ/ppm = 8.62 (d, J = 8.5 Hz, 3H, H^{A3}), 8.36 (d, J = 8.5 Hz, 3H, H^{A4}), 8.06 (s, 3H, H^{A5}), 7.34 (t, J = 8.0 Hz, 3H, H^{B5}), 7.04 (d, J = 7.7 Hz, 3H, H^{B6}), 6.97 (d, J = 8.3 Hz, 3H, H^{B4}), 6.94 (s, 3H, H^{B2}), 3.70 (s, 9H, OMe).

¹³C NMR (126 MHz, CD₃CN) δ/ppm = 161.3 (C^{B3}), 156.7 (C^{A2}), 151.0 (C^{A6}), 140.3 (C^{A5}), 137.1 (C^{B1}), 136.8 (C^{A4}), 131.6 (C^{B5}), 125.5 (C^{A3}), 120.5 (C^{B6}), 116.4 (C^{B4}), 113.3 (C^{B2}), 56.2 (C^{OMe}).

MS (ESI): m/z = 603.1 [M-2PF₆]²⁺ (calc. 603.2).

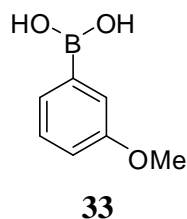
mp.: 151-153 °C.

UV-Vis (MeCN, $\lambda_{\text{max}}(\text{nm})$ [ϵ (cm⁻¹ M⁻¹)] = 470 [10900], 321 [110000].

Emission (MeCN, $\lambda_{\text{max}}(\text{nm})$) = 636.

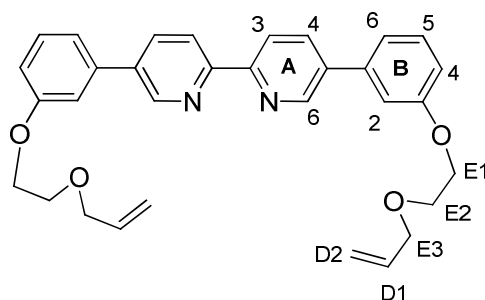
IR (ATR): $\tilde{\nu}/\text{cm}^{-1}$ = 2970w, 2839w, 1736m, 1582s, 1466s, 1366w, 1304w, 1219s, 1173m, 1026m, 825s, 779m, 694w.

Anal. calc. for $\text{C}_{72}\text{H}_{60}\text{F}_{12}\text{N}_6\text{O}_6\text{P}_2\text{Ru}$ C 57.80, H 4.04, N 5.62; found C 57.81, H 4.02, N 5.52.

3-Methoxyphenylboronic acid (**33**)

1-Bromo-3-methoxybenzene (18.5 mL, 145 mmol) was dissolved in 500 mL anhydrous THF and cooled to $-78\text{ }^{\circ}\text{C}$. *N*-butyl lithium (100 mL, 1.6M solution in hexane, 160 mmol) was added drop wise to this solution. The reaction mixture was stirred over a period of 2 h at this temperature whereby a slight yellow colouring was observed and LiCl precipitated. Trimethyl borate (17.8 mL, 160 mmol) was added, and the reaction mixture (now colourless) was stirred at room temperature over night. Hydrochloric acid (250 mL, 4M) was added and the solvents were removed *in vacuo*. The solvents were removed and the milky precipitate was taken in 300 mL water and 300 mL diethyl ether. The organic phase was extracted twice with 200 mL 1M NaOH. The combined aqueous extracts were acidified to pH 1 with 37% HCl before extraction with to portions of diethyl ether (200 mL). The solvents were evaporated *in vacuo* to yield a white solid (18.3 g, 120 mmol, 83%).

MS (EI): $m/z = 152.1$ $[\text{M}]^+$ (calc. 152.06).

Ligand **42**

5,5'-Bis(3'-hydroxyphenyl)-2,2'-bipyridine (1.63 g, 4.79 mmol), 3-(2-bromoethoxy)prop-1-ene (1.57 g, 9.63 mmol) and Cs_2CO_3 (6.24 g, 19.0 mmol) were dissolved in dry DMF (200 mL). The reaction mixture was heated for 4 d at $120\text{ }^{\circ}\text{C}$. Removal of DMF, column chromatography (SiO_2 , CH_2Cl_2 : MeOH (66:1)) and filtration over Al_2O_3 yielded **42** as a colourless crystalline solid (2.17 g, 4.27 mmol, 89%).

^1H NMR (500 MHz, CDCl_3) δ/ppm = 8.97 (d, J = 2.1 Hz, 2H, H^{A6}), 8.54 (d, J = 8.2 Hz, 2H, H^{A3}), 8.06 (dd, J = 2.3, 8.3 Hz, 2H, H^{A4}), 7.45 (t, J = 7.9 Hz, 2H, H^{B5}), 7.32 – 7.26 (m, 4H, $\text{H}^{\text{B2+B6}}$), 7.03 (dd, J = 2.2, 8.2 Hz, 2H, H^{B4}), 6.05 – 5.94 (m, 2H, H^{D1}), 5.37 (dd, J = 1.6, 17.2 Hz, 2H, $\text{H}^{\text{D2,trans}}$), 5.27 (dd, J = 1.2, 10.4 Hz, 2H, $\text{H}^{\text{D2,cis}}$), 4.29 – 4.24 (m, 4H, H^{E1}), 4.19 – 4.14 (m, 4H, H^{E3}), 3.92 – 3.86 (m, 4H, H^{E2}).

^{13}C NMR (126 MHz, CDCl_3) δ/ppm = 159.3 (C^{B3}), 154.70 (C^{A2}), 147.7 (C^{A6}), 138.9 (C^{B1}), 136.2 (C^{A5}), 135.2 (C^{A4}), 134.5 (C^{D1}), 130.1 (C^{B5}), 120.9 (C^{A3}), 119.7 (C^{B6}), 117.4 (C^{D2}), 114.0 (C^{B4}), 113.6 (C^{B2}), 72.4 (C^{E3}), 68.4 (C^{E2}), 67.5 (C^{E1}).

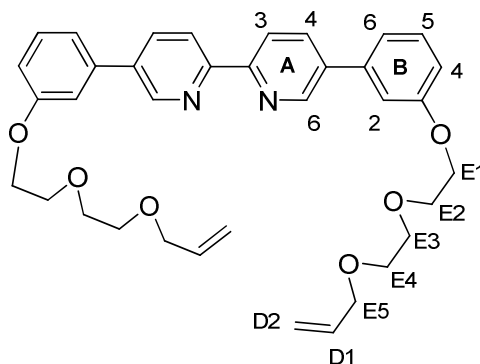
MS (EI): m/z = 508.2 [M^+] (calc. 508.2), 424.2[($\text{M}-\text{C}_5\text{H}_8\text{O}$) $^+$] (calc. 424.2), 340.1[($\text{M}-2\text{C}_5\text{H}_8\text{O}$) $^+$] (calc. 340.1).

mp.: 96-98 °C.

IR (ATR): $\tilde{\nu}/\text{cm}^{-1}$ = 3005w, 2932w, 2856w, 1605m, 1576s, 1464m, 1452s, 1441m, 1358m, 1300m, 1279m, 1205s, 1142m, 1130m, 1099m, 1068m, 1016m, 947m, 937m, 918m, 835m, 781s, 694s.

Anal. calc. for $\text{C}_{32}\text{H}_{32}\text{N}_2\text{O}_2$ C 75.57 H 6.34 N 5.51; found C 75.54 H 6.50 N 5.39.

Ligand 43



Ligand **43** was synthesised according to the procedure described for **42** from 5,5'-bis(3'-hydroxyphenyl)-2,2'-bipyridine (2.40 g, 7.05 mmol), 3-(2-(2-bromoethoxy)ethoxy)prop-1-ene (3.24 g, 15.5 mmol) and Cs_2CO_3 (8.00 g, 24.5 mmol). Column chromatography (SiO_2 , CH_2Cl_2 : MeOH (49:1)) yielded **43** as a colourless crystalline solid (3.33 g, 5.58 mmol 79%).

^1H NMR (500 MHz, CD_2Cl_2) δ/ppm = 8.93 (s, 2H, H^{A6}), 8.55 (d, J = 8.2 Hz, 2H, H^{A3}), 8.06 (dd, J = 2.2, 8.3 Hz, 2H, H^{A4}), 7.43 (t, J = 7.9 Hz, 2H, H^{B5}), 7.29 (d, J = 7.7 Hz, 2H, H^{B6}), 7.26 – 7.22 (m, 2H, H^{B2}), 6.99 (dd, J = 2.1, 8.2 Hz, 2H, H^{B4}), 5.97 – 5.87 (m, 2H, H^{D1}), 5.27 (dd, J = 1.6, 17.2 Hz, 2H, $\text{H}^{\text{D2,trans}}$), 5.16 (dd, J = 1.5, 10.4 Hz, 2H, $\text{H}^{\text{D2,cis}}$), 4.26 – 4.16 (m,

4H, H^{E1}), 4.01 (m_c, 4H, H^{E5}), 3.92 – 3.84 (m, 4H, H^{E2}), 3.76 – 3.67 (m, 4H, H^{E3}), 3.65 – 3.59 (m, 4H, H^{E4}).

¹³C NMR (126 MHz, CD₂Cl₂) δ/ppm = 160.0 (C^{B3}), 155.2 (C^{A2}), 148.2 (C^{A6}), 139.6 (C^{B1}), 136.8 (C^{A5}), 135.8 (C^{A4}), 135.6 (C^{D1}), 130.73 (C^{B5}), 121.3 (C^{A3}), 120.1 (C^{B6}), 117.0 (C^{D2}), 114.7 (C^{B4}), 113.9 (C^{B2}), 72.6 (C^{E5}), 71.4 (C^{E3}), 70.2 (C^{E2}), 70.1 (C^{E4}), 68.2 (C^{E1}).

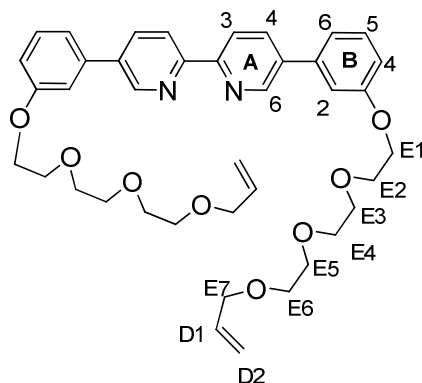
MS (EI): *m/z* = 596.3 [M⁺] (calc. 596.3), 508.2, 495.2, 481.2, 468.2 [(M-C₇H₁₄O)⁺] (calc. 468.2), 453.2.

mp.: 73-75 °C.

IR (ATR): $\tilde{\nu}/\text{cm}^{-1}$ = 3010w, 2872m, 1724w, 1605m, 1578s, 1460s, 1441m, 1362w, 1298m, 1277m, 1231w, 1202m, 1119m, 1099m, 1059m, 1018w, 933m, 841s, 777s, 744w, 692m, 611m.

Anal. calc. for C₃₆H₄₀N₂O₆ C 72.46 H 6.76 N 4.69; found C 72.26 H 6.66 N 4.49.

Ligand 44



Ligand **44** was synthesised according to the procedure described for **42** from 5,5'-Bis(3'-hydroxyphenyl)-2,2'-bipyridine (1.11 g, 3.26 mmol), 3-(2-(2-(2-bromoethoxy)ethoxy)ethoxy)prop-1-ene (2.06 g, 8.15 mmol) and Cs₂CO₃ (4.25 g, 13.0 mmol). Column chromatography (SiO₂, CH₂Cl₂ : MeOH (49:1)) yielded **44** as a colourless solid (2.01 g, 2.93 mmol, 90%).

¹H NMR (500 MHz, CD₂Cl₂) δ/ppm = 8.94 (d, *J* = 1.8 Hz, 2H, H^{A6}), 8.56 (d, *J* = 8.2 Hz, 2H, H^{A3}), 8.07 (dd, *J* = 2.1, 8.3 Hz, 2H, H^{A4}), 7.43 (t, *J* = 7.9 Hz, 2H, H^{B5}), 7.29 (d, *J* = 7.7 Hz, 2H, H^{B6}), 7.25 (d, *J* = 1.9 Hz, 2H, H^{B2}), 6.99 (dd, *J* = 2.1, 8.2 Hz, 2H, H^{B4}), 5.96 – 5.85 (m, 2H, H^{D1}), 5.26 (dd, *J* = 1.6, 17.2 Hz, 2H, H^{D2,trans}), 5.15 (dd, *J* = 1.3, 10.4 Hz, 2H, H^{D2,cis}), 4.24 – 4.19 (m, 4H, H^{E1}), 3.99 (d, *J* = 5.6 Hz, 4H, H^{E7}), 3.88 – 3.86 (m, 4H, H^{E2}), 3.73 – 3.68 (m, 4H, H^{E3}), 3.67 – 3.60 (m, 8H), 3.59 – 3.55 (m, 4H).

^{13}C NMR (101 MHz, CD_2Cl_2) δ/ppm = 160.0 ($\text{C}^{\text{B}3}$), 155.2 ($\text{C}^{\text{A}2}$), 148.1 ($\text{C}^{\text{A}6}$), 139.6 ($\text{C}^{\text{B}1}$), 136.7 ($\text{C}^{\text{A}5}$), 135.7 ($\text{C}^{\text{A}4}$), 135.6 ($\text{C}^{\text{D}1}$), 130.7 ($\text{C}^{\text{B}5}$), 121.3 ($\text{C}^{\text{A}3}$), 120.1 ($\text{C}^{\text{B}6}$), 116.9 ($\text{C}^{\text{D}2}$), 114.6 ($\text{C}^{\text{B}2}$), 113.9 ($\text{C}^{\text{B}4}$), 72.5, 71.3, 71.1 (2 C), 70.2, 70.1, 68.2 ($\text{C}^{\text{E}1}$).

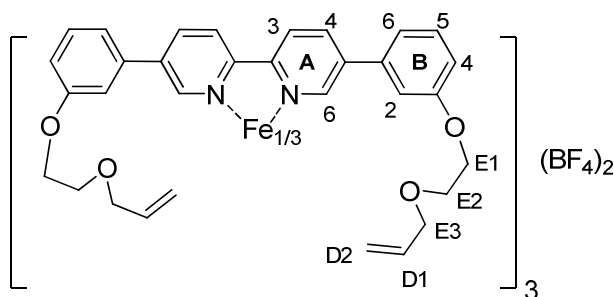
MS (EI): m/z = 685.4 [M^+] (calc. 685.4).

mp.: 57-58 °C.

IR (ATR): $\tilde{\nu}/\text{cm}^{-1}$ = 2868m, 1599m, 1582m, 1464s, 1364m, 1300m, 1232w, 1209m, 1126m, 1107m, 1067m, 932m, 633w.

Anal. calc. for $\text{C}_{40}\text{H}_{48}\text{N}_2\text{O}_8$ C 70.16 H 7.06 N 4.09; found C 70.03 H 7.06 N 4.00.

[Fe(**42**) $_3$](BF $_4$) $_2$ (**46**)



Ligand **42** (735 mg, 1.45 mmol) was dissolved in acetonitrile (40 mL) and an aqueous solution (40 mL) of iron(II) tetrafluoroborate hexahydrate (488 mg, 1.45 mmol) was added. The solution turned red immediately and was heated at reflux for 12 h. A ^1H NMR spectrum of the crude product showed still roughly 10% of unreacted ligand, 300 mg of iron(II) tetrafluoroborate hexahydrate were added and the solution was heated at reflux for three more days. The reaction mixture was filtered over Celite and Al_2O_3 in order to remove excess [Fe(BF $_4$) $_2$]. The analytically pure red solid was dried *in vacuo* (848 mg, 438 μmol , quant.).

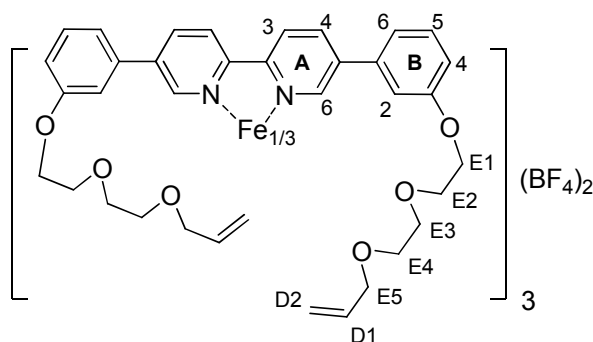
^1H NMR (400 MHz, CDCl_3) δ/ppm = 8.91 (d, J = 8.3 Hz, 6H $\text{H}^{\text{A}3}$), 8.36 (d, J = 7.7 Hz, 6H, $\text{H}^{\text{A}4}$), 7.54 (s, 6H, $\text{H}^{\text{A}6}$), 7.27 (t, J = 8.0, 6H, $\text{H}^{\text{B}5}$), 6.93 (d, J = 8.4 Hz, 6H, $\text{H}^{\text{B}6}$), 6.79 (m, 12H, $\text{H}^{\text{B}2+\text{B}4}$), 5.96 – 5.83 (m, 6H, $\text{H}^{\text{D}1}$), 5.33 – 5.23 (m, 6H, $\text{H}^{\text{D}2, \text{trans}}$), 5.18 (dd, J = 1.4, 10.4 Hz, 6H, $\text{H}^{\text{D}2, \text{cis}}$), 4.08 – 3.98 (m, 24H), 3.77 – 3.70 (m, 12H).

^{13}C NMR (101 MHz, CDCl_3) δ/ppm = 159.8, 157.5, 150.6, 140.5, 137.8, 135.2, 134.4, 131.0, 125.4, 119.2, 117.4, 116.5, 112.8, 72.3, 68.3, 67.7.

MS (ESI): m/z = 790.8 [$\text{M}-2\text{BF}_4$] $^{2+}$ (calc. 790.3).

Anal. calc. for $\text{C}_{96}\text{H}_{96}\text{B}_2\text{F}_8\text{FeN}_6\text{O}_{12}$ C 65.69 H 5.51 N 4.79; found C 65.37 H 5.54 N 4.72.

[Fe(**43**)₃](BF₄)₂ (**47**)



Ligand **43** (1.84 g, 3.08 mmol) and iron(II) tetrafluoroborate hexahydrate (1.04 g, 3.08 mmol) were dissolved in acetonitrile (300 mL) and heated at reflux for three days. Filtration over Al₂O₃ and removal of the solvent yielded iron complex **47** (1.93 g, 999 μmol, 93%) as a red oil.

¹H NMR (500 MHz, CD₃CN) δ/ppm = 8.66 (d, *J* = 8.5 Hz, 6H, H^{A3}), 8.44 (dd, *J* = 1.8, 8.5 Hz, 6H, H^{A4}), 7.75 (d, *J* = 1.3 Hz, 6H, H^{A6}), 7.33 (t, *J* = 8.0 Hz, 6H, H^{B5}), 7.06 (d, *J* = 7.7, 6H, H^{B6}), 6.96 (dd, *J* = 2.1, 8.3 Hz, 6H, H^{B4}), 6.89 (s, 6H, H^{B2}), 5.92 – 5.82 (m, 6H, H^{D1}), 5.22 (dd, *J* = 1.7, 17.3 Hz, 6H, H^{D2, trans}), 5.10 (dd, *J* = 1.5, 10.4 Hz, 6H, H^{D2, cis}), 3.99 – 3.91 (m, 24H, H^{E1+E5}), 3.71 – 3.65 (m, 12H, H^{E2}), 3.61 – 3.56 (m, 12H, H^{E3}), 3.53 (m_c, 12H, H^{E4}).

¹⁹F NMR (376 MHz, CDCl₃) δ/ppm = -153.1 (s).

¹³C NMR (126 MHz, CD₃CN) δ/ppm = 160.5 (C^{B3}), 158.8 (C^{A2}), 153.5 (C^{A6}), 140.0 (C^{A5}), 137.7 (C^{A4}), 137.1 (C^{B1}), 136.3 (C^{D1}), 131.7 (C^{B5}), 125.3 (C^{A3}), 120.6 (C^{B6}), 117.2 (C^{B4}), 117.0 (C^{D2}), 113.4 (C^{B2}), 72.5 (C^{E5}), 71.4 (C^{E3}), 70.4 (C^{E4}), 70.2 (C^{E2}), 68.7 (C^{E1}).

MS (ESI): *m/z* = 923.2 [M-2BF₄]²⁺ (calc. 922.9)

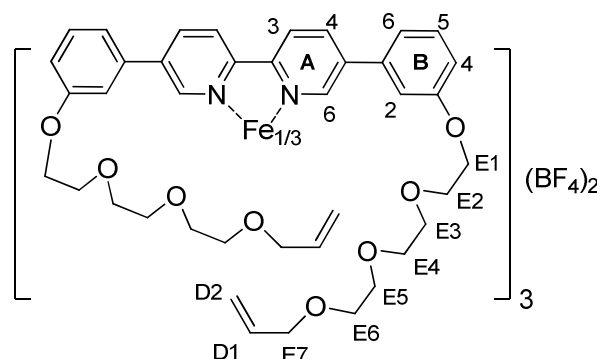
UV-Vis (MeCN, λ_{max}(nm) [ε' (cm⁻¹ M⁻¹)] = 336 [102700], 544 [8960].

Emission (MeCN, λ_{exc} = 340 nm, λ_{max}(nm)) = 406.

IR (ATR): $\tilde{\nu}$ /cm⁻¹ = 2922m, 2905m, 2870m, 1636m, 1599w, 1582m, 1504w, 1468m, 1408m, 1373w, 1302m, 1246w, 1213m, 1124m, 1092m, 1059m, 995w, 943w, 876m, 827s, 781m, 739m, 694m, 660m, 644m, 623w, 602w. (as PF₆ salt).

Anal. calc. for C₁₀₈H₁₂₀N₆O₁₈B₂F₈Fe·2 H₂O C 63.10 H 6.08 N 4.09; found C 63.10 H 6.10 N 4.24

[Fe(**44**)₃](BF₄)₂ (**48**)



Ligand **44** (666 mg, 973 μ mol) and iron(II) tetrafluoroborate hexahydrate (328 mg, 973 μ mol) were dissolved in acetonitrile (50 mL) and water (50 mL) and heated at reflux for five days. The acetonitrile was removed and the aqueous phase was extracted with CH₂Cl₂ (3 x 40 mL). The combined organic layers were dried over MgSO₄, filtered and the solvent was removed *in vacuo* to yield a red oil (681 mg, 298 μ mol, 92%).

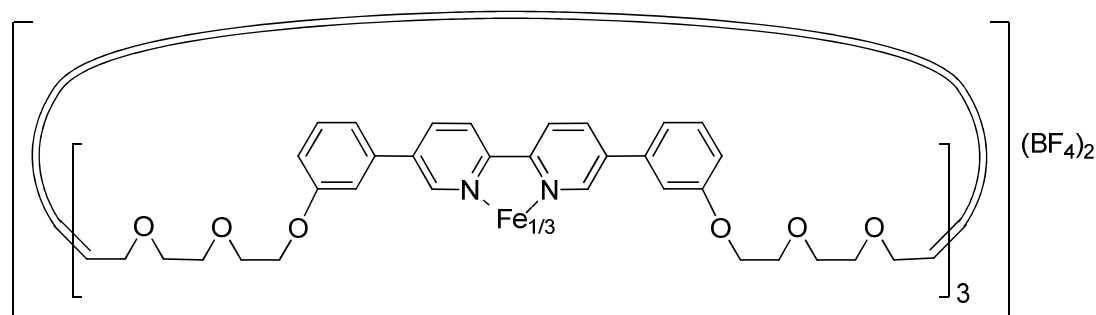
¹H NMR (400 MHz, CDCl₃) δ /ppm = 8.84 (s, 6H), 8.42 (s, 6H), 7.54 (s, 6H), 7.26 (s, 6H), 6.92 (s, 6H), 6.79 (s, 12H), 5.92 – 5.75 (m, 6H), 5.21 (d, *J* = 17.0, 6H), 5.10 (d, *J* = 10.3, 6H), 4.11 – 3.88 (m, 24H), 3.79 (s, 12H), 3.75 – 3.61 (m, 36H), 3.57 (s, 12H).

¹³C NMR (126 MHz, CDCl₃) δ /ppm = 159.7, 157.4, 150.6, 140.5, 137.8, 135.1, 134.6, 131.0, 125.0, 119.1, 117.0, 116.5, 112.7, 72.1, 70.7, 70.5 (2 C), 69.4, 69.3, 67.6.

¹⁹F NMR (376 MHz, CDCl₃) δ /ppm = -153.2.

MS (ESI): *m/z* = 1054.9 [M-2BF₄]²⁺ (calc. 1055.0)

Macrocycle **54**

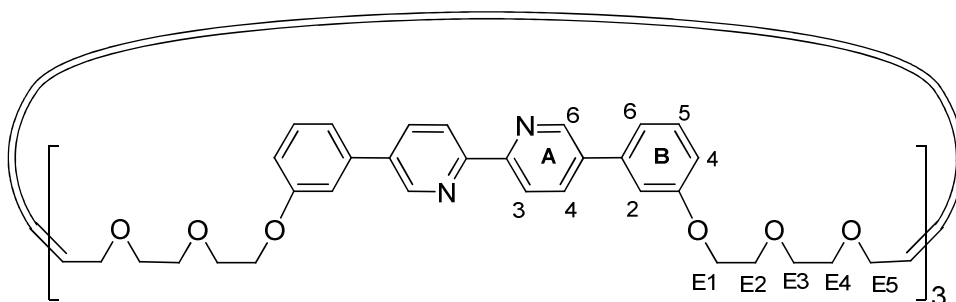


Iron complex **47** (1.93 g, 955 μ mol) and (1,3-bis-(2,4,6-trimethylphenyl)-2-imidazolylidene)dichloro(*o*-isopropoxyphenylmethylene)ruthenium(II) (75.0 mg, 120 μ mol) were dissolved in absolute CH₂Cl₂ (955 mL) and stirred at r.t. for 30 days under N₂. After 8 days,

75 mg and after 20 days 30 mg of catalyst were again added. The reaction was quenched with ethyl-vinylether (5 mL) and the solvents removed *in vacuo* yielding a red solid. ^1H NMR and ESI-MS confirmed almost full conversion (>95%). The compound was used further without purification.

MS (ESI): $m/z = 881.1$ $[\text{M}-2\text{BF}_4]^{2+}$ (calc. 880.9)

Macrocycle **57**

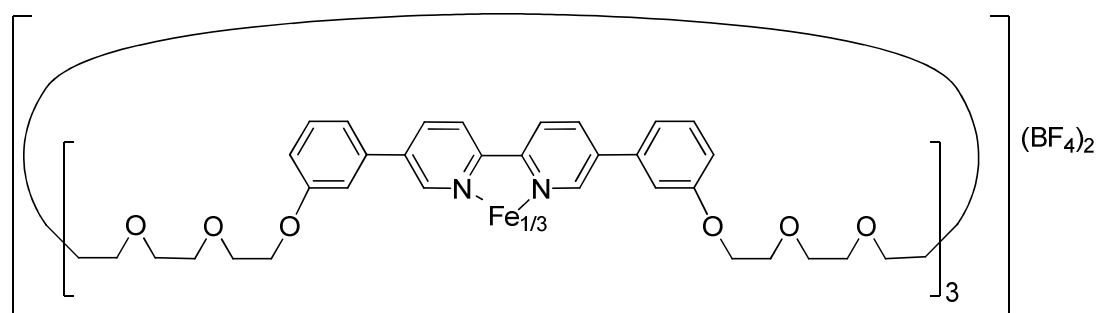


Crude iron complex **54** (200 mg, ~100 μmol) was dissolved in acetonitrile. $\text{Na}_2\text{EdtaH}_2$ (192 mg, 517 μmol) and Na_2CO_3 (192 mg, 517 μmol) in 30 mL water were added. The reaction mixture was stirred at 50 $^\circ\text{C}$ for 1 h, after 30 min the red colour had disappeared. Most of the acetonitrile has been distilled off and the solution was extracted with CH_2Cl_2 (3 x 100 mL). The combined organic layers were dried over MgSO_4 , filtered and the solvent was removed in vacuum to yield a brownish oil. Purification was attempted via Column chromatography (SiO_2 , CH_2Cl_2 : MeOH (1%-7%)) yielding macrocyclic ligand **57** (170 mg, 99.6 μmol , 70%, 70% pure) as a colourless oil. The crude compound was hydrogenated in the next step without further purification.

^1H NMR (600 MHz, CD_2Cl_2) $\delta/\text{ppm} = 8.89$ (d, $J = 1.8$ Hz, 6H, $\text{H}^{\text{A}6}$), 8.49 (d, $J = 8.3$ Hz, 6H, $\text{H}^{\text{A}3}$), 8.00 (dd, $J = 2.3, 8.2$ Hz, 6H, $\text{H}^{\text{A}4}$), 7.38 (t, $J = 7.9$ Hz, 6H, $\text{H}^{\text{B}5}$), 7.24 (d, $J = 7.6$ Hz, 6H, $\text{H}^{\text{B}6}$), 7.22 – 7.21 (m, 6H, $\text{H}^{\text{B}2}$), 6.95 (dd, $J = 1.7, 8.3$ Hz, 6H, $\text{H}^{\text{B}4}$), 5.82 – 5.77 (m, 6H, CH_2CH), 4.20 – 4.15 (m, 12H, $\text{H}^{\text{E}1}$), 4.01 – 3.98 (m, 12H, $\text{H}^{\text{E}2}$), 3.85 – 3.81 (m, 12H, $\text{H}^{\text{E}3}$), 3.69 – 3.65 (m, 12H, $\text{H}^{\text{E}5}$), 3.62 – 3.56 (m, 12H, $\text{H}^{\text{E}4}$).

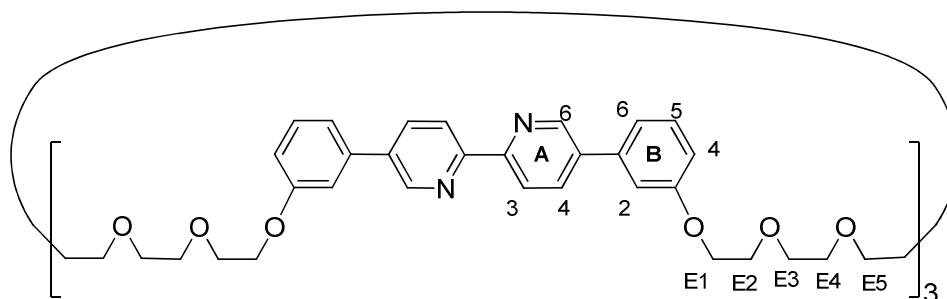
^{13}C NMR (151 MHz, CD_2Cl_2) $\delta/\text{ppm} = 160.0$ ($\text{C}^{\text{B}3}$), 155.1 ($\text{C}^{\text{A}2}$), 148.1 ($\text{C}^{\text{A}6}$), 139.5 ($\text{C}^{\text{B}1}$), 136.7 ($\text{C}^{\text{A}5}$), 135.7 ($\text{C}^{\text{A}4}$), 130.7 ($\text{C}^{\text{B}5}$), 129.9 (CH_2CH), 121.3 ($\text{C}^{\text{A}3}$), 120.1 ($\text{C}^{\text{B}6}$), 114.7 ($\text{C}^{\text{B}4}$), 114.0 ($\text{C}^{\text{B}2}$), 71.6 ($\text{C}^{\text{E}1}$), 71.4 ($\text{C}^{\text{E}2}$), 70.2 ($\text{C}^{\text{E}3}$), 70.1 ($\text{C}^{\text{E}4}$), 68.2 ($\text{C}^{\text{E}5}$).

MS (ESI): $m/z = 1728.6$ $[\text{M}+\text{Na}]^+$ (calc. 1728.7).

[Fe(309)](BF₄)₂ (56)

To a solution of crude iron complex **54** (955 μmol) in 150 mL EtOH and 150 mL of CH₂Cl₂, 500 mg of Pd/C (25 mol% Pd) were added. The reaction mixture was stirred in a hydrogen atmosphere (1 bar) at r.t. for 12 h. ¹H NMR and ESI-MS confirmed full conversion. The compound was used further without purification.

MS (ESI): $m/z = 884.0$ [M-2BF₄]²⁺ (calc. 883.9)

Macrocycle 31

To a solution of crude iron complex **56** (~955 μmol) in acetonitrile (200 mL), Na₂EdtaH₂ (1.86 g, 5.00 mmol) and Na₂CO₃ (1.06 g, 10.0 mmol) in 20 mL water were added. The reaction mixture was stirred at 50 °C for 3 h, after 30 min the red colour had disappeared. The organic solvent was removed in vacuum and the aqueous residue was extracted with CH₂Cl₂ (5 x 50 mL). The combined organic layers were dried over MgSO₄, filtered and the solvent was removed in vacuum to yield a brown oil (1.65 g). From the residue 4/15 parts (440 mg) were purified via preparative thin layer chromatography (Al₂O₃, CH₂Cl₂/MeOH (1.1%), 6h elution) on 8 plates to yield macrocyclic ligand **31** (113 mg, 26%, three steps) as a colourless oil.

^1H NMR (500 MHz, CD_2Cl_2) δ/ppm = 8.90 (d, J = 1.8, 6H, $\text{H}^{\text{A}6}$), 8.50 (d, J = 8.3 Hz, 6H, $\text{H}^{\text{A}3}$), 8.01 (dd, J = 2.2, 8.3 Hz, 6H, $\text{H}^{\text{A}4}$), 7.39 (t, J = 7.9 Hz, 6H, $\text{H}^{\text{B}5}$), 7.24 (d, J = 7.9 Hz, 6H, $\text{H}^{\text{B}6}$), 7.22 (d, J = 1.8, 6H, $\text{H}^{\text{B}2}$), 6.96 (dd, J = 2.1, 8.2, 6H, $\text{H}^{\text{B}4}$), 4.20 – 4.14 (m, 12H, $\text{H}^{\text{E}1}$), 3.86 – 3.80 (m, 12H, $\text{H}^{\text{E}2}$), 3.69–3.66 (m, 12H, $\text{H}^{\text{E}3}$), 3.60 – 3.54 (m, 12H, $\text{H}^{\text{E}4}$), 3.49 – 3.43 (m, 12H, $\text{H}^{\text{E}5}$), 1.65 – 1.58 (m, 12H, CH_2CH_2).

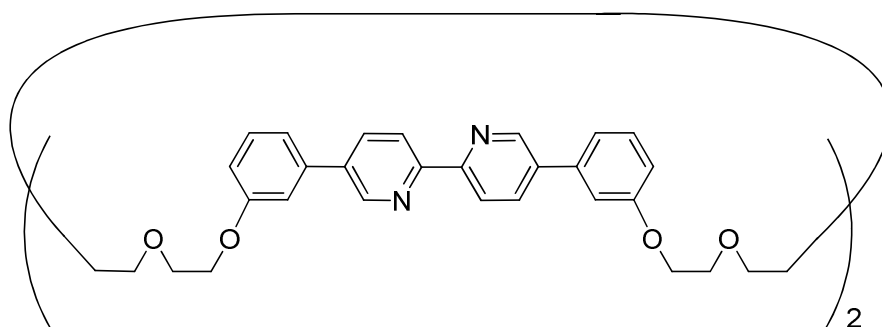
^{13}C NMR (126 MHz, CD_2Cl_2) δ/ppm = 160.0 ($\text{C}^{\text{B}3}$), 155.2 ($\text{C}^{\text{A}2}$), 148.1 ($\text{C}^{\text{A}6}$), 139.5 ($\text{C}^{\text{B}1}$), 136.6 ($\text{C}^{\text{A}5}$), 135.6 ($\text{C}^{\text{A}4}$), 130.7 ($\text{C}^{\text{B}5}$), 121.3 ($\text{C}^{\text{A}3}$), 120.0 ($\text{C}^{\text{B}6}$), 114.6 ($\text{C}^{\text{B}4}$), 113.9 ($\text{C}^{\text{B}2}$), 71.6 ($\text{C}^{\text{E}1}$), 71.4 ($\text{C}^{\text{E}2}$), 70.7 ($\text{C}^{\text{E}3}$), 70.2 ($\text{C}^{\text{E}4}$), 68.2 ($\text{C}^{\text{E}5}$), 27.0 (CH_2CH_2).

MS (ESI): m/z = 1735.0 [$\text{M}+\text{Na}$] $^+$ (calc. 1734.8).

IR (ATR): $\tilde{\nu}/\text{cm}^{-1}$ = 2920m, 2862m, 1722w, 1682m, 1597m, 1580m, 1462s, 1439m, 1362w, 1298m, 1281w, 1231w, 1205m, 1103s, 1063m, 1018m, 995s, 937w, 839s, 779s, 744m, 694m, 652w, 604m.

Anal. calc. for $\text{C}_{102}\text{H}_{114}\text{N}_6\text{O}_{18}\cdot 2\text{H}_2\text{O}$ C 70.08 H 6.80 N 4.81; found C 70.18 H 6.94 N 4.92.

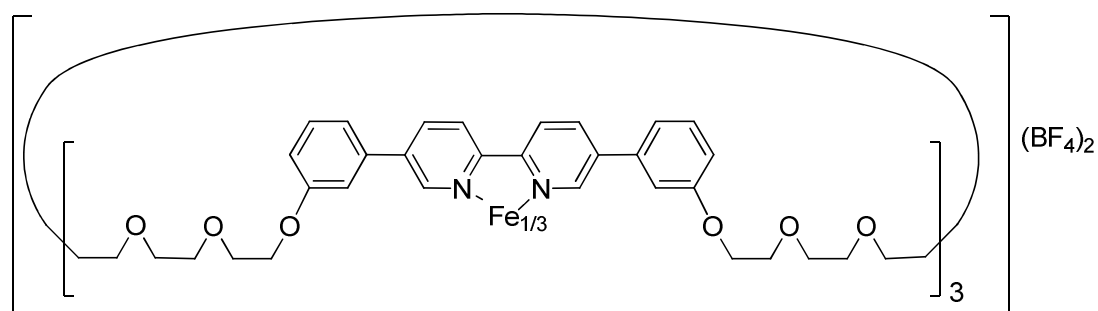
Macrocycle **55**



Tetradentate ligand **55** was obtained after preparative layer chromatography Al_2O_3 , $\text{CH}_2\text{Cl}_2/\text{MeOH}$ (1.1%), 6h elution) after an analogous reaction sequence as described for **31**.

^1H NMR (400 MHz, CD_2Cl_2) δ/ppm = 8.88 – 8.83 (m, 4H), 8.45 (d, J = 8.3, 4H), 7.97 (dd, J = 2.3, 8.3 Hz, 4H), 7.38 (t, J = 7.9, 4H), 7.26 – 7.18 (m, 8H), 6.99 – 6.92 (m, 4H), 4.21 – 4.13 (m, 8H), 3.82 – 3.75 (m, 8H), 3.57 (m_c , 8H), 1.68 (m_c , 8H).

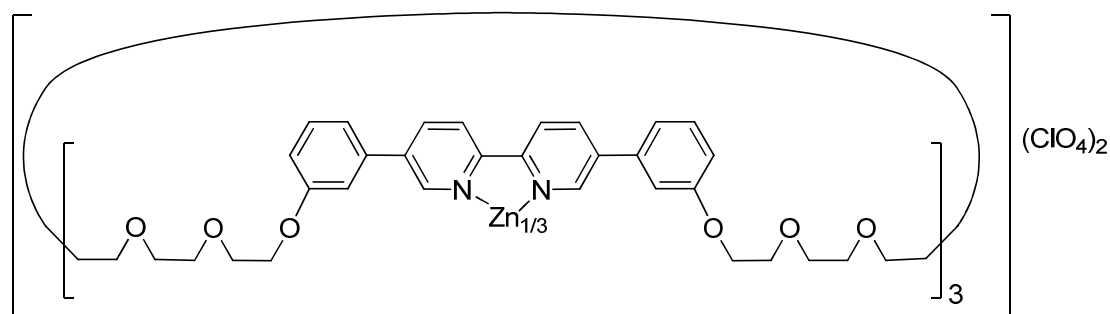
MS (ESI): m/z = 988.0 [$\text{M}+\text{Na}$] $^+$ (calc. 988.1).

[Fe(31)](BF₄)₂ (56)

Ligand **31** (26.1 mg, 15.2 μmol) and iron(II) tetrafluoroborate hexahydrate (5.1 mg, 15.2 μmol) were dissolved in acetonitrile (20 mL) and refluxed for 4 d. The solvent was removed and the residue filtered over SiO₂ (CH₂Cl₂/MeOH (10%)). After removal of the solvents a red residue (29.7 mg, quant.) could be obtained.

¹H NMR (400 MHz, CDCl₃) δ /ppm = 9.19 – 8.78 (m), 8.64 – 8.14 (m), 7.78 – 7.42 (m), 7.43 – 7.08 (m), 7.05 – 6.58 (m), 6.42 (s), 4.31 – 3.27 (m), 3.18 (s), 1.76 – 1.46 (m).

MS (ESI): m/z = 883.5 [M-2BF₄]²⁺(calc. 883.9).

[Zn(31)](ClO₄)₂ (58)

To a solution of Ligand **31** (23.3 mg, 13.6 μmol) in CH₂Cl₂ (1 mL) of a 13.6 mM solution of [Zn(ClO₄)₂] \cdot 6 H₂O in MeCN was added and the reaction mixture was stirred at r.t. over night. The solvents were removed under reduced pressure yielding a yellow oil (26.6 mg, 13.5 μmol , 99%).

¹H NMR (400 MHz, CD₂Cl₂) δ /ppm = 9.02 – 7.87 (m, 18H), 7.57 – 6.43 (m, 24H), 4.04 (m, 12H), 3.86 – 3.17 (m, 48H), 1.56 (s, 12H).

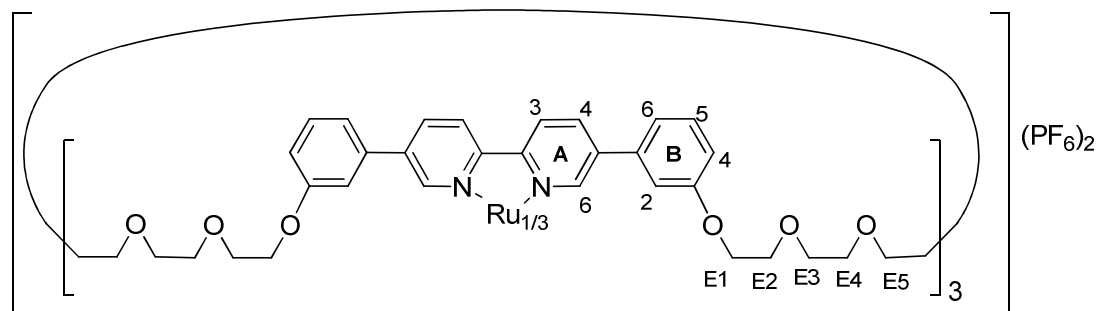
¹³C NMR (101 MHz, CD₂Cl₂) δ /ppm = 160.3, 148.5, 145.9, 141.0, 139.9, 136.3, 131.3, 125.0, 120.3, 120.0, 116.4, 114.0, 113.9, 71.7, 71.4, 70.7, 70.6, 70.0, 68.4, 68.3, 27.2, 27.0, 26.9.

MS (ESI): $m/z = 888.6$ $[M-2ClO_4]^{2+}$ (calc. 887.9).

UV-Vis (MeCN, λ_{max} (nm) [ϵ ($cm^{-1} M^{-1}$)] = 293 [82000], 344[21600].

Emission (MeCN, $\lambda_{exc} = 354$ nm, λ_{max} (nm)) = 468.

[Ru(**31**)](PF₆)₂ (**59**) (mixture of two geometrical isomers)



Ligand **31** (162 mg, 94.3 μ mol) and [Ru(DMSO)₄Cl₂] (45.7 mg, 94.3 μ mol) were suspended in EtOH (10 mL). The reaction mixture was stirred in the microwave (140 °C, 1h) leading to a homogeneous orange-brown solution. The solution was reduced to 5 mL and treated with 50 mL of an aqueous NH₄PF₆ solution (163 mg, 1 mmol). The precipitate was collected by filtration and washed with water and ether. Column chromatography (Al₂O₃, CH₂Cl₂/MeOH (0%→3%)) and preparative thin layer chromatography (Al₂O₃, CH₂Cl₂/MeOH (2%), 4h elution) on 2 plates yielded an orange solid (38.6 mg, 18.4 μ mol, 19 %).

¹H NMR (500 MHz, CDCl₃) δ /ppm = 8.94 – 8.74 (m, 18H, H^{A3, Iso1+Iso2}), 8.49 (d, $J = 8.4$, 2H, H^{A4, Iso1}), 8.40 (d, $J = 8.4$ Hz, 4H, H^{A4, Iso2}), 8.37 (d, $J = 8.1$ Hz, 4H, H^{A4, Iso1}), 8.30 (d, $J = 8.2$ Hz, 8H, H^{A4, Iso2}), 7.93 (s, 4H, H^{A6, Iso2}), 7.91 (s, 2H, H^{A6, Iso1}), 7.90 (s, 2H, H^{A6, Iso1}), 7.84 (s, 4H, H^{A6, Iso2}), 7.83 (s, 4H, H^{A6, Iso2}), 7.80 (s, 2H, H^{A6, Iso1}), 7.37 – 7.27(m, 18H, H^{B5, Iso1+Iso2}), 7.21 (d, $J = 7.6$ Hz, 2H, H^{B6, Iso1}), 7.00 – 6.88 (m, 34H, H^{B2/B4/B6, Iso1+Iso2}), 6.85 – 6.76 (m, 12H, H^{B2/B4/B6, Iso1+Iso2}), 6.71 (s, 4H, H^{B2, Iso2}), 6.45 (s, 2H, H^{B2, Iso1}), 4.18 – 3.90 (m, 36H, H^{E1}), 3.89 – 3.69 (m, 36H, H^{E2}), 3.68 – 3.58 (m, 36H, H^{E3/E4}), 3.58 – 3.48 (m, 36H, H^{E3/E4}), 3.48 – 3.32 (m, 36H, H^{E5}), 1.57 (s, 36H, CH₂CH₂).

¹³C NMR (126 MHz, CDCl₃) δ /ppm = 159.8, 159.7, 159.6, 155.2, 155.1, 155.1, 148.3, 148.0, 141.1, 141.0, 140.7, 137.1, 135.4, 135.2, 135.2, 131.1, 131.0, 130.9, 125.2, 119.9, 119.5, 119.3, 118.9, 116.8, 116.6, 116.4, 113.8, 113.3, 113.2, 112.8, 112.4, 71.1, 71.03, 70.98, 70.87, 70.83, 70.77, 70.64, 70.05, 69.95, 69.52, 69.35, 69.09, 67.87, 67.73, 67.62, 67.55, 26.51, 26.30, 26.26, 26.18.

¹⁹F NMR (376 MHz, CD₃CN) δ /ppm = -74.0 (d, $J = 707$ Hz).

MS (ESI): $m/z = 906.6$ [M-2PF₆]²⁺ (calc. 906.8).

UV-Vis (MeCN, $\lambda_{\max}(\text{nm})$ [ϵ' (cm⁻¹ M⁻¹)] = 204 [105800], 323 [86010], 471 [8520].

Emission (MeCN, $\lambda_{\text{exc}} = 366$ nm, $\lambda_{\max}(\text{nm}) = 634$.

IR (ATR): $\tilde{\nu}/\text{cm}^{-1} = 2922\text{m}, 2856\text{m}, 1715\text{w}, 1666\text{w}, 1599\text{m}, 1580\text{m}, 1466\text{m}, 1369\text{w}, 1302\text{m}, 1246\text{m}, 1213\text{m}, 1097\text{m}, 1059\text{m}, 1040\text{m}, 945\text{w}, 831\text{s}, 781\text{m}, 739\text{m}, 694\text{w}.$

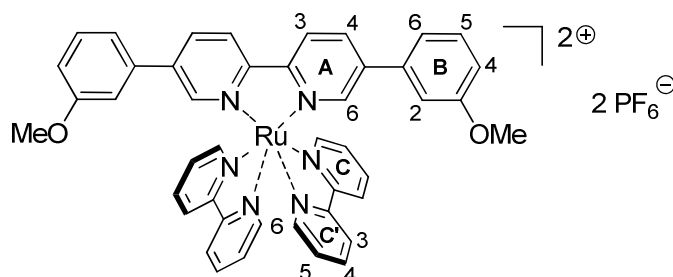
mp.: 84-90 °C.

Anal. calc. for C₁₀₂H₁₁₄F₁₂N₆O₁₈P₂Ru·H₂O C 57.76 H 5.51 N 3.96; found C 57.77 H 5.67 N 3.54

Complexes	Ru ^{II} /Ru ^{III}	Reduction 1	2	3	4	5	6
Ru(bpy)₃²⁺	0.89	-1.73	-1.93	-2.17			
49²⁺	0.93	-1.56	-1.66	-1.92	-2.31	-2.46	-2.65
59²⁺	0.95	-1.57	-1.72	-1.91	-2.30	-2.46	-2.66

In deoxygenated MeCN +0.1 M Bu₄NPF₆ at scan rate of 100 mV s⁻¹. vs. Fc/Fc⁺.

6.4 Experimental for Compounds in Chapter 3

[Ru(**34**)(bpy)₂](PF₆)₂ (**67**)

General procedure 67

5,5'-bis(3-methoxyphenyl)-2,2'-bipyridine (**34**) (86.6 mg, 235 μmol) and *cis*-[Ru(bpy)₂Cl₂] (116 mg, 240 μmol) were suspended in 5 mL of EtOH. The reaction mixture was heated in a microwave reactor for 40 min to 140 °C. To the resulting orange solution was added 100 mL of an aqueous NH₄PF₆-solution (4.00 mmol). An orange precipitate formed which was filtered and washed with water (50 mL) and ether (50 mL) yielding the ruthenium complex **67** (234 mg, 218 μmol , 93%) as an orange powder.

¹H NMR (500 MHz, CD₃CN) δ /ppm = 8.58 (d, $J = 8.5$ Hz, 2H, H^{A3}), 8.51 (m_c, 4H, H^{C3+C3'}), 8.33 (dd, $J = 2.0, 8.5$ Hz, 2H, H^{A4}), 8.07 (td, $J = 1.3, 8.0$ Hz, 4H, H^{C4+C4'}), 7.89 (d, $J = 5.3$ Hz, 2H, H^{C6}), 7.82 (d, $J = 5.3$ Hz, 2H, H^{C6'}), 7.80 (d, $J = 1.8$ Hz, 2H, H^{A6}), 7.48 – 7.40 (m, 4H, H^{C5+C5'}), 7.36 (t, $J = 8.0$ Hz, 2H, H^{B5}), 7.00 (dd, $J = 2.0, 8.0$ Hz, 4H, H^{B4+B6}), 6.92 (t, $J = 2.0$ Hz, 2H, H^{B2}), 3.77 (s, 6H, OMe).

¹³C NMR (126 MHz, CD₃CN) δ /ppm = 161.35 (C^{B3}), 158.28 (C^{C2}), 157.97 (C^{C2'}), 156.53 (C^{A2}), 153.13 (C^{A6}), 150.01 (C^{C6} + C^{C6'}), 140.63 (C^{B1}), 138.91 (C^{C4/C4'}), 138.86 (C^{C4/C4'}), 137.22 (C^{A5}), 136.79 (C^{A4}), 131.64 (C^{B5}), 128.68 (C^{C5}), 128.61 (C^{C5'}), 125.53 (C^{A3/C3/C3'}), 125.33 (C^{A3/C3/C3'}), 125.32 (C^{A3/C3/C3'}), 120.38 (C^{B4/B6}), 116.33 (C^{B4/B6}), 113.31 (C^{B2}), 56.21 (OMe).

¹⁹F NMR (376 MHz, CD₃CN) δ /ppm = -74.1 (d, $J = 706$ Hz).

MS (ESI): $m/z = 391.2$ [M-2PF₆]²⁺ (calc. 391.1), 927.1 [M- PF₆]⁺ (calc. 927.2)

UV-Vis (CH₂Cl₂, λ_{max} (nm) [ϵ / (cm⁻¹ M⁻¹)] = 467.0 [15000], 289.0 [85900].

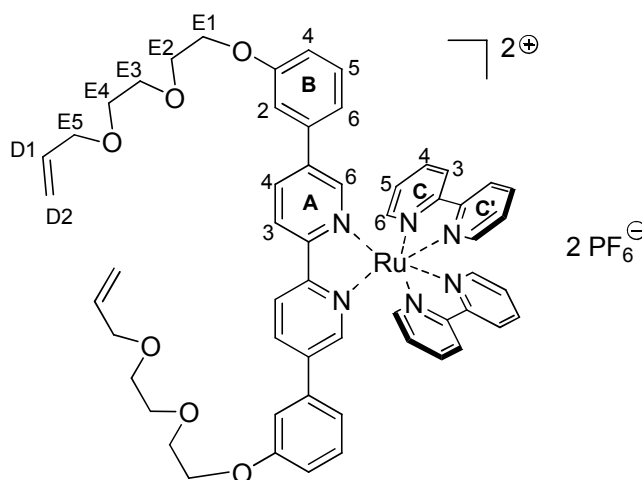
Emission (CH₂Cl₂, $\lambda_{\text{exc}} = 350$ nm, λ_{max} (nm)) = 616.

m.p.: 327-329 °C.

IR (ATR): $\tilde{\nu}/\text{cm}^{-1} = 3088\text{w}, 2934\text{w}, 1601\text{w}, 1578\text{w}, 1464\text{m}, 1447\text{m}, 1427\text{m}, 1285\text{w}, 1215\text{w}, 1171\text{w}, 1051\text{w}, 1028\text{w}, 878\text{w}, 829\text{s}, 791\text{m}, 762\text{m}, 731\text{m}, 698\text{w}.$

Anal. calc. for $C_{44}H_{36}F_{12}N_6O_2P_2Ru$ C 49.31, H 3.39, N 7.86; found C 49.20, H 3.39, N 7.70.

[Ru(**43**)(bpy)₂](PF₆)₂ (**68**)



Complex **68** was synthesised according to procedure **67** with 5,5'-bis(3-(2-(2-(allyloxy)ethoxy)ethoxy)phenyl)-2,2'-bipyridine (**PR157**) (71.7 mg, 120 μ mol) and *cis*-[Ru(bpy)₂Cl₂] (58.8 mg, 121 μ mol). Column chromatography (SiO₂, CH₂Cl₂ : MeOH (20:1)) yielded title compound **69** (141 mg, 108 μ mol, 90%) as an orange solid.

¹H NMR (500 MHz, CD₃CN) δ /ppm = 8.58 (d, J = 8.6 Hz, 2H, H^{A3}), 8.52 (mc, 4H, H^{C3+C3'}), 8.33 (dd, J = 2.0, 8.5 Hz, 2H, H^{A4}), 8.12 – 8.06 (m, 4H, H^{C4+C4'}), 7.89 (d, J = 5.5 Hz, 2H, H^{C6}), 7.82 (d, J = 5.6 Hz, 2H, H^{C6'}), 7.81 (d, J = 1.7 Hz, 2H, H^{A6}), 7.47 – 7.42 (m, 4H, H^{C5+C5'}), 7.35 (t, J = 8.0 Hz, 2H, H^{B5}), 7.03 – 6.97 (m, 4H, H^{B4+B6}), 6.93 (s, 2H, H^{B2}), 5.95 – 5.85 (m, 2H, H^{D2}), 5.25 (dd, J = 3.3, 17.3 Hz, 2H, H^{D1, trans}), 5.12 (dd, J = 1.4, 10.4 Hz, 2H, H^{D1, cis}), 4.07 (dd, J = 5.3, 9.7 Hz, 4H, H^{E1}), 3.97 (dd, J = 1.2, 4.2 Hz, 4H, H^{E5}), 3.82 – 3.77 (m, 4H, H^{E2}), 3.65 (dd, J = 3.5, 5.7 Hz, 4H, H^{E3/E4}), 3.57 (dd, J = 3.5, 5.6 Hz, 4H, H^{E3/E4}).

¹³C NMR (126 MHz, CD₃CN) δ /ppm = 160.5 (C^{B3}), 158.27 (C^{A2}), 157.96 (C^{C2}), 156.51 (C^{C2}), 153.13 (2 C^{C3+C3'}), 150.03 (C^{A6}), 140.57 (C^{A5}), 138.93 (C^{C4/C4'}), 138.86 (C^{C4/C4'}), 137.23 (C^{B1}), 136.77 (C^{A4}), 136.34 (C^{D2}), 131.66 (C^{B5}), 128.69 (C^{C5/C5'}), 128.62 (C^{C5/C5'}), 125.54 (C^{A3}), 125.33 (2 C^{C5+C5'}), 120.54 (C^{B6}), 117.03 (C^{D1}), 116.99 (C^{B4}), 113.82 (C^{B2}), 72.53 (C^{E5}), 71.44 (C^{E3/E4}), 70.43 (C^{E3/E4}), 70.23 (C^{E2}), 68.75 (C^{E1}).

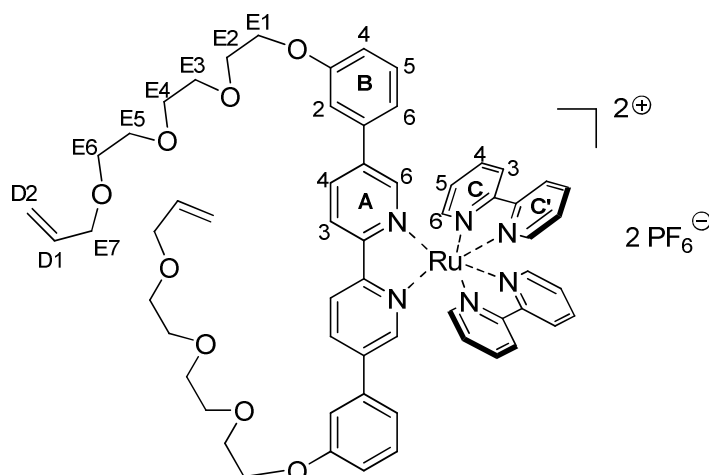
¹⁹F NMR (376 MHz, CD₃CN) δ /ppm = -74.1 (d, J = 706 Hz).

m.p.: 99-102 °C.

MS (ESI): m/z = 1155.4 [M-PF₆]⁺ (calc. 1155.3), 505.2 [M- 2 PF₆]²⁺ (calc. 505.2).

Anal. calc. for C₅₆H₅₆F₁₂N₆O₆P₂Ru C 51.74, H 4.34, N 6.46; found C 51.78, H 4.25, N 6.24.

[Ru(**44**)(bpy)₂](PF₆)₂ (**69**)



Complex **69** was synthesised according to procedure **67** with 5,5'-bis(3-(2-(2-(2-(allyloxy)ethoxy)ethoxy)ethoxy)phenyl)-2,2'-bipyridine (**44**) (420 mg, 613 μ mol) and *cis*-[Ru(bpy)₂Cl₂] (300 mg, 619 μ mol). Column chromatography (SiO₂, CH₂Cl₂ : MeOH (20:1)) yielded title compound **69** (793 mg, 571 μ mol, 93%) as an orange solid.

¹H NMR (500 MHz, CDCl₃) δ /ppm = 8.50 (d, J = 8.6 Hz, 2H, H^{A3}), 8.48 – 8.41 (m, 4H, H^{C3+C3'}), 8.13 (d, J = 8.3 Hz, 2H, H^{A4}), 7.99 (t, J = 8.0 Hz, 2H, H^{C4/C4'}), 7.95 (t, J = 7.9 Hz, 2H, H^{C4/C4'}), 7.79 (d, J = 4.1 Hz, 4H, H^{C6+C6'}), 7.65 (s, 2H, H^{A6}), 7.49 – 7.45 (m, 4H, H^{C5+C5'}), 7.22 (t, J = 8.0 Hz, 2H, H^{B5}), 6.85 – 6.81 (m, 6H, H^{B2+B4+B6}), 5.88 – 5.80 (m, 2H, H^{D1}), 5.20 (dd, J = 1.4, 17.2 Hz, 2H, H^{D2, trans}), 5.09 (d, J = 10.4 Hz, 2H, H^{D2, cis}), 4.10 – 4.00 (m, 4H, H^{E1}), 3.95 (d, J = 5.6 Hz, 4H, H^{E7}), 3.83 – 3.79 (m, 4H, H^{E2}), 3.70 – 3.68 (m, 4H, H^{E3/E4}), 3.68 – 3.62 (m, 8H, H^{E3/E4+E5}), 3.59 – 3.53 (m, 4H, H^{E7}).

¹³C NMR (126 MHz, CDCl₃) δ /ppm = 159.61 (C^{B3}), 156.77 (C^{C2/C2'}), 156.29 (C^{C2/C2'}), 155.09 (C^{A2}), 151.72 (C^{C6/C6'}), 151.44 (C^{C6/C6'}), 148.10 (C^{A6}), 140.47 (C^{A5}), 138.33 (C^{C4/C4'}), 138.25 (C^{C4/C4'}), 136.34 (C^{A4}), 135.69 (C^{B1}), 134.74 (C^{D1}), 130.82 (C^{B5}), 128.63 (C^{C5/C5'}), 128.26 (C^{C5/C5'}), 124.57 (C^{C3/C3'}), 124.50 (C^{C3/C3'}), 124.28 (C^{A3}), 119.57 (C^{B6}), 117.13 (C^{D2}), 116.50 (C^{B4}), 112.69 (C^{B2}), 72.14 (C^{E7}), 70.66 (C^{E3/E4}), 70.56 (C^{E3/E4}), 69.51 (C^{E2}), 69.41 (C^{E6}), 67.64 (C^{E1}).

¹⁹F NMR (376 MHz, CD₃CN) δ /ppm = -74.09 (d, J = 706 Hz).

MS (ESI): m/z = 1243.2 [M-PF₆]⁺ (calc. 1243.3), 549.1 [M- 2 PF₆]²⁺ (calc. 549.2).

UV-Vis (MeCN, λ_{\max} (nm) [ϵ / (cm⁻¹ M⁻¹)] = 456.0 [16200], 318.0 [56900].

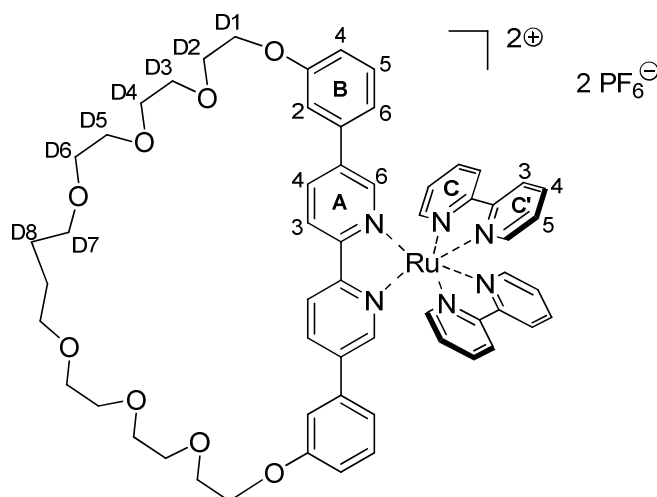
Emission (MeCN, λ_{exc} = 350 nm, λ_{\max} (nm)) = 636.

IR (ATR): $\tilde{\nu}/\text{cm}^{-1} = 3080\text{w}, 2864\text{m}, 1601\text{m}, 1580\text{m}, 1464\text{w}, 1445\text{w}, 1423\text{w}, 1369\text{m}, 1302\text{m}, 1217\text{m}, 1095\text{m}, 1063\text{m}, 945\text{w}, 827\text{s}, 764\text{m}, 731\text{m}, 698\text{w}.$

m.p.: 77-79 °C.

Anal. calc. for $\text{C}_{60}\text{H}_{64}\text{F}_{12}\text{N}_6\text{O}_8\text{P}_2\text{Ru}$ C 51.91, H 4.65, N 6.05; found C 51.93, H 4.68, N 5.87.

Complex **64**



Ruthenium complex **69** (193 mg, 139 μmol) and (1,3-bis-(2,4,6-trimethylphenyl)-2-imidazolylidene)dichloro(*o*-isopropoxyphenylmethylene)ruthenium (6.0 mg, 9.6 μmol) were dissolved in absolute CH_2Cl_2 (13.9 mL) and stirred at r.t. for 5 d under N_2 . ^1H NMR and ESI-MS indicated roughly 40% conversion to the desired cyclic molecule. Again 16 mg of catalyst were added immediately and 8 mg of catalyst were added after 7 days. After 5 days the starting material was consumed (ESI-MS). The crude complex was filtered over Al_2O_3 (CH_2Cl_2 : MeOH (40:1)) and hydrogenated with molecular H_2 (1 atm) and a catalytic amount of Pd/C (30 mg) in 20 mL of EtOH and 20 mL of CH_2Cl_2 . Preparative thick layer chromatography (SiO_2 , CH_2Cl_2 : MeOH (25:1)) yielded title compound **64** (20.2 mg, 14.8 μmol , 10%) as a mixture of the pure complex and the complex with one sodium cation coordinated to the ether chain as an orange solid.

^1H NMR (500 MHz, CD_3CN) $\delta/\text{ppm} = 8.63$ (d, $J = 8.1$ Hz, 2H, $\text{H}^{\text{C}3}$), 8.56 (t, $J = 8.0$ Hz, 4H, $\text{H}^{\text{C}3+\text{A}3}$), 8.35 (dd, $J = 2.0, 8.5$ Hz, 2H, $\text{H}^{\text{A}4}$), 8.22 (td, $J = 1.2, 7.9$ Hz, 2H, $\text{H}^{\text{C}4}$), 8.09 – 8.03 (m, 2H $\text{H}^{\text{C}4}$), 7.90 (d, $J = 5.0$ Hz, 2H, $\text{H}^{\text{C}6}$), 7.84 (d, $J = 5.5$ Hz, 2H, $\text{H}^{\text{C}6}$), 7.82 (d, $J = 1.8$ Hz, 2H, $\text{H}^{\text{A}6}$), 7.58 – 7.52 (m, 2H, $\text{H}^{\text{C}5}$), 7.42 (t, $J = 6.6$ Hz, 2H, $\text{H}^{\text{C}5}$), 7.38 (t, $J = 8.0$ Hz, 2H, $\text{H}^{\text{B}5}$), 7.27 (d, $J = 7.8$ Hz, 2H, $\text{H}^{\text{B}6}$), 6.96 (dd, $J = 2.2, 8.2$ Hz, 2H, $\text{H}^{\text{B}4}$), 6.75 – 6.70 (m, 2H,

H^{B2}), 3.98 (t, $J = 6.1$ Hz, 4H, D1), 3.76 (t, $J = 6.0$ Hz, 4H, D2), 3.72 – 3.45 (m, 8H), 3.42 – 3.35 (m, 4H), 2.35 – 2.24 (m, 4H, D7), 1.65 – 1.52 (m, 4H, D8) .

^{13}C NMR (126 MHz, CD_3CN) $\delta/ppm = 160.78 (C^{B3}), 158.33 (C^{C2/C2}), 158.23 (C^{C2/C2}), 156.71 (C^{A2}), 153.54 (C^{A6}), 150.26 (C^{C2} + C^{C2}), 140.34 (C^{B1}), 140.14 (C^{C4}), 139.22 (C^{C4}), 137.04 (C^{A5}), 136.33 (C^{A4}), 132.06 (C^{B5}), 129.47 (C^{C5}), 128.99(C^{C5}), 125.97 (C^{C3/C3/A3}), 125.89 (C^{C3/C3/A3}), 125.55 (C^{C3/C3/A3}), 120.88 (C^{B6}), 118.85 (C^{B4}), 113.01 (C^{B2}), 71.95, 71.78, 71.60, 71.22, 70.10 (C^{D2}), 68.70 (C^{D1}), 34.57 (C^{D7}), 26.97 (C^{D8}).$

^{19}F NMR (376 MHz, CD_3CN) $\delta/ppm = -74.09$ (d, $J = 706$ Hz).

MS (ESI, 130 °C): $m/z = 1217.6 [M-PF_6]^+$ (calc. 1217.3), 536.2 $[M-2 PF_6]^{2+}$ (calc. 536.2).

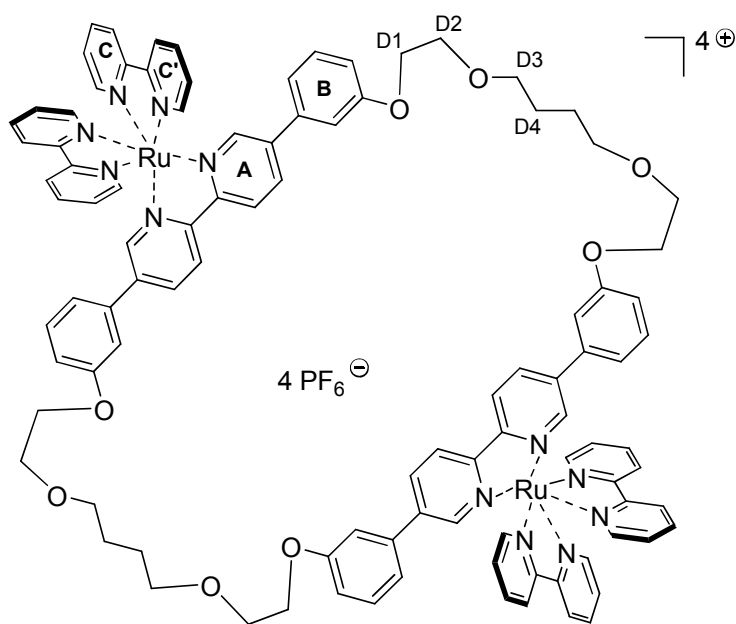
UV-Vis (CH_2Cl_2 , $\lambda_{max}(nm)$ [ϵ ($cm^{-1} M^{-1}$)] = 457.0 [14700], 354 [39200, shoulder], 321.0 [45700], 290 [86800].

Emission (MeCN, $\lambda_{exc} = 350$ nm, $\lambda_{max}(nm)$) = 641.

IR (ATR): $\tilde{\nu}/cm^{-1} = 2921m, 2892w, 2853m, 1728m, 1717m, 1601m, 1585w, 1464m, 1446m, 1423m, 1372w, 1352w, 1302w, 1275m, 1243m, 1215m, 1121m, 1093m, 1055m, 1032m, 940w, 876w, 829s, 792m, 767s, 740w, 732m, 695m, 690m, 660m.$

Anal. calc. for $C_{58}H_{62}F_{12}N_6O_8P_2Ru \cdot 2.5H_2O \cdot 0.35NaCl$ C 48.80, H 4.73, N 5.89; found C 49.06, H 4.85, N 4.48.

$[Ru_2(55)(bpy)_4](PF_6)_4$ (**65**)



Dinuclear Complex **65** was synthesised according to procedure **67** with ligand **55** (10.8 mg, 11.2 μmol) and *cis*-[Ru(bpy)₂Cl₂] (10.8 mg, 22.4 μmol). Preparative thick layer chromatography (Al₂O₃, CH₂Cl₂ : MeOH (20:1)) yielded title compound **65** (12.1 mg, 5.1 μmol , 46%) as an orange solid.

¹H NMR (600 MHz, CD₃CN) δ /ppm = 8.48 (m_c 8H, H^{C3+C3}), 8.41 (dd, *J* = 2.7, 8.5 Hz, 4H, H^{A3}), 8.19 – 8.14 (m, 4H, H^{A4}), 8.06 – 7.96 (m, 8H, H^{C4+C4}), 7.89 – 7.82 (m, 4H, H^{C6}), 7.81 – 7.75 (m, 8H, H^{A6+C6}), 7.43 – 7.35 (m, 8H, H^{C5+C5}), 7.32 (t, *J* = 8.1 Hz, 4H, H^{B5}), 6.98 (dd, *J* = 2.0, 8.7 Hz, 4H, H^{B4}), 6.91 (m_c, 8H, H^{B2+B6}), 4.06 – 4.02 (m, 8H, H^{D1}), 3.71 (m_c, 8H, H^{D2}), 3.48 (m_c, 8H, H^{D3}), 1.59 – 1.55 (m_c, 8H, H^{D4}).

¹³C NMR (151 MHz, CD₃CN) δ /ppm = 160.01 (C^{B3}), 157.55 (C^{C2}), 157.25 (C^{C2}), 155.70 (C^{A2}), 152.40 (C^{C6} + C^{C6}), 149.26 (C^{A6}), 139.86 (C^{A5}), 138.21 (C^{C4}), 136.40 (C^{B1}), 135.99 (C^{A4}), 131.03 (C^{B5}), 128.05 (C^{C5}), 127.96 (C^{C5}), 124.85 (C^{C3}), 124.67 (C^{C3}), 124.55 (C^{A3}), 119.68 (C^{B6}), 116.16 (C^{B4}), 113.65 (C^{B2}), 71.12 (C^{D3}), 69.30 (C^{D2}), 68.24 (C^{D1}), 26.64 (C^{D4}).

¹⁹F NMR (376 MHz, CD₃CN) δ /ppm = -74.09 (d, *J* = 706 Hz).

MS (ESI): *m/z* = 1041.3 [M-2 PF₆]²⁺ (calc. 1041.2), 646.0 [M- 3 PF₆]³⁺ (calc. 645.8), 448.2 [M- 4 PF₆]⁴⁺ (calc. 448.1).

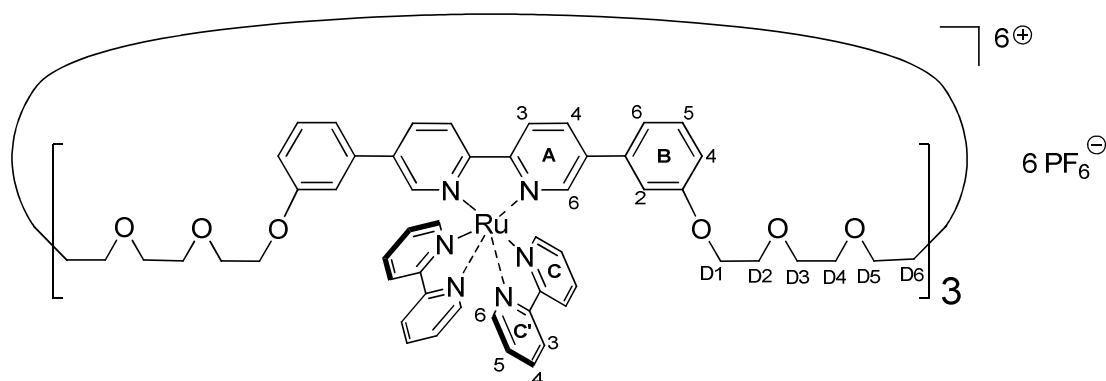
m.p.: 192-196 °C.

UV-Vis (CH₂Cl₂, λ_{max} (nm) [ϵ ' (cm⁻¹ M⁻¹)] = 457.0 [19700], 315.0 [shoulder, 61800], 290.0 [114300].

Emission (CH₂Cl₂, λ_{exc} = 450 nm, λ_{max} (nm)) = 617.

IR (ATR): $\tilde{\nu}$ /cm⁻¹ = 3086w, 2922m, 2853m, 1601m, 1582m, 1464m, 1445m, 1369w, 1301w, 1211m, 1119m, 1055w, 825s, 761m.

Anal. calc. for C₁₀₀H₉₂F₂₄N₁₂O₈P₄Ru₂ C 50.64, H 3.91, N 7.09; found C 50.58, H 4.12, N 7.13.

$[\text{Ru}_3(\mathbf{31})(\text{bpy})_6](\text{PF}_6)_6$ (**66**)

Trinuclear Complex **66** was synthesised according to procedure **67** with ligand **31** (27.3 mg, 15.9 μmol) and *cis*-[Ru(bpy)₂Cl₂] (23.6 mg, 48.6 μmol). The mixture of the two diastereoisomers (ratio 5:1 from NMR) was synthesised as an orange solid (56.2 mg, 14.7 μmol , 92%). Attempts to separate the two diastereoisomers chromatographically were not successful.

¹H NMR (500 MHz, CD₃CN) δ/ppm = 8.55 (d, J = 8.6 Hz, 6H, H^{A3}), 8.50 (t, J = 7.5 Hz, 12H, H^{C3+C3'}), 8.29 (d, J = 8.5 Hz, 6H, H^{A4}), 8.11 – 8.01 (m, 12H, H^{C4+C4'}), 7.88 (d, J = 5.3 Hz, 6H, H^{C6}), 7.81 (d, J = 5.4 Hz, 6H, H^{C6'}), 7.79 (d, J = 1.5 Hz, 6H, H^{A6}), 7.47 – 7.39 (m, 12H, H^{C5+C5'}), 7.30 (t, J = 7.9 Hz, 6H, H^{B5}), 6.99 – 6.90 (m, 18H, H^{B2+B4+B6}), 4.09 – 4.00 (m, 12H, H^{D1}), 3.79 – 3.71 (m, 12H, H^{D2}), 3.63 – 3.55 (m, 12H, H^{D3/D4}), 3.55 – 3.47 (m, 12H, H^{D3/D4}), 3.42 – 3.33 (m, 12H, H^{D5}), 1.52 (m_c, 12H, H^{D6}).

¹³C NMR (126 MHz, CD₃CN) δ/ppm = 160.54 (C^{B3}), 158.25 (C^{C2}), 157.95 (C^{C2}), 156.49 (C^{A2}), 153.12 (C^{C6} + C^{C6'}), 149.99 (C^{A6}), 140.56 (C^{B1}), 138.95 (C^{C4/C4'}), 138.88 (C^{C4/C4'}), 137.20 (C^{A5}), 136.77 (C^{A4}), 131.66 (C^{B5}), 128.72 (C^{C5}), 128.65 (C^{C5}), 125.54 (C^{C3/C3'}), 125.33 (C^{C3/C3'}), 120.49 (C^{B4/B6}), 116.98 (C^{B4/B6}), 113.88 (C^{B2}), 71.57 (C^{D5}), 71.45 (C^{D3/D4}), 70.86 (C^{D3/D4}), 70.21 (C^{D2}), 68.75 (C^{D1}), 27.25 (C^{D6}).

UV-Vis (CH₂Cl₂, $\lambda_{\text{max}}(\text{nm})$ [$\epsilon/(\text{cm}^{-1} \text{M}^{-1})$]) = 457.0 [31200], 290.0 [181000].

Emission (CH₂Cl₂, $\lambda_{\text{exc}} = 350 \text{ nm}$, $\lambda_{\text{max}}(\text{nm})$) = 621.

m.p.: 170-176 °C.

MS (ESI): m/z = 1765.7 [M-2 PF₆]²⁺ (calc. 1766.4), 1128.5 [M- 3 PF₆]³⁺ (calc. 1129.28), 811.1 [M- 4 PF₆]⁴⁺ (calc. 810.7) 619.8 [M- 5 PF₆]⁵⁺ (calc. 619.6), 492.4 [M- 6 PF₆]⁶⁺ (calc. 492.2).

IR (ATR): $\tilde{\nu}/\text{cm}^{-1}$ = 3061w, 2929m, 2864m, 1738m, 1728m, 1601m, 1582m, 1464m, 1447m, 1369w, 1302w, 1217m, 1099m, 1059w, 827s, 761m.

Anal. calc. for $C_{162}H_{162}F_{36}N_{18}O_{18}P_6Ru_3$ C 50.91, H 4.27, N 6.60; found C 50.63, H 4.19, N 6.20.

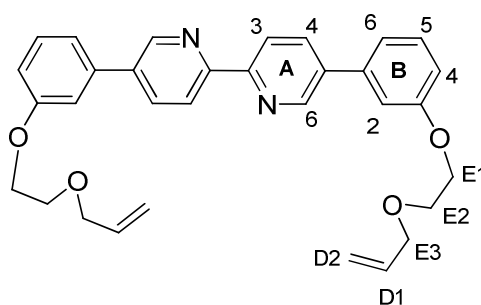
Determination of sodium in **64** via atomic absorption spectroscopy

Only ultrapure water (Milli-Q, $>18\text{ M}\Omega\text{ cm}^{-3}$) and HPLC quality acetonitrile were used throughout these experiments. A sodium stock solution (10^{-4} M) was prepared by dissolving 58.4 mg of NaCl in 100 mL of water and a 1 to 100 dilution of this solution. The standards were prepared by adding 1, 2, 3, 4, 6, 10 mL of the stock solution to a 100 mL volumetric flask. To each were 5 mL of acetonitrile added and the flask was filled to 100 mL with water yielding 1, 2, 3, 4, 6, 10 μM standard solutions.

The sample was prepared by dissolving 8.9 mg of the ruthenium complex **64** (M_r 1386.6, **64** \cdot 0.35NaCl) in 2.5 mL of acetonitrile in a 50 mL flask which was then filled with water until the mark. This solution was diluted 1/100 with a 5% acetonitrile/water solution yielding a 12.9 μM solution of **64**.

The atomic absorption of sodium of a blank and the standards were measured and a linear least square fit was calculated for standards 2,3,4, 6 and 10 μM solutions after correction of background absorption. The slope was calculated as 0.0113(3) a.u./ μM and an intercept of 0.001(1) was found. The atomic absorption of the sample was measured and the sodium concentration of the sample could then be calculated as 4.46 μM .

6.3 Experimental for Compounds in Chapter 4

Ligand **42**

5,5'-Bis(3'-hydroxyphenyl)-2,2'-bipyridine (1.63 g, 4.79 mmol), 3-(2-bromoethoxy)prop-1-ene (1.57 g, 9.63 mmol) and Cs_2CO_3 (6.24 g, 19.0 mmol) were dissolved in dry DMF (200 mL). The reaction mixture was heated for 4 d at 120 °C. Removal of DMF, column chromatography (SiO_2 , CH_2Cl_2 : MeOH (66:1)) and filtration over Al_2O_3 yielded **42** as a colourless crystalline solid (2.17 g, 4.27 mmol, 89%).

^1H NMR (500 MHz, CDCl_3) δ/ppm = 8.97 (d, J = 2.1 Hz, 2H, H^{A6}), 8.54 (d, J = 8.2 Hz, 2H, H^{A3}), 8.06 (dd, J = 2.3, 8.3 Hz, 2H, H^{A4}), 7.45 (t, J = 7.9 Hz, 2H, H^{B5}), 7.32 – 7.26 (m, 4H, $\text{H}^{\text{B2+B6}}$), 7.03 (dd, J = 2.2, 8.2 Hz, 2H, H^{B4}), 6.05 – 5.94 (m, 2H, H^{D1}), 5.37 (dd, J = 1.6, 17.2 Hz, 2H, $\text{H}^{\text{D2,trans}}$), 5.27 (dd, J = 1.2, 10.4 Hz, 2H, $\text{H}^{\text{D2,cis}}$), 4.29 – 4.24 (m, 4H, H^{E1}), 4.19 – 4.14 (m, 4H, H^{E3}), 3.92 – 3.86 (m, 4H, H^{E2}).

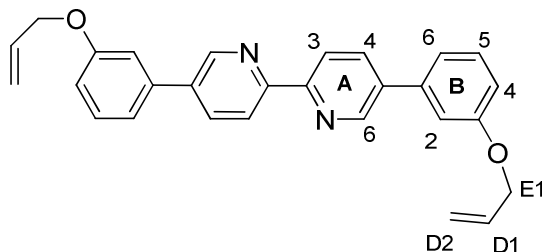
^{13}C NMR (126 MHz, CDCl_3) δ/ppm = 159.3 (C^{B3}), 154.70 (C^{A2}), 147.7 (C^{A6}), 138.9 (C^{B1}), 136.2 (C^{A5}), 135.2 (C^{A4}), 134.5 (C^{D1}), 130.1 (C^{B5}), 120.9 (C^{A3}), 119.7 (C^{B6}), 117.4 (C^{D2}), 114.0 (C^{B4}), 113.6 (C^{B2}), 72.4 (C^{E3}), 68.4 (C^{E2}), 67.5 (C^{E1}).

MS (EI): m/z = 508.2 [M^+] (calc. 508.2), 424.2[($\text{M}-\text{C}_5\text{H}_8\text{O}$) $^+$] (calc. 424.2), 340.1[($\text{M}-2\text{C}_5\text{H}_8\text{O}$) $^+$] (calc. 340.1).

mp.: 96-98 °C.

IR (ATR): $\tilde{\nu}/\text{cm}^{-1}$ = 3005w, 2932w, 2856w, 1605m, 1576s, 1464m, 1452s, 1441m, 1358m, 1300m, 1279m, 1205s, 1142m, 1130m, 1099m, 1068m, 1016m, 947m, 937m, 918m, 835m, 781s, 694s.

Anal. calc. for $\text{C}_{32}\text{H}_{32}\text{N}_2\text{O}_2$ C 75.57 H 6.34 N 5.51; found C 75.54 H 6.50 N 5.39.

5,5'-Bis(3-(allyloxy)phenyl)-2,2'-bipyridine (**72**)

5,5'-Bis(3'-hydroxyphenyl)-2,2'-bipyridine (88.4 mg, 260 μmol), allyl bromide (1.0 mL, 11.5 mmol) and Cs_2CO_3 (350 mg, 1.07 mmol) were heated in THF to 100 $^\circ\text{C}$ in a microwave reactor for 45 min. Column chromatography (SiO_2 , CH_2Cl_2 : MeOH (100:1)) yielded ligand **72** as a colourless solid (106 mg, 252 μmol , 96%).

^1H NMR (500 MHz, CDCl_3) δ/ppm = 8.93 (d, J = 2.1 Hz, 2H, $\text{H}^{\text{A}6}$), 8.50 (d, J = 8.2 Hz, 2H, $\text{H}^{\text{A}3}$), 8.03 (dd, J = 8.2, 2.3 Hz, 2H, $\text{H}^{\text{A}4}$), 7.42 (t, J = 7.9 Hz, 2H, $\text{H}^{\text{B}5}$), 7.26 – 7.24 (m, 2H, $\text{H}^{\text{B}6}$), 7.22 – 7.21 (m, 2H, $\text{H}^{\text{B}2}$), 6.98 (dd, J = 8.2, 2.4 Hz, 2H, $\text{H}^{\text{B}4}$), 6.15 – 6.04 (m, 2H, $\text{H}^{\text{D}1}$), 5.47 (dd, J = 17.3, 1.5 Hz, 2H, $\text{H}^{\text{D}2, \text{trans}}$), 5.33 (dd, J = 10.5, 1.3 Hz, 2H, $\text{H}^{\text{D}2, \text{cis}}$), 4.63 (d, J = 5.3 Hz, 4H, $\text{H}^{\text{E}1}$).

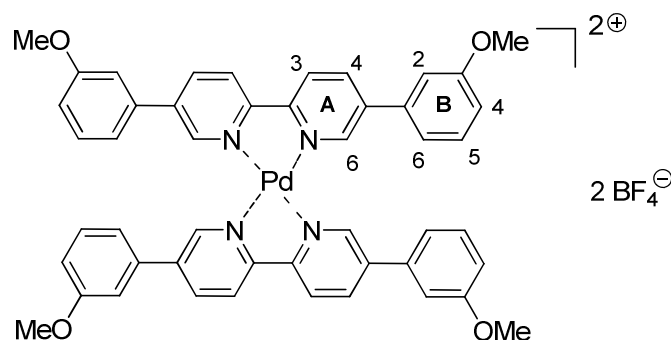
^{13}C NMR (126 MHz, CDCl_3) δ/ppm = 159.2 ($\text{C}^{\text{B}3}$), 154.8 ($\text{C}^{\text{A}2}$), 147.7 ($\text{C}^{\text{A}6}$), 139.0 ($\text{C}^{\text{B}1}$), 136.3 ($\text{C}^{\text{A}5}$), 135.3 ($\text{C}^{\text{A}4}$), 133.1 ($\text{C}^{\text{D}1}$), 130.2 ($\text{C}^{\text{B}5}$), 121.0 ($\text{C}^{\text{A}3}$), 119.7 ($\text{C}^{\text{B}6}$), 117.9 ($\text{C}^{\text{D}2}$), 114.3 ($\text{C}^{\text{B}4}$), 113.7 ($\text{C}^{\text{B}2}$), 68.9 ($\text{C}^{\text{E}1}$).

m.p.: 135-137 $^\circ\text{C}$.

IR (ATR): $\tilde{\nu}/\text{cm}^{-1}$ = 2874m, 2869m, 1605m, 1578s, 1460s, 1435m, 1362w, 1297m, 1278m, 1201s, 1175w, 1113m, 1099m, 1068m, 1016m, 947m, 934m, 937m, 918m, 841m, 779s.

MS (EI): m/z = 421.2 $[\text{M}+\text{H}]^+$ (calc. 421.2).

Anal. calc. for $\text{C}_{28}\text{H}_{24}\text{N}_2\text{O}_2 \cdot 0.2 \text{H}_2\text{O}$ C 79.30 H 5.80 N 6.61; found C 79.13 H 6.10 N 6.31.

$[\text{Pd}(\mathbf{34})_2](\text{BF}_4)_2$ (**74**)

5,5'-Bis(3-methoxyphenyl)-2,2'-bipyridine (**34**) (227 mg, 617 μmol) in abs. CH_2Cl_2 (10 mL) was added to a solution of $[\text{Pd}(\text{CH}_3\text{CN})_4](\text{BF}_4)_2$ (137 mg, 308 μmol) in abs. CH_3CN (10 mL) and stirred at room temperature for 24 h. The solution turned pale yellow and a yellow precipitate was formed. All volatiles were removed in vacuum yielding the desired complex **74** (313 mg, 308 μmol , quant.).

^1H NMR (500 MHz, DMSO) δ/ppm = 9.15 (s_b, 4H, $\text{H}^{\text{A}6}$), 8.90 (s_b, 8H, $\text{H}^{\text{A}3+\text{A}4}$), 7.43 (m, 8H, $\text{H}^{\text{B}2+\text{B}6}$), 7.39 (t, J = 7.8 Hz, 4H, $\text{H}^{\text{B}5}$), 7.13 (d, J = 7.4 Hz, 4H, $\text{H}^{\text{B}4}$), 3.73 (s, 12H, OMe).

^{13}C NMR (101 MHz, DMSO) δ/ppm = 160.1 ($\text{C}^{\text{B}3}$), 154.5 ($\text{C}^{\text{A}2}$), 149.5 ($\text{C}^{\text{A}6}$), 140.0 ($\text{C}^{\text{A}3/\text{A}4}$), 139.2 ($\text{C}^{\text{A}5}$), 135.6 ($\text{C}^{\text{B}1}$), 130.5 ($\text{C}^{\text{B}5}$), 124.3 ($\text{C}^{\text{A}3/\text{A}4}$), 119.7 ($\text{C}^{\text{B}6}$), 115.6 ($\text{C}^{\text{B}4}$), 112.8 ($\text{C}^{\text{B}2}$), 55.2 (OCH₃).

^{19}F NMR (376 MHz, DMSO) δ/ppm = -149 (s).

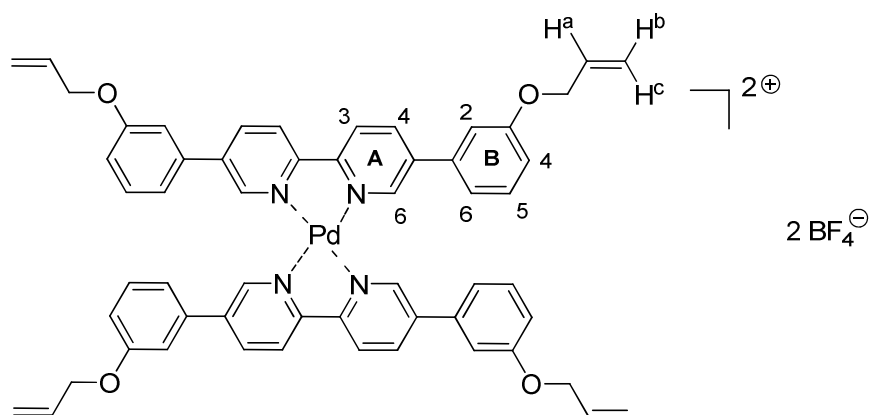
MS (FAB): m/z = 929.1 (0.68, $[\text{PdL}_2](\text{BF}_4)^+$, calc. 929.2), 861.1 (8.70), 842.1 (9.35, $[\text{PdL}_2]^+$, calc. 842.2), 474.0 (37.05, $[\text{PdL}]^+$, calc. 474.1), 369.1 (100, LH^+ , calc. 369.2).

MS (ESI): m/z = 879.0 $[\text{M}-2\text{BF}_4+\text{Cl}]^+$ (calc. 878.7), 448.7 (?), 369.4 $[\text{LH}^+]$ (calc. 369.2).

IR (ATR): $\tilde{\nu}/\text{cm}^{-1}$ = 3005w, 2932w, 2856w, 1738m, 1605m, 1576m, 1464m, 1452s, 1435m, 1300m, 1231m, 1205m, 1063m, 1016m, 843m, 837m, 779s, 692s.

Anal. calc. for $\text{C}_{48}\text{H}_{40}\text{B}_2\text{F}_8\text{N}_4\text{O}_4\text{Pd}$ C 56.70, H 3.96, N 5.51; found C 56.53, H 4.10, N 5.41.

[Pd(**72**)₂](BF₄)₂ (**75**)



Complex **75** (85.1 mg, 75.9 μmol , 99.9%) was synthesised according to procedure for **74** from ligand **72** (64.1mg, 152 μmol) and [Pd(CH₃CN)₄](BF₄)₂ (34.2 mg, 77.0 μmol).

¹H NMR (500 MHz, acetone-*d*₆) δ /ppm = 9.33 (s_b, 4H, H^{A6}), 8.89 – 8.78 (m, 8H, H^{A3+A4}), 7.47 – 7.44 (m, 4H, H^{B2}), 7.43 – 7.40 (m, 8H, H^{B5+B6}), 7.17 – 7.10 (m, 4H, H^{B4}), 6.10 – 5.98 (m, 4H, H^a), 5.39 (dq, *J* = 1.7, 17.3 Hz, 4H, H^c), 5.24 (dq, *J* = 1.5, 10.6 Hz, 4H, H^b), 4.60 (dt, *J* = 1.5, 5.2 Hz, 8H, -OCH₂).

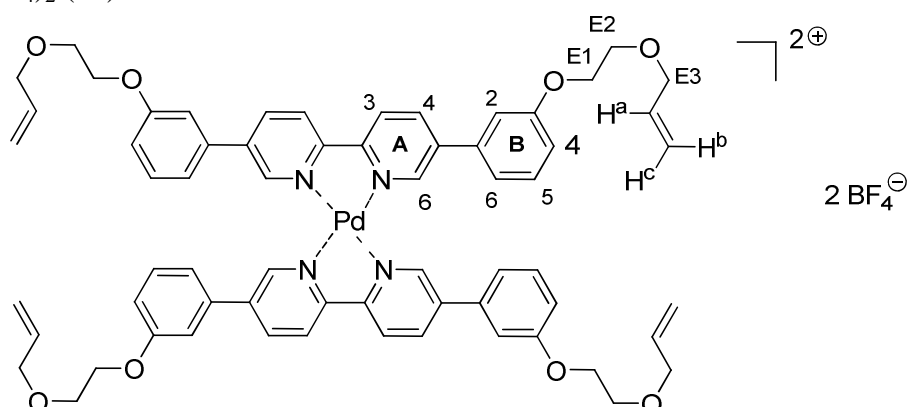
¹³C NMR (126 MHz, acetone-*d*₆) δ /ppm = 160.5 (C^{B3}), 156.2 (C^{A2}), 150.3 (C^{A6}), 140.91 (C^{A5}), 140.90 (C^{A3/A4}), 137.0 (C^{B1}), 134.4 (OCH₂CH), 131.6 (C^{B5}), 125.3 (C^{A3/A4}), 120.7 (C^{B6}), 117.8 (OCH₂CHCH₂), 117.1 (C^{B2}), 114.5 (C^{B4}), 69.5 (OCH₂).

¹⁹F NMR (376 MHz, acetone-*d*₆) δ /ppm = -152.2 (s).

MS (ESI): *m/z* = 473.3 [M- 2BF₄]²⁺ (calc. 473.2).

IR (ATR): $\tilde{\nu}$ /cm⁻¹ = 3070m, 2924m, 2168m, 2037w, 1736w, 1582w, 1466m, 1373w, 1304m, 1250m, 1211m, 1026s, 918m, 841m, 779m, 687m.

Anal. calc. for C₅₆H₄₈B₂F₈N₄O₄Pd C 60.00, H 4.32, N 5.00; found C 60.64, H 4.49, N 4.80.

[Pd(42)₂](BF₄)₂ (76)

Complex **76** (129 mg, 99.4 μmol , quant.) was synthesised according to procedure **74** from ligand **42** (100 mg, 197 μmol) and $[\text{Pd}(\text{CH}_3\text{CN})_4](\text{BF}_4)_2$ (44.1 mg, 99.3 μmol).

^1H NMR (500 MHz, $\text{CD}_3\text{CN}/\text{CDCl}_3$) δ/ppm = 8.76 (s_b, 4H, $\text{H}^{\text{A}6}$), 8.46 (s_b, 8H, $\text{H}^{\text{A}3+\text{A}4}$), 7.30 (t, J = 7.9 Hz, 4H, $\text{H}^{\text{B}5}$), 7.17 (s, 4H, $\text{H}^{\text{B}2}$), 7.14 (d, J = 7.6 Hz, 4H, $\text{H}^{\text{B}6}$), 7.00 (d, J = 8.2 Hz, 4H, $\text{H}^{\text{B}4}$), 5.92 – 5.79 (m, 4H, H^{a}), 5.25 (dd, J = 1.4, 17.3 Hz, 4H, H^{b}), 5.14 (d, J = 10.4 Hz, 4H, H^{c}), 4.10 – 4.04 (m, 8H, $\text{CH}_2^{\text{E}1}$), 4.01 (d, J = 5.5 Hz, 8H, $\text{CH}_2^{\text{E}3}$), 3.75 – 3.68 (m, 8H, $\text{CH}_2^{\text{E}2}$).

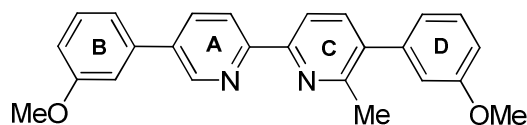
^{13}C NMR (126 MHz, $\text{CD}_3\text{CN}/\text{CDCl}_3$) δ/ppm = 160.0 ($\text{C}^{\text{B}3}$), 155.0 ($\text{C}^{\text{A}2}$), 148.9 ($\text{C}^{\text{A}6}$), 140.1 ($\text{C}^{\text{A}3/\text{A}4}$), 136.0 ($\text{C}^{\text{A}5/\text{B}1}$), 135.8 ($\text{C}^{\text{A}5/\text{B}1}$), 134.8 (CHCH_2), 131.0 ($\text{C}^{\text{B}5}$), 124.7 ($\text{C}^{\text{A}3/\text{A}4}$), 119.9 ($\text{C}^{\text{B}6}$), 117.2 (CHCH_2), 116.6 ($\text{C}^{\text{B}4}$), 113.4 ($\text{C}^{\text{B}2}$), 72.3 ($\text{C}^{\text{E}3}$), 68.6 ($\text{C}^{\text{E}2}$), 67.9 ($\text{C}^{\text{E}1}$).

^{19}F NMR (376 MHz, acetone- d_6) δ/ppm = -152.6 (s).

MS (ESI): m/z = 1157.6 $[\text{Pd}(\mathbf{42})_2\text{Cl}]^+$ (calc. 1157.4).

IR (ATR): $\tilde{\nu}/\text{cm}^{-1}$ = 3070m, 2924m, 2168m, 2037w, 1736w, 1582w, 1466m, 1373w, 1304m, 1250m, 1211m, 1026s, 918m, 841m, 779m, 686m.

Anal. calc. for $\text{C}_{64}\text{H}_{64}\text{B}_2\text{F}_8\text{N}_4\text{O}_4\text{Pd}$ C 59.26, H 4.97, N 4.32; found C 60.03, H 5.15, N 4.36.

5,5'-Bis(3-methoxyphenyl)-6-methyl-2,2'-bipyridine (77)

5,5'-Bis(3-methoxyphenyl)-2,2'-bipyridine (**34**) (1.28 g, 3.47 mmol) was dissolved in anhydrous toluene (250 mL) and cooled to -78 $^\circ\text{C}$. Methyl lithium (2.4 mL, 1.6M solution in

hexane, 3.82 mmol) was added drop wise to this solution. A slight colour change from colourless to orange was observed. The reaction mixture was allowed to warm to room temperature over night and the colour changed to intense blue/violet. To ensure complete conversion the solution was stirred again for 30 min at 100 °C (colour change to orange). Then the solution was cooled to room temperature and was extracted with H₂O (200 mL). The water phase was extracted with CH₂Cl₂ (3 x 20 mL) and the combined organic layers were dried over MgSO₄, filtered and stirred in the presence of MnO₂ (10 g) for 6h. Filtration and removal of solvents yielded colourless bipyridine **77** (1.09 g, 2.85mmol, 82%).

¹H NMR (500 MHz, CDCl₃) δ /ppm = 8.93 (d, J = 2.2 Hz, 1H, H^{A6}), 8.54 (d, J = 8.2 Hz, 1H, H^{A3}), 8.30 (d, J = 7.9 Hz, 1H, H^{C3}), 8.02 (dd, J = 8.2, 2.3 Hz, 1H, H^{A4}), 7.68 (d, J = 8.0 Hz, 1H, H^{C4}), 7.42 (t, J = 7.9 Hz, 1H, H^{B5}), 7.38 (t, J = 7.8 Hz, 1H, H^{D5}), 7.25 (d, J = 7.5 Hz, 1H, H^{B6}), 7.20 – 7.18 (m, 1H, H^{B2}), 6.99 – 6.91 (m, 4H, H^{B4+D2+D4+D6}), 3.90 (s, 3H, H^{B, OMe}), 3.86 (s, 3H, H^{D, OMe}), 2.63 (s, 3H, H^{C, Me}).

¹³C NMR (126 MHz, CDCl₃) δ /ppm = 160.12 (C^{B3}), 159.48 (C^{D3}), 155.36 (C^{A2}), 155.18 (C^{C2}), 154.08 (C^{C6}), 147.67 (C^{A6}), 141.33 (C^{D1}), 139.17 (C^{B1}), 138.01 (C^{C4}), 136.81 (C^{C5}), 136.08 (C^{A5}), 135.18 (C^{A4}), 130.13 (C^{B5}), 129.42 (C^{D5}), 121.49 (C^{D6}), 120.97 (C^{A3}), 119.51 (C^{B6}), 118.28 (C^{C3}), 114.82 (C^{D4}), 113.37 (C^{B4}), 112.85 (C^{D2}), 112.81 (C^{B2}), 55.34 (C^{B, OMe}), 55.29 (C^{D, OMe}), 23.72 (C^{C, Me}).

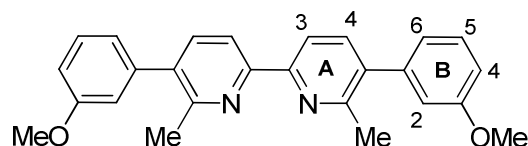
MS (EI): m/z = 382.2 [M]⁺ (calc. 282.2).

mp.: 143-144 °C.

IR (ATR): $\tilde{\nu}/\text{cm}^{-1}$ = 3060w, 2993w, 2929w, 2832w, 1606m, 1578m, 1458s, 1439m, 1432m, 1418m, 1295m, 1283s, 1209s, 1178m, 1167m, 1048m, 1035m, 1019m, 841s, 697s.

Anal. calc. for C₂₅H₂₂N₂O₂ C 78.51 H 5.80 N 7.32; found C 78.34 H 5.98 N 7.13.

5,5'-Bis(3-methoxyphenyl)-6,6'-dimethyl-2,2'-bipyridine (**78**)



5,5'-Bis(3-methoxyphenyl)-6-methyl-2,2'-bipyridine (**77**) (102 mg, 267 μ mol) was dissolved in anhydrous toluene (30 mL) and cooled to –20 °C. Methyl lithium (180 μ L, 1.6M solution in hexane, 293 μ mol) was added drop wise and an intense blue coloration appeared. The reaction mixture was stirred for 1h at this temperature, allowed to warm to room temperature and H₂O

(5 mL) was added. The water phase was separated and extracted with CH_2Cl_2 (3 x 10 mL). The combined organic layers were treated with MnO_2 (2 g) and stirred for 5 h at room temperature. Column chromatography (Al_2O_3 , CH_2Cl_2) yielded colourless title compound **78** (58.3 mg, 147 μmol 55%).

^1H NMR (500 MHz, CDCl_3) δ/ppm = 8.93 (d, J = 2.2 Hz, 1H, H^{A6}), 8.54 (d, J = 8.2 Hz, 1H, H^{A3}), 8.30 (d, J = 7.9 Hz, 1H, H^{C3}), 8.02 (dd, J = 8.2, 2.3 Hz, 1H, H^{A4}), 7.68 (d, J = 8.0 Hz, 1H, H^{C4}), 7.42 (t, J = 7.9 Hz, 1H, H^{B5}), 7.38 (t, J = 7.8 Hz, 1H, H^{D5}), 7.25 (d, J = 7.5 Hz, 1H, H^{B6}), 7.20 – 7.18 (m, 1H, H^{B2}), 6.99 – 6.91 (m, 4H, $\text{H}^{\text{B4+D2+D4+D6}}$), 3.90 (s, 3H, $\text{H}^{\text{B, OMe}}$), 3.86 (s, 3H, $\text{H}^{\text{D, OMe}}$), 2.63 (s, 3H, $\text{H}^{\text{C, Me}}$).

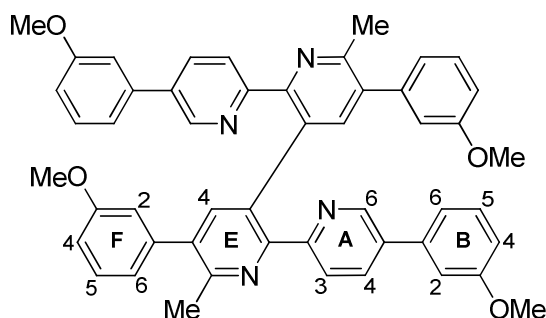
^{13}C NMR (126 MHz, CDCl_3) δ/ppm = 160.12 (C^{B3}), 159.48 (C^{D3}), 155.36 (C^{A2}), 155.18 (C^{C2}), 154.08 (C^{C6}), 147.67 (C^{A6}), 141.33 (C^{D1}), 139.17 (C^{B1}), 138.01 (C^{C4}), 136.81 (C^{C5}), 136.08 (C^{A5}), 135.18 (C^{A4}), 130.13 (C^{B5}), 129.42 (C^{D5}), 121.49 (C^{D6}), 120.97 (C^{A3}), 119.51 (C^{B6}), 118.28 (C^{C3}), 114.82 (C^{D4}), 113.37 (C^{B4}), 112.85 (C^{D2}), 112.81 (C^{B2}), 55.34 ($\text{C}^{\text{B, OMe}}$), 55.29 ($\text{C}^{\text{D, OMe}}$), 23.72 ($\text{C}^{\text{C, Me}}$).

MS (ESI): m/z = 397.4 $[\text{M}+\text{H}]^+$ (calc. 397.2), 419.2 $[\text{M}+\text{Na}]^+$ (calc. 419.2), 815.6 $[2\text{M}+\text{Na}]^+$ (calc. 815.4).

IR (ATR): $\tilde{\nu}/\text{cm}^{-1}$ = 3077w, 3052w, 2989m, 2959m, 2924m, 2832m, 1606m, 1575m, 1456m, 1289m, 1209s, 1179m, 1049m, 1018m, 879w, 841s, 781s.

Found C, 76.12; H, 6.15; N, 6.70; $\text{C}_{26}\text{H}_{24}\text{N}_2\text{O}_2 \cdot 0.75\text{H}_2\text{O}$ requires C, 76.17; H, 6.27; N, 6.83 %.

Compound 79



Compound **34** (1.92 g, 5.21 mmol) was dissolved in toluene (250 mL). Methyl lithium (3.9 mL, 1.6 M solution in hexane, 6.25 mmol) was added dropwise at r. t. resulting in a blue/violet solution. Water (40 mL) was added and the organic phase was separated. The water phase was extracted with CH_2Cl_2 and the combined organic layers were dried over MgSO_4 , filtered and stirred in the presence of MnO_2 (25 g) for 6h. After final filtration, spot

tlc showed the presence of two components. These were separated using column chromatography (Al_2O_3 , $\text{CH}_2\text{Cl}_2 \rightarrow \text{CH}_2\text{Cl}_2 : \text{MeOH}$ (20:1)) and solvent removed from the fractions to yield **5** (first fraction, 668 mg, 1.75 mmol, 34%) and **7** (second fraction, 621 mg, 814 μmol , 31%).

^1H NMR (500 MHz, CDCl_3) δ/ppm = 8.68 (d, J = 1.7 Hz, 2H, H^{A6}), 7.72 (dd, J = 8.1, 2.2 Hz, 2H, H^{A4}), 7.53 (s, 2H, H^{E4}), 7.52 (d, J = 8.1 Hz, 2H, H^{A3}), 7.40 (t, J = 7.9 Hz, 2H, H^{B5}), 7.31 (t, J = 7.9 Hz, 2H, H^{F5}), 7.17 (d, J = 7.7 Hz, 2H, H^{B6}), 7.10 (s, 2H, H^{B2}), 6.95 (dd, J = 8.2, 2.1 Hz, 2H, H^{B4}), 6.91 – 6.86 (m, 4H, $\text{H}^{\text{F4+F6}}$), 6.81 (s, 2H, H^{F2}), 3.87 (s, 6H, $\text{H}^{\text{B, OMe}}$), 3.78 (s, 6H, $\text{H}^{\text{F, OMe}}$), 2.63 (s, 6H, H^{Me}).

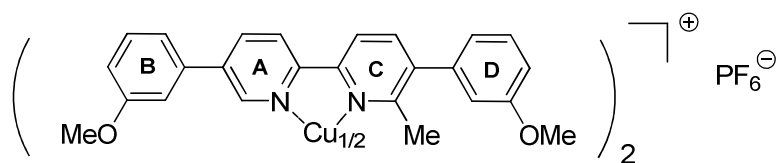
^{13}C NMR (126 MHz, CDCl_3) δ/ppm = 160.06 (C^{B3}), 159.41 (C^{F3}), 156.54 (C^{A2}), 154.46 (C^{E6}), 153.30 (C^{E2}), 147.20 (C^{A6}), 140.55 (C^{F1}), 140.40 (C^{E4}), 139.10 (C^{B1}), 136.14 (C^{E5}), 134.85 (C^{A5}), 134.40 (C^{A4}), 131.86 (C^{E3}), 130.07 (C^{B5}), 129.33 (C^{F5}), 124.16 (C^{A3}), 121.46 (C^{F6}), 119.47 (C^{B6}), 114.65 (C^{F2}), 113.21 (C^{B4}), 113.00 (C^{F4}), 112.89 (C^{B2}), 55.29 ($\text{C}^{\text{B, OMe}}$), 55.19 ($\text{C}^{\text{F, OMe}}$), 23.31 (C^{Me}).

MS (ESI): m/z = 763.4 [$\text{M} + \text{H}$] $^+$ (calc. 763.3).

IR (ATR): $\tilde{\nu}/\text{cm}^{-1}$ = 3001w, 2932w, 2831 w, 1599s, 1578s, 1450m, 1424s, 1363w, 1285m, 1211s, 1163m, 1037m, 1013m, 844m, 777s, 690s.

Found C, 77.36; H, 5.70; N, 7.22; $\text{C}_{50}\text{H}_{42}\text{N}_4\text{O}_4 \cdot 0.75\text{H}_2\text{O}$ requires C, 77.35; H, 5.65; N, 7.22 %.

[Cu(**77**) $_2$](PF $_6$) (**80**)



To a solution of ligand **77** (32.0 mg, 83.7 μmol) in abs. CH_2Cl_2 (5 mL) $[\text{Cu}(\text{CH}_3\text{CN})_4](\text{PF}_6)$ (15.7 mg, 42.0 μmol) dissolved in abs. CH_3CN (5 mL) was added in N_2 -atmosphere. The red solution was stirred for 30 min at room temperature filtered over Al_2O_3 and the solvents were removed in vacuum. The copper(I) complex **80** (40.1 mg, 41.2 μmol , 98%) was analytically pure.

^1H NMR (500 MHz, CD_3CN) δ/ppm = 8.91 (d, J = 1.7 Hz, 2H, H^{A6}), 8.48 (d, J = 8.4 Hz, 2H, H^{A3}), 8.30 (d, J = 8.1 Hz, 2H, H^{C3}), 8.24 (d, J = 7.1 Hz, 2H, H^{A4}), 7.83 (d, J = 8.0 Hz, 2H,

^1H NMR (500 MHz, CD_3CN) δ/ppm = 7.41 – 7.35 (m, 4H, $\text{H}^{\text{B}5+\text{D}5}$), 7.25 (d, J = 7.8 Hz, 2H, $\text{H}^{\text{B}6}$), 7.24 – 7.20 (m, 2H, $\text{H}^{\text{B}2}$), 7.01 – 6.91 (m, 8H, $\text{H}^{\text{B}4+\text{D}2+\text{D}4+\text{D}6}$), 3.81 (s, 6H, $\text{H}^{\text{B}, \text{OMe}}$), 3.80 (s, 6H, $\text{H}^{\text{D}, \text{OMe}}$), 2.39 (s, 6H, H^{Me}).

^{13}C NMR (126 MHz, CD_3CN) δ/ppm = 161.39 ($\text{C}^{\text{B}3}$), 160.74 ($\text{C}^{\text{D}3}$), 156.25 ($\text{C}^{\text{C}6}$), 153.74 ($\text{C}^{\text{A}2}$), 152.71 ($\text{C}^{\text{C}2}$), 148.42 ($\text{C}^{\text{A}6}$), 141.54 ($\text{C}^{\text{D}1}$), 139.60 ($\text{C}^{\text{C}4}$), 139.29 ($\text{C}^{\text{C}5}$), 139.01 ($\text{C}^{\text{B}1}$), 138.39 ($\text{C}^{\text{A}5}$), 136.66 ($\text{C}^{\text{A}4}$), 131.41 ($\text{C}^{\text{B}5}$), 130.75 ($\text{C}^{\text{D}5}$), 122.44 ($\text{C}^{\text{A}3}$), 122.31 ($\text{C}^{\text{D}6}$), 120.36 ($\text{C}^{\text{B}6}$), 119.86 ($\text{C}^{\text{C}3}$), 115.75 ($\text{C}^{\text{D}2}$), 115.17 ($\text{C}^{\text{D}4}$), 114.32 ($\text{C}^{\text{B}4}$), 113.60 ($\text{C}^{\text{B}2}$), 56.12 ($\text{C}^{\text{B}, \text{OMe}}$), 56.08 ($\text{C}^{\text{D}, \text{OMe}}$), 24.64 (C^{Me}).

^{19}F NMR (376 MHz, CD_3CN) δ/ppm = -74.1 (d, J = 705 Hz).

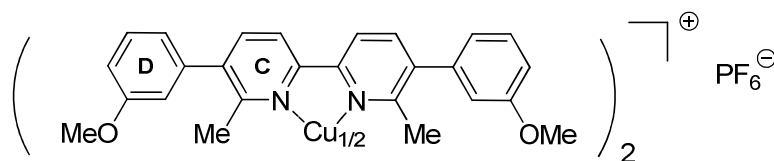
IR (ATR): $\tilde{\nu}/\text{cm}^{-1}$ = 3062 w, 2954 w, 2922 m, 2850 w, 1599 m, 1581 m, 1470 m, 1447 m, 1435 m, 1377 w, 1300 m, 1251 w, 1224 m, 1045 s, 1021 s, 837 s, 786 s, 690 m.

UV-Vis (CH_2Cl_2 , $\lambda_{\text{max}}(\text{nm})$ [ϵ' ($\text{cm}^{-1} \text{M}^{-1}$)]) = 468 [6000], 319.0 [61000], 277.0 [50500].

Emission (CH_2Cl_2 , $\lambda_{\text{max}}(\text{nm})$, exc 350 nm) = 379.

Found C, 61.39; H, 4.75; N, 5.54; $\text{C}_{50}\text{H}_{44}\text{CuN}_4\text{O}_4\text{PF}_6$ requires C, 61.69; H, 4.56; N, 5.76 %.

[Cu(**80**)₂](PF₆) (**81**)



Copper(I) complex **81** was prepared analogue to procedure for **80** with ligand **78** (40.0 mg, 101 μmol) and $[\text{Cu}(\text{CH}_3\text{CN})_4](\text{PF}_6)$ (19 mg, 50.9 μmol). Filtration over Al_2O_3 yielded title compound **81** (48.1 mg, 48.0 μmol , 94%).

^1H NMR (500 MHz, CD_3CN) δ/ppm = 8.35 (d, J = 7.1 Hz, 4H, $\text{H}^{\text{C}3}$), 7.98 (d, J = 7.3 Hz, 4H, $\text{H}^{\text{C}4}$), 7.39 (t, J = 7.8 Hz, 4H, $\text{H}^{\text{D}5}$), 7.03 – 6.94 (m, 12H, $\text{H}^{\text{D}2+\text{D}4+\text{D}6}$), 3.80 (s, 12H, OMe), 2.32 (s, 12H, Me).

^{13}C NMR (126 MHz, CD_3CN) δ/ppm = 160.77 ($\text{C}^{\text{D}3}$), 156.22 ($\text{C}^{\text{C}6}$), 151.52 ($\text{C}^{\text{C}2}$), 141.00 ($\text{C}^{\text{D}1}$), 140.32 ($\text{C}^{\text{C}5}$), 140.10 ($\text{C}^{\text{C}4}$), 130.85 ($\text{C}^{\text{D}5}$), 122.35 ($\text{C}^{\text{D}6}$), 120.70 ($\text{C}^{\text{C}3}$), 115.83 ($\text{C}^{\text{D}4}$), 114.57 ($\text{C}^{\text{D}2}$), 56.13 (C^{OMe}), 24.83 (C^{Me}).

^{19}F NMR (376 MHz, CD_3CN) δ/ppm = -74.1 (d, J = 703 Hz).

MS (ESI): m/z = 856.0 [$\text{M} - \text{PF}_6$]⁺ (calc. 855.3)

mp.: 240-243 °C.

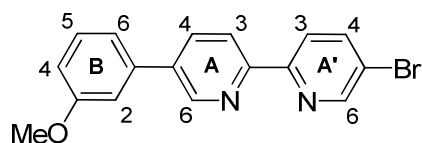
UV-Vis (CH_2Cl_2 , $\lambda_{\text{max}}(\text{nm})$ [ϵ' ($\text{cm}^{-1} \text{M}^{-1}$)]) = 467 [6100], 320.0 [61000], 277.0 [50600].

Emission (CH_2Cl_2 , $\lambda_{\text{max}}(\text{nm})$, exc 350 nm) = 383.

IR (ATR): $\tilde{\nu}/\text{cm}^{-1} = 3057\text{w}, 2972\text{w}, 2918\text{w}, 2842\text{w}, 1589\text{m}, 1448\text{m}, 1230\text{w}, 1223\text{m}, 1047\text{w}, 1022\text{m}, 831\text{s}, 787\text{m}, 702\text{m}.$

Anal. calc. for $\text{C}_{52}\text{H}_{48}\text{CuF}_6\text{N}_6\text{O}_6\text{P}$ C 62.36, H 4.83, N 5.59; found C 62.96, H 4.95, N 5.58.

5-Bromo-5'-(3-methoxyphenyl)-2,2'-bipyridine (**82**)



3-Methoxyphenylboronic acid (**33**) (851 mg, 5.60 mmol) was added to 5,5'-dibromo-2,2'-bipyridine (**32**) (1.90 g, 6.05 mmol) followed by toluene (200 mL), Na_2CO_3 (1.78 g, 17.8 mmol) and water (50 mL). The biphasic mixture was then degassed for 20 min by bubbling nitrogen through the solution. $[\text{Pd}(\text{PPh}_3)_4]$ (195 mg, 168 μmol) was added and the mixture was heated to reflux for 20 h. After cooling to room temperature, the phases were separated and the aqueous layer extracted with CH_2Cl_2 (3×50 mL). The organic extracts were combined and dried with MgSO_4 . After purification via chromatography (Al_2O_3 , DCM) and (SiO_2 , CH_2Cl_2 : MeOH (100:1)) a colourless solid (820 mg, 2.40 mmol, 40%) could be isolated.

^1H NMR (500 MHz, CDCl_3) $\delta/\text{ppm} = 8.89$ (d, $J = 1.9$ Hz, 1H, $\text{H}^{\text{A}6}$), 8.73 (d, $J = 2.1$ Hz, 1H, $\text{H}^{\text{A}6}$), 8.43 (d, $J = 8.3$ Hz, 1H, $\text{H}^{\text{A}3}$), 8.35 (d, $J = 8.5$ Hz, 1H, $\text{H}^{\text{A}3}$), 8.00 (dd, $J = 8.2, 2.3$ Hz, 1H, $\text{H}^{\text{A}4}$), 7.94 (dd, $J = 8.5, 2.3$ Hz, 1H, $\text{H}^{\text{A}4}$), 7.41 (t, $J = 7.9$ Hz, 1H, $\text{H}^{\text{B}5}$), 7.23 (d, $J = 7.8$ Hz, 1H, $\text{H}^{\text{B}6}$), 7.18 – 7.14 (m, 1H, $\text{H}^{\text{B}2}$), 6.97 (dd, $J = 8.2, 2.1$ Hz, 1H, $\text{H}^{\text{B}4}$), 3.88 (s, 3H, OMe).

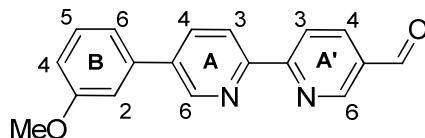
^{13}C NMR (126 MHz, CDCl_3) $\delta/\text{ppm} = 160.1$ ($\text{C}^{\text{B}3}$), 154.3 ($\text{C}^{\text{A}2}$), 154.0 ($\text{C}^{\text{A}2}$), 150.2 ($\text{C}^{\text{A}6}$), 147.7 ($\text{C}^{\text{A}6}$), 139.5 ($\text{C}^{\text{A}4}$), 138.9 ($\text{C}^{\text{B}1}$), 136.6 ($\text{C}^{\text{A}5}$), 135.3 ($\text{C}^{\text{A}4}$), 130.2 ($\text{C}^{\text{B}5}$), 122.3 ($\text{C}^{\text{A}3}$), 121.1 ($\text{C}^{\text{A}5}$), 120.8 ($\text{C}^{\text{A}3}$), 119.5 ($\text{C}^{\text{B}6}$), 113.5 ($\text{C}^{\text{B}4}$), 112.9 ($\text{C}^{\text{B}2}$), 55.3 (OMe).

MS (EI): $m/z = 340.0$ [M^+] (calc. 340.0).

m.p.: 149-150 $^\circ\text{C}$.

IR (ATR): $\tilde{\nu}/\text{cm}^{-1} = 3080\text{w}, 3003\text{w}, 2952\text{w}, 2931\text{w}, 2834\text{w}, 1605\text{m}, 1575\text{m}, 1454\text{s}, 1433\text{m}, 1360\text{m}, 1298\text{m}, 1283\text{m}, 1215\text{m}, 1170\text{w}, 1090\text{m}, 1052\text{m}, 1013\text{s}, 1003\text{m}, 928\text{m}, 833\text{s}, 816\text{m}, 783\text{m}, 779\text{m}, 771\text{m}, 733\text{m}, 692\text{w}.$

Anal. calc. for $\text{C}_{17}\text{H}_{13}\text{BrN}_2\text{O}$ C 59.84, H 3.84, N 8.21; found C 59.75, H 3.80, N 8.16.

5'-(3-Methoxyphenyl)-2,2'-bipyridine-5-carbaldehyde (**83**)

5-Bromo-5'-(3-methoxyphenyl)-2,2'-bipyridine (**82**) (760 mg, 2.23 mmol) was dissolved in abs. toluene (80 mL) and cooled to $-78\text{ }^{\circ}\text{C}$. *N*-butyl lithium (1.46 mL, 1.6 M solution in hexane, 2.34 mmol) was added drop wise. The dark red solution was stirred for 30 min at this temperature before abs. DMF (3.44 ml) was added. The reaction mixture was gradually allowed to warm to room temperature and then poured to H_2O (500 mL). The organic phase was separated and the water phase extracted with CH_2Cl_2 (3 x 50 mL). The combined organic layers were treated with MgSO_4 and filtered. Column chromatography (Al_2O_3 , CH_2Cl_2 : MeOH (0% \rightarrow 2%)) yielded aldehyde **83** (190 mg, 654 μmol , 29%).

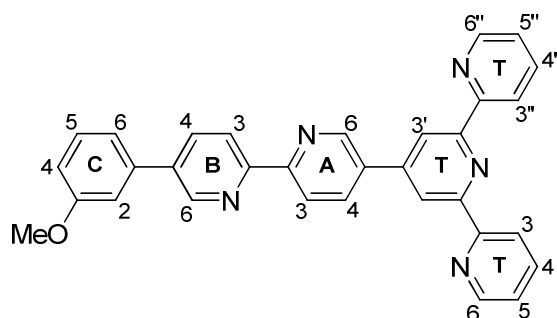
^1H NMR (500 MHz, CDCl_3) δ/ppm = 10.15 (s, 1H, CHO), 9.12 (d, $J = 1.6$ Hz, 1H, $\text{H}^{\text{A}6}$), 8.94 (d, $J = 1.9$ Hz, 1H, $\text{H}^{\text{A}6}$), 8.63 (d, $J = 8.2$ Hz, 1H, $\text{H}^{\text{A}3}$), 8.56 (d, $J = 8.2$ Hz, 1H, $\text{H}^{\text{A}3}$), 8.28 (dd, $J = 8.2, 2.1$ Hz, 1H, $\text{H}^{\text{A}4}$), 8.03 (dd, $J = 8.2, 2.4$ Hz, 1H, $\text{H}^{\text{A}4}$), 7.42 (t, $J = 7.5$ Hz, 1H, $\text{H}^{\text{B}5}$), 7.23 (d, $J = 7.7$ Hz, 1H, $\text{H}^{\text{B}6}$), 7.18 – 7.16 (m, 1H, $\text{H}^{\text{B}2}$), 6.97 (dd, $J = 8.2, 2.1$ Hz, 1H, $\text{H}^{\text{B}4}$), 3.88 (s, 3H, OMe).

^{13}C NMR (126 MHz, CDCl_3) δ/ppm = 190.53 (C^{CHO}), 160.33 ($\text{C}^{\text{A}2}$), 160.16 ($\text{C}^{\text{B}3}$), 153.53 ($\text{C}^{\text{A}2}$), 151.69 ($\text{C}^{\text{A}6}$), 147.94 ($\text{C}^{\text{A}6}$), 138.61 ($\text{C}^{\text{B}1}$), 137.37 ($\text{C}^{\text{A}5}$), 136.85 ($\text{C}^{\text{A}4}$), 135.31 ($\text{C}^{\text{A}4}$), 130.97 ($\text{C}^{\text{A}5}$), 130.23 ($\text{C}^{\text{B}5}$), 122.09 ($\text{C}^{\text{A}3}$), 121.17 ($\text{C}^{\text{A}3}$), 119.53 ($\text{C}^{\text{B}6}$), 113.70 ($\text{C}^{\text{B}4}$), 112.93 ($\text{C}^{\text{B}2}$), 55.34 (C^{OMe}).

IR (ATR): $\tilde{\nu}/\text{cm}^{-1}$ = 2952w, 2852w, 1696s, 1676s, 1590m, 1583m, 1572m, 1545m, 1465s, 1359m, 1285m, 1210m, 1171w, 1114m, 1050m, 1010s, 994m, 838s, 772m, 740m, 695m.

MS (EI): m/z = 290.1 [M] $^+$ (calc. 290.1).

m.p.: 151-154 $^{\circ}\text{C}$.

Heteroditopic ligand **73**

5'-(3-Methoxyphenyl)-2,2'-bipyridine-5-carbaldehyde (**83**) (180 mg, 620 μmol), 1-(pyridin-2-yl)ethanone (146 μl , 1.30 mmol), KOH (powder, 73.0 mg, 1.30 mmol) and NH_3 (25%, 1.4 mL) were stirred at 50 $^\circ\text{C}$ for 30 min in EtOH. The reaction mixture was stirred over night at room temperature and all volatiles were removed in vacuum. Column chromatography (Al_2O_3 , CH_2Cl_2 : MeOH (0% \rightarrow 1%)) yielded the heteroditopic ligand **73** (80.3 mg, 163 μmol , 26%).

^1H NMR (500 MHz, CDCl_3) δ/ppm = 9.22 (d, J = 1.5 Hz, 1H, $\text{H}^{\text{A}6}$), 8.95 (d, J = 1.6 Hz, 1H, $\text{H}^{\text{B}6}$), 8.81 (s, 2H, $\text{H}^{\text{T}3'}$), 8.75 (d, J = 4.2 Hz, 2H, $\text{H}^{\text{T}6+\text{T}6''}$), 8.69 (d, J = 7.9 Hz, 2H, $\text{H}^{\text{T}3+\text{T}3''}$), 8.59 (d, J = 8.4 Hz, 1H, $\text{H}^{\text{A}3}$), 8.57 (d, J = 8.4 Hz, 1H, $\text{H}^{\text{B}3}$), 8.34 (dd, J = 8.2, 2.1 Hz, 1H, $\text{H}^{\text{A}4}$), 8.05 (dd, J = 8.2, 2.0 Hz, 1H, $\text{H}^{\text{B}4}$), 7.90 (t, J = 7.7 Hz, 2H, $\text{H}^{\text{T}4+\text{T}4''}$), 7.43 (t, J = 7.9 Hz, 1H, $\text{H}^{\text{C}5}$), 7.41 – 7.35 (m, 2H, $\text{H}^{\text{T}5+\text{T}5''}$), 7.26 (d, J = 3.8 Hz, 2H, $\text{H}^{\text{C}6}$), 7.19 (s, 1H, $\text{H}^{\text{C}2}$), 7.01 – 6.95 (m, 1H, $\text{H}^{\text{C}4}$), 3.89 (s, 3H, OMe).

^{13}C NMR (126 MHz, CDCl_3) δ/ppm = 160.16 ($\text{C}^{\text{C}3}$), 156.23 ($\text{C}^{\text{T}2'}$), 156.12 ($\text{C}^{\text{A}2}$), 155.88 ($\text{C}^{\text{T}2+\text{T}2''}$), 154.51 ($\text{C}^{\text{B}2}$), 149.17 ($\text{C}^{\text{T}6+\text{T}6''}$), 147.90 ($\text{C}^{\text{T}4'}$), 147.74 ($\text{C}^{\text{A}6}$), 147.01 ($\text{C}^{\text{B}6}$), 139.01 ($\text{C}^{\text{B}1}$), 136.99 ($\text{C}^{\text{T}4+\text{T}4''}$), 136.61 ($\text{C}^{\text{B}5}$), 135.58 ($\text{C}^{\text{A}4}$), 135.35 ($\text{C}^{\text{B}4}$), 133.96 ($\text{C}^{\text{A}5}$), 130.19 ($\text{C}^{\text{C}5}$), 124.04 ($\text{C}^{\text{T}5+\text{T}5''}$), 121.42 ($\text{C}^{\text{T}3+\text{T}3''}$), 121.30 ($\text{C}^{\text{A}3}$), 120.96 ($\text{C}^{\text{B}3}$), 119.56 ($\text{C}^{\text{C}6}$), 118.67 ($\text{C}^{\text{T}3'}$), 113.56 ($\text{C}^{\text{C}4}$), 112.86 ($\text{C}^{\text{C}2}$), 55.37 (OMe).

MS (EI): m/z = 493.2 [M] $^+$.

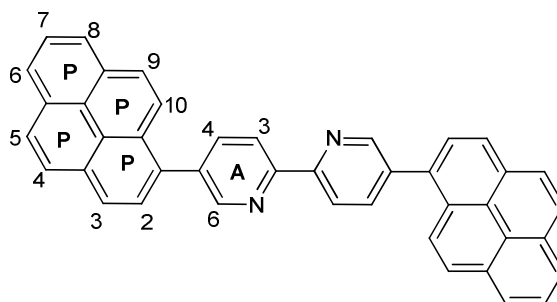
m.p.: 221-225 $^\circ\text{C}$ (with partial decomposition).

IR (ATR): $\tilde{\nu}/\text{cm}^{-1}$ = 3052w, 3000w, 2964w, 1603m, 1582m, 1576m, 1565m, 1558m, 1465s, 1406m, 1358m, 1300m, 1234m, 1210m, 1179w, 1121m, 1035m, 1012s, 990m, 849m, 843m, 836s, 788m, 780m, 741m, 731m, 697m, 651m.

Anal. calc. for $C_{32}H_{23}N_5O \cdot 1.75 H_2O$ C 73.20, H 5.09, N 13.34; found C 73.10, H 5.11, N 13.41.

6.6 Experimental for Compounds in Chapter 5

5,5'-Di(pyren-1-yl)-2,2'-bipyridine (**84**)



Pyren-2-ylboronic acid (1.00 g, 4.06 mmol), 5,5'-dibromo-2,2'-bipyridine (**32**) (593 mg, 1.89 mmol) and Na_2CO_3 (801 mg, 7.56 mmol) were dissolved in toluene (200 mL) and water (50 mL). The biphasic reaction mixture was degassed with N_2 (30 min) prior to the addition of $[\text{Pd}(\text{PPh}_3)_4]$ (219 mg, 189 μmol). The reaction mixture was stirred at reflux for 3 d under rigorous exclusion of light. An insoluble solid formed which was collected on a frit, washed with water (50 mL) and Et_2O (50 mL) yielding title compound **84** (1.05 g, 1.89 mmol, quant.).

^1H NMR (500 MHz, $\text{CD}_2\text{Cl}_2/\text{TFA}$ (1:1)) δ/ppm = 9.43 (d, J = 1.8 Hz, 2H, H^{A6}), 9.15 (dd, J = 2.0, 8.2 Hz, 2H, H^{A4}), 8.91 (d, J = 8.3 Hz, 2H, H^{A3}), 8.46 (d, J = 7.9 Hz, 2H, H^{P}), 8.39 (mc, 4H, $\text{H}^{2\text{xP}}$), 8.36 – 8.29 (m, 4H, $\text{H}^{2\text{xP}}$), 8.26 – 8.13 (m, 8H, $\text{H}^{4\text{xP}}$).

^{13}C NMR (126 MHz, $\text{CD}_2\text{Cl}_2/\text{TFA}$ (1:1)) δ/ppm = 149.48, 146.92, 145.58, 142.36, 134.77, 132.73, 132.05, 131.63, 130.96, 129.93, 128.65, 128.33, 128.26, 128.20, 128.17, 127.94, 127.59, 126.69, 126.31, 125.64, 122.79.

MS (ED): m/z = 556.2 [M^+] (calc. 556.2), 278.1 [M^{2+}] (calc. 278.1).

UV-Vis (CH_2Cl_2 , $\lambda_{\text{max}}(\text{nm})$ [$\epsilon/(\text{cm}^{-1} \text{M}^{-1})$]) = 243 [93050], 280 [55100], 357 [55500].

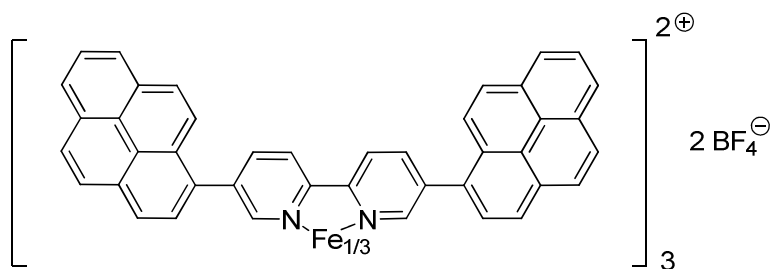
Emission (CH_2Cl_2 , $\lambda_{\text{max}}(\text{nm})$, $\lambda_{\text{exc}} = 355 \text{ nm}$) = 476.

84H⁺:

UV-Vis ($\text{CH}_2\text{Cl}_2/\text{TFA}$ (1%), $\lambda_{\text{max}}(\text{nm})$ [$\epsilon/(\text{cm}^{-1} \text{M}^{-1})$]) = 276 [43300], 341 [46100], 432 [14500].

Emission ($\text{CH}_2\text{Cl}_2/\text{TFA}$ (1%), $\lambda_{\text{max}}(\text{nm})$, $\lambda_{\text{exc}} = 355 \text{ nm}$) = 609.

Anal. calc. for $\text{C}_{42}\text{H}_{24}\text{N}_2 \cdot 1.25\text{H}_2\text{O}$ C 87.10, H 4.61, N 4.84; found C 87.08, H 4.38, N 4.76.

[Fe(**84**)₃](BF₄)₂ (**85**)

5,5'-Di(pyren-1-yl)-2,2'-bipyridine (**84**) (70.7 mg, 127 μmol) and iron(II) tetrafluoroborate hexahydrate (42.8 mg, 127 μmol) were suspended in MeCN (10 mL) and stirred in a microwave reactor (110 $^{\circ}\text{C}$, 30 min). The solution was reduced to 2 mL and the compound was precipitated with H₂O, filtered and washed with H₂O (30 mL) and ether (30 mL). The resulting red iron(II) complex (50.9 mg, 26.7 μmol , 21%) is poorly soluble in MeCN and DMSO and unstable in DMSO (decolouration after 20 h).

¹H NMR (400 MHz, DMSO-*d*₆) δ/ppm = 9.03 (d, J = 7.2 Hz, 6H), 8.37 (dd, J = 1.7, 8.1 Hz, 6H), 8.27 (d, J = 5.3 Hz, 6H), 8.20 (d, J = 9.3 Hz, 6H), 8.10 (d, J = 9.1 Hz, 6H), 8.04 (s_b, 6H), 8.00 – 7.88 (m, 12H), 7.62 (s, 6H), 7.06 (s_b, 6H), 6.06 (s_b, 6H), 5.49 (s_b, 6H).

¹⁹F NMR (376 MHz, CD₃CN) δ/ppm = -152.30 (s).

MS (EI): m/z = 863.1 [M-2BF₄]²⁺ (calc. 862.8).

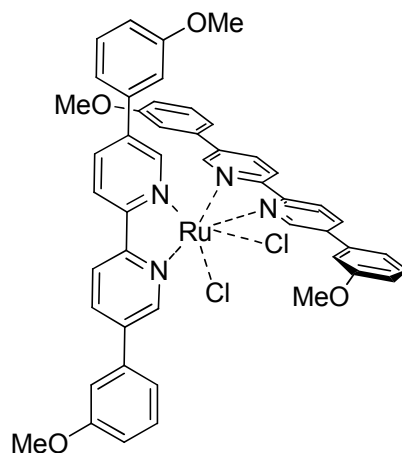
UV-Vis (MeCN, $\lambda_{\text{max}}(\text{nm})$ [ϵ' (cm⁻¹ M⁻¹)] = 240 [279 000], 276 [160 000], 313 [128 800], 322 [130 000], 544 [8 140].

Emission (MeCN, $\lambda_{\text{max}}(\text{nm})$, λ_{exc} = 355 nm) = 479.

IR (ATR): $\tilde{\nu}/\text{cm}^{-1}$ = 3043w, 2922m, 2851w, 1593w, 1583w, 1470m, 1377w, 1238w, 1049s, 1034s, 841s, 762m, 721m, 683m.

Anal. calc. for C₁₂₆H₈₀B₂F₈FeN₆ · 3 H₂O C 77.47, H 4.02, N 4.30; found C 77.56, H 4.49, N 3.66.

cis-[Ru(**34**)₂Cl₂] (**89**)



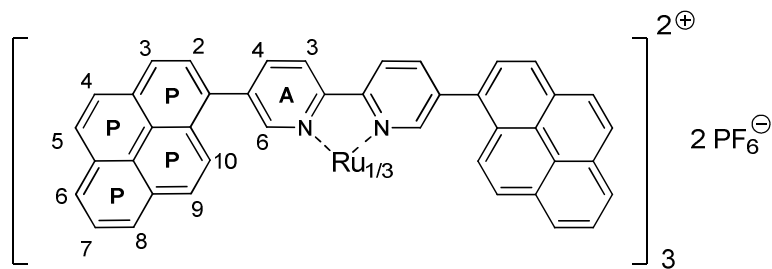
89

Commercial ruthenium trichloride trihydrate (267 mg, 1.02 mmol) and 5,5'-bis(3-methoxyphenyl)-2,2'-bipyridine (**34**) (760 mg, 2.06 mmol) were heated to reflux in DMF (100 mL) for 4 h. The reaction mixture was reduced to 5 mL, cooled to room temperature, treated with acetone (100 mL) and kept at 4 °C over night. The precipitate was collected by suction filtration and washed with water (40 mL). The crude product was suspended in 500 mL of water–ethanol (1:1) and heated to reflux for 1 h, filtered from insoluble solid and treated carefully with 40 g of lithium chloride. Ethanol was removed *in vacuo* and the resulting water solution was cooled in an ice bath. Dark crystals formed. They were ground and dried *in vacuo* for 24 h. The dark powder (518 mg, 570 μmol, 44%) was spectroscopically pure.

¹H NMR (400 MHz, DMSO-*d*₆) δ/ppm = 10.44 (s, 1H), 8.80 (s, 1H), 8.62 (s, 1H), 8.49 (s, 1H), 8.07 (s, 1H), 7.80 (s, 1H), 7.56 (s, 1H), 7.44 (s, 2H), 7.28 (s, 1H), 7.14 (s, 1H), 6.93 (s, 2H), 6.84 (s, 1H), 3.88 (s, 3H), 3.62 (s, 3H).

MS (FAB): *m/z* = 908.1 [M] (calc. 908.1), 873.3 [M- Cl] (calc. 873.2), 838.2 [M- 2Cl] (calc. 838.2).

Anal. calc. for C₄₈H₄₀Cl₂N₄Ru · 3.5 H₂O C 59.32, H 4.87, N 5.76; found C 59.33, H 4.52, N 5.68.

[Ru(84)₃](PF₆)₂ (86)

5,5'-Di(pyren-1-yl)-2,2'-bipyridine (**84**) (127 mg, 228 μmol) and $[\text{Ru}(\text{DMSO})_4\text{Cl}_2]$ (37.1 mg, 76.6 μmol) were suspended in 10 mL of ethylene glycol. The reaction mixture was stirred for 2h at 250 $^\circ\text{C}$ in a microwave reactor. The orange mixture was added to 200 mL of an aqueous NH_4PF_6 solution (1.00 mmol). An orange precipitate formed which was filtered and washed with water (50 mL) and ether (50 mL) yielding the ruthenium complex **86** (131 mg, 63.6 μmol , 83%) as an orange powder.

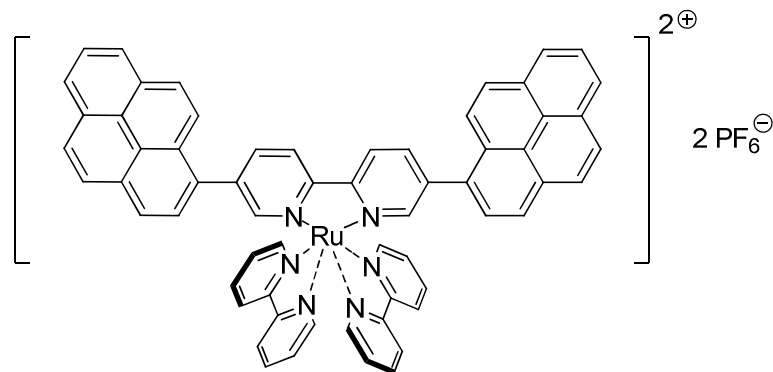
^1H NMR (500 MHz, $\text{DMSO}-d_6$, 355 K) δ/ppm = 9.35 (d, J = 8.3 Hz, 6H, $\text{H}^{\text{A}3}$), 8.51 (d, J = 8.1 Hz, 6H, $\text{H}^{\text{A}4}$), 8.38 (s, 6H, $\text{H}^{\text{A}6}$), 8.31 (d, J = 7.6 Hz, 6H, $\text{H}^{\text{P}6}$), 8.24 (d, J = 8.9 Hz, 6H, $\text{H}^{\text{P}5}$), 8.14 (dd, J = 4.5, 8.1 Hz, 12H, $\text{H}^{\text{P}3+\text{P}4}$), 7.99 (t, J = 7.6 Hz, 6H, $\text{H}^{\text{P}7}$), 7.80 (d, J = 7.8 Hz, 6H, $\text{H}^{\text{P}2}$), 7.66 (d, J = 7.1 Hz, 6H, $\text{H}^{\text{P}8}$), 7.22 (d, J = 9.1 Hz, 6H, $\text{H}^{\text{P}10}$), 6.88 (d, J = 8.5 Hz, 6H, $\text{H}^{\text{P}9}$).

MS (ESI): m/z = 885.7 $[\text{M} - 2 \text{PF}_6]^{2+}$ (calc. 885.7).

Emission (MeCN, $\lambda_{\text{max}}(\text{nm})$) = 476.

UV-Vis (MeCN, $\lambda_{\text{max}}(\text{nm})$ [ϵ' ($\text{cm}^{-1} \text{M}^{-1}$)] = 240 [129000], 276 [76100], 297 [69300], 323 [66600], 379 [43300], 401 [43200].

Anal. calc. for $\text{C}_{126}\text{H}_{72}\text{F}_{12}\text{N}_6\text{P}_2\text{Ru}\cdot\text{H}_2\text{O}$ C 72.79, H 3.59, N 4.04; found C 72.70, H 3.66, N 3.87.

[Ru(84)(bpy)₂](PF₆)₂ (87)

Complex **87** was synthesised according to procedure **67** with 5,5'-di(pyren-1-yl)-2,2'-bipyridine (**84**) (94.2 mg, 169 μmol) and *cis*-[Ru(bpy)₂Cl₂] (82.0 mg, 169 μmol). Column chromatography (Al₂O₃, CH₂Cl₂ : MeOH (20:1)) yielded title compound **87** (201 mg, 160 μmol , 94%) as an orange solid.

¹H NMR (500 MHz, CD₃CN) δ/ppm = 8.82 (d, *J* = 8.3 Hz, 2H), 8.66 (d, *J* = 8.1 Hz, 2H), 8.50 – 8.46 (m, 2H), 8.43 (dd, *J* = 8.3, 1.8 Hz, 2H), 8.38 – 8.33 (m, 4H), 8.32 (d, *J* = 8.0 Hz, 2H), 8.25 – 8.19 (m, 4H), 8.19 – 8.12 (m, 8H), 7.98 (d, *J* = 7.9 Hz, 2H), 7.96 (d, *J* = 1.6 Hz, 2H), 7.81 – 7.75 (m, 4H), 7.65 (d, *J* = 9.0 Hz, 2H), 7.63 – 7.57 (m, 2H), 7.20 (t, *J* = 6.6 Hz, 2H).

¹³C NMR (126 MHz, CD₃CN) δ/ppm = 158.07, 158.01, 156.55, 153.41, 153.27, 152.97, 141.25, 140.30, 139.18, 138.72, 132.92, 132.36, 131.68, 131.62, 129.76, 129.64, 129.21, 128.96, 128.90, 128.54, 128.31, 127.87, 127.26, 126.79, 126.20, 125.58, 125.49, 125.38, 125.30, 125.19, 124.03.

¹⁹F NMR (376 MHz, CD₃CN) δ/ppm = -74.09 (d, *J* = 706.4 Hz).

MS (ESI): *m/z* = 485.2 [M - 2 PF₆]²⁺ (calc. 485.1).

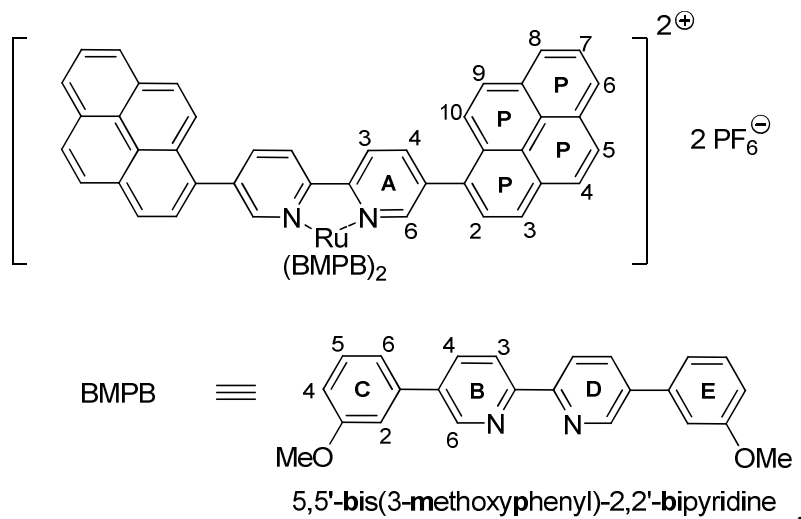
UV-Vis (MeCN, $\lambda_{\text{max}}(\text{nm})$ [ϵ (cm⁻¹ M⁻¹)] = 241 [134000], 288 [117000], 405 [47730].

Emission (MeCN, $\lambda_{\text{max}}(\text{nm})$, $\lambda_{\text{exc}} = 355 \text{ nm}$) = 495, 645.

IR (ATR): $\tilde{\nu}/\text{cm}^{-1}$ = 3043w, 1601w, 1464w, 1447m, 1240m, 1161w, 831s, 762m, 729w.

Anal. calc. for C₆₂H₄₀F₁₂N₆P₂Ru·H₂O C 58.27, H 3.31, N 6.58; found C 58.26, H 3.43, N 6.52.

[Ru(**84**)(**34**)₂](PF₆)₂ (**88**)



Complex **88** was synthesised according to procedure **67** with 5,5'-di(pyren-1-yl)-2,2'-bipyridine (**84**) (64.1 mg, 115 μmol) and $[\text{Ru}(\text{bmpb})_2\text{Cl}_2]$ (**89**) (108 mg, 119 μmol). Column chromatography (SiO_2 , $\text{CH}_2\text{Cl}_2 \rightarrow \text{CH}_2\text{Cl}_2$: MeOH (50:1)) yielded title compound **88** (120 mg, 71.2 μmol , 62%) as an orange solid.

^1H NMR (500 MHz, CD_3CN) $\delta/\text{ppm} = 8.88$ (d, $J = 8.4$ Hz, 2H, $\text{H}^{\text{A}3}$), 8.75 (d, $J = 8.5$ Hz, 2H, $\text{H}^{\text{B}3}$), 8.57 (d, $J = 8.5$ Hz, 2H, $\text{H}^{\text{D}3}$), 8.50 (dd, $J = 8.5$ Hz, 1.7, 2H, $\text{H}^{\text{B}4}$), 8.47 (dd, $J = 8.3$ Hz, 1.7, 2H, $\text{H}^{\text{A}4}$), 8.32 – 8.23 (m, 10H, $\text{H}^{\text{B}6+\text{A}6+3\text{xP}}$), 8.18 (d, $J = 9.0$ Hz, 2H, H^{P}), 8.14 – 8.09 (m, 4H, $\text{H}^{2\text{xP}}$), 8.06 (dd, $J = 8.5$, 1.8 Hz, 2H, $\text{H}^{\text{D}4}$), 7.97 (d, $J = 8.3$ Hz, 4H, $\text{H}^{\text{D}6+\text{P}}$), 7.90 (d, $J = 9.2$ Hz, 2H, H^{P}), 7.70 (d, $J = 9.2$ Hz, 2H, H^{P}), 7.46 (t, $J = 8.0$ Hz, 2H, $\text{H}^{\text{C}5}$), 7.21 – 7.18 (m, 2H, $\text{H}^{\text{C}6}$), 7.17 (t, $J = 6.7$ Hz, 2H, $\text{H}^{\text{E}5}$), 7.13 (s, 2H, $\text{H}^{\text{C}2}$), 7.06 (dd, $J = 8.3$, 2.3 Hz, 2H, $\text{H}^{\text{C}4}$), 6.86 (dd, $J = 8.3$, 2.3 Hz, 2H, $\text{H}^{\text{E}6}$), 6.76 (d, $J = 7.8$ Hz, 2H, $\text{H}^{\text{E}4}$), 6.65 (s, 2H, $\text{H}^{\text{E}2}$), 3.80 (s, 6H, $\text{H}^{\text{C-OMe}}$), 3.55 (s, 6H, $\text{H}^{\text{E-OMe}}$).

^{13}C NMR (126 MHz, CD_3CN) $\delta/\text{ppm} = 161.51$, 161.10, 156.84, 156.79, 156.47, 154.14, 150.95, 150.43, 141.22, 140.73, 140.38, 140.22, 137.29, 137.09, 136.76, 136.55, 132.89, 132.30, 131.82, 131.71, 131.54, 131.44, 129.72, 129.60, 129.26, 128.84, 128.26, 127.85, 127.27, 126.81, 126.18, 125.71, 125.57, 125.52 (2x), 125.15, 123.91, 120.55, 120.11, 116.42, 116.20, 113.58, 113.08, 56.36, 55.96.

^{19}F NMR (376 MHz, CD_3CN) $\delta/\text{ppm} = -74.09$ (d, $J = 706.4$ Hz).

MS (ESI): $m/z = 1539.5$ $[\text{M} - \text{PF}_6]^+$ (calc. 1539.4) 697.3 $[\text{M} - 2 \text{PF}_6]^{2+}$ (calc. 697.2).

UV-Vis (MeCN, $\lambda_{\text{max}}(\text{nm})$ [ϵ ($\text{cm}^{-1} \text{M}^{-1}$)] = 241 [134700], 275 [91900], 321 [139100], 403 [40200, shoulder].

Emission (MeCN, $\lambda_{\text{max}}(\text{nm})$, $\lambda_{\text{exc}} = 355$ nm) = 464, 498, 638.

IR (ATR): $\tilde{\nu}/\text{cm}^{-1} = 3047\text{w}$, 2835w, 1597m, 1580m, 1466m, 1369m, 1300m, 1219m, 1175m, 1022m, 825s, 777m, 685m.

Anal. calc. for $\text{C}_{90}\text{H}_{64}\text{F}_{12}\text{N}_6\text{O}_4\text{P}_2\text{Ru}\cdot\text{H}_2\text{O}$ C 63.49, H 3.91, N 6.94; found C 63.33, H 3.91, N 4.52.

7 Appendix

7.1 Crystal Structures from Chapter 2

[Fe(34)₃]²⁺ (45²⁺)

	Crystal Data
Formula	C ₇₂ H ₆₀ FeN ₆ O ₆ , 3(C ₂ H ₄ Cl ₂), 2(F ₆ P)
Formula Weight	1747.95
Crystal System	Orthorhombic
Space group	Pbca ba-c (No. 61)
a, b, c [Å]	22.5632(1) 25.4589(2) 28.8665(2)
alpha, beta, gamma [deg]	
V [Å ³]	16581.91(19)
Z	8
D(calc) [g/cm ³]	1.400
Mu(MoKa) [mm ⁻¹]	0.495
F(000)	7168
Crystal Size [mm]	0.21 x 0.28 x 0.34
	Data Collection
Temperature (K)	173
Radiation [Å]	MoKa 0.71073
Theta Min-Max [deg]	1.4, 27.9
Dataset	-29: 29 ; -33: 29 ; -37: 36
Tot., Uniq. Data, R(int)	113362, 19770, 0.049
Observed data [I > 2.0 sigma(I)]	11198
	Refinement
Nref, Npar	11198, 1081
R, ωR2, S	0.0704, 0.0960, 1.05
Max. and Av. Shift/Error	0.03, 0.00
Min. and Max. Resd. Dens. [e/Å ³]	-0.86, 1.53

[Ru(31)]²⁺ (59²⁺)

	Crystal Data
Formula	C ₁₁₂ F ₁₂ N ₁₁ O ₁₈ P ₂ Ru
Formula Weight	2178.29
Crystal System	Monoclinic
Space group	P2 ₁ /n (No. 14)
a, b, c [Å]	22.8533(6) 17.8126(3) 28.7516(7)
alpha, beta, gamma [deg]	90 99.5680(8) 90
V [Å ³]	11541.3(5)
Z	4
D(calc) [g/cm ³]	1.254
Mu(MoKa) [mm ⁻¹]	0.248
F(000)	4300
Crystal Size [mm]	0.12 x 0.25 x 0.44
	Data Collection
Temperature (K)	173
Radiation [Å]	MoKa 0.71073
Theta Min-Max [deg]	1.7, 26.0
Dataset	-28: 27 ; -14: 21 ; -32: 35
Tot., Uniq. Data, R(int)	47722, 21737, 0.040
Observed data [I > 2.0 sigma(I)]	11003
	Refinement
Nref, Npar	11003, 625
R, ωR2, S	0.3143, 0.4047, 3.53
Max. and Av. Shift/Error	1.65, 0.00
Min. and Max. Resd. Dens. [e/Å ³]	-3.86, 9.61

[Ru(34)₃]²⁺ (49²⁺)

Formula	C ₇₂ H ₆₀ N ₆ O ₆ Ru, 2(F ₆ P), 3(C ₂ H ₄ Cl ₂)
Formula Weight	1793.18
Crystal System	Trigonal
Space group	P-3 (No.147)
a, b, c [Å]	14.5348(1) 14.5348(1) 21.8419(2)
alpha, beta, gamma [deg]	90 90 120
V [Å ³]	3996.13(5)
Z	2
D(calc) [g/cm ³]	1.490
Mu(MoKa) [mm ⁻¹]	0.521
F(000)	1828
Crystal Size [mm]	0.10 x 0.22 x 0.27
Temperature (K)	173
Radiation [Å]	MoKa 0.71073
Theta Min-Max [deg]	1.6, 27.9
Dataset	-18: 16 ; -19: 19 ; -28: 28
Tot., Uniq. Data, R(int)	31117, 6383, 0.050
Observed data [I > 2.0 sigma(I)]	3852
Nref, Npar	3852, 358
R, ωR2, S	0.0525, 0.0792, 1.03
Max. and Av. Shift/Error	0.03, 0.00
Min. and Max. Resd. Dens. [e/Å ³]	-0.72, 1.32

34H⁺

Formula	C ₂₄ H ₂₀ N ₂ O ₂ , F ₆ P, H ₂ O
Formula Weight	531.41
Crystal System	Monoclinic
Space group	P2 ₁ /a (No. 14)
a, b, c [Å]	13.0892(2) 10.5206(2) 18.0328(3)
alpha, beta, gamma [deg]	90 109.5695(8) 90
V [Å ³]	2339.79(7)
Z	4
D(calc) [g/cm ³]	1.509
Mu(MoKa) [mm ⁻¹]	0.196
F(000)	1092
Crystal Size [mm]	0.08 x 0.13 x 0.25
Temperature (K)	173
Radiation [Å]	MoKa 0.71073
Theta Min-Max [deg]	2.3, 27.8
Dataset	-17: 17 ; -13: 13 ; -23: 23
Tot., Uniq. Data, R(int)	20955, 5546, 0.045
Observed data [I > 2.0 sigma(I)]	3605
Nref, Npar	3605, 325
R, ωR2, S	0.0562, 0.0983, 1.13
Max. and Av. Shift/Error	0.00, 0.00
Min. and Max. Resd. Dens. [e/Å ³]	-0.28, 1.56

7.2 Crystal Structures from Chapter 3

[Ru(34)(bpy)₂]²⁺ (67²⁺)

Formula	C ₄₄ H ₃₆ N ₆ O ₂ Ru, 2(F ₆ P), C ₂ H ₃ N
Formula Weight	1112.85
Crystal System	Triclinic
Space group	P-1 (No. 2)
a, b, c [Å]	12.449(3) 13.757(3) 14.219(3)
alpha, beta, gamma [deg]	76.49(3) 74.54(3) 83.29(3)
V [Å ³]	2278.2(10)
Z	2
D(calc) [g/cm ³]	1.622
Mu(MoKa) [mm ⁻¹]	0.512
F(000)	1124
Crystal Size [mm]	0.07 x 0.25 x 0.30
Temperature (K)	446
Radiation [Å]	MoKa 0.71073
Theta Min-Max [deg]	2.5, 25.0
Dataset	-14: 14 ; -16: 16 ; -16: 16
Tot., Uniq. Data, R(int)	33505, 8048, 0.126
Observed data [I > 2.0 sigma(I)]	7300
Nref, Npar	8048, 669
R, ωR2, S	0.0572, 0.1493, 1.10
Max. and Av. Shift/Error	0.00, 0.00
Min. and Max. Resd. Dens. [e/Å ³]	-1.86, 2.03

[Ru(N[^]N)(bpy)₂]²⁺ (64²⁺)

Formula	C ₅₈ H ₆₂ N ₆ O ₈ Ru, C ₅₈ H ₆₂ F ₁₂ N ₆ NaO ₈ P ₂ Ru, 3(F ₆ P)
Formula Weight	1446.13
Crystal System	Triclinic
Space group	P-1 (No. 2)
a, b, c [Å]	15.154(3) 17.614(4) 26.892(5)
alpha, beta, gamma [deg]	86.54(3) 82.28(3) 84.31(3)
V [Å ³]	7070(3)
Z	4
D(calc) [g/cm ³]	1.359
Mu(MoKa) [mm ⁻¹]	0.372
F(000)	2952
Crystal Size [mm]	0.16 x 0.28 x 0.45
Temperature (K)	173
Radiation [Å]	MoKa 0.71073
Theta Min-Max [deg]	1.4, 25.0
Dataset	-18: 18 ; -20: 20 ; -32: 32
Tot., Uniq. Data, R(int)	89634, 24992, 0.083
Observed data [I > 2.0 sigma(I)]	21321
Nref, Npar	24992, 1741
R, ωR2, S	0.0658, 0.1755, 1.05
Max. and Av. Shift/Error	0.04, 0.00
Min. and Max. Resd. Dens. [e/Å ³]	-0.90, 0.87



Formula	C ₁₀₀ H ₉₂ N ₁₂ O ₈ Ru ₂ · C ₂ H ₄ Cl ₂ · 2.5(C ₄ H ₈ O ₂)
Formula Weight	2691.12
Crystal System	Triclinic
Space group	P-1 (No. 2)
a, b, c [Å]	14.1156(13) 20.075(2) 23.409(2)
alpha, beta, gamma [deg]	77.354(5) 73.193(5) 85.179(5)
V [Å ³]	6194.5(10)
Z	2
D(calc) [g/cm ³]	1.443
Mu(MoKa) [mm ⁻¹]	0.437
F(000)	2748
Crystal Size [mm]	0.05 x 0.13 x 0.29
Temperature (K)	123
Radiation [Å]	MoKa 0.71073
Theta Min-Max [deg]	1.9, 33.7
Dataset	-21: 21 ; -31: 31 ; -35: 36
Tot., Uniq. Data, R(int)	386895, 48568, 0.050
Observed data [I > 2.0 sigma(I)]	18510
Nref, Npar	18510, 1825
R, ωR2, S	0.0679, 0.1851, 1.04
Max. and Av. Shift/Error	0.03, 0.00
Min. and Max. Resd. Dens. [e/Å ³]	-0.84, 1.70

7.3 Crystal Structures from Chapter 4

[Pd(34)₂]²⁺ (74²⁺)

Formula	C ₄₈ H ₄₀ N ₄ O ₄ Pd, C ₂₄ H ₂₀ N ₂ O ₂ , 2(BF ₄)
Formula Weight	1385.31
Crystal System	Triclinic
Space group	P-1 (No. 2)
a, b, c [Å]	8.7623(2) 11.1136(2) 16.3282(3)
alpha, beta, gamma [deg]	75.8896(11) 77.9053(12) 89.1174(12)
V [Å ³]	1506.78(5)
Z	1
D(calc) [g/cm ³]	1.527
Mu(MoKa) [mm ⁻¹]	0.396
F(000)	710
Crystal Size [mm]	0.05 x 0.25 x 0.34
Temperature (K)	173
Radiation [Å]	MoKa 0.71073
Theta Min-Max [deg]	1.9, 27.8
Dataset	-11: 11 ; -14: 14 ; -21: 21
Tot., Uniq. Data, R(int)	13865, 7175, 0.023
Observed data [I > 2.0 sigma(I)]	5977
Nref, Npar	5977, 430
R, ωR2, S	0.0274, 0.0351, 1.11
Max. and Av. Shift/Error	0.00, 0.00
Min. and Max. Resd. Dens. [e/Å ³]	-0.65, 0.43

Ligand 78

Formula	C ₂₆ H ₂₄ N ₂ O ₂
Formula Weight	396.49
Crystal System	Monoclinic
Space group	P2 ₁ /c (No. 14)
a, b, c [Å]	10.0276(2) 8.1544(1) 12.9843(2)
alpha, beta, gamma [deg]	90 111.960(1) 90
V [Å ³]	984.68(3)
Z	2
D(calc) [g/cm ³]	1.337
Mu(MoKa) [mm ⁻¹]	0.085
F(000)	420
Crystal Size [mm]	0.12 x 0.21 x 0.41
Temperature (K)	123
Radiation [Å]	MoKa 0.71073
Theta Min-Max [deg]	2.2, 35.5
Dataset	-16: 16 ; -12: 11 ; -21: 20
Tot., Uniq. Data, R(int)	25410, 4279, 0.036
Observed data [I > 2.0 sigma(I)]	2689
Nref, Npar	2689, 136
R, ωR2, S	0.0512, 0.0608, 1.07
Max. and Av. Shift/Error	0.00, 0.00
Min. and Max. Resd. Dens. [e/Å ³]	-0.41, 0.50

[Cu(77)₂]⁺ (80⁺)

Formula	C ₅₀ H ₄₄ CuN ₄ O ₄ , F ₆ P, 0.1(C ₂ H ₄ Cl ₂), 0.15(CH ₂ Cl ₂)
Formula Weight	996.07
Crystal System	Triclinic
Space group	P-1 (No. 2)
a, b, c [Å]	10.3190(8) 15.0783(14) 16.6032(11)
alpha, beta, gamma [deg]	90.627(7) 98.169(6) 106.230(7)
V [Å ³]	2451.7(4)
Z	2
D(calc) [g/cm ³]	1.349
Mu(MoKa) [mm ⁻¹]	0.575
F(000)	1027
Crystal Size [mm]	0.07 x 0.13 x 0.25
Temperature (K)	173
Radiation [Å]	MoKa 0.71073
Theta Min-Max [deg]	2.8, 35.1
Dataset	-15: 16 ; -24: 24 ; -26: 26
Tot., Uniq. Data, R(int)	74714, 21403, 0.140
Observed data [I > 2.0 sigma(I)]	7665
Nref, Npar	7665, 757
R, ωR2, S	0.0958, 0.1300, 1.03
Max. and Av. Shift/Error	0.03, 0.00
Min. and Max. Resd. Dens. [e/Å ³]	-0.74, 0.79

Compound 73

Formula	C ₃₂ H ₂₃ N ₅ O
Formula Weight	493.57
Crystal System	Monoclinic
Space group	P2 ₁ /c (No. 14)
a, b, c [Å]	6.4613(2) 18.9013(5) 19.9753(6)
alpha, beta, gamma [deg]	90 96.853(2) 90
V [Å ³]	2422.09(12)
Z	4
D(calc) [g/cm ³]	1.354
Mu(MoKa) [mm ⁻¹]	0.085
F(000)	1032
Crystal Size [mm]	0.03 x 0.05 x 0.23
Temperature (K)	173
Radiation [Å]	MoKa 0.71073
Theta Min-Max [deg]	2.2, 31.0
Dataset	-9: 9 ; -27: 27 ; -28: 28
Tot., Uniq. Data, R(int)	93608, 7731, 0.050
Observed data [I > 2.0 sigma(I)]	4127
Nref, Npar	4127, 343
R, ωR2, S	0.0377, 0.0595, 1.13
Max. and Av. Shift/Error	
Min. and Max. Resd. Dens. [e/Å ³]	-0.17, 0.37

7.4 Crystal Structures from Chapter 5

Compound **84**

Formula	C ₄₂ H ₂₄ N ₂
Formula Weight	556.67
Crystal System	Monoclinic
Space group	P21/c (No. 14)
a, b, c [Å]	7.378(3) 6.923(3) 26.070(12)
alpha, beta, gamma [deg]	90 94.21(3) 90
V [Å ³]	1328.0(10)
Z	2
D(calc) [g/cm ³]	1.392
Mu(MoKa) [mm ⁻¹]	0.081
F(000)	580
Crystal Size [mm]	0.01 x 0.10 x 0.33
Temperature (K)	
Radiation [Å]	MoKa 0.71073
Theta Min-Max [deg]	3.0, 28.6
Dataset	-9: 9; -9: 9; -34: 34
Tot., Uniq. Data, R(int)	13452, 3235, 0.149
Observed data [I > 2.0 sigma(I)]	1624
Nref, Npar	1624, 200
R, ωR2, S	0.1048, 0.1196, 1.10
Max. and Av. Shift/Error	0.00, 0.00
Min. and Max. Resd. Dens. [e/Å ³]	-0.50, 0.45

[Ru(**84**)₃](PF₆)₂ (**86**)

Formula	C ₁₂₆ H ₇₂ N ₆ Ru, 2(F ₆ P), C ₄ O ₂ , 2(O _{0.90}), 0.2(O)
Formula Weight	2172.95
Crystal System	Monoclinic
Space group	C2/c (No. 15)
a, b, c [Å]	31.036(6) 14.554(3) 30.004(6)
alpha, beta, gamma [deg]	90 117.56(3) 90
V [Å ³]	12015(5)
Z	4
D(calc) [g/cm ³]	1.201
Mu(MoKa) [mm ⁻¹]	0.229
F(000)	4432
Crystal Size [mm]	0.06 x 0.10 x 0.35
Temperature (K)	
Radiation [Å]	MoKa 0.71073
Theta Min-Max [deg]	2.4, 27.5
Dataset	-40: 40; -18: 18; -38: 38
Tot., Uniq. Data, R(int)	153371, 13745, 0.102
Observed data [I > 2.0 sigma(I)]	12531
Nref, Npar	13745, 834
R, ωR2, S	0.0749, 0.2272, 1.19
Max. and Av. Shift/Error	0.03, 0.00
Min. and Max. Resd. Dens. [e/Å ³]	-0.60, 0.79

[Ru(84)(bpy)₂](PF₆)₂ (87)

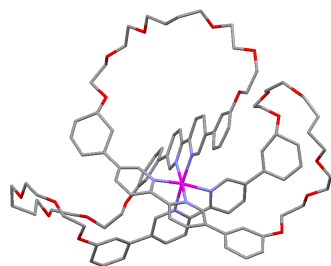
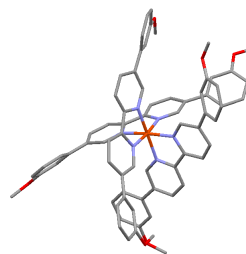
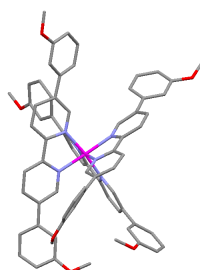
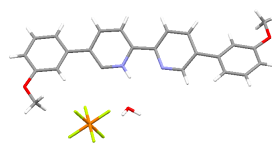
Formula	C ₆₂ H ₄₀ N ₆ Ru, C ₄ H ₈ O ₂ , 3(C ₃ H ₇ NO), 2(F ₆ P)
Formula Weight	1567.42
Crystal System	Triclinic
Space group	P-1 (No. 2)
a, b, c [Å]	12.3207(4) 15.9054(5) 19.8308(5)
alpha, beta, gamma [deg]	113.507(1) 96.569(2) 92.992(2)
V [Å ³]	3519.78(19)
Z	2
D(calc) [g/cm ³]	1.479
Mu(MoKa) [mm ⁻¹]	0.359
F(000)	1608
Crystal Size [mm]	0.04 x 0.09 x 0.39
Temperature (K)	
Radiation [Å]	MoKa 0.71073
Theta Min-Max [deg]	2.1, 34.1
Dataset	-19: 19 ; -24: 25 ; -30: 29
Tot., Uniq. Data, R(int)	171563, 27495, 0.041
Observed data [I > 2.0 sigma(I)]	17707
Nref, Npar	17707, 937
R, ωR2, S	0.0399, 0.0516, 1.07
Max. and Av. Shift/Error	0.00, 0.00
Min. and Max. Resd. Dens. [e/Å ³]	-0.59, 0.98

[Ru(84)(34)₂](PF₆)₂ (88)

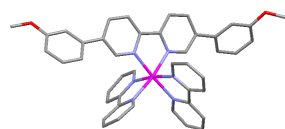
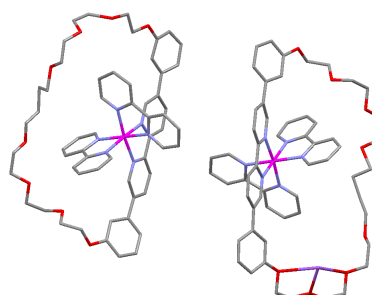
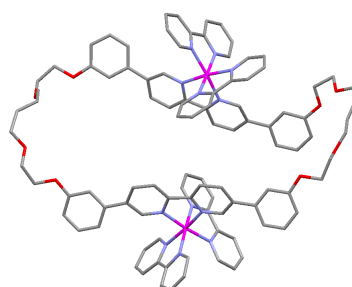
Formula	2(C ₉₀ H ₆₄ N ₆ O ₄ Ru), 2(C ₄ H ₁₀ O), 4(F ₆ P), 10(C ₂ H ₃ N), C ₂ H ₃ N
Formula Weight	3968.88
Crystal System	Monoclinic
Space group	P21/n (No. 14)
a, b, c [Å]	16.7663(9) 30.4322(17) 18.6382(11)
alpha, beta, gamma [deg]	90 97.028(3) 90
V [Å ³]	9438.4(9)
Z	2
D(calc) [g/cm ³]	1.396
Mu(MoKa) [mm ⁻¹]	0.285
F(000)	4092
Crystal Size [mm]	0.25 x 0.32 x 0.40
Temperature (K)	
Radiation [Å]	MoKa 0.71073
Theta Min-Max [deg]	1.7, 30.2
Dataset	-23: 23 ; -42: 42 ; -26: 26
Tot., Uniq. Data, R(int)	235317, 27749, 0.000
Observed data [I > 2.0 sigma(I)]	22984
Nref, Npar	19573, 1315
R, ωR2, S	0.0627, 0.0853, 1.02
Max. and Av. Shift/Error	0.04, 0.00
Min. and Max. Resd. Dens. [e/Å ³]	-1.05, 1.78

7.5 Overview Crystal Structures

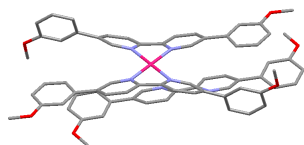
Chapter 2

 $[\text{Ru}(\mathbf{31})]^{2+}$ ($\mathbf{59}^{2+}$) $[\text{Fe}(\mathbf{34})_3]^{2+}$ ($\mathbf{45}^{2+}$) $[\text{Ru}(\mathbf{34})_3]^{2+}$ ($\mathbf{49}^{2+}$) $\mathbf{34H}^+$

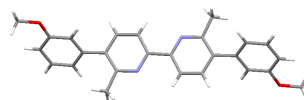
Chapter 3

 $[\text{Ru}(\mathbf{34})(\text{bpy})_2]^{2+}$ ($\mathbf{67}^{2+}$) $[\text{Ru}(\text{N}^{\wedge}\text{N})(\text{bpy})_2]^{2+}$ ($\mathbf{64}^{2+}$) $[\text{Ru}_2(\mathbf{55})(\text{bpy})_4]^{4+}$ ($\mathbf{52-F1}^{2+}$)

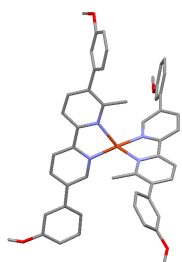
Chapter 4



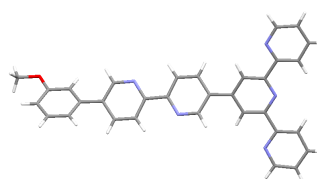
$[\text{Pd}(\mathbf{34})_2]^{2+}$ ($\mathbf{74}^{2+}$)



Ligand **78**

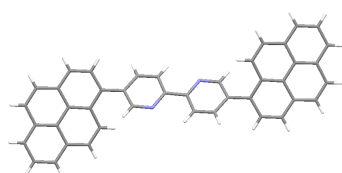


$[\text{Cu}(\mathbf{77})_2]^+$ ($\mathbf{80}^+$)

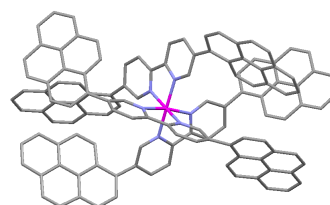


Compound **73**

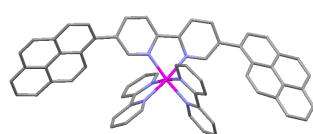
Chapter 5



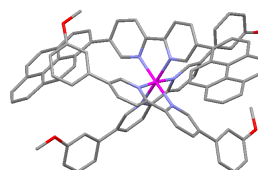
Compound **84**



$[\text{Ru}(\mathbf{84})_3](\text{PF}_6)_2$ ($\mathbf{86}$)



$[\text{Ru}(\mathbf{84})(\text{bpy})_2](\text{PF}_6)_2$ ($\mathbf{87}$)



$[\text{Ru}(\mathbf{84})(\mathbf{34})_2](\text{PF}_6)_2$ ($\mathbf{88}$)

8 References

- [1] M. Schliwa, *Molecular Motors*, Wiley-VCH, Weinheim, **2003**.
- [2] P. D. Boyer, *Nature* **1999**, *402*, 247.
- [3] K. Kinbara, T. Aida, *Chem. Rev.* **2005**, *105*, 1377.
- [4] H. L. Frisch, E. Wasserman, *J. Am. Chem. Soc.* **1961**, *83*, 3789.
- [5] E. Wasserman, *J. Am. Chem. Soc.* **1960**, *82*, 4433.
- [6] G. Schill, K. Murjahn, *Chem. Ber.-Recl.* **1971**, *104*, 3587.
- [7] G. Schill, H. Neubauer, *Annalen Der Chemie-Justus Liebig* **1971**, *750*, 76.
- [8] C. O. Dietrich-Buchecker, P. A. Marnot, J. P. Sauvage, J. P. Kintzinger, P. Maltese, *New J. Chem.* **1984**, *8*, 573.
- [9] C. O. Dietrich-Buchecker, J. P. Sauvage, J. P. Kintzinger, *Tetrahedron Lett.* **1983**, *24*, 5095.
- [10] C. O. Dietrich-Buchecker, J. P. Sauvage, J. M. Kern, *J. Am. Chem. Soc.* **1984**, *106*, 3043.
- [11] K. Y. Ng, A. R. Cowley, P. D. Beer, *Chem. Commun.* **2006**, 3676.
- [12] M. Fujita, F. Ibukuro, H. Hagihara, K. Ogura, *Nature* **1994**, 367, 720.
- [13] H. Ogino, *J. Am. Chem. Soc.* **1981**, *103*, 1303.
- [14] P. R. Ashton, M. C. T. Fyfe, M. V. Martinez-Diaz, S. Menzer, C. Schiavo, J. F. Stoddart, A. J. P. White, D. J. Williams, *Chem. Eur. J.* **1998**, *4*, 1523.
- [15] F. G. Gatti, D. A. Leigh, S. A. Nepogodiev, A. M. Z. Slawin, S. J. Teat, J. K. Y. Wong, *J. Am. Chem. Soc.* **2001**, *123*, 5983.
- [16] P. L. Anelli, P. R. Ashton, R. Ballardini, V. Balzani, M. Delgado, M. T. Gandolfi, T. T. Goodnow, A. E. Kaifer, D. Philp, M. Pietraszkiwicz, L. Prodi, M. V. Reddington, A. M. Z. Slawin, N. Spencer, J. F. Stoddart, C. Vicent, D. J. Williams, *J. Am. Chem. Soc.* **1992**, *114*, 193.
- [17] D. G. Hamilton, N. Feeder, L. Prodi, S. J. Teat, W. Clegg, J. K. M. Sanders, *J. Am. Chem. Soc.* **1998**, *120*, 1096.
- [18] K. Hiratani, J. Suga, Y. Nagawa, H. Houjou, H. Tokuhisa, M. Numata, K. Watanabe, *Tetrahedron Lett.* **2002**, *43*, 5747.
- [19] M. Asakawa, P. R. Ashton, S. Iqbal, J. F. Stoddart, N. D. Tinker, A. J. P. White, D. J. Williams, *Chem. Commun.* **1996**, 483.
- [20] P. R. Ashton, S. J. Langford, N. Spencer, J. F. Stoddart, A. J. P. White, D. J. Williams, *Chem. Commun.* **1996**, 1387.
- [21] C. A. Hunter, *J. Am. Chem. Soc.* **1992**, *114*, 5303.
- [22] F. Vögtle, T. Dunnwald, T. Schmidt, *Acc. Chem. Res.* **1996**, *29*, 451.
- [23] F. Vögtle, S. Meier, R. Hoss, *Angew. Chem. Int. Ed.* **1992**, *31*, 1619.
- [24] A. S. Lane, D. A. Leigh, A. Murphy, *J. Am. Chem. Soc.* **1997**, *119*, 11092.
- [25] A. Harada, J. Li, M. Kamachi, *Nature* **1992**, *356*, 325.
- [26] G. Wenz, M. B. Steinbrunn, K. Landfester, *Tetrahedron* **1997**, *53*, 15575.
- [27] C. G. Gong, H. W. Gibson, *J. Am. Chem. Soc.* **1997**, *119*, 5862.
- [28] A. Harriman, J. P. Sauvage, *Chem. Soc. Rev.* **1996**, *25*, 41.
- [29] J. D. Badjic, V. Balzani, A. Credi, S. Silvi, J. F. Stoddart, *Science* **2004**, *303*, 1845.
- [30] V. Balzani, A. Credi, M. Venturi, *Molecular Devices and Machines. A Journey into the Nanoworld*, Wiley-VCH, Weinheim, **2003**.
- [31] A. M. Brouwer, C. Frochot, F. G. Gatti, D. A. Leigh, L. Mottier, F. Paolucci, S. Roffia, G. W. H. Wurpel, *Science* **2001**, *291*, 2124.

- [32] W. R. Browne, B. L. Feringa, *Nat. Nanotechnol.* **2006**, *1*, 25.
- [33] E. R. Kay, D. A. Leigh, F. Zerbetto, *Angew. Chem. Int. Ed.* **2007**, *46*, 72.
- [34] I. Poleschak, J. M. Kern, J. P. Sauvage, *Chem. Commun.* **2004**, 474.
- [35] J. P. Sauvage, *Chem. Commun.* **2005**, 1507.
- [36] L. Raehm, J. M. Kern, J. P. Sauvage, *Chem. Eur. J.* **1999**, *5*, 3310.
- [37] J. P. Collin, F. Durolo, P. Mobian, J. P. Sauvage, *Eur. J. Inorg. Chem.* **2007**, 2420.
- [38] F. Durolo, D. Hanss, P. Roesel, J. P. Sauvage, O. S. Wenger, *Eur. J. Org. Chem.* **2007**, 125.
- [39] F. Durolo, L. Russo, J. P. Sauvage, K. Rissanen, O. S. Wenger, *Chem. Eur. J.* **2007**, *13*, 8749.
- [40] F. Durolo, J. P. Sauvage, *Angew. Chem. Int. Ed.* **2007**, *46*, 3537.
- [41] F. Durolo, J. P. Sauvage, O. S. Wenger, *Chem. Commun.* **2006**, 171.
- [42] F. Durolo, J. P. Sauvage, O. S. Wenger, *Helv. Chim. Acta* **2007**, *90*, 1439.
- [43] A. I. Prikhod'ko, F. Durolo, J. P. Sauvage, *J. Am. Chem. Soc.* **2008**, *130*, 448.
- [44] B. Ventura, F. Barigelletti, F. Durolo, L. Flamigni, J. P. Sauvage, O. S. Wenger, *Dalton Trans.* **2008**, 491.
- [45] M. Scholl, T. M. Trnka, J. P. Morgan, R. H. Grubbs, *Tetrahedron Lett.* **1999**, *40*, 2247.
- [46] M. Weck, B. Mohr, J. P. Sauvage, R. H. Grubbs, *J. Org. Chem.* **1999**, *64*, 5463.
- [47] H. Fukumi, H. Kurihara, *Heterocycles* **1978**, *9*, 1197.
- [48] J. Majnusz, J. M. Catala, R. W. Lenz, *Eur. Polym. J.* **1983**, *19*, 1043.
- [49] M. Rehahn, A. D. Schluter, W. J. Feast, *Synthesis* **1988**, 386.
- [50] R. Franzen, Y. J. Xu, *Can. J. Chem.* **2005**, *83*, 266.
- [51] A. Jutand, A. Mosleh, *J. Org. Chem.* **1997**, *62*, 261.
- [52] C. C. Adams, *The Knot Book*, W. H. Freeman, New York, **1994**.
- [53] J. D. Griffith, H. A. Nash, *Proc. Natl. Acad. Sci. U. S. A.* **1985**, *82*, 3124.
- [54] S. A. Wasserman, N. R. Cozzarelli, *Proc. Natl. Acad. Sci. U. S. A.* **1985**, *82*, 1079.
- [55] S. A. Wasserman, J. M. Dungan, N. R. Cozzarelli, *Science* **1985**, *229*, 171.
- [56] C. Z. Liang, K. Mislow, *J. Am. Chem. Soc.* **1994**, *116*, 11189.
- [57] C. Z. Liang, K. Mislow, *J. Am. Chem. Soc.* **1995**, *117*, 4201.
- [58] W. R. Taylor, *Nature* **2000**, *406*, 916.
- [59] W. R. Taylor, K. Lin, *Nature* **2003**, *421*, 25.
- [60] H. X. Zhou, *J. Am. Chem. Soc.* **2003**, *125*, 9280.
- [61] O. Lukin, F. Vogtle, *Angew. Chem. Int. Ed.* **2005**, *44*, 1456.
- [62] K. R. Gustafson, R. C. Sowder, L. E. Henderson, I. C. Parsons, Y. Kashman, J. H. Cardellina, J. B. McMahon, R. W. Buckheit, L. K. Pannell, M. R. Boyd, *J. Am. Chem. Soc.* **1994**, *116*, 9337.
- [63] J. H. Chen, N. C. Seeman, *Nature* **1991**, *350*, 631.
- [64] S. M. Du, B. D. Stollar, N. C. Seeman, *J. Am. Chem. Soc.* **1995**, *117*, 1194.
- [65] E. Flapan, N. C. Seeman, *J. Chem. Soc.-Chem. Commun.* **1995**, 2249.
- [66] J. E. Mueller, S. M. Du, N. C. Seeman, *J. Am. Chem. Soc.* **1991**, *113*, 6306.
- [67] N. C. Seeman, *Acc. Chem. Res.* **1997**, *30*, 357.
- [68] N. C. Seeman, J. H. Chen, S. M. Du, J. E. Mueller, Y. W. Zhang, T. J. Fu, Y. L. Wang, H. Wang, S. W. Zhang, *New J. Chem.* **1993**, *17*, 739.
- [69] N. C. Seeman, J. H. Chen, J. E. Mueller, S. M. Du, Y. L. Wang, Y. W. Zhang, *Faseb Journal* **1992**, *6*, A364.
- [70] J. C. Chambron, C. Dietrich-Buchecker, J. P. Sauvage, *Top. Curr. Chem.* **1993**, *165*, 131.
- [71] N. van Gülick, *New J. Chem.* **1993**, *17*, 619.
- [72] Boeckman, J. G. Schill, *Tetrahedron* **1974**, *30*, 1945.
- [73] G. Schill, G. Doerjter, E. Logemann, H. Fritz, *Chem. Ber.-Recl.* **1979**, *112*, 3603.

- [74] V. I. Sokolov, *Uspekhi Khimii* **1973**, *42*, 1037.
- [75] D. M. Walba, R. M. Richards, R. C. Haltiwanger, *J. Am. Chem. Soc.* **1982**, *104*, 3219.
- [76] D. M. Walba, *Tetrahedron* **1985**, *41*, 3161.
- [77] J. P. Sauvage, C. O. Dietrich-Buchecker, in *Molecular Catenanes, Rotaxanes and Knots, A Journey Through the World of Molecular Topology* (Eds.: J. P. Sauvage, C. O. Dietrich-Buchecker), Wiley-VCH, Weinheim, **1999**, pp. 107.
- [78] C. O. Dietrich-Buchecker, J. P. Sauvage, *Angew. Chem.-Int. Edit. Engl.* **1989**, *28*, 189.
- [79] C. O. Dietrich-Buchecker, G. Rapenne, J. P. Sauvage, *Chem. Commun.* **1997**, 2053.
- [80] C. O. Dietrich-Buchecker, J. F. Nierengarten, J. P. Sauvage, N. Armaroli, V. Balzani, L. Decola, *J. Am. Chem. Soc.* **1993**, *115*, 11237.
- [81] C. O. Dietrich-Buchecker, J. Guilhem, C. Pascard, J. P. Sauvage, *Angew. Chem. Int. Ed.* **1990**, *29*, 1154.
- [82] G. Rapenne, C. Dietrich-Buchecker, J. P. Sauvage, *J. Am. Chem. Soc.* **1996**, *118*, 10932.
- [83] R. F. Carina, C. Dietrich-Buchecker, J. P. Sauvage, *J. Am. Chem. Soc.* **1996**, *118*, 9110.
- [84] P. R. Ashton, O. A. Matthews, S. Menzer, F. M. Raymo, N. Spencer, J. F. Stoddart, D. J. Williams, *Liebigs Annalen-Recueil* **1997**, 2485.
- [85] O. Safarowsky, M. Nieger, R. Fröhlich, F. Vögtle, *Angew. Chem. Int. Ed.* **2000**, *39*, 1616.
- [86] in *Spectroscopic methods for determining protein structure in solution* (Ed.: H. A. Havel), Wiley-VCH, New York, **1995**.
- [87] M. Feigel, R. Ladberg, S. Engels, R. Herbst-Irmer, R. Frohlich, *Angew. Chem. Int. Ed.* **2006**, *45*, 5698.
- [88] H. Adams, E. Ashworth, G. A. Breault, J. Guo, C. A. Hunter, P. C. Mayers, *Nature* **2001**, *411*, 763.
- [89] G. H. Searle, *Bull. Chem. Soc. Jpn.* **1989**, *62*, 4021.
- [90] D. J. Royer, G. J. Grant, D. G. Vanderveer, M. J. Castillo, *Inorg. Chem.* **1982**, *21*, 1902.
- [91] Y. Yoshikawa, *Chem. Lett.* **1978**, 109.
- [92] F. M. Romero, R. Ziessel, *Tetrahedron Lett.* **1995**, *36*, 6471.
- [93] O. Henze, U. Lehmann, A. D. Schlüter, *Synthesis* **1999**, 683.
- [94] P. F. H. Schwab, F. Fleischer, J. Michl, *J. Org. Chem.* **2002**, *67*, 443.
- [95] E. C. Constable, C. E. Housecroft, B. M. Kariuki, C. B. Smith, *Supramol. Chem.* **2006**, *18*, 305.
- [96] Al. Williamson, *Justus Liebigs Ann. Chem.* **1851**, *77*, 37.
- [97] M. Neuburger, Personal communication ed., Basel, **2008**.
- [98] C. E. Housecroft, E. C. Constable, *Chemistry*, 2 ed., Pearson Education, Harlow, **2002**.
- [99] A. Goetzberger, C. Hebling, H. W. Schock, *Mater. Sci. Eng. R-Rep.* **2003**, *40*, 1.
- [100] M. Graetzel, *Inorg. Chem.* **2005**, *44*, 6841.
- [101] S. Campagna, F. Puntoriero, F. Nastasi, G. Bergamini, V. Balzani, in *Photochemistry and Photophysics of Coordination Compounds I, Vol. 280*, Springer-Verlag Berlin, Berlin, **2007**, pp. 117.
- [102] A. Juris, V. Balzani, F. Barigelletti, S. Campagna, P. Belser, A. von Zelewsky, *Coord. Chem. Rev.* **1988**, *84*, 85.
- [103] F. Barigelletti, in *CUSO-Summer School: The Challenge of Future Energy Sources*, Villars-sur-Ollon, CH, **2008**.
- [104] G. Sprintschnik, H. W. Sprintschnik, P. P. Kirsch, D. G. Whitten, *J. Am. Chem. Soc.* **1976**, *98*, 2337.
- [105] G. Sprintschnik, H. W. Sprintschnik, P. P. Kirsch, D. G. Whitten, *J. Am. Chem. Soc.* **1977**, *99*, 4947.

- [106] J. G. Vos, J. M. Kelly, *Dalton Trans.* **2006**, 4869.
- [107] V. Balzani, A. Juris, M. Venturi, S. Campagna, S. Serroni, *Chem. Rev.* **1996**, 96, 759.
- [108] A. Hagfeldt, M. Grätzel, *Acc. Chem. Res.* **2000**, 33, 269.
- [109] B. O' Regan, M. Grätzel, *Nature* **1991**, 353, 737.
- [110] T. Bessho, E. C. Constable, M. Graetzel, A. Hernandez Redondo, C. E. Housecroft, W. Kylberg, M. K. Nazeeruddin, M. Neuburger, S. Schaffner, *Chem. Commun.* **2008**, 3717.
- [111] G. J. Meyer, *Inorg. Chem.* **2005**, 44, 6852.
- [112] J. Barber, *Q. Rev. Biophys.* **2003**, 36, 71.
- [113] J. Andersson, F. Puntoriero, S. Serroni, A. Yartsev, T. Pascher, T. Polivka, S. Campagna, V. Sundstrom, *Faraday Discuss.* **2004**, 127, 295.
- [114] V. Balzani, S. Campagna, G. Denti, A. Juris, S. Serroni, M. Venturi, *Acc. Chem. Res.* **1998**, 31, 26.
- [115] Y. H. Xu, G. Eilers, M. Borgstrom, J. X. Pan, M. Abrahamsson, A. Magnuson, R. Lomoth, J. Bergquist, T. Polivka, L. C. Sun, V. Sundström, S. Styring, L. Hammarström, B. Akermark, *Chem. Eur. J.* **2005**, 11, 7305.
- [116] M. Ruben, J. Rojo, F. J. Romero-Salguero, L. H. Uppadine, J.-M. Lehn, *Angew. Chem. Int. Ed.* **2004**, 43, 3644.
- [117] G. S. Hanan, C. R. Arana, J.-M. Lehn, D. Fenske, *Angew. Chem. Int. Ed.* **1995**, 34, 1122.
- [118] A. Credi, V. Balzani, S. Campagna, G. S. Hanan, C. R. Arana, J.-M. Lehn, *Chem. Phys. Lett.* **1995**, 243, 102.
- [119] D. M. Bassani, J.-M. Lehn, S. Serroni, F. Puntoriero, S. Campagna, *Chem. Eur. J.* **2003**, 9, 5936.
- [120] A. M. Stadler, F. Puntoriero, S. Campagna, N. Kyritsakas, R. Welter, J.-M. Lehn, *Chem. Eur. J.* **2005**, 11, 3997.
- [121] V. Balzani, S. Campagna, G. Denti, A. Juris, S. Serroni, M. Venturi, *Acc. Chem. Res.* **1998**, 31, 26.
- [122] V. Balzani, P. Ceroni, M. Maestri, C. Saudan, V. Vicinelli, in *Dendrimers V: Functional and Hyperbranched Building Blocks, Photophysical Properties, Applications in Materials and Life Sciences*, Vol. 228, Springer-Verlag Berlin, Berlin, **2003**, pp. 159.
- [123] V. Balzani, F. Vögtle, *C. R. Chim.* **2003**, 6, 867.
- [124] M. Plevoets, F. Vögtle, L. De Cola, V. Balzani, *New J. Chem.* **1999**, 23, 63.
- [125] B. Bozic-Weber, E. C. Constable, E. Figgemeier, C. E. Housecroft, W. Kylberg, *Energy & Environmental Science* **2009**, 2, 299.
- [126] M. W. Cooke, G. S. Hanan, F. Loiseau, S. Campagna, M. Watanabe, Y. Tanaka, *Angew. Chem. Int. Ed.* **2005**, 44, 4881.
- [127] M. I. J. Polson, G. S. Hanan, N. J. Taylor, B. Hasenknopf, R. Thouvenot, *Chem. Commun.* **2004**, 1314.
- [128] A. Inagaki, Y. Takaya, T. Takemori, H. Suzuki, M. Tanaka, M. A. Haga, *J. Am. Chem. Soc.* **1997**, 119, 625.
- [129] K. Matsubara, R. Okamura, M. Tanaka, H. Suzuki, *J. Am. Chem. Soc.* **1998**, 120, 1108.
- [130] N. Shan, S. J. Vickers, H. Adams, M. D. Ward, J. A. Thomas, *Angew. Chem. Int. Ed.* **2004**, 43, 3938.
- [131] G. Süssfink, J. L. Wolfender, F. Neumann, H. Stoeckli-evans, *Angew. Chem. Int. Ed.* **1990**, 29, 429.
- [132] S. Katsuta, Y. Iwabe, Y. Kato, Y. Kudo, Y. Takeda, *Inorg. Chim. Acta* **2008**, 361, 103.
- [133] E. C. Constable, B. A. Hermann, C. E. Housecroft, M. Neuburger, S. Schaffner, L. J. Scherer, *New J. Chem.* **2005**, 29, 1475.

- [134] E. C. Constable, C. E. Housecroft, M. Neuburger, S. Schaffner, E. J. Shardlow, *Dalton Trans.* **2005**, 234.
- [135] E. C. Constable, K. Harris, C. E. Housecroft, M. Neuburger, S. Schaffner, *Chem. Commun.* **2008**, 5360.
- [136] G. Sprintschnik, H. W. Sprintschnik, P. P. Kirsch, D. G. Whitten, *J. Am. Chem. Soc.* **1977**, *99*, 4947.
- [137] H. Clavier, K. Grela, A. Kirschning, M. Mauduit, S. P. Nalon, *Angew. Chem. Int. Ed.* **2007**, *46*, 6786.
- [138] R. H. Grubbs, S. Chang, *Tetrahedron* **1998**, *54*, 4413.
- [139] H. G. Schmalz, *Angew. Chem. Int. Ed.* **1995**, *34*, 1833.
- [140] M. Schuster, S. Blechert, *Angew. Chem. Int. Ed.* **1997**, *36*, 2037.
- [141] S. B. Garber, J. S. Kingsbury, B. L. Gray, A. H. Hoveyda, *J. Am. Chem. Soc.* **2000**, *122*, 8168.
- [142] K. Grela, M. Kim, *Eur. J. Org. Chem.* **2003**, 963.
- [143] A. Michrowska, L. Gulajski, K. Grela, *Chem. Commun.* **2006**, 841.
- [144] D. P. Rillema, D. S. Jones, H. A. Levy, *J. Chem. Soc.-Chem. Commun.* **1979**, 849.
- [145] H. C. Stynes, J. A. Ibers, *Inorg. Chem.* **1971**, *10*, 2304.
- [146] R. A. Kirgan, P. A. Witek, C. Moore, D. P. Rillema, *Dalton Trans.* **2008**, 3189.
- [147] M. Hesse, H. Meier, B. Zeeh, *Spektroskopische Methoden in der Organischen Chemie*, 7 ed., Thieme, Stuttgart, **2005**.
- [148] J. B. Fenn, *Angew. Chem. Int. Ed.* **2003**, *42*, 3871.
- [149] J. P. Paris, W. W. Brandt, *J. Am. Chem. Soc.* **1959**, *81*, 5001.
- [150] N. E. Tokel-Takvoryan, R. E. Hemingway, A. J. Bard, *J. Am. Chem. Soc.* **1973**, *95*, 6582.
- [151] F. Bolletta, M. Ciano, V. Balzani, N. Serpone, *Inorganica Chimica Acta-Articles* **1982**, *62*, 207.
- [152] A. Juris, V. Balzani, P. Belser, A. von Zelewsky, *Helv. Chim. Acta* **1981**, *64*, 2175.
- [153] A. Juris, F. Barigelletti, V. Balzani, P. Belser, A. von Zelewsky, *Inorg. Chem.* **1985**, *24*, 202.
- [154] C. T. Lin, W. Bottcher, M. Chou, C. Creutz, N. Sutin, *J. Am. Chem. Soc.* **1976**, *98*, 6536.
- [155] <http://www.chem.qmul.ac.uk/iupac/stereo/BC.html#17>.
- [156] J. Lacour, C. Ginglinger, C. Grivet, G. Bernardinelli, *Angew. Chem. Int. Ed.* **1997**, *36*, 608.
- [157] J. Cavezzan, G. Etemadmoghadam, M. Koenig, A. Kläbe, *Tetrahedron Lett.* **1979**, 795.
- [158] M. Koenig, A. Kläbe, A. Munoz, R. Wolf, *J. Chem. Soc.-Perkin Trans. 2* **1979**, 40.
- [159] F. Favarger, C. Goujon-Ginglinger, D. Monchaud, J. Lacour, *J. Org. Chem.* **2004**, *69*, 8521.
- [160] P. S. P. Eloísa Martínez-Viviente, L. Vial, C. Herse, J. Lacour, *Chem. Eur. J.* **2004**, *10*, 2912.
- [161] C. Ginglinger, D. Jeannerat, J. Lacour, S. Jugé, J. Uziel, *Tetrahedron Lett.* **1998**, *39*, 7495.
- [162] J. L. Olivier Maury, H. Le Bozec, *Eur. J. Inorg. Chem.* **2001**, *2001*, 201.
- [163] H. A. Régis Caspar, M. Gruselle, C. Cordier, B. Malézieux, R. Duval, H. Leveque, *Eur. J. Inorg. Chem.* **2003**, *2003*, 499.
- [164] K. H. Shuichi Hiraoka, T. Tanaka, M. Shiro, M. Shionoya, *Angew. Chem. Int. Ed.* **2003**, *42*, 5182.
- [165] H. Amouri, R. Caspar, M. Gruselle, C. Guyard-Duhayon, K. Boubekeur, D. A. Lev, L. S. B. Collins, D. B. Grotjahn, *Organometallics* **2004**, *23*, 4338.

- [166] M. Chavarot, S. Menage, O. Hamelin, F. Charnay, J. Pecaut, M. Fontecave, *Inorg. Chem.* **2003**, *42*, 4810.
- [167] O. Hamelin, J. Pecaut, M. Fontecave, *Chem. Eur. J.* **2004**, *10*, 2548.
- [168] J. Lacour, C. Goujon-Ginglinger, S. Torche-Haldimann, J. J. Jodry, *Angew. Chem. Int. Ed.* **2000**, *39*, 3695.
- [169] E. C. Constable, R. Frantz, C. E. Housecroft, J. Lacour, A. Mahmood, *Inorg. Chem.* **2004**, *43*, 4817.
- [170] J. Lacour, C. Ginglinger, S. Torche-Haldimann, *Angew. Chem. Int. Ed.* **1998**, *37*, 2379.
- [171] D. Monchaud, J. J. Jodry, D. Pomeranc, V. Heitz, J. C. Chambron, J. P. Sauvage, J. Lacour, *Angew. Chem. Int. Ed.* **2002**, *41*, 2317.
- [172] L. Vial, M. H. Goncalves, P. Y. Morgantini, J. Weber, G. Bernardinelli, J. Lacour, *Synlett* **2004**, 1565.
- [173] T. Le Bouder, O. Maury, A. Bondon, K. Costuas, E. Amouyal, I. Ledoux, J. Zyss, H. Le Bozec, *J. Am. Chem. Soc.* **2003**, *125*, 12284.
- [174] L. Viau, S. Bidault, O. Maury, S. Bresselet, I. Ledoux, J. Zyss, E. Ishow, K. Nakatani, H. Le Bozec, *J. Am. Chem. Soc.* **2004**, *126*, 8386.
- [175] G. Bruylants, C. Bresson, A. Boisdenghien, F. Pierard, A. Kirsch-De Mesmaeker, J. Lacour, K. Bartik, *New J. Chem.* **2003**, *27*, 748.
- [176] A. Streitwieser, C. H. Heathcock, E. M. Kosower, *Organische Chemie*, VCH, Weinheim, **1994**.
- [177] R. W. Hoffmann, *Angew. Chem. Int. Ed.* **2003**, *42*, 1096.
- [178] N. Matsuura, A. Igashira-Kamiyama, T. Kawamoto, T. Konno, *Inorg. Chem.* **2006**, *45*, 401.
- [179] J. A. Dean, T. C. Rains, Marcel Dekker, New York, **1969-1975**.
- [180] D. A. Skoog, F. J. Holler, T. A. Nieman, *Principles of Instrumental Analysis*, 5 ed., Saunders, Philadelphia etc, **1998**.
- [181] V. A. Fassel, R. N. Kniseley, *Anal. Chem.* **1974**, *46*, 1110.
- [182] J. Yin, R. L. Elsenbaumer, *Inorg. Chem.* **2007**, *46*, 6891.
- [183] U. Knof, A. von Zelewsky, *Angew. Chem. Int. Ed.* **1999**, *38*, 302.
- [184] J. H. van Vleck, *Physical Review* **1932**, *41*, 208.
- [185] W. W. Brandt, F. P. Dwyer, E. C. Gyrfas, *Chem. Rev.* **1954**, *54*, 959.
- [186] E. C. Constable, C. E. Housecroft, B. M. Kariuki, C. B. Smith, *Aust. J. Chem.* **2006**, *59*, 30.
- [187] C. B. Smith, E. C. Constable, C. E. Housecroft, B. M. Kariuki, *Chem. Commun.* **2002**, 2068.
- [188] K. J. Arm, J. A. G. Williams, *Dalton Trans.* **2006**, 2172.
- [189] E. C. Constable, E. Figgemeier, C. E. Housecroft, J. Olsson, Y. C. Zimmermann, *Dalton Trans.* **2004**, 1918.
- [190] E. C. Constable, C. E. Housecroft, I. Poleschak, *Inorg. Chem. Commun.* **1999**, *2*, 565.
- [191] E. Figgemeier, E. C. Constable, C. E. Housecroft, Y. C. Zimmermann, *Langmuir* **2004**, *20*, 9242.
- [192] B. Galland, D. Limosin, H. Laguitton-Pasquier, A. Deronzier, *Inorg. Chem. Commun.* **2002**, *5*, 5.
- [193] V. Grosshenny, A. Harriman, M. Hissler, R. Ziessel, *J. Chem. Soc., Faraday Trans.* **1996**, *92*, 2223.
- [194] F. Loiseau, R. Passalacqua, S. Campagna, M. I. J. Polson, Y. Q. Fang, G. S. Hanan, *Photochem. Photobiol. Sci.* **2002**, *1*, 982.
- [195] J. Lombard, J. C. Lepretre, J. Chauvin, M. N. Collomb, A. Deronzier, *Dalton Trans.* **2008**, 658.

- [196] B. Milani, A. Anzilutti, L. Vicentini, A. Sessanta o Santi, E. Zangrando, S. Geremia, G. Mestroni, *Organometallics* **1997**, *16*, 5064.
- [197] E. C. Constable, *Adv. Inorg. Chem.* **1989**, *34*, 1.
- [198] F. H. Allen, *Acta Crystallogr., Sect. B* **2002**, *58*, 380.
- [199] I. J. Bruno, J. C. Cole, P. R. Edgington, M. Kessler, C. F. Macrae, P. McCabe, J. Pearson, R. Taylor, *Acta Crystallogr., Sect. B* **2002**, *58*, 389.
- [200] B. Milani, A. Anzilutti, L. Vicentini, A. S. O. Santi, E. Zangrando, S. Geremia, G. Mestroni, *Organometallics* **1997**, *16*, 5064.
- [201] P. C. Chieh, *J. Chem. Soc., Dalton Trans.* **1972**, 1207.
- [202] A. Hazell, O. Simonsen, O. Wernberg, *Acta Crystallogr., Sect. C* **1986**, *42*, 1707.
- [203] S. Maeda, Y. Nishida, H. Okawa, S. Kida, *Bull. Chem. Soc. Jpn.* **1986**, *59*, 2013.
- [204] T. N. Fedotova, L. K. Minacheva, G. N. Kuznetsova, *Russ. J. Inorg. Chem.* **2003**, *48*, 351.
- [205] B. R. Clare, C. S. McInnes, A. G. Blackman, *Acta Crystallogr., Sect. E* **2005**, *61*, M2042.
- [206] S. Geremia, L. Randaccio, G. Mestroni, B. Milani, *J. Chem. Soc., Dalton Trans.* **1992**, 2117.
- [207] M. Kato, K. Sasano, C. Kosuge, M. Yamazaki, S. Yano, M. Kimura, *Inorg. Chem.* **1996**, *35*, 116.
- [208] S. Stoccoro, G. Alesso, M. A. Cinellu, G. Minghetti, A. Zucca, A. Bastero, C. Claver, M. Manassero, *J. Organomet. Chem.* **2002**, *664*, PII S0022.
- [209] J. R. Stork, D. Rios, D. Pham, V. Bicocca, M. M. Olmstead, A. L. Balch, *Inorg. Chem.* **2005**, *44*, 3466.
- [210] M. Tominaga, T. Kusukawa, S. Sakamoto, K. Yamaguchi, M. Fujita, *Chem. Lett.* **2004**, *33*, 794.
- [211] H. Endres, H. J. Keller, W. Moroni, D. Nothe, V. Dong, *Acta Crystallogr., Sect. B* **1978**, *34*, 1823.
- [212] R. Palmans, D. B. MacQueen, C. G. Pierpont, A. J. Frank, *J. Am. Chem. Soc.* **1996**, *118*, 12647.
- [213] V. Dong, H. Endres, H. J. Keller, W. Moroni, D. Nothe, *Acta Crystallogr., Sect. B* **1977**, *33*, 2428.
- [214] V. Maheshwari, M. Carlone, F. R. Fronczek, L. G. Marzilli, *Acta Crystallogr., Sect. B* **2007**, *63*, 603.
- [215] P. Wehman, G. C. Dol, E. R. Moorman, P. C. J. Kamer, P. Vanleeuwen, J. Fraanje, K. Goubitz, *Organometallics* **1994**, *13*, 4856.
- [216] J. Durand, E. Zangrando, C. Carfagna, B. Milani, *Dalton Trans.* **2008**, 2171.
- [217] C. Y. Yue, F. L. Jiang, D. Q. Yuan, L. Chen, M. Y. Wu, M. C. Hong, *Chin. J. Struct. Chem.* **2008**, *27*, 467.
- [218] E. C. Constable, S. M. Elder, J. Healy, M. D. Ward, D. A. Tocher, *J. Am. Chem. Soc.* **1990**, *112*, 4590.
- [219] E. C. Constable, S. M. Elder, M. J. Hannon, A. Martin, P. R. Raithby, D. A. Tocher, *J. Chem. Soc., Dalton Trans.* **1996**, 2423.
- [220] G. Rapenne, C. Dietrich-Buchecker, J. P. Sauvage, *J. Am. Chem. Soc.* **1999**, *121*, 994.
- [221] K. H. Song, S. O. Kang, J. Ko, *Chem. Eur. J.* **2007**, *13*, 5129.
- [222] L. E. Perret-Aebi, A. von Zelewsky, C. D. Dietrich-Buchecker, J. P. Sauvage, *Angew. Chem. Int. Ed.* **2004**, *43*, 4482.
- [223] A. Fürstner, *Topics Organomet. Chem.* **1998**, *1*, 37.
- [224] C. Dietrich-Buchecker, M. C. Jimenez, J. P. Sauvage, *Tetrahedron Lett.* **1999**, *40*, 3395.
- [225] M. Shaul, Y. Cohen, *J. Org. Chem.* **1999**, *64*, 9358.
- [226] D. A. Bryant, N. U. Frigaard, *Trends Microbiol.* **2006**, *14*, 488.

- [227] D. A. Van Dyke, B. A. Pryor, P. G. Smith, M. R. Topp, *J. Chem. Educ.* **1998**, *75*, 615.
- [228] T. Förster, K. Kasper, *Z. Phys. Chem. (Munich)* **1954**, *1*, 275.
- [229] T. Förster, K. Kasper, *Z. Elektrochem.* **1955**, *59*, 976.
- [230] H. Saigusa, E. C. Lim, *Acc. Chem. Res.* **1996**, *29*, 171.
- [231] K. E. Wilzbach, L. Kaplan, *J. Am. Chem. Soc.* **1966**, *88*, 2066.
- [232] J. Mattay, *Angew. Chem. Int. Ed.* **2007**, *46*, 663.
- [233] P. Conlon, C. Y. J. Yang, Y. R. Wu, Y. Chen, K. Martinez, Y. M. Kim, N. Stevens, A. A. Marti, S. Jockusch, N. J. Turro, W. H. Tan, *J. Am. Chem. Soc.* **2008**, *130*, 336.
- [234] M. Kadirvel, B. Arsic, S. Freeman, E. V. Bichenkova, *Organic & Biomolecular Chemistry* **2008**, *6*, 1966.
- [235] M. Kasha, *Faraday Soc. Discuss.* **1950**, 14.
- [236] M. K. DeArmond, C. M. Carlin, *Coord. Chem. Rev.* **1981**, *36*, 325.
- [237] R. L. Blakley, M. L. Myrick, M. K. DeArmond, *J. Am. Chem. Soc.* **1986**, *108*, 7843.
- [238] T. E. Keyes, C. O'Connor, J. G. Vos, *Chem. Commun.* **1998**, 889.
- [239] D. S. Tyson, C. R. Luman, X. Zhou, F. N. Castellano, *Inorg. Chem.* **2001**, *40*, 4063.
- [240] L.-Q. Song, J. Feng, X.-S. Wang, J.-H. Yu, Y.-J. Hou, P.-H. Xie, B.-W. Zhang, J.-F. Xiang, X.-C. Ai, J.-P. Zhang, *Inorg. Chem.* **2003**, *42*, 3393.
- [241] R. L. Blakley, M. L. Myrick, M. K. DeArmond, *J. Am. Chem. Soc.* **1986**, *108*, 7843.
- [242] C. Carlin, M. K. DeArmond, *J. Lumin.* **1972**, *5*, 225.
- [243] R. J. Watts, M. J. Brown, B. G. Griffith, J. S. Harrington, *J. Am. Chem. Soc.* **1975**, *97*, 6029.
- [244] A. I. Baba, J. R. Shaw, J. A. Simon, R. P. Thummel, R. H. Schmehl, Colchester, Vermont, **1997**, pp. 43.
- [245] E. C. Glazer, D. Magde, Y. Tor, *J. Am. Chem. Soc.* **2005**, *127*, 4190.
- [246] E. C. Glazer, D. Magde, Y. Tor, *J. Am. Chem. Soc.* **2007**, *129*, 8544.
- [247] G. J. Wilson, A. Launikonis, W. H. F. Sasse, A. W. H. Mau, *J. Phys. Chem. A* **1997**, *101*, 4860.
- [248] G. J. Wilson, W. H. F. Sasse, A. W. H. Mau, *Chem. Phys. Lett.* **1996**, *250*, 583.
- [249] W. E. Ford, M. A. J. Rodgers, *J. Phys. Chem.* **1992**, *96*, 2917.
- [250] N. D. McClenaghan, F. Barigelletti, B. Maubert, S. Campagna, *Chem. Commun.* **2002**, 602.
- [251] A. F. Morales, G. Accorsi, N. Armaroli, F. Barigelletti, S. J. A. Pope, M. D. Ward, *Inorg. Chem.* **2002**, *41*, 6711.
- [252] G. J. Wilson, A. Launikonis, W. H. F. Sasse, A. W. H. Mau, *J. Phys. Chem. A* **1998**, *102*, 5150.
- [253] D. S. Tyson, K. B. Henbest, J. Bialecki, F. N. Castellano, *J. Phys. Chem. A* **2001**, *105*, 8154.
- [254] J. M. Robertson, J. G. White, *J. Chem. Soc.* **1947**, 358.
- [255] S. K. Burley, G. A. Petsko, *Science* **1985**, *229*, 23.
- [256] C. Janiak, *J. Chem. Soc., Dalton Trans.* **2000**, 3885.
- [257] C. Janiak, S. Temizdemir, S. Dechert, *Inorg. Chem. Commun.* **2000**, *3*, 271.
- [258] Y. Umezawa, S. Tsuboyama, K. Honda, J. Uzawa, M. Nishio, *Bull. Chem. Soc. Jpn.* **1998**, *71*, 1207.
- [259] E. G. Cox, D. W. J. Cruickshank, J. A. S. Smith, *Proc. Roy. Soc. London, Ser. A.* **1958**, *247*, 1.
- [260] T. Shoda, K. Yamahara, K. Okazaki, D. E. Williams, *Theochem-J. Mol. Struct.* **1994**, *119*, 321.
- [261] D. E. Williams, Y. L. Xiao, *Acta Crystallogr., Sect. A* **1993**, *49*, 1.
- [262] A. Harriman, M. Hissler, A. Khatyr, R. Ziessel, *Chem. Commun.* **1999**, 735.
- [263] A. Harriman, M. Hissler, R. Ziessel, *Phys. Chem. Chem. Phys.* **1999**, *1*, 4203.

- [264] J. A. Simon, S. L. Curry, R. H. Schmehl, T. R. Schatz, P. Piotrowiak, X. Q. Jin, R. P. Thummel, *J. Am. Chem. Soc.* **1997**, *119*, 11012.
- [265] U. Pischel, *Angew. Chem. Int. Ed.* **2007**, *46*, 4026.
- [266] COLLECT Software, Nonius BV 1997-2001.
- [267] C. W. Carter, R. M. Sweet, *Vol. 276* (Eds.: Z. Otwinowski, W. Minor), Academic Press, New York, **1997**, p. 307.
- [268] A. Altomare, G. Cascarano, C. Giacovazzo, A. Guagliardi, e. al., *J. Appl. Cryst.* **1994**, *27*, 1045.
- [269] Stoe & Cie, IPDS software v 1.26, Stoe & Cie, Darmstadt, Germany, **1996**.
- [270] G. M. Sheldrick, *Acta Crystallogr., Sect. A* **2008**, *64*, 112.
- [271] P. W. Betteridge, J. R. Carruthers, R. I. Cooper, K. Prout, D. J. Watkin, *J. Appl. Cryst.* **2003**, *36*, pt.6, 1487.
- [272] K. Nakamaru, *Bull. Chem. Soc. Jpn.* **1982**, *55*, 2697.
- [273] S. Lebedkin, T. Langetepe, P. Sevillano, D. Fenske, M. M. Kappes, *J. Phys. Chem. B* **2002**, *106*, 9019.

Curriculum vitae

Pirmin Rösel

PERSONAL DETAILS

Ryffstr. 16
4056 Basel
Switzerland
Home Phone: +41(0)613217510
Work Phone: +41(0)612671035
E-Mail: P.Roesel@stud.unibas.ch

Marital Status: Single
Place of birth: Lörrach, Germany
Date of birth: 02/08/1979
Citizenship: German

EDUCATION

07/2005 – 05/2009 **PhD studies**, *Mononuclear and Oligonuclear Transition Metal Complexes with Acyclic and Macrocyclic Ligands*,
Supervisors: Prof. Dr. Edwin Constable, University of Basel, Prof. Dr. Jean-Pierre Sauvage, University Louis Pasteur, Strasbourg.

10/2004 – 02/2005 **Diploma work** (equivalent to an MSc), *ESI-MS als Instrument zur Ligandenentwicklung (ESI-MS as tool for ligand development)*,
Supervisor: Prof. Dr. Andreas Pfaltz, University of Basel.

2000 – 2004 Studies in chemistry at the University of Basel

1999 – 2000 Military service in Sigmaringen (Germany)

1999 Abitur at *Wirtschaftsgymnasium Lörrach*, Germany

TEACHING

05/2009 – present Supervising of one 4th year student (Wahlpraktikum), University Basel
2006 – present Laboratory Demonstrator, General chemistry (1st year), University Basel

Während meiner Ausbildung an der Universität Basel habe ich Vorlesungen und Seminare der folgenden Dozenten besucht:

T. Briellmann, H. Burkhart, E. C. Constable, O. Dopfer, F. Dussy, B. Giese, M. Guggisberg, H.-J. Güntherodt, P. Hauser, C. E. Housecroft, H. Huber, H.-C. Imhof, B. Jung, M. Jungen, T. Kaden, J. P. Maier, M. Mayor, W. P. Meier, M. Meuwly, W. Nau, M. Neuburger-Zehnder, M. Oehme, A. Pfaltz, C. Schönenberger, U. Séquin, H. Sigel, P. Strazewski, A. Vedani, C. Wattinger, H. A. Wegener, H. Wennemers, J. Wirz, W.-D. Woggon, A. Zuberbühler.